VALORISATION OF ALKANES AND ALKYNES BY TRANSHYDROGENATION IN PETROCHEMICAL PROCESSES

MUSTAPHA DANLAMI GARBA

MSc Oil & Gas Chemistry, 2012
University of Aberdeen, United Kingdom

BSc (Hons) Chemistry, 2010
Bayero University Kano, Nigeria

Supervisor: Professor S. David Jackson

School of Chemistry
College of Science and Engineering
University of Glasgow

October, 2017

‘Luck is what happens when preparation meets opportunity…’

Abstract

The production of high premium fuel is an issue of priority to every refinery. The trans-hydrogenation process was devised to convert two low value refinery cracked products to premium products; the conversion processes involve the combination of dehydrogenation and hydrogenation reactions as a single step process. The low value refinery products (i.e. alkanes and alkynes or alkadienes) have been converted to alkenes (olefins) by trans-hydrogenation using catalysts system based on VOx, CrOx and Pt all supported on alumina. Although trans-hydrogenation has been disclosed in many patents over decades, only little academic literature is available. The success of the process over various catalysts has been claimed in many of these patents. However, further studies are still required to ascertain the actual reaction mechanism, mitigating carbon deposition and catalyst deactivation, and the role of different catalysts to optimize the reaction desired products. The current research work evaluates the potential of CrO_x/Al_2O_3, K-CrO_x/Al_2O_3, Pt/Al_2O_3 and K-Pt/Al_2O_3 to investigate the trans-hydrogenation of the pentane (P)/1-hexyne (1HY) system, the pentane (P)/1,5-hexadiene (1,5-HD) system and the pentane (P)/2,4-Hexadiene (2,4-HD) system over a range temperatures (523-773 K).

The fresh catalysts were first characterised by N_2 adsorption using the BET method, X-ray diffraction, Raman spectroscopy, Thermogravimetric analysis, Temperature programme oxidation (TPO), Temperature programmed reduction (TPR), Electron paramagnetic resonance (EPR), Atomic absorption spectroscopy (AAS) and colorimetric analysis.

The Free energy (ΔG) for the reaction of pentane with 1-hexyne, 1,5-hexadiene and 2,4-hexadiene shows that trans-hydrogenation is thermodynamically favoured at most temperatures for the reaction of pentane with 1-hexyne, however this is not always the case when hexadienes are the hydrogen acceptors. When 2,4-HD is the acceptor, ΔG is +ve at all the reaction temperatures tested. When pentane or hexyne/hexadiene or a 5:1 mixture was passed over the catalyst, in the temperature range of 523K -773 K, it was found that trans-hydrogenation process had taken place but many of the products are alkylated olefinic and alkylated hydrocarbons. Regarding all systems previously mentioned above, the ratio of olefin to alkylated olefin products was ~50:50 at

773K, however, this ratio was found to vary at other temperatures. The lowest ratio of ~10:90 was obtained at 523K. Dissociation of the hydrocarbon reactant was also observed leading to production of cracked products such as CH_4, C_2H_4 and subsequent formation of a carbonaceous overlayer on the catalyst surface. This was not the case with the 2,4-hexadiene reactant, the trans-hydrogenation is poor, as expected from the free energies.

The trans-hydrogenation process was shown to improve the conversion of pentane when co-fed with the hexyne to ~26% and to ~90% when co-fed with 1,5HD using the chromia catalyst at 773K, both values are much higher than the equilibrium conversion of the pentane dehydrogenation. Higher conversions of the pentane were subsequently obtained with other catalysts, but the chromia/alumina and K-CrO_x/Al_2O_3 catalyst exhibits greater trans-hydrogenation activity. With the 2,4HD acceptor, very low conversions of pentane were obtained with all the catalysts: in general conversions lower than when the pentane was run alone were obtained.

The products observed were unique for each catalyst. However, it was observed that for each catalyst, only the distribution of the products changed with temperature. This also accounted for changes in both the cracking products and the carbon laydown on the catalyst.

The deactivation regeneration cycles shows very similar conversion of both reactants. There is a small deactivation observed for the longer time run; however these were not very significant. It was observed that some of the major products were consumed with time, but are used for the formation of other major products. However, this is more prominent with pentane/hexyne run using the CrO_x/Al_2O_3 catalyst

The TGA-TPO analysis of the post reaction catalysts shows desorption of species from all catalyst, and analysis of the eluant gas by mass spectrometry (m/e, 44) confirms carbon deposition. Traces of other species (i.e H_2, CH_4, C_2H_4 and H_2O) were also observed with some of the catalysts, more especially with the chromia catalyst. Evidence for the evolution of CO_2 was only observed for 1,5HD and 2,4HD and the same combustion species were observed for all catalysts. However, the 1HY presented different combustion species with the use of the

various catalysts. One and three types of carbonaceous species were evolved using CrO_x/Al_2O_3 and $K\text{-}CrO_x/Al_2O_3$ respectively. There is reduction to the amount of carbon deposition with the trans-hydrogenation process compared to when run individually with all the catalysts. Pentane presents very less carbon deposition at all temperatures compared to the hexyne/hexadienes or their mixed feed.

The Raman analysis shows both the D and G bands associated with coke depositions observed with the hydrogen acceptors. However, many of the trans-hydrogenation reactions present predominantly G bands except for a few reactions. The formation of the D and G bands is also observed to be related to the amount of carbon material deposited on the catalyst.

Dedication

My humble parents, my siblings

&

The wonderful people of Nigeria

Acknowledgement

To God is the glory…

First and foremost, I consider it worthwhile to express my profound gratitude to my supervisor, not only as a supervisor but as a father; words will not be enough to express how grateful I am toward all he did to me during this work, may God bless you more. I will want be like you when I grow up, because it is very rare to be so influential combined with such intelligence, awesomeness and fame in one person. The thesis would have not been done without his continuous guidance, valuable recommendations, smiling face, patience and endless support. A big thank you to my second supervisor, prof. Justin Hargreaves for your valuable support and advice.

I would like to use this opportunity, to thank Dr Florent, Dr Ashley for their guidance during the start of my PhD, both of you greatly assisted me. Dr Stephen Sproules, thank you for the EPR analysis. To you Cory I owe you a lot, without you I wouldn't have enjoy my stay in Glasgow. Lots of memories that cannot be mention here, you're indeed a sister and hopefully small Cory to be will emulate you and all you good characters, it is very difficult to find person like you.

Words are not enough to express my sincere gratitude and gratefulness to the new and old catalysis team, all of you have been amazing, I still remember all the BBQ and dinners with Ihfaf, Nicola you've been amazing, and you've encapsulated me with lots of memories, Yalin you're indeed a sister, Kathleen, Angela, Ahmad, Said and Danielle, you've all been great.

My appreciation also goes to technical staff UoG, in the person of Andy, Jim, Gangi, Claire, Stuart, and all the great and hardworking members of the team for all the help you have rendered me during my PhD.

I would like to acknowledge, Petroleum technology development fund (PTDF) for the research funding and financial support.

Finally, to my parents and siblings for their tireless prayer and support.

Declaration

The work contained in this thesis, submitted for the degree of Doctor of Philosophy, is my own work, except where due reference is made to other authors. It has not been accepted in any previous application for a degree. It is a record of my work and all verbatim extracts have been distinguished by quotation marks. My sources of information have been specifically acknowledged.

Mustapha Danlami Garba

Table of content

GLOSSARY

Catalyst metals

Chromium	Cr
Chromia	CrO_x
Platinum	Pt
Potassium	K

Gases, Compounds and Solvents etc.

Hydrogen	H_2
Oxygen	O_2
Nitrogen	N_2
Argon	Ar
Helium	He
Methane	CH_4
Water	H_2O
Carbon Monoxide	CO
Liquefied petroleum gas	LPG
Methyl tert-butyl ether	MTBE
Carbon Dioxide	CO_2

Analysis Methods

Brunauer, Emmett and Teller	BET
X-ray Diffraction	XRD
Thermo-gravimetric Analysis	TGA
Differential Thermo-gravimetric analysis	DTA
Temperature-Programmed Reduction	TPR
Temperature-Programmed Oxidation	TPO
Carbon, Nitrogen and Hydrogen (analysis)	CHN
Gas Chromatography	GC
Mass Spectroscopy	MS
Atomic Absorption Spectroscopy	ASS
UV-Visible Spectroscopy	UV-Vis
Electron Paramagnetic Resonance	EPR

Other Terms

Flame Ionization Detector	FID
European Spectrometry Systems	ESS
BET Surface Area	S_{BET}
Gas Hourly Speed Velocity	GHSV
Weight Hourly Speed Velocity	WHSV

Enthalpy	ΔH
Entropy	ΔS
Gibbs free energy	ΔG
Specific heat capacity	C_p
Thermo-couple	TC

1.0 Introduction

Background

The demand and consumption of energy is increasingly becoming a critical factor for development, welfare, and social activities & stability [1]. This could be linked to the rapid increase in human population and the associated development in science and technology, particularly given the emphasis to increased production and usage of high performance gasoline engines and production of petrochemical allied chemicals. Therefore devising the most appropriate method of upgrading and effective isolation of the petroleum product is an inevitable issue from both research and policy perspectives.

The production of olefins has been of major industrial importance since World War II using catalysts to yield high octane aviation fuel [2]. Since then the petroleum industries have been constantly developing new processes for improved olefin production, involving new catalyst formulations and modifications to reactor and plant design. This effort has also been extended to accommodate different hydrocarbon feeds in order to maximize production. Currently, olefins are produced via number of processes in oil refining industries to successfully maximize the production. For example in the late 1980s, the Catofin™ process was designed for the on-demand production of propylene and isobutylene using propane and isobutene respectively [3-5]

Gasoline is a hydrocarbon based fuel obtained from petroleum fraction. However its exact chemical composition can be varied by blending with other specific hydrocarbons to produce a very high grade fuel depending on the demand, applications and environmental constraints. The major component of fuel used in internal combustion engines comprises of mainly straight chain and isomers of light and medium alkanes with specific concentrations of aromatics to achieve an optimum octane number [6-8]. Environmental problems associated with aromatics however have recently resulted in a ban on their usage due to health concerns [9, 10]. Even with this restriction, gasoline will remain a popular fuel for transportation, combustion engines and industrial applications [11, 12] for many years to come. Therefore devising the most appropriate

method of upgrading the octane number is an important issue from both research and policy perspectives.

Olefins are class of hydrocarbons that are unsaturated with a single double bond and general chemical formula of C_nH_{2n}. Olefins are regarded as the building block of the petrochemical industry due to their relatively high reactivity, making the olefin molecule ideal for the conversions into valuable end products [13].

The global production of olefins is around 400 MT per year generated from one billion tons of various hydrocarbon feedstocks, with about 60 % of the global feedstock processed within the fluid catalytic cracking unit of oil refineries, whilst the other 40 % are processed within the steam cracking of naphtha, steam cracking, ethylene plants, and liquefied petroleum gas [14]. Currently this is an area of globally active R&D targeted at maximizing production due to worldwide high demands.

The primary purpose of the trans-hydrogenation process historically has been to convert low-value cracked hydrocarbons into valued distillate products. Although trans-hydrogenation is not a new technology for production of olefins there is scant scientific attention toward the invention. The trans-hydrogenation of alkanes and alkynes (or alkadienes) into alkenes (olefins) is a method of converting two low value chemicals into two high value chemicals. It is well known that hydrocarbon feed stock streams, such as naphtha, LPG, or gas oil are cracked in a furnace to produce mixtures of hydrocarbons of varying molecular weight [15-20], a typical percentage composition (by weight) is presented in Table 1. The olefin component is generally the most important, used for the production of high-octane fuel and polymerization [15, 20].

Therefore, there is a need to maximize its production as the most valuable product of the cracked component. However inevitably compounds such as alkanes and alkynes are also products of cracking and although the alkyne can be hydrogenated to the respective alkene, this uses hydrogen. Similarly the alkane can be dehydrogenated but there is then the need for separation.

Table 1: typical percentage composition by weight of naphtha cracking products

Component	Wt. % Composition
Hydrogen	1
Benzene	6
Methane	16
Toluene	3
Ethene	32
Aromatics	2
Propene	16
Fuel oil	4
C4 hydrocarbons	8
Others	12

In contrast when both react via catalytic trans-hydrogenation the yield of the olefin is increased without the need of hydrogen or separation technology. The two low value products can be mixed and fed into a simple refinery process (Figure 1).

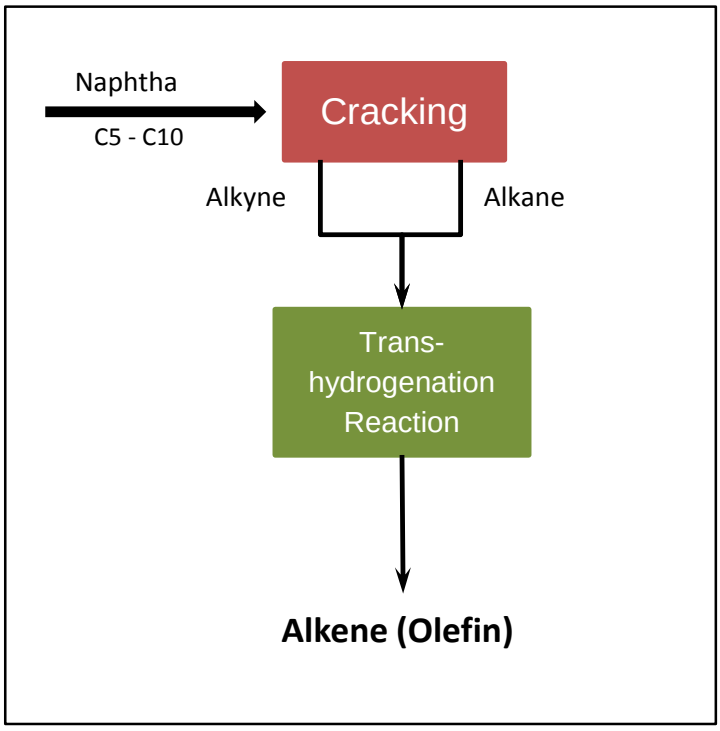

Figure 1: Proposed operation unit for Trans-hydrogenation process in a refinery

Trans-hydrogenation has been disclosed in a numbers of patents over a period of decades [20-25]. However it has only recently been studied in the academic literature [26-28]. The trans-hydrogenation process has significance as a safe environmentally acceptable technique for up-grading feedstock containing C2-C5 alkanes and alkynes/alkadienes

1.1 Dehydrogenation and hydrogenation processes in trans-hydrogenation

1.1.1 Dehydrogenation process

Alkane dehydrogenation is endothermic (~124 $kJ.mol^{-1}$) and a significant amount of energy is required to break C-H bonds in a molecule. The equilibrium conversion of the process is limited by the reaction temperature and as that increases so does conversion [29]. Hence to accommodate the thermodynamic limitations typical reaction temperatures are ≥ 823 K: at these temperatures all C-H bonds in an alkane have equal chance to react [30-33]. However at such high temperatures secondary reactions such as cracking and carbon deposition are also favoured, therefore the reaction tends to get less selective as temperature and conversion increase. The equilibrium conversion can also be increased by decreasing the pressure and indeed some on-demand dehydrogenation processes operate at partial pressure less than 1 atm often with the use of a diluent in the alkane feed [34]. Carbon deposition during dehydrogenation is a major process problem and limits the time on-stream for the catalysts. Carbon deposition occurs via a series of progressive dehydrogenation, condensation, polymerisation and cyclisation processes leading eventually to graphitic precursors such as pyrene, perylene and fluoranthene. To cope with such carbon laydown all current processes operate cyclically to regenerate deactivated catalysts and use the heat liberated to offset the reaction endotherm.

The dehydrogenation equilibrium of alkanes to alkenes shows that high molecular alkane need lower temperature than the low molecular alkane for dehydrogenation [30]. However, because of the equal chance of C-H bond breakage in the alkane molecule chain, if two neighbouring C-H are split a double bond is formed converting alkane to alkene. However, in another

scenario if the splitting took place in non-neighbouring carbon or other reaction conditions, possible other compounds different from alkene could be formed. These compounds are formed due to process as listed below:

- Dehydrocyclization
- Aromatization
- Isomerisation
- Oligomerization to form high molecular weight hydrocarbon
- Hydrogen gas and coke

These products could be formed depending on the two C-H splitting and number of carbon atom of the alkane reactant (Figure 2).

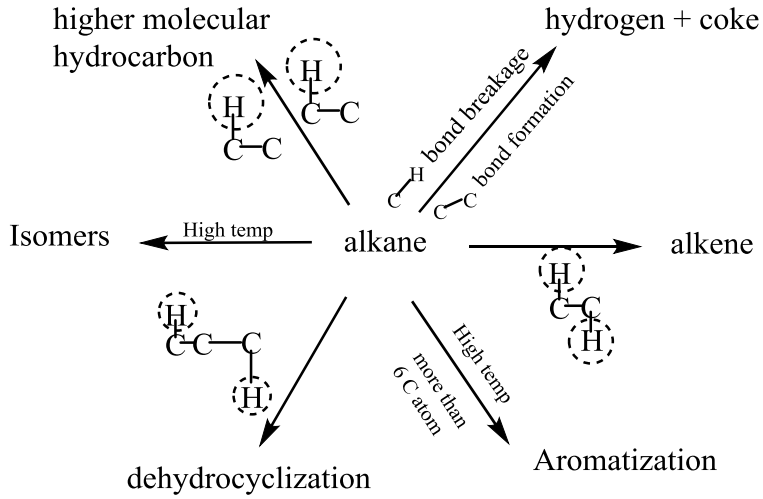

Figure 2: Likely products during alkane dehydrogenation

According to Le Chatelier's principle which shows that higher conversion is obtained by either high temperature or low pressure as expressed below:

$$Xe^2 = \frac{Kp}{Kp + P}$$

Where:

Xe = equilibrium conversion

P = total absolute pressure

Kp = dehydrogenation constant

Kp can be calculated from Gibb's free energy from sources of thermodynamic data.

Bhasin et al., [2] illustrated the effect of low pressure in dehydrogenation reaction to investigate the equilibrium conversion of propane. The investigations were performed using 1 and 0.23 atmospheric pressure. The results are presented in figure 3, it is observed that higher equilibrium conversions are obtained at the low pressure 0.23 atm abs reaction (Figure 3-1) compares to the higher pressure 1 atm abs reaction (Figure 3-2).

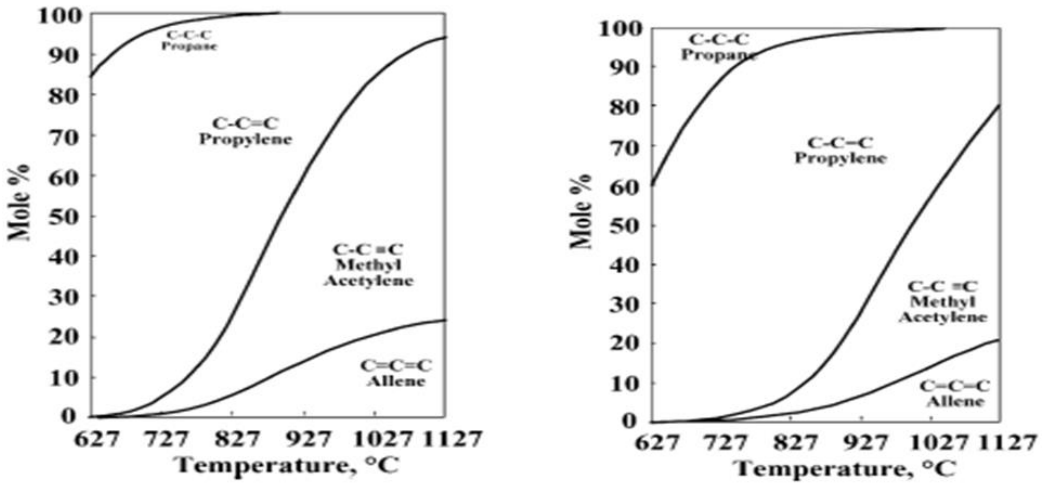

Figure 3: Propane dehydrogenation equilibrium at 1) 0.23 atm abs. pressure & 2) 1.00 atm abs [35]

In alkane dehydrogenation it is reported that the equilibrium constant increases with increasing carbon number. Figure 4 adapted from Imai, *et al.*,[2] shows the trend in the equilibrium constant with increase in carbon number for dehydrogenation of alkane to alkene and hydrogen. Thus, this could show that high molecular alkane need lower temperature that the lower alkane dehydrogenation.

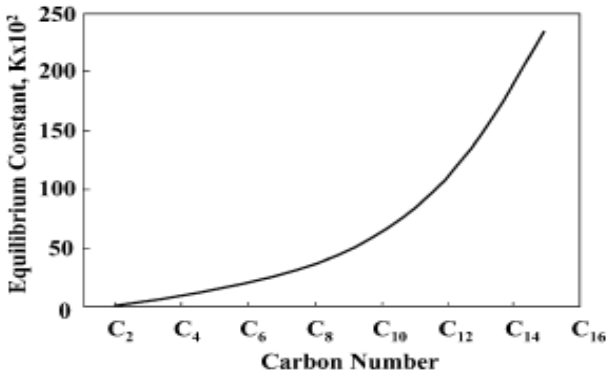

Figure 4: Equilibrium constants for n-paraffin dehydrogenation at 500 °C [2]

However, based on the equilibrium constant, a temperature plot could be formed and used to determine a certain required equilibrium conversion. This shows the temperature dependence for the dehydrogenation of lighter to heavier alkane, lighter alkane requiring much higher temperature as illustrated by Bahsin *et al.*, as presented in Figure 5.

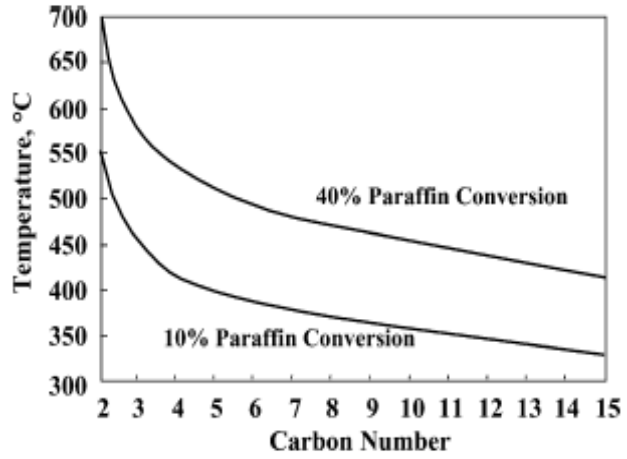

Figure 5: temperature dependency on paraffin conversion [2]

1.1.2 Hydrogenation processes

Alkyne hydrogenation in contrast is exothermic and produces a significant amount heat. Alkynes are thermodynamically less stable than the respective alkene due to the nature of their bonding and strongly adsorb on catalyst surfaces. Therefore, in catalytic hydrogenation there are significant numbers of hydrogenation catalysts effective in promoting the addition of hydrogen however

few are selective in producing the desired alkene rather than the alkane. Palladium is the metal of choice for selective hydrogenation of alkynes but even then palladium catalysts may be partially deactivated, as in Lindlar's catalyst, or poisoned, as in the addition of carbon monoxide in ethyne hydrogenation, to limit the production of the alkane. Although alkene hydrogenation is inhibited by the presence of alkynes, in the absence of the alkyne research indicates that the alkene will react more rapidly [36]. Research has also shown that in a competitive environment the alkyne can influence the reactivity of other alkynes and alkenes [37, 38]. However, all of these studies have been performed at low temperatures (typically < 373 K), whereas in trans-hydrogenation the reaction will take place at moderate to high temperatures (> 673 K). Although this has little effect on the thermodynamics of hydrogenation, it does have a significant effect on the potential for side reactions due to the high reactivity of alkynes or alkadienes.

Although, alkyne and alkene show different behaviours toward catalytic hydrogenation research indicates that alkenes react more rapidly[36]. Therefore, hydrogenation is done carefully because at a given point the produced alkene will rapidly hydrogenate to alkane. This can be explained by stages involved in hydrogenation reaction of alkynes as outlined below:

$C_nH_{2n-2}(ads) + 2H\ (ads) \rightarrow C_nH_{2n}\ (ads)$

$C_nH_{2n}\ (ads) \rightarrow C_nH_{2n}\ (g)$

This can further be hydrogenated to corresponding alkane

$C_nH_{2n}\ (ads) + 2H\ (ads) \rightarrow C_nH_{2n+2}(ads)$

$C_nH_{2n+2}(ads) \rightarrow C_nH_{2n+2}(g)$

The alkyne is first adsorbed on the catalyst surface before hydrogen can be added to the multiple bonds. A formation of the stable complex with the catalyst metal is normally achieved.

The reaction may encounter some problems as reported by [39, 40] in the hydrogenation of acetylenic bonds using platinum group metal catalyst. The summarized problems are outlined below:

1. Selective production of desire intermediates could be uncontrollable

2. Hydrogenation may be accompanied by hydropolymerization leading to higher hydrocarbons

1.1.3 Trans-hydrogenation processes

Trans-hydrogenation involves the dehydrogenation of an alkane to produce an alkene (olefin) and hydrogen and hydrogenation of an alkyne or alkadiene with the hydrogen generated from the dehydrogenation step to produce another alkene (Figure 6).

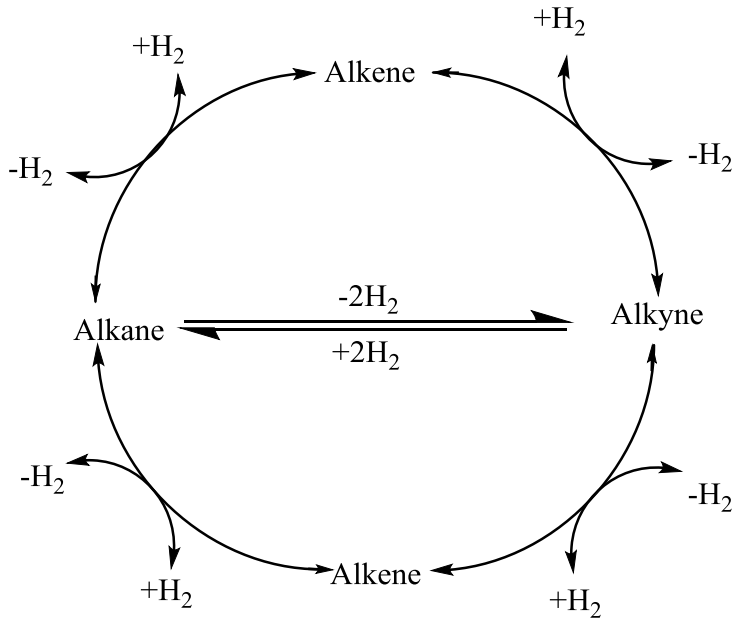

Figure 6: General concept of a trans-hydrogenation process

The dehydrogenation and hydrogenation processes should ideally occur simultaneously during the trans-hydrogenation reaction with the aim of obtaining two olefinic molecules. Dehydrogenation proceeds by the removal of hydrogen from the alkane in the feed using an appropriate catalyst to form the olefin and hydrogen. The hydrogenation reaction involves the addition of

absorbed hydrogen on the catalyst surface to the alkyne or alkadiene hydrocarbon in the feed and producing the corresponding olefin. A generic simplified mechanism is outlined below

$C_nH_{2n+2}(g) \rightarrow C_nH_{2n+1}(ads) + H(ads)$

$C_nH_{2n+1}(ads) \rightarrow C_nH_{2n}(g) + H(ads)$

$C_nH_{2n-2}(g) + H(ads) \rightarrow C_nH_{2n-1}(ads)$

$C_nH_{2n-1}(ads) + H(ads) \rightarrow C_nH_{2n}(g)$

Overall: $C_nH_{2n-2} + C_nH_{2n+2} \rightarrow 2C_nH_{2n}$

By coupling the endothermic dehydrogenation process with the exothermic hydrogenation process it is possible to generate a process where the reaction conditions may be adjusted in order to produce a reaction that is net endothermic, net exothermic, or thermally stable, which can simplify and reduce the cost involved in the process [25]. For example with propane and propyne, the dehydrogenation reaction is significantly endothermic:

$C_3H_8 \rightarrow C_3H_6 + H_2 \quad (\Delta H = +124 \text{ kJ/mol})$

However the hydrogenation reaction is even more significantly exothermic:

$C_3H_4 + H_2 \rightarrow C_3H_6 \quad (\Delta H = -157 \text{ kJ/mol})$

Taken together results in an overall exothermic process

$C_3H_8 + C_3H_4 \rightarrow 2C_3H_6 \ (\Delta H = -33 \text{ kJ/mol})$

However in many instances the ratio of alkane to alkyne will not be 1:1 but an overall heat balance can be deduced from the enthalpy of reactions and the number of moles of the converted reactant. This can be represented by:

$$\frac{n_{hydrog}\, x\, \Delta H_{hydrog}}{n_{dehydrog}\, x\, \Delta H_{dehydrog}}\, x\, 100$$

So for example, if 30 moles and 15 moles of propane and propyne respectively are converted in a trans-hydrogenation reaction, the hydrogenation reaction step would provide about 63 % of the heat required for the dehydrogenation reaction step.

1.2 Catalytic processes for trans-hydrogenation

Trans-hydrogenation is carried out using any catalyst system that will enable the dehydrogenation of the H-donor for the reaction conditions used during the process. This also depends on the nature of both the H-donor/acceptor reactants used in the process.

1.2.1 Trans-hydrogenation catalysts

As outlined above catalysts used in trans-hydrogenation reactions are typically based on dehydrogenation catalysts [21]. The logic that underlies this is the evidence that dehydrogenation is the more difficult reaction. Although alkanes can exchange hydrogen at low temperatures on a catalyst surface [31, 32, 41] indicating that breaking the first C-H bond in an alkane is not necessarily difficult, removal of the second hydrogen is rate determining and thermodynamic limits ensure that high temperatures are needed [42, 43]. In contrast the addition of hydrogen to an alkyne or alkadiene is thermodynamically favoured at most temperatures.

Although many metals and oxides are claimed in the patent examples cited above only two catalytically active materials are used with any regularity, these are Pt and chromia. However it is interesting to note that the catalyst rarely is mentioned in the claims of the patents as usually they are standard commercial catalysts used in dehydrogenation processes. Hence the platinum catalyst is typically modified with tin, while the chromia is modified with potassium. The role of both these modifiers is to reduce carbon deposition and more general by-product formation from the dehydrogenation process. Vanadia has also been used in the academic literature [28].

1.2.1.1 Catalyst systems based on chromia catalysts

Chromia catalysts have been subject to extensive characterisation using a variety of techniques such as electron spin resonance (ESR) [44, 45], infrared spectroscopy (IR) [46, 47], diffuse reflectance spectroscopy (DRS) [48, 49], photon electron spectroscopy (XPS) [50, 51], X-ray diffraction(XRD) [52-54], thermo-gravimetric analysis (TGA) [53, 54] and Raman spectroscopy [55, 56]. Although in the as-prepared catalyst chromia is often in a 6+ oxidation state, the active phase for dehydrogenation and hydrogenation is thought to be Cr^{3+} in the form of a polychromate following reduction either by hydrogen or the reactants.

Table 2: Surface characterization of Cr/Al2O3 catalyst as determine by several characterization techniques

Cr oxide Loading (wt% Cr)	XPS	DRS	RS	ESR	XRD
0 - 1	Cr^{6+}	Chromate	Chromate; Polychromate	Traces of Cr^{5+}	No Cr oxide phase
1-7	Cr^{6+} ; Cr^{3+}	Chromate; Polychromate; Traces of Cr^{3+}	Chromate; polychromate	Traces of Cr^{5+} ; Cr^{6+}	No Cr oxide phase
>7	Cr^{6+} ; Cr^{3+}	Chromate Polychromate Traces of Cr^{3+}	Chromate; Polychromate; Cr_2O_3	Traces of Cr^{5+}	α-Cr_2O_3

XPS= X-ray proton spectroscopy, DRS= Diffuse reflectance spectroscopy, RS= Raman spectroscopy, ESR= Electron spin resonance, XRD= X-ray diffraction

Wang and Hall, 1983 [57] first performed an *in situ* Raman study on supported rhenium oxide and subsequently several other Raman studies have been reported[58]. Ideally, *in situ* Raman Spectroscopy is suitable and presents no inherent limitation on temperature, pressure and reaction gases. However, sources of confusion as a result of hydration/dehydration have hampered progress in the understanding of the supported metal oxide catalyst. Many studies on the supported metal oxide [58-60], show drastic changes in the spectra upon dehydration. For example it is observed that a symmetric

stretching frequency of the metal oxygen bonds shifts upward except for vanadium oxide system which has been observed recently [55, 61]. Thus, same surface metal oxide species can be observed under hydration and dehydration conditions.

One of the earliest patents relating to trans-hydrogenation was reported in 1985 by Parris et *al.,* [24]. In this patent the reaction between ethylene and isobutane was exemplified as a way of increasing isobutene yield at lower temperatures as part of an MTBE process. Typical dehydrogenation catalysts such as chromia/alumina were used. Here the transhydrogenation reaction was used to produce a more valuable olefin at the expense of a cheaper one. Reaction conditions were typically ~773 K and atmospheric pressure although temperatures between 673 and 773 K and pressures between 1 and 10 bar were claimed. In one example with an inlet ratio of 1:2 ethylene:isobutene at 773 K and 1 bar, an outlet of 25 % ethane and 21 % isobutene was obtained.

In another patent relating to trans-hydrogenation, granted in 1994 [62], the reaction of propane 80% v/v and 1,3-butadiene 20% v/v was exemplified to demonstrate the effectiveness of trans-hydrogenation for promoting the production of propene. A typical dehydrogenation catalyst CrOx/alumina was used in the process. The reaction conditions were typically 823 K temperature at 1 atm pressure and a WHSV of 5.4 hr^{-1}. About 15 % by volume of propene was produced after ~2 h into the reaction together with other valuable hydrocarbons. The amount of carbon deposit formed during the reaction, which resulted in catalyst deactivation, was also determined. Therefore, catalyst regeneration was performed online using an air stream to remove the deposited carbon. The catalyst was then reduced in flow of hydrogen at same reaction temperature (823 K) and the reaction repeated again.

There is only a very limited academic literature on trans-hydrogenation reactions. However in a series of papers Jackson *et al.,* studied the trans-hydrogenation of propane and propyne over a chromia/alumina catalyst in a 1:1 ratio to generate two alkenes [27]. The catalyst was activated by reducing in hydrogen before use and the reaction temperature varied between 773 and 873 K. The reactants were first passed over the catalyst individually to determine their reactivity in the absence of the other reactant. When propyne was passed

over the catalyst all the propyne reacted and further reduced the catalyst. There was also a decrease in carbon deposition with increasing reaction temperature. This was a surprising result, which was due to the way that propyne fragmented at high temperature forming a methyl fragment which was hydrogenated to methane faster as the temperature increased leaving less carbon deposit on the catalyst surface [27]. When propane was passed over the catalyst, almost no dehydrogenation took place at the lowest temperature (773 K) in keeping with the thermodynamic limitations. The dehydrogenation of propane increased with increasing temperature but so did by-product reactions. Isotopic studies revealed that each propane fragmented to produce a species (CH or CH_2) that had an equal chance of hydrogenation to methane. However in contrast, with propyne the extent of carbon deposition on the catalyst surface increased with increasing temperature [26].

Almost no trans-hydrogenation occurred when both the reactants were passed over the catalyst at lowest temperature of 773 K, however by 823 K trans-hydrogenation was clearly observed. Using isotopic labels to elucidate the mechanism, the trans-hydrogenation reaction was shown to produce propene above the equilibrium value expected from propane dehydrogenation at 823 K. By 873 K the conversion of propane was about 80 % however the yield of propene was low, which was suggested to be due to secondary reaction of the propene forming methane and carbon deposits. These results suggested that at high temperatures a short residence time was required.

1.2.1.2 Catalyst systems based on platinum catalysts

In a patent by Gough *et al*. [22], trans-hydrogenation was disclosed for the processing of hydrocarbons from naphtha cracking feedstock. Processed cracked products from the cracking unit were subjected to a trans-hydrogenation process using streams of poly-unsaturated hydrocarbons as the hydrogen acceptor and that of paraffins as the hydrogen donors. Reaction between a stream containing butadiene and propane was exemplified in the patent. A Pt-Sn/Alumina catalyst was used for the process and the reaction conditions were typically in the 773-873 K temperature range and 1 atm pressure. There was no clear information to the amount of the reactant fed during the process but a ratio around 10:1

paraffin to poly-unsaturated hydrocarbon was emphasised with the paraffin concentration always higher than the concentration of the hydrogen acceptor.

In another patent showing trans-hydrogenation [20], a non-acidic intermediate pore size zeolite (ZSM-5) with a Pt active phase and a Sn modifier was used. In one example from the patent, a Sn free Pt-high silica ZSM-5 catalyst was used to dehydrogenate isobutane at 550 ^{o}C. The reaction was initially conducted with equimolar volume of helium which was subsequently replaced with ethene. When the ethene was added the isobutene yield fell as the ethene inhibited the alkane adsorption. To mitigate against this inhibition tin was added to the catalyst and a subsequent example reports trans-hydrogenation of propene with isobutene. The patent also reports a split bed system where the top bed has a single feed of alkane and is used for dehydrogenation, while just above the bottom bed the alkene is introduced so that the bottom bed has a feed of alkenes and hydrogen.

In another patent by Turner [25], trans-hydrogenation was disclosed for the production of isobutene to be subsequently used in the in the production of methyl tertiary butyl ether (MTBE). The catalyst employed was 1 % Pt-Sn/alumina with a weight ratio of 1:1 Pt:Sn. The trans-hydrogenation conditions employed were typically 773 K, 1 atm pressure and a WHSV of 5.5 hr^{-1}. The catalyst was first pre-treated in a flow of hydrogen to be fully reduced before commencement of the reaction. An increase yield in the olefinic C4 stream was achieved with about 2.7 % and 98.8 % conversion of propane and butadiene respectively.

In trans-hydrogenation, because hydrogen is not co-fed in the process, there is a high tendency for the formation of bulk coke deposit. This happens especially with amorphous catalyst supports such as alumina, which have acid sites that promote cracking and alkylation. The use of metal doping and non-acidic catalyst supports are reportedly used to suppressed the effects. A diluent such as steam may also be added, which leads to coke suppression and can serve to activate the catalyst. Methane can also be used as a diluent [26]. Coke deposition is detrimental to the catalyst and leads to catalyst deactivation, however regeneration processes are often used to remove the deposit and regenerate the catalyst. In patent number WO 1994010264 [22] the

regeneration of a Pt/Sn-ZSM-5 catalyst used for trans-hydrogenation was performed in a flow of hydrogen at 60 psi pressure and 823 K temperature for 4-24 hr. In another patent [25] regeneration of the catalyst was reported to be have been conducted in a stream of pre-heated oxygen-containing gas like air. Regeneration of the catalyst burned off the deposited carbon on the catalyst surface reactivating the catalysts and generating heat.

The reaction stream may comprise of a mixture of reactants instead of same carbon number reactant. For instance, the hydrogen acceptor could be admixture of alkadienes and alkynes of different carbon number, equally the hydrogen donor stream could also be admixture of different carbon number atom alkanes.

1.2.1.3 Catalyst systems based on vanadia catalyst

In a recent study by Wigzell et al. [28] a trans-hydrogenation reaction was performed between propyne and butane over a 1 % vanadia/θ-alumina catalyst at 873 K. Propyne and butane were co-fed, which resulted in an increase conversion of propyne to propene compared to when it was fed singly over the catalyst. The trans-hydrogenation reaction was observed to deliver a 72 % increase in propene yield, while all the butane reacted was converted to butene isomers.

1.2.2 Role of dopants

Trans-hydrogenation reactions over potassium doped chromia catalyst [27] have been reported. However, the dopant has little direct effect on the trans-hydrogenation process rather it is used to remove and/or neutralize acid sites on a support such as alumina reducing catalyst deactivation [63]. It does not generally change the reaction mechanism [63, 64]. Use of dopants to enhance trans-hydrogenation reactions has also been disclosed in patents. Gough *et al*. [62] reported that a chromia admixture with a platinum group metal and doped with alkali on alumina effected good trans-hydrogenation activity. The doped alkali metal was either potassium or caesium ($Cr/Pt\text{-}K\text{-}Al_2O_3$ or $Cr/Pt\text{-}Cs\text{-}Al_2O_3$). Catalyst modification using dopants has also been disclosed in other patents.[20, 25, 64]

The effect of tin on a platinum dehydrogenation catalyst is much more significant as it forms an alloy changing the electronic properties of the platinum in such a way as to enhance dehydrogenation activity [65]. The Sn not only modifies the electronic properties of Pt but also reduces the carbon deposition on the platinum. However the alloy is not stable during regeneration with the Sn segregating from the Pt/Sn alloy during coke burning. The alloy reforms during hydrogen reduction but with multiple reaction/regeneration/reduction cycles there is a slow Sn enrichment of the alloy, resulting in a permanent decrease in the activity

1.2.3 Catalyst deactivation/regeneration and stability

Catalyst deactivation is responsible for loss of activity and/or selectivity; as a result, the catalyst will have a limited life time. However, the life of a catalyst depends on the reaction parameters upon which the catalyst is used and therefore, some catalyst lose their activity quickly within short period of time while others retained their activity for years. A long life time activity catalyst is always a desired due to economic viability and catalyst deactivation prevention cannot be over emphasised whilst numerous effort are made to avoid it. However, catalyst deactivation cannot be completely stopped but slow deactivation of catalyst has always been a priority to increase long term activity. The desire activity of a catalyst has be described by Hagen, 2015 [66] as presented in Figure 7

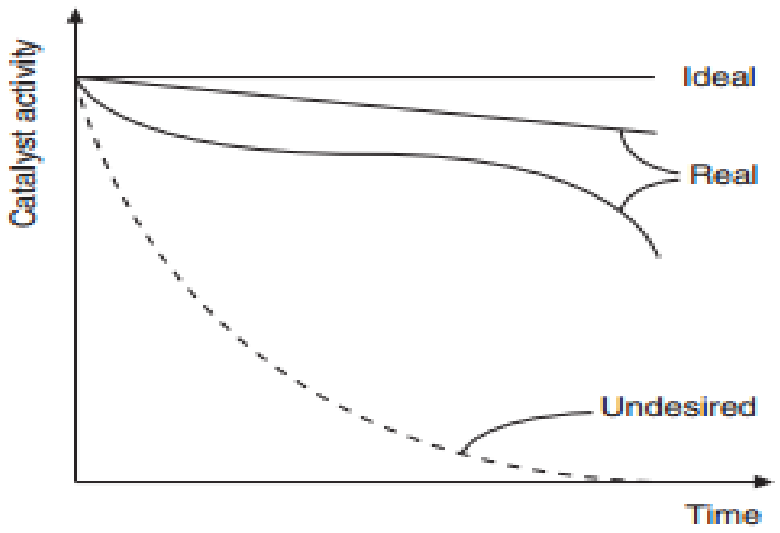

Figure 7: Deactivation behaviour of catalyst

There are four main and common causes of catalyst deactivation as reported by Hagen, 2015 as listed below:

i. Poisoning of catalyst (H_2S, Pb, Hg, S, & P)

ii. Deposition on catalyst (coke formation)

iii. Thermal process and sintering (loss of active surface area)

iv. Loss of activity by evaporation active component

These processes are explained further by the used of schematic diagram presented in Figure 8

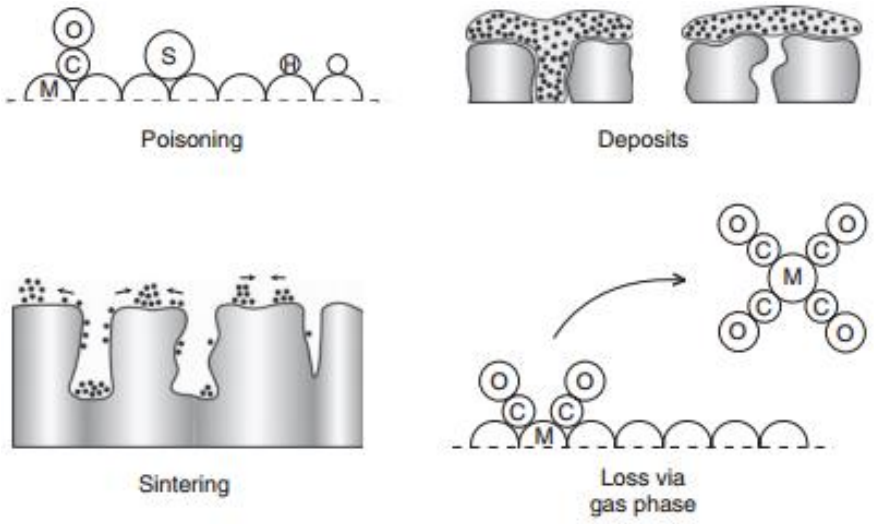

Figure 8: Mechanism of catalyst deactivation (M= metal)

In a trans-hydrogenation process, catalyst coking is one of the major forms of catalyst deactivation. Both the dehydrogenation and hydrogenation reaction contribute to the coke formation. The dehydrogenation of lighter alkanes is performed at higher temperature of above 873 K while that of higher alkanes require temperature of about 673-773 K which give the catalyst long life even and high catalyst productivity. The temperature difference is due to equilibrium limitations, which reveal that lighter alkanes require higher temperatures. However the higher temperature conditions make the catalyst more likely to deactivate due to coke formation and make frequent regenerations of catalyst

necessary. Carbon formations are also formed due to the alkane hydrogenation and reactivity of the alkyne/alkadiene which are very prone to cracking activity.

For optimizing the CrO_x/Al_2O_3 system and every other related catalyst, a periodic regeneration with air is needed to burn off the coke; in this case the catalyst undergoes a cycle between exposure to hydrocarbon where the coke is formed and then exposure to oxygen and/or steam to remove the coke periodically. The regeneration cycles are usually performed at a temperature of ~873 K or less. Hence, this enables the catalyst to retain its morphological structure, chemical stability in a range of high temperature conditions.

1.3 Mechanistic understanding of trans-hydrogenation

One of the early investigations of trans-hydrogenation process was carried-out in department of Chemistry, University of Glasgow by Isobel [67]. The investigation was conducted using pulses of unlabelled & perdeutero propane, and propyne over Pt/alumina and CrO_x/alumina at 673, 723, 773 and 823 K. She investigated the dehydrogenation of the of the unlabelled & perdeutero propane over the listed range of temperatures using both Pt/alumina and CrO_x/alumina. She then investigated the hydrogenation of propyne over chromia/alumina catalyst at 673 K for analogical description.

Dissociation of the propane was reported when alternate pulses of the perdeutero and unlabelled propane were passed over the Pt/alumina catalyst at the reaction temperature. However, reaction at 673 K presented some remained of the unreacted propane. The mass spectral data shows that CH_4 was the most abundant products regardless of whether perdeutero or unlabelled propane was used. However, small amount of CH_3D, CH_2D_2, CHD_3 and CD_4 were also observed. Analysis of the spent catalyst showed that both carbon and hydrogen were lost from the catalyst during these experiments. Treatment of the spent catalyst with dioxygen at 673 K produced CO_2.

When the chromia/alumina catalyst was used, dehydrogenation and some dissociation of the propane were both observed and propene was detected. The propene was detected using GC-MS when the unlabelled propane was used. Whilst scanning mass spectrometry technique was conducted to be able to

observe the alkenes produced with the perdeutero propane. The highest obtained presented 51% propene yield during the 2nd pulse, and increased to only 51.2 % by the 6th pulse. This trend was observed with all the other temperatures except for 673 K. However, higher percentage yield of propene was obtained with reaction at 823 K and a good increase was observed with increase temperature, 19.2%, 34.7% and 51.2% obtained at 723, 773 and 823 K respectively.

When using perdeutero propane as the adsorbate during alternate pulses, the resulting products were isotopic methanes, CH_4, C_3D_7H and C_3D_8. On the other hand, when unlabelled propane was used as the adsorbate, isotopic methanes, $C_3H_4D_2$, C_3H_5D, C_3H_6, $C_3H_6D_2$, C_3H_7D, and C_3H_8 were the resulting products. Isobel deduced that either single or double deuterium/hydrogen exchange had contributed towards both propene and propane desorption from chromia/alumina catalyst. When comparing both adsorbates used, this reaction mainly took place using unlabelled propane at the elevated temperatures of 773 K and 823 K. Carbon and hydrogen were lost to catalyst surface during the experiment and CO_2 was produced when the spent catalyst was treated with O_2 at 673 K.

When propyne was passed over the chromia/alumina catalyst, the products observed were, methane, carbon monoxide and small amount of propene. There is also significant amount of carbon and small amount of hydrogen lost to the catalyst on each reaction pulse. These investigations were performed with the view to establish conditions under which trans-hydrogenation could be affected.

1.4 Research objectives

The research is aimed at preparation, characterization and investigation of the activity of CrO_x/alumina, K-CrO_x/Al_2O_3, Pt/Al_2O_3 and K-Pt/Al_2O_3 catalysts for the trans-hydrogenation process of non-valuable refinery cracked products, for the production of alkenes. This was performed using alkane, alkyne and alkadienes models reactants with a view of establishing conditions under which trans-hydrogenation could be effected. The research objectives include:

1. Preparation and characterisation of CrO_x/alumina, K-CrO_x/Al_2O_3, Pt/Al_2O_3 and K-Pt/Al_2O_3 catalysts.

2. Investigating the alkane dehydrogenation reactions to establish detailed information appropriate trans-hydrogenation conditions for these catalysts and compare their conversions with during the trans-hydrogenation

3. To verify the hydrogenation and dehydrogenation processes individually and as trans-hydrogenation using thermodynamic data, this includes the calculations of parameters such as $\Delta G°$, $\Delta S°$ and $\Delta H°$.

4. Investigating the activity of each catalyst on the model reactants run individually and compared to the trans-hydrogenation process

5. Characterization and analysis of the carbonaceous species formed on the spent catalyst during the individual run and as trans-hydrogenation process.

6. Investigating catalyst deactivation and regeneration over series of trans-hydrogenation processes

2.0 Experimental

2.1 Introduction

Four catalyst, chromia/alumina, platinum/alumina, chromia/alumina promoted with potassium (chromia/K/alumina) and platinum/alumina promoted with potassium (platinum/K/alumina) were prepared by incipient wet impregnations. The catalysts were tested for dehydrogenation, hydrogenation individually alone and a mixture trans-hydrogenation activity using a specially designed rig. Products of the reactions were analysed by GS-MS and an online ESS mass spectrometer.

Characterization of the pre and post catalyst were carried using micrometrics (BET), X-ray diffraction (X.R.D.) thermal gravimetric analysis (T.G.A), Temperature program oxidation (TPO) temperature program reduction (TPR), temperature program desorption (TPD) and Raman.

2.2 Materials

The alumina support used was a gamma-alumina extrudate supplied by Johnson Matthey, with a surface area 208 $m^2 g^{-1}$ and a pore volume 0.52 $cm^3 g^{-1}$. This was pre-dried in an oven overnight at 253 K prior to catalyst preparation.

2.2.1 Catalyst preparation

2.2.1.1 Chromia/alumina catalyst

A 4 wt. % CrOx/alumina catalyst was prepared by incipient wetness impregnation of the γ-alumina support. An aqueous $(NH_4)_2Cr_2O_7$ (99+ % Aldrich) solution was used to prepare the catalyst with a 4% w/w loading. The amount of the liquid solution of the precursor require to fill the pore volume of the support was ~0.52 cm^3g^{-1}. After the impregnation, the samples were mixed thoroughly using a rota vap. for 2hr at 253K and dried at ~393 K overnight. 50g of the 4 wt. % loading catalyst was prepared. Finally, the samples were calcined at 873 K for 6hr. after the calcination the sample was ground using a mortar and pestle and sieved to a uniform particle size of 250-425 μm.

2.2.1.2 Potassium doped chromia/alumina catalyst

50g of the potassium-doped catalyst was prepared. The amount of potassium used was calculated relative to the hydroxyl population of the support. For the purpose of these calculations a hydroxyl density of 8 OH groups per nm^2 was used [68-71]. Given the surface area of the catalyst it was determined that 268 mmoles potassium should be added per g of (S_{BET}= 203 $m^2 g^{-1}$). This was them used to calculate the appropriate amount of KOH to be used (15.008 g). This was prepared by incipient wetness impregnation using the above catalyst (section 2.2.1.2). The catalyst was treated with a solution of KOH sufficient to generate a ~10 % loading of potassium. This was then dried at 353 K for 2 h and then at 393 K overnight. Finally, the samples were calcined at 873 K for 6 h.

3.2.1.3 Platinum/alumina catalyst

The catalyst was a commercial catalyst supplied by Johnson Matthey (ref no: 1074). The catalyst has a BET surface area (S_{BET}) 119 $m^2 g^{-1}$ and pore volume 0.49 $cm^3 g^{-1}$. The samples were calcined at 873 K for 4hr. after the calcination the sample catalyst were grounded using mortar and pestle and sieved to a uniform particle size of 250-425 μm.

3.2.1.4 Potassium doped platinum/alumina catalyst

50g of the potassium doped catalyst prepared. The amount of potassium used was calculated relative to the hydroxyl population of the support. For the purpose of these calculations a hydroxyl density of 8 OH groups per nm^2 was used [68-71]. Given the surface area of the catalyst it was determined that 158 mmoles potassium should be added per g of catalyst (S_{BET} = 119 $m^2 g^{-1}$). This was them used to calculate the appropriate amount of KOH to be used (8.90 g). This was prepared by incipient wetness impregnation using the above catalyst (Section 3.2.1.3). The catalyst was treated with a solution of KOH sufficient to generate ~6 % loading of potassium. This was then dried at 353 K for 2 h and then at 393 K overnight. Finally, the samples were calcined at 873 K for 6 h.

2.3 Reaction studies

2.3.1 Reactor set-up and sampling method

The reactions were carried out in an atmospheric, flow micro-reactor shown as a block schematic in Figure 9. the reactants were vaporized individually using a bubbler with argon as the carrier gas using 30 ml min^{-1} flowrate and mixed in mixer chamber before passing through the reactor. The vapour pressure of each reactant was taken into consideration using the Clapeyron equation (eqn. 1) for feeding the reactor. An appropriate reactants ratio was therefore achievable. Temperatures of the reactants were varied using ice bath for the calculation. The mixed reactant was then passed over the catalyst bed for the reaction and the products collected over a solvent while the light gases were analysed by online mass spectrometry (MS). The thermocouples (TC) were fixed at each section to monitor the temperatures. The temperature can be controlled to ±1 K

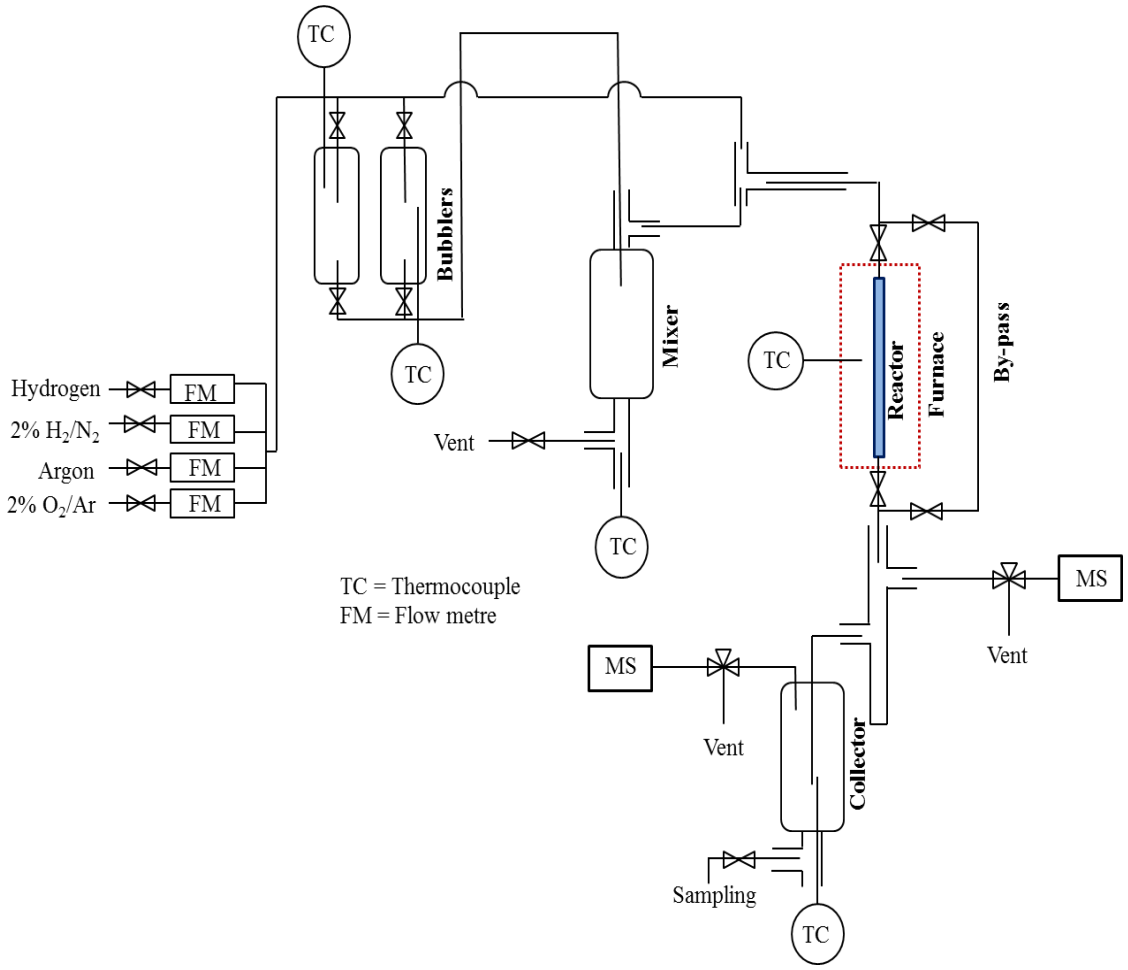

Figure 9: Schematic diagram of the reaction rig: (continuous flow micro reactor type)

2.3.2 Evaluation of rig accuracy

All flow meters were tested and calibrated to ensure an accurate flow of reactants was achieved. All joints and taps were properly and repeatedly checked for leaks, all reactants were individually introduced into the reaction rig through the bypass and collected over the heptane solvent for the accuracy of my reactant feed calculations. This was subsequently used to calculate the WHSV and GHSV of the process. The differential error obtained for my first and second collector is less than 1%. A ratio of 5:1 of alkane and alkyne/alkadiene was targeted and therefore the rig setup was tested for the reliability of the anticipated reaction mixture to tally with calculated figures. All other components of the rig were also similarly tested.

2.3.3 Setting the feed ratio

The equation was used to determine the reactant temperature required to achieve a given feed ratio. For example, for the ratio of 5:1 pentane to hexyne, 1,5-hexadiene and or 2,4-hexadiene respectively, a temperature of 273 K was maintained for pentane while the temperature was changed for the C_6H_{10} reactants to obtain the desired ratios. Therefore, the temperatures were changed according to the C_6H_{10} molecule in used and a right vapour pressure is obtained for the calculation. The ΔH_{vap} of each reactant could be obtained and then used in subsequent calculations of the vapour pressure as shown in eqn 1 below

$$\ln\left(P_2/p_1\right) = -\frac{\Delta H_{vap}}{R}\left(\frac{1}{T_2} - \frac{1}{T_1}\right) \ldots\ldots Eqn\ 1$$

Table 3: Reactant Clausiu clyperon parameters

Reactant	ΔH_{vap} (J mol^{-1})	Temperature (K)	Vapour pressure (atm)	Target ratio
Pentane	28180	273	0.242	5
1-Hexyne	37285	273	0.046	1
1,5-Hexadiene	30142	258	0.045	1
2,4-Hexadiene	30750	273	0.043	1

2.3.4 Trans-hydrogenation procedure and activity evaluation

The trans-hydrogenation of pentane (P) and 1-hexyne (1-HY)/1,5-hexadiene (1,5-HD)/2,4-hexadiene (2,4-HD), was investigated using a glass-line u-tube continuous flow micro reactor. The catalyst (0.5 g) was reduced *in-situ* with hydrogen (40 ml min^{-1}) for 2 h at 873 K. The flow was switched to Argon (40 cm^3 min^{-1}) and the system purged for 30 min while the reactor temperature was reduced to the required reaction temperature (523-773 K) thereafter. After the reduction was completed, the reactant pentane (99+ % Aldrich), hexyne (97+ % Aldrich), 1,5-hexadiene (97+ % Aldrich), 2,4-hexadiene (97+ % Aldrich) was introduced to the reaction chamber at 30 ml min^{-1} flowrate using argon as carrier gas. This is on by-pass for 15 min to allow good saturation of reactant before its switched to the reactor tube. A ratio 5:1 C_5H_{12}/C_6H_{10} was used. The reactions were performed using each component individually as well as the 5:1 mixture over a temperature range of 523-773 K. The reaction products were collected over a solvent (25 ml heptane) for the reaction period time of 2 hr. From the collected reaction products 1 ml was then mixed with 10 µl toluene internal standard and analysed by gas chromatography (ThermoQuest CE Trace GC 2000 Series, FID detector) fitted with a 150 m Petrocol column. The gaseous

products were followed continuously over the time-period of the reaction using an ESS mass spectrometer.

2.4.7 Gas Chromatography

The samples were analysed using ThermoQuest CE Trace GC 2000 Series gas chromatograph fitted with a flame ionization detector (FID). The column used was a Petrocol column 150 m, 0.25 mm, 1 μm film thickness with helium as the carrier gas. Samples were pre-prepared in vials and the GC automatically injected the sample using auto-sampler.

2.4.7.1 GC Conditions

Oven: 333 K held for 70 min; ramped to 453 K at 10 K min^{-1}

Inlet: 513 K; split flow 75 ml min^{-1}; split ratio 50

Detector: 523 K; H_2 35 ml min^{-1}; Air 350 ml min^{-1}; makeup 30 ml min^{-1}

2.4.7.2 GC calibrations

For the purpose of this study, calibrations were made based on the number of carbon atom. There is not much difference in response factor for types of hydrocarbons that have the same number of carbon atoms. Therefore, calibration factors for C5, C6, C7 and C8 hydrocarbons were obtained, which the major products are obtained.

The calibration was made by measuring out a known quantity of the compound into solution and passing different known concentrations through the GC. This was done for pentene, pentane, hexane, hexyne, toluene and iso-octane, for C5, C6, C7 and C8 respectively. Stock solutions were made for each compound and diluted with heptane to 50%, 25%, 10%, 5%, 1%, 0.5% and 0.1%. The number of moles in each component could be calculated taking into consideration of the following parameters.

- Density

- Molar mass
- Volume
- % purity
- Mass
- Moles
- Moles injected

Toluene was used as the internal standard as the retention time does not overlap with that of any other product. This was then used to calculate the response factor using internal standard (10 μl v/v). Equation (2) was used to calculate the response factor (α).

$$\alpha = \frac{Peak\ area\ of refrence}{Peak\ area\ of\ internal\ standard} \times \frac{Moles\ of\ internal\ standard}{Moles\ of\ refrence} \ldots\ldots Eqn\ 2$$

Using the equation above (Eqn 2), it was possible to obtain a straight line graph and a linear relationship of the peak intensity against moles for each of the reference compounds used. The resultant gradient obtained is equal to the response factor (α). The graphs figures of the various reference compounds used are presented in Figure 10-12.

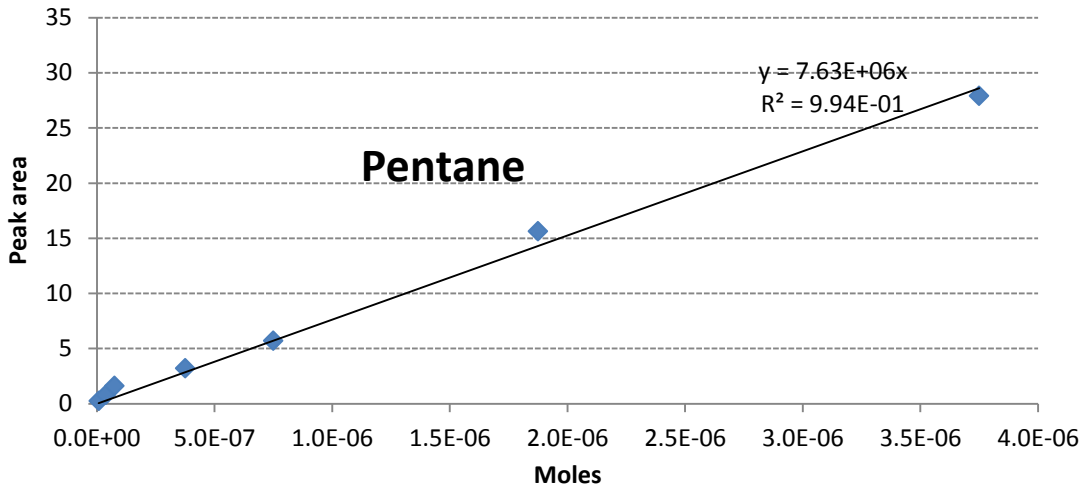

Figure 10: Pentane calibration curve

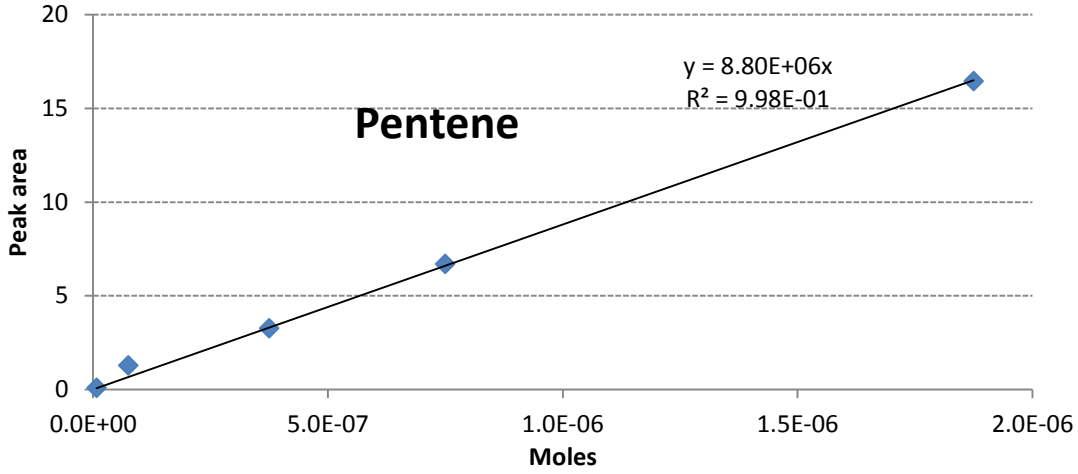

Figure 11: 1-Pentene calibration curve

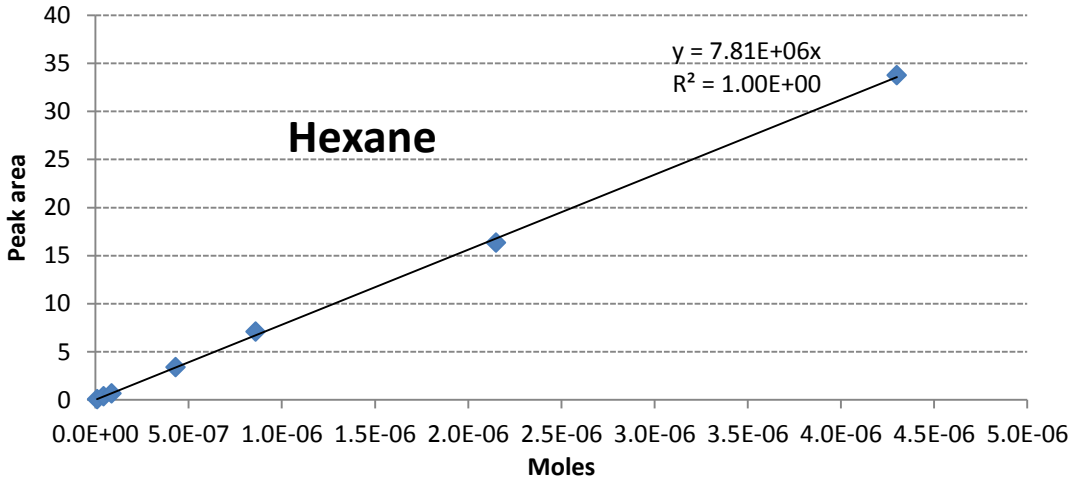

Figure 12: Hexane calibration curve

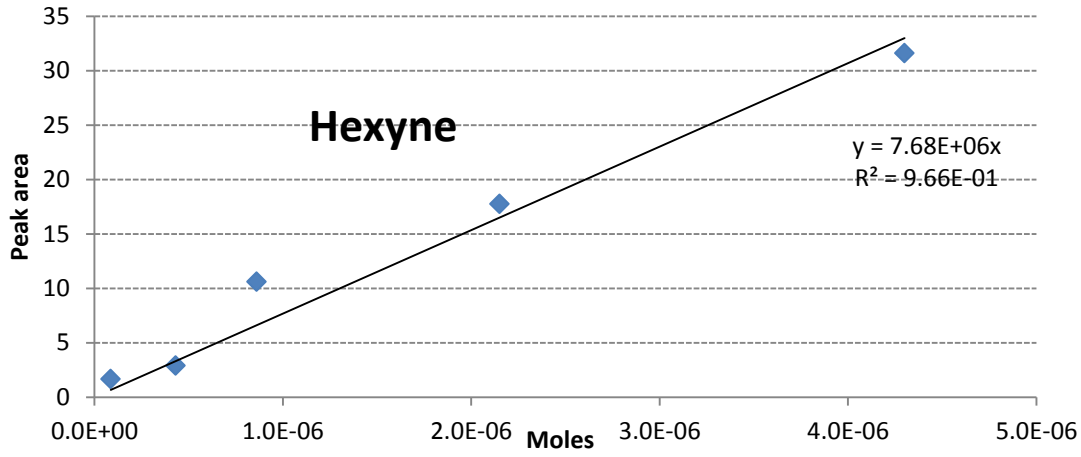

Figure 13: 1-Hexyne calibration curve

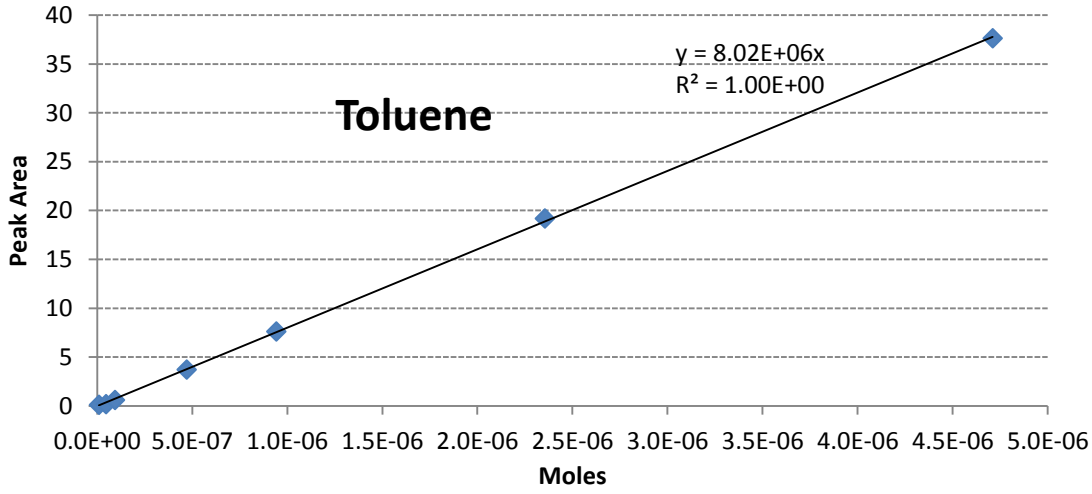

Figure 14: Toluene calibration curve

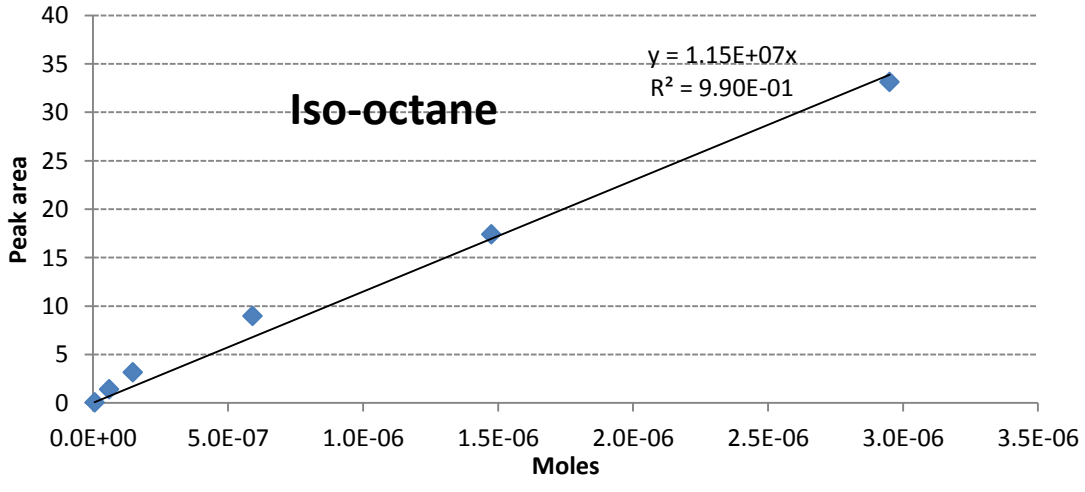

Figure 15: Iso-octane calibration curve

2.4.7.3 Response factor

Response factor is an important parameter for both reactant and products to determine quantitative data from the GC-FID. The response factors used for this piece of work are presented in Table 4.

Table 4: Reference factor for the various reference compounds used

Reference group	Unit type	Response factor (α)
Pentane	C5	7.63×10^{6}
Pentene	C5	7.50×10^{6}
Hexane	C6	7.81×10^{6}
Hexyne	C6	7.68×10^{6}
Toluene	C7	8.02×10^{6}
Iso-octane	C8	1.15×10^{7}

2.4.7.4 GC-MS and product identification

The reaction products were analysed using a Shimadzu GC-MS-QP2010S coupled to a Shimadzu GC-2010 equipped with a PetrocolTH DH columns (100 m × 0.25 mm × 0.5 µm) with Helium as a carrier to identify each product (GC peaks) for better precision. The GC-MS analysis of the products provided a means for identifying all the possible reaction products. Twenty one products of isomerization, alkylation, cyclization and further hydrogenation & dehydrogenation together with the trans-hydrogenation products were successfully identified through the mass fragment data analysis for each peak which was compared and identified by the software library. The mass data were later compared with reference standard for better precision and accuracy. For the purpose of the products analysis and easier graph plots, letter abbreviations were adopted for each identified products and this is presented in Table 5.

Table 5: Identified products and their unit type

S/N	Abbreviation	products	Unit type
1	IP	Iso-pentane	C5
2	T2P	Trans-2-pentene	C5
3	C2P	Cis-2-pentne	C5
4	MB	2-Methyl-2-butene	C5
5	4MP	4-Methylpentene	C5
6	P1	Pentene	C5
7	P2	2-Pentene	C5
8	H	Hexane	C6
9	H1	1-Hexene	C6
10	H2	2-Hexene	C6
11	H3	3-Hexene	C6
12	1,3HD	1,3-Hexadiene	C6
13	3MPY	3-Methylpentyne	C6
14	3MH1	3-Methylhexene	C6
15	2MH1	2-Methylhexene	C6
16	3MH	3-Methylhexane	C6
17	3MPD	3-Methyl-1,3-pentadiene	C6
18	B	Benzene	C6
19	1,4HD	1,4-Hexadiene	C6
20	MCH	Methylcyclohexane	C7
21	ECP	Ethylcyclopentane	C8

2.4.7.5 Product quantification

Using this methodology it was possible to approximately quantify each product, making use of equation 3.

$$moles = \frac{Peak\ area\ of product}{Peak\ area\ of\ internal\ standard} \times \frac{1}{\alpha} \ldots\ldots..Eqn\ 3$$

The conversion for each reactant feed was therefore calculated as:

$$\frac{\text{moles of reactant converted}}{\text{total moles fed}} \times 100 \ldots\ldots\ldots\ldots Eqn\ 4$$

The yield as:

$$P\ alone = \frac{\text{moles of C for each product formed}}{\text{Total moles of C for P fed}} \times 100 \ldots\ldots\ldots\ldots Eqn\ 5$$

$$H\ alone = \frac{\text{moles of C for each product formed}}{\text{Total moles of C for H fed}} \times 100 \ldots\ldots\ldots\ldots\ldots Eqn\ 6$$

$$P + H = \frac{\text{moles of C for each product formed}}{\text{Total moles of C for (P + H)fed}} \times 100 \ldots\ldots\ldots Eqn\ 7$$

Where H = 1HY, 1,5HD and 2,4HD

In order to determine the efficacy of the trans-hydrogenation process, the catalysts were subjected to reaction with P, 1HY, 1,5HD and 2,4HD individually and as a molar mixture of P:H in the ratio (5:1). The yield of each product formed was calculated from the individual run and summed as the yield P+H theory:

$$\mathrm{P_{alone}} + \mathrm{H_{alone}} = \mathrm{P + H\ Theory}$$

This is then compared to the mixed feed runs termed as trans-hydrogenation yield

2.4 Catalyst characterization

2.4.1 BET analysis

The surface area of the catalysts was determined using a Micrometrics Gemimi III 2375. Approximately ~ 0.03-0.05 g of catalyst was weight into a glass tube and purged in a flow of N2 gas overnight at 383 K before the measurement was carried out.

The BET equation 8 can be expresses as:

$$\frac{P}{V(Po-P)} = \frac{1}{V_m C} + \frac{(C-1)P}{V_m CPo} \ldots\ldots\ldots\ldots Eqn\ 8$$

Where: P = Pressure of adsorbate gas; Po = Saturated pressure of adsorbate

V = Volume of adsorbate gas; Vm = Volume of monolayer adsorbed gas

C = BET constant: $C = e^{\frac{q1-q2}{RT}}$; q1 = heat of adsorption on the first layer

q2 = heat of liquefaction on 2nd and higher layers; R = the gas constant.

The graph plot $\frac{P}{V(Po-P)}$ vs. $\frac{P}{Po}$ gives a straight line with a slope of $\frac{C-1}{V_m C}$ and an intercept of $\frac{1}{V_m C}$

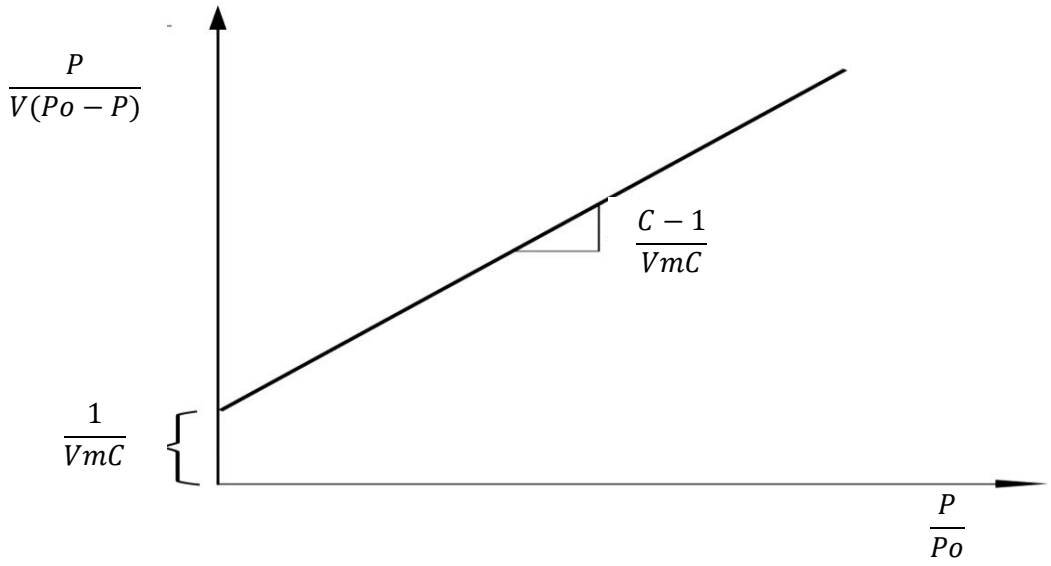

The Vm can be calculated by using the following equation

$Vm = \frac{1}{I+J}$ Where, I & J are intercept and slope respectively.

The surface area of the catalyst can be determined by using the following

$$S_{Total} = \frac{VmN\sigma}{Mv}$$

Where, N = Avogadro's number

Mv = Molar vol. of adsorbed gas

σ = adsorption cross section of the adsorbed gas molecule (N_2 gas)

The surface are per unit weight of the catalyst can be calculated from the equation $S = \frac{S_{Total}}{m}$ where m= mass of the catalyst.

2.4.2 XRD analysis

The XRD diffraction patterns of the catalysts were measured using a Siemens D500 X-ray diffractometer (40 Kv, 40mA, monochromatised) using a CuK α source (1.5418 Å). The scanning range was 5-85° 2θ with a scanning rate of 1 second step^{-1} and step size of 0.02°. Crushed catalyst was placed in the sample holder and the sample was levelled with the aid of a glass slide. The XRD spectral analysis was carried out using Bruker advanced X-ray solution Diffrac^{plus} release 2004 EVA version 10.0 rev.0 software.

The detector moves in a circle around the sample and records at the angle 2θ (Figure 16). The detector record the number of scattered x-rays observed at each angle 2θ and the x-ray intensity is usually recorded as counts or counts per second. However, to keep the x-ray beam properly focused, the sample will also rotate.

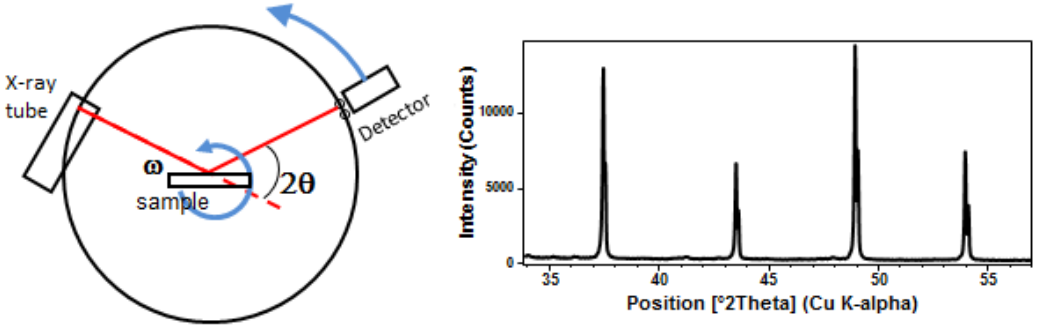

Figure 16: pattern operation of XRD

The Scherrer equation (Eqn 9) can be used to calculated crystal size from the XRD data

$$d = \frac{K\lambda}{\beta cos\theta} \ldots\ldots\ldots Eqn\ 9$$

Where: d = Average crystal size

K = Scherrer constant

λ = Wavelength of X-ray source (1.5418 Å)

β = Full width at half maximum (degree)

θ = Diffraction angle (degree)

X-ray diffraction is used to study the crystalline phase by powder pattern analysis. This provides information for identification and quantification of the phase composition in multi-component mixtures. The 2θ position of the peaks (CuK α) and intensities are therefore very important [72].

2.4.3 TGA-MS analysis

Thermo-gravimetric analysis was performed on the catalysts using a combined TGA/DSC SDT Q600 thermal analyser coupled to an ESS evolution mass spectrometer for evolved gas analysis. The samples (~10-30 mg) were heated from ambient temperature to 1273 K using a heating ramp of 15 K/min. The temperature profile was employed in 2% H_2/N_2 or O_2/Ar gas. Relevant mass fragments were followed by online mass spectrometry.

Thermo-gravimetric analysis is a technique in which the changes in mass of a particular substance are determined as a function of temperature. This can then be used to deduce the loss in the amount of the catalyst with temperatures and also the transformation that take place when the catalyst is heated at elevated temperatures [73, 74].

The use of combined TGA & DTA provides details on the transformation phenomenon of the catalyst material. Thus, this could be possibly deduced when the catalyst material undergoes heating. The TGA is the measure of amount of mass change as a function of temperature while DTA is the measure of the amount of heat that absorbed or evolved with temperature at the point that changes that takes place within the catalyst.

The couple TGA-MS helps in determining the volatiles evolved during the thermal degradation of the sample and has rapid scan capabilities for detection. In so doing, the sample weight variation could be monitored and the gaseous products could be monitored simultaneously during the temperature scan.

Reduction/oxidation cycles (Red-Ox cycles) were performed on the fresh CrO_x/Al_2O_3 and Pt/Al_2O_3 catalysts. Reduction of the catalyst was conducted by heating the sample in 2% H_2/N_2 from room temperature to 873 K using a heating ramp of 15 K/min and a hold for 15 min at 873 K. The sample was then cooled to room temperature and the gas switched to argon (100 ml min^{-1}) to purge. This was followed by oxidation in 2% O_2/Ar (100 ml min^{-1}) from room temperature to 873 K using a ramp of 15 K min^{-1} and hold for 15 min. The sample was then cooled to room temperature and gas switched to argon (100 ml min^{-1}) to purge. Lastly a reduction temperature profile was then employed in 2% H_2/N_2 from room temperature to 873 K using ramp of 15 K min^{-1} and hold for 15 min. Relevant masses were followed by online mass spectrometry for the processes.

2.4.3.1 Temperature program oxidation (TPO)

The TPO was performed on the post reaction catalyst using the TGA-DTA-MS facility. The samples were heated in a flow of 2% O2/Air (100 $mlmin^{-1}$) to 1273 K from ambient temperature, at a ramp of 10 Kmin-1. The following masses were monitored for desorbed species, m/z 2(H_2), 16(CH_4) 18(H_2O), 28 (C_2H_4), 44(CO_2) and 32 (O_2).

2.4.3.2 Temperature program reduction (TPR)

The TPR was performed on the Fresh catalyst using the TGA-DTA-MS facility. The samples were heated in a flow of 2% H_2/ N_2 (100 ml min^{-1}) to 1273 K from ambient temperature, at a ramp of 10 K min-1. The following masses were

monitored for desorbed species, m/z 2 (H_2), 16 (CH_4) 18 (H_2O), 28 (C_2H_4), 44 (CO_2) and 32 (O_2).

2.4.4 Electron paramagnetic resonance (EPR)

The EPR analysis were performed using A Bruker ELEXSYS E500 spectrometer to produce the X-band EPR spectra. The experimental conditions were frequency 9.4325 GHz; modulation 0.1 mT; power 6.3 μW, temperature 293 K. all the EPR analysis were carried out by Dr. Stephen Sproules at the university of Glasgow.

2.4.5 CHN Elemental analysis

The CHN analysis was performed by combustion using a CE-440 elemental analyser. All CHN analysis was carried out by Mr Gangi Reddy Ubbara at the University of Glasgow.

2.4.6 Raman spectroscopy

The Raman spectra were collected using Horiba Jobin Yvon LabRAM High Resolution spectrometer, with all the scattered photons collected by an ellipsoidal mirror focused into nitrogen cooled charge-coupled detector CCD. The signal from the detector was subsequently analysed by a computer using LabSpec5 software.

The UV Raman spectroscopy was obtained using a helium cadmium IK3201R-F 20 mW, 325 nm UV laser as the excitation source, focused for 10 s using a 15x UV objective lens and a grating of 1200 cm^{-1}. The visible Raman spectroscopy was obtained using a Ventus 532 laser system, 100mW, 562 nm green laser as the excitation source, focused for 10 s using a 50x objective lens and a grating of 600 cm^{-1}. Both UV and Visible Raman were collected under ambient conditions on slit glass disk.

2.4.7 UV-Vis analysis

The wax on the catalyst was extracted using Soxhlet extractor (~0.2 g of the spent catalyst with ~25 ml hexane solvent) was used. This was then manipulated to obtain various concentrations by diluting further with the hexane solvent, 100

%, 50% and 25 %. The absorbance measurements of each sample were monitored using a UV-160A Shimadzu UV-Visible spectrophotometer in the range of 900-200 nm. The spectra were collected in order to determine the presence or absence of the yellowish oil classified as wax observed during the course of the trans-hydrogenation process.

2.4.8 AAS analysis

The Elemental analysis was carried out using Perkin Elmer analyst 400, atomic absorption spectrometer, with winlab 32. Typically 0.1g of catalyst was accurately measured to 0.001 g and digested with *aqua regia* reagent (1:3 HNO_3/HCl). This was then filtered and filled up to mark of 25 ml volumetric flask and used for the analysis.

2.4.9 Colorimetric analysis

Colorimetric analysis was conducted to determine the oxidation state of the chromium on the catalyst (dry catalyst, un-calcined, calcined and the reduced catalyst). Although this is not a precise experiment it gives a very good insight on the various oxidation states exist on the catalyst. This method has not been reported previously to have been used on catalyst samples, but it was useful in investigating the various oxidation states of chromium on the chromia catalyst even if only a qualitative result was obtained.

Cr(VI) reacts with diphenylcarbazide in acid solution to produce a red-violet colour of unknown composition which is measured at 540 nm. The procedure is nearly specific for Cr(VI). Interferences occur due to copper, iron, mercury, molybdate, permanganate and vanadium which form similarly coloured products but the colour intensities are much weaker than the Cr complex. The acid range is critical, the final acidity must be between 0.7 and 1.3 M H^+.

3.4.9.1 Reagents used

1. Sulphuric Acid 0.5M

28 ml Analar concentrated (98%) H_2SO_4 was carefully added to approximately 500 ml water in a 1 litre volumetric flask. Cool and make up to volume.

2. Diphenylcarbazide Solution

250 mg 1,5-diphenylcarbazide was dissolved in 50 ml acetone. The solution however is only stable for few days, this is discarded when it becomes coloured.

3. Chromium Stock Solution (1000 mg/litre Cr as dichromate)

Analytical grade $K_2Cr_2O_7$ was dried in an oven at 378 K and cool in a desiccator. 2.829 g was carefully weighed and dissolve in water, this was then transfer quantitatively to a 1 litre volumetric flask and make up to the mark.

4. Chromium Standard 5 mg Cr per litre

5 ml of the stock Cr solution was carefully diluted to 1000 ml in a volumetric flask.

3.4.9.2 Procedure

Calibration was first made by preparing 0 to 5 ml of 5 mg/litre Cr standard and pipetted into a series of 50 ml volumetric flasks and diluted to approximately 40 ml and mixed well. 5 ml 0.5 M of the prepared sulphuric acid was then added and mix well. 1 ml diphenylcarbazide solution also added, make up to the mark and further mix well. This then allow to stand 5 to 10 minutes for colour development and the absorbance measured at 540 nm.

Sample containing no more than 25 µg Cr was pipetted into a 50 ml volumetric flask, diluted to approximately 40 ml and mix well. 5 ml 0.5 M sulphuric acid and Add 1 ml diphenylcarbazide solution were added, make up to the mark and mix well. This then allow to stand 5 to 10 minutes for colour development and the absorbance measured at 540 nm.

3.0 Results

3.1 Thermodynamics analysis of the reactions

3.1.1 Basic thermodynamics data

The Gibbs free energy for the production of two alkenes via pentane and hexyne/hexadienes reactions were calculated in order to determine whether the reactions were spontaneous or not. Their basic thermodynamic data at 298 K were obtained from the book of Physical Chemistry [75],for pentane, 1-hexyne, 1,5-hexadiene, 2,4-hexadiene, 1-pentene, 1-hexene and H_2 are listed and presented in Table 6 and 7.

Table 6: ΔH_f^o (298 *K*), ΔS_f^o (298 *K*) and ΔG_f^o (298 *K*) of reactants and products

	ΔH_f^o (298 *K*) (kJ mol^{-1})	ΔS_f^o (298 *K*) (kJ mol^{-1})	ΔG_f^o (298 *K*) (kJ mol^{-1})
Pentane	-146.44	348.95	-8.37
1-Hexyne	*123.64*	*368.74*	*218.57*
1,5-Hexadiene	84.06	*376.98*	*175.32*
2,4-Hexadiene	*48.11*	*367.77*	*160.08*
1-Pentene	-20.92	345.80	*79.08*
1-Hexene	-41.67	*384.64*	*87.45*
H_2	0	130.59	*0*

Table 7: C_p of reactants and products at various temperatures

	C_p *(cal mol^{-1} K^{-1})*						
	298 K	*300 K*	*400 K*	*500 K*	*600 K*	*700 K*	*800 K*
Pentane	*28.73*	*28.87*	*36.53*	*43.58*	*49.64*	*54.83*	*59.30*

1-Hexyne	*30.65*	*30.77*	*37.87*	*44.18*	*49.59*	*54.20*	*58.16*
1,5-Hexadiene	*31.81*	*31.93*	*38.83*	*44.43*	*49.03*	*53.73*	*57.23*
2,4-Hexadiene	*31.38*	*31.50*	*37.49*	*42.90*	*47.48*	*51.51*	*55.01*
1-Pentene	*26.19*	*26.31*	*33.10*	*39.23*	*44.56*	*49.06*	*52.95*
1-Hexene	*31.63*	*31.78*	*40.03*	*47.47*	*53.90*	*59.34*	*64.02*
H_2	*6.892*	*6.895*	*6.974*	*6.993*	*7.008*	*7.035*	*7.078*

3.1.2 Calculation of ΔG_r^o and ΔS_r^o at different temperatures

Using these variables, the Gibbs free energy can be calculated using the following equations below. Equation 10 represents the Gibbs function at its non-standard state is, whereas equation 11 represents its standard state.

$$\Delta G_r(T) = \Delta G_r^o\ (T) + RT \ln K \ldots\ldots\ldots.. Eqn\ 10$$

$$\Delta G_r^o\ (T) = \Delta H_r^o\ (T) - T\Delta S_r^o\ (T) \ldots\ldots\ldots \text{Eqn } 11$$

$$K = \frac{[P(C_5H_{10})/P^o\,]\,[P(C_6H_{12})/P^o\,]}{[P(C_5H_{12})/P^o\,]\,[P(C_6H_{10})/P^o\,]} \ldots\ldots.. Eqn\ 12$$

The ΔH_r^o and ΔS_r^o were initially calculated at different temperatures. The relationship between the ΔH_r^o /ΔS_r^o can be expressed in the following equations:

$$\mathrm{d}\,\Delta H_r^o\ /\,dT\ =\ \Delta C_p\ \ldots\ldots\ldots\ldots\ldots Eqn\ 13$$

$$\mathrm{d}\,\Delta S_r^o\ /\,dT\ =\ \Delta C_p/T\ \ \ldots\ldots\ldots\ldots Eqn\ 14$$

Hence, this is to say that,

$$\Delta H_r^o\ (T_j) = \sum v_i \Delta H_f^o\ (T_{j-1}) + \sum v_i\, \bar{C}_{pi}\, x(T_j - T_{j-1}) \ldots\ldots. Eqn\ 15$$

$$\Delta S_r^o\ (T_j) = \sum v_i \Delta S_f^o\ (T_{j-1}) + \sum v_i\, \bar{C}_{pi}\, x\, ln(T_j - T_{j-1}) \ldots\ldots\ldots Eqn\ 16$$

$$\bar{C}_{pi} = \frac{C_{pi}\ (T_{j-1}) + C_{pi}\ (T_J)}{2} \ldots\ldots\ldots\ldots\ldots Eqn\ 17$$

Therefore, the variables ΔH_r^o and ΔS_r^o could be calculated through equations 15, 16 and 17 at different temperatures for the basic thermodynamics data of C_5H_{12}, C_6H_{10}, C_6H_{12}, C_5H_{10} and H_2 in the three reaction systems outlined previously: 1HY, 1,5HD and 2,4HD trans-hydrogenations.

3.1.3 Equilibrium constant variations with temperature with regards to ΔH_r^o and ΔS_r^o

The equilibrium constant of the reaction process can equally be described by the equation 18 below relating the variables $\Delta H_r^o\ /-RT$ and $\Delta S_r^o\ /R$ as outline by Van't Hoff. The $\ln K_{eq}$ is calculated at different reaction temperatures with a plot relationship of $\frac{1}{T}$ being obtained for each reaction system. This is then compared to the plot of the pentane dehydrogenation; where it is observed that the trans-hydrogenation reaction with the 2,4HD system has only slightly changed from the pentane dehydrogenation compared to the other systems where significant changes were made. This is presented Figure 17.

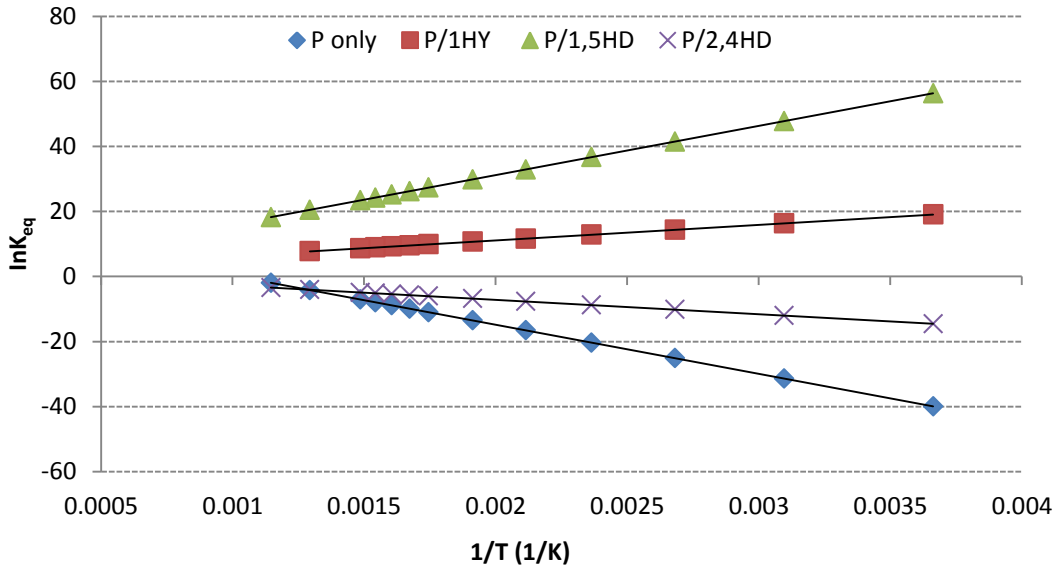

Figure 17: Van't Hoff plots for the comparison of the pentane dehydrogenation with the trans-hydrogenation over the three systems

$$\ln K_{eq} = -\frac{\Delta H^{\circ}}{R}\frac{1}{T} + \frac{\Delta S^{\circ}}{R} \ldots\ldots\ldots\ldots Eqn\ 18$$

The variables $\Delta H_r^o\ /-RT$ and $\Delta S_r^o\ /R$ are calculated for each reaction system at various temperatures. Meanwhile, the effect of temperature on both the ΔH_r^o and ΔS_r^o is quite small, this can also be due to the fact that the variation in temperature has minimal effect on the C_p. Therefore, the ΔG at the different temperatures can be calculated using equation 11. The calculated results are presented in table 6. It can be observed that the trans-hydrogenation is thermodynamically favoured at most temperatures for the reaction of alkanes with alkynes, however this is not always the case when alkadienes are the hydrogen acceptors. According to the calculated free energies for the trans-hydrogenation of pentane with 1-hexyne, 1,5-hexadiene and 2,4-hexadiene, we find that the ΔG of the process moves from negative to positive (Table 8). Therefore, there can be thermodynamic constraints on the process.

Table 8: Free energy for the reaction of pentane with 1-hexyne, 1,5-hexadiene and 2,4-hexadiene

	Free energy (ΔG) of reaction of pentane with the hydrogen acceptors at			
	473 K	573 K	673 K	773 K
1-Hexyne	-45.83	-47.10	-48.38	-49.65
1,5-Hexadiene	-2.35	-2.80	-3.25	-3.70
2,4-Hexadiene	+30.34	+28.87	+27.50	+26.13

3.1.4 Lifting dehydrogenation equilibrium constrain by trans-hydrogenation

Dehydrogenation processes of alkane to olefins have risen to a position of importance, especially in petroleum industries. The production of olefin by dehydrogenation is presented by the following typical equation below.

Alkane = alkene + H_2 (ΔH = 124 $kJmol^{-1}$)

The equilibrium for pentane dehydrogenation is favourable at thermal cracking temperatures; this consequently allows the decomposition of the reactant. The equilibrium data calculated at various reaction temperatures (T) and the equilibrium conversions (α) plotted against temperature presented in Figure 18, shows that the equilibrium conversions are limited by the reaction temperature, and that reasonable conversions are obtained at a temperature >823 K.

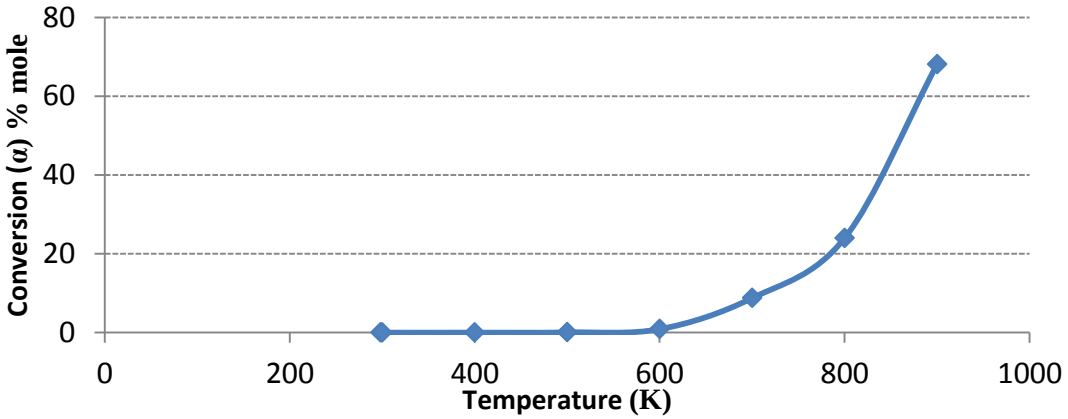

Figure 18: Equilibrium conversion with temperature of n-pentane dehydrogenation

The plotted data are presented in Table 9

Table 9: the equilibrium conversion at various temperatures over pentane dehydrogenation

	298 K	400 K	500 K	600 K	700 K	800 K	900 K
α (%)	2.1×10^{-6}	1.4×10^{-3}	7.0×10^{-2}	8.8×10^{-1}	8.76	24.0	68.0

3.1.5 Equilibrium partial pressure in mixture of ideal gases phase

As mentioned, the trans-hydrogenation process is thermodynamically favoured at most temperatures, this in effect also provides the advantage to push the equilibrium constrain of the alkane dehydrogenation as illustrated in the Fig. 19

below. In accordance to Le Chatelier's principle, the continuous removal of the hydrogen molecule by unsaturated reactants pulls the conversion of pentane.

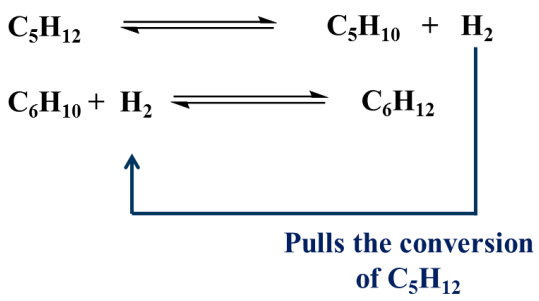

Figure 19: Illustration for pushing the conversion of alkane dehydrogenation by trans-hydrogenation

The pressure dependence of the three reaction system is introduced in order to determine the reaction dependency on conversion

Dehydrogenation system: C_5H_{12} ⇌ C_5H_{10} + H_2

	C_5H_{12} ⇌ C_5H_{10} + H_2		
	C_5H_{12}	C_5H_{10}	H_2
Initial moles	1	0	0
Equilibrium moles	$1-\alpha$	α	α
Mole fractions	$\frac{1-\alpha}{1+\alpha}$	$\frac{\alpha}{1+\alpha}$	$\frac{\alpha}{1+\alpha}$
Partial pressure	$(\frac{1-\alpha}{1+\alpha})P$	$(\frac{\alpha}{1+\alpha})P$	$(\frac{\alpha}{1+\alpha})P$

Equilibrium Constant (K_p)

$$K_p = \frac{P_{C5H10} \cdot P_{H2}}{P_{C5H12}}$$

Therefore,

$$K_p = \frac{\left(\frac{\alpha}{1+\alpha}\right)P \cdot \left(\frac{\alpha}{1+\alpha}\right)P}{\left(\frac{1-\alpha}{1+\alpha}\right)P}$$

$$K_p = \left(\frac{\alpha}{1+\alpha^2}\right) = \frac{K}{P} \ldots\ldots\ldots\ldots\ldots Eqn\ 19$$

The conversion (α) is inversely dependent on pressure as illustrated in eqn 19. Hence K_p is strongly dependent on temperature. The ideal gas equation (PV=nRT) shows that pressure (P) is dependent of temperature (T). Therefore, (α) will be a strong function of temperature.

Trans-hydrogenation system: $C_5H_{12} + C_6H_{10} \rightleftharpoons C_5H_{10} + C_6H_{12}$

	$C_5H_{12} + C_6H_{10} \rightleftharpoons C_5H_{10} + C_6H_{12}$			
	C_5H_{12}	C_6H_{10}	C_5H_{10}	C_6H_{12}
Initial moles	1	1	0	0
Equilibrium moles	1- α	1- α	α	α
Mole fractions	$\left(\frac{1-\alpha}{2}\right)$	$\left(\frac{1-\alpha}{2}\right)$	$\left(\frac{\alpha}{2}\right)$	$\left(\frac{\alpha}{2}\right)$
Partial pressure	$\left(\frac{1-\alpha}{2}\right)P$	$\left(\frac{1-\alpha}{2}\right)P$	$\left(\frac{\alpha}{2}\right)P$	$\left(\frac{\alpha}{2}\right)P$

Equilibrium Constant

$$K_p = \frac{P_{C5H10} \cdot P_{C6H12}}{P_{C5H12} \cdot P_{C6H10}}$$

Therefore,

$$K_p = \frac{\left(\frac{\alpha}{2}\right)P \cdot \left(\frac{\alpha}{2}\right)P}{\left(\frac{1-\alpha}{2}\right)P \cdot \left(\frac{1-\alpha}{2}\right)P}$$

$$K_p = \left(\frac{\alpha^2}{(1+\alpha)^2}\right) \ldots\ldots\ldots\ldots\ldots Eqn\ 20$$

Hence conversion (α) is not dependent of the pressure as illustrated in eqn. 20. Thus, using the trans-hydrogenation technique, which involves the hydrogen acceptor, the effect of pressure is completely removed.

3.2. CrO_x/Al_2O_3 catalyst

3.2.1 Pre-reaction catalyst characterisation

3.2.1.1 BET surface area and pore volume determination

Table 10 shows the summary of the parameters extracted from the BET analysis. The result indicated that the BET surface area (S_{BET}) and the pore volume of the alumina support show a slight decrease upon impregnation of the metal precursor, which is in keeping with previous literature [76].

Table 10: BET surface areas, pore volume and average pore diameter of the support and the CrO_x/Al_2O_3 catalyst

	S_{BET} (m^2/g)	V_p(cm^3g^{-1})	D_p(Å)
Y-Al2O3	208	0.52	100
CrOx/Al2O3	203	0.46	91

The adsorption isotherm for the catalyst and the support were found to be similar, obeying the type II model typical for mesoporous material (fig 20).

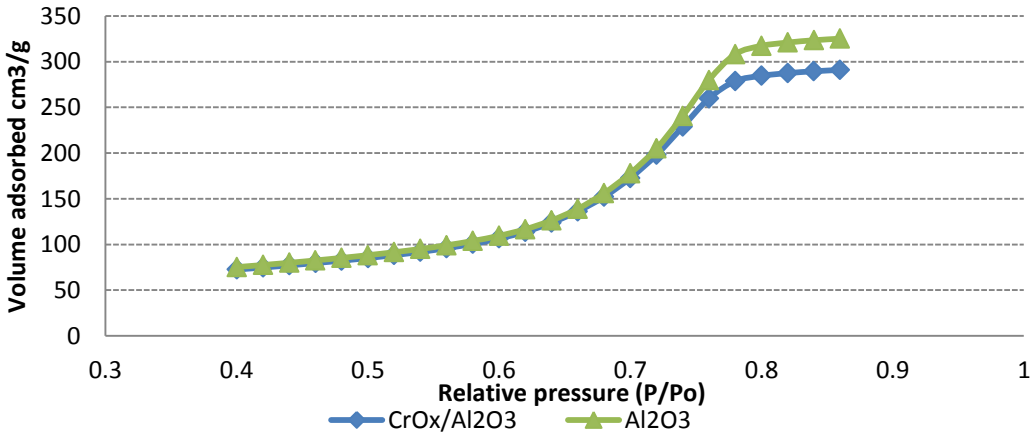

Figure 20: Nitrogen adsorption isotherm at 78K for the support and the CrO_x/Al_2O_3 catalyst

The pore volume distribution as measured in the mesopore range for the support is illustrated in Figure 21. It presents a more uniform distribution and it is very clear that the chromia loading slightly decreases the pore volume of both mesopores and micropores of the alumina support upon the impregnation. This shows a slight loss surface area of the alumina support after the impregnation. In both cases mesopores fall within range of 3-11 nm and micropores 0.5 to <2 nm.

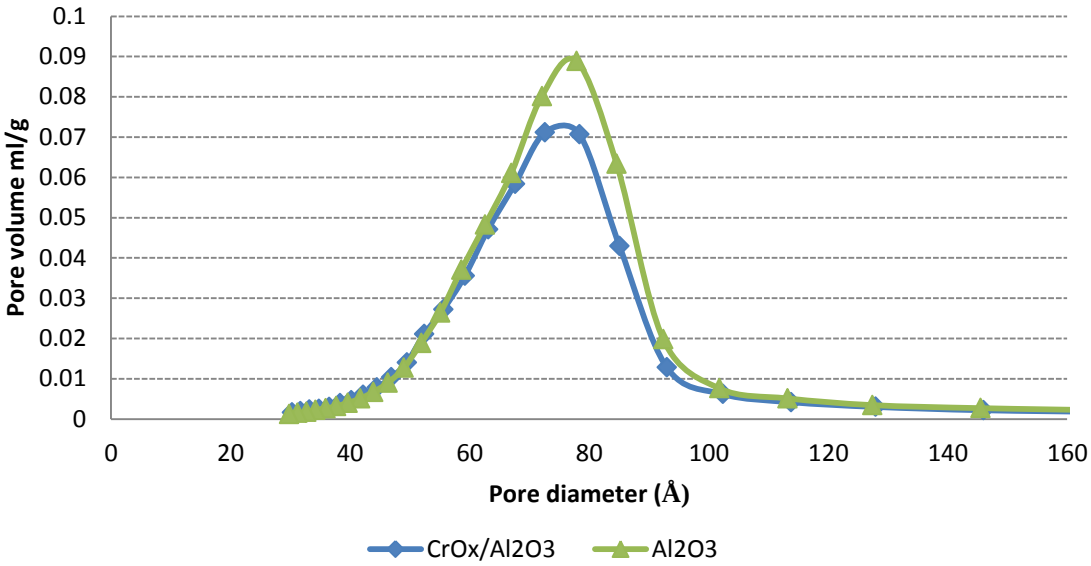

Figure 21: Pore volume distribution of the support and the CrO_x/Al_2O_3 catalyst

3.2.1.2 XRD analysis

The XRD analysis of the catalyst and the γ- alumina both revealed the same diffraction pattern associated with only the alumina and no evidence observed for the crystalline phase of chromium oxide. This is expected for this loading, as it has been reported in previous studies[34] that the crystalline chromium oxide phases are only observed with loadings >10 %. The result is presented in Figure 22.

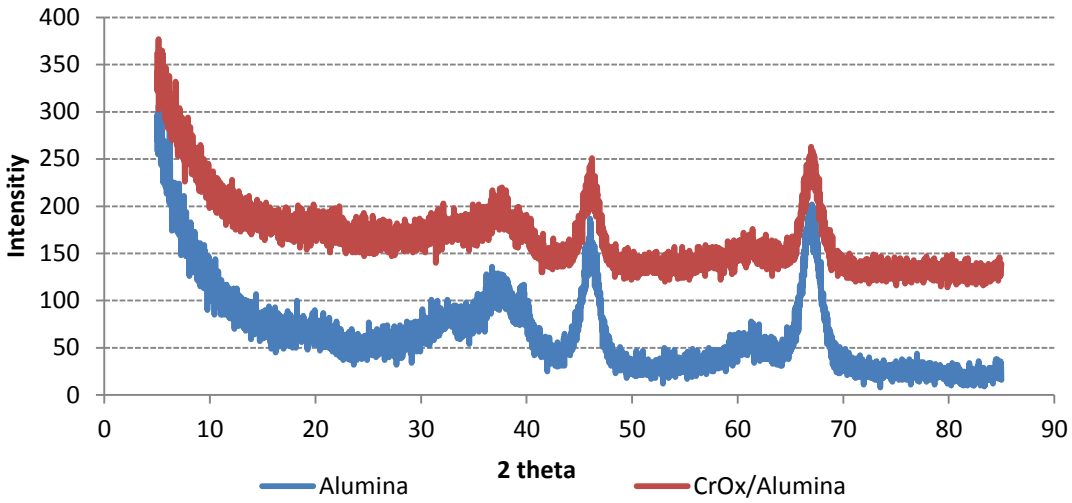

Figure 22: XRD diffraction pattern of the support and the CrO_x/Al_2O_3 catalyst

3.2.1.3 Thermogravimetric analysis

The standard TGA-TPR obtained from ambient temperature to 1273 K presented in Figure 23, is found to be consistent with the Red-Ox cycle as explained below, and the reduction peak observed at ~650 K perfectly match ones obtained with the reduction cycles.

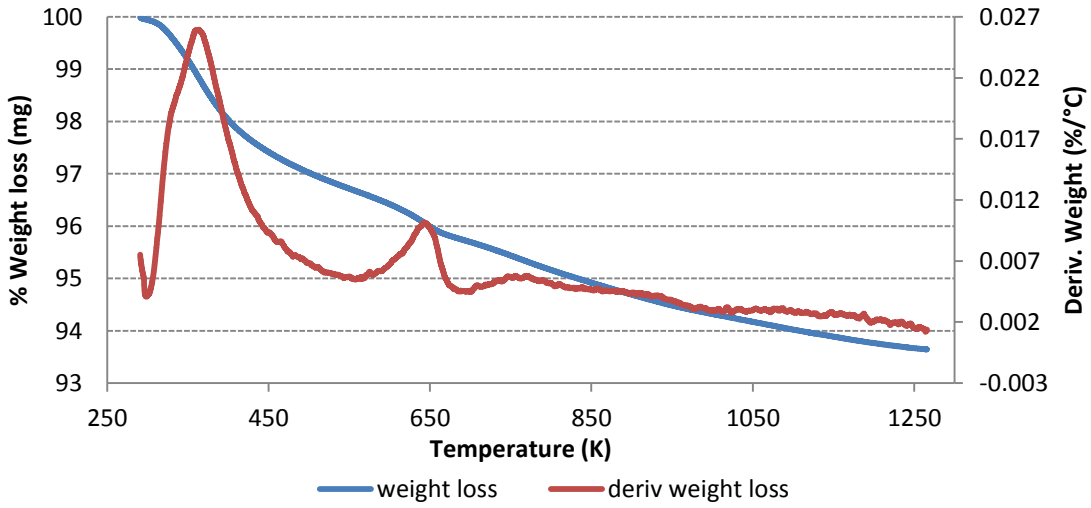

Figure 23: The standard TGA-TPR profile of the CrO_x/Al_2O_3 catalyst

The TGA-TPR obtained during the Red-Ox cycles (section 2.4.3) showed a single peak at ~650 K associated with H_2 consumption observed with both 1st and 2nd cycles, which would be an indicative of a single chromium reduction stage. The

TPR result for the 2nd cycle showed a lower H_2 consumption compared to the 1st cycle. The first peak obtained at ~373 K is associated to desorption of physisorbed H_2O absorbed on the catalyst from atmosphere (Figure 24).

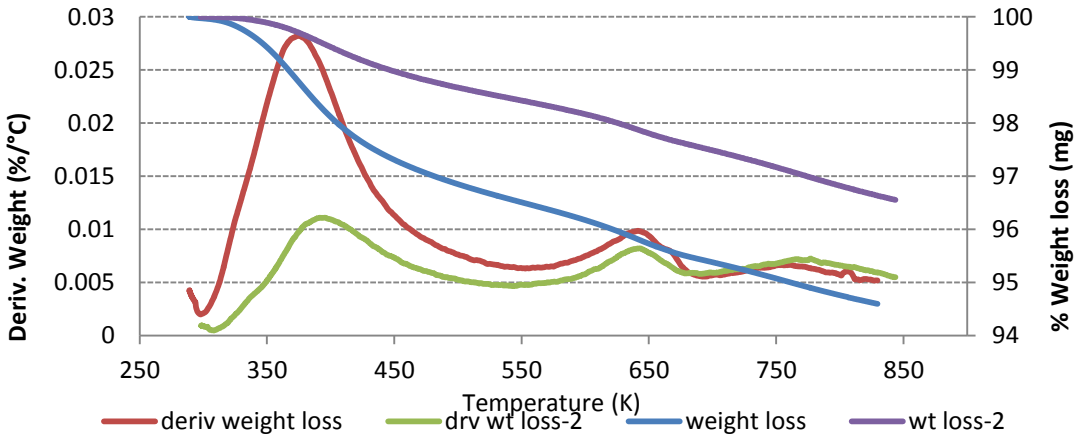

Figure 24: The TGA-TPR profile during the Red-Ox cycles of the CrO_x/Al_2O_3 catalyst

From the TGA-TPR-MS result (m/e 2), the hydrogen consumption perfectly matched the reduction peak at ~650 K observed with both cycles. Trace water (m/e 18) was also detected during the first cycle at ~373K confirming desorption of the physisorbed water on the catalyst. This perfectly matches the peak at ~373 K. There is almost no physisorbed water detected during the second cycle as expected, only ~1% loss was observed. The result is presented in Figure 25

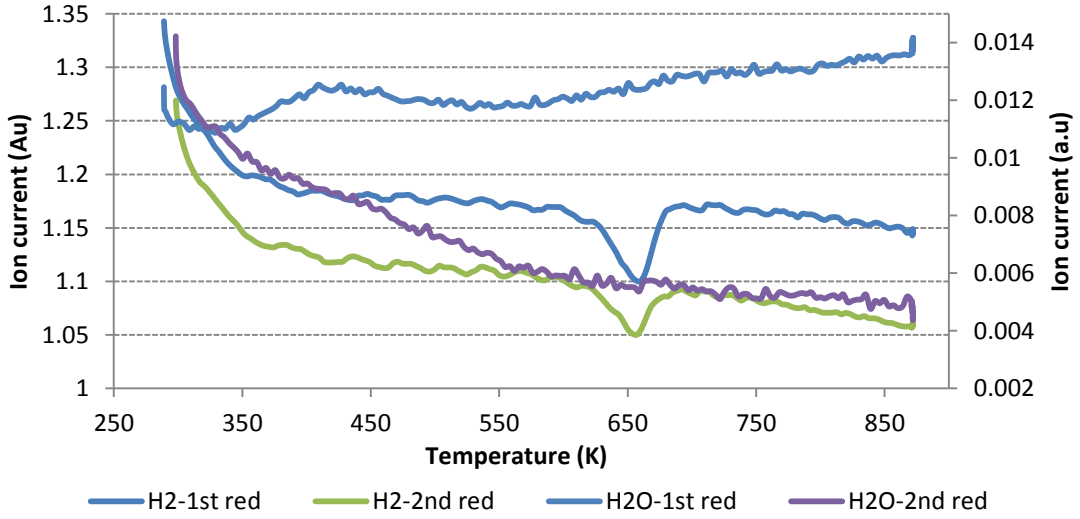

Figure 25: mass spectra data obtained during the TGA-TPR Red-Ox cycle of the CrO_x/Al_2O_3 catalyst

The DTA of the first reduction cycle shows one endothermic response at ~373 K ascribed to the removal physisorbed water corresponding to moisture loss mainly from the alumina support: the weight loss is ~4%. There is no obvious effect observed due to this, during the second cycle. The exothermic peak at ~ 650 K corresponds to weight loss of ~2% due to loss of oxygen; ~0.22 mg of the 25.9 mg of the catalyst was lost. This corresponds to the loss of ~0.5 O_2 atom per chromium atom. This could be a reduction step of the chromium oxide between Cr^{6+} and Cr^{3}. The result is presented in Figure 26.

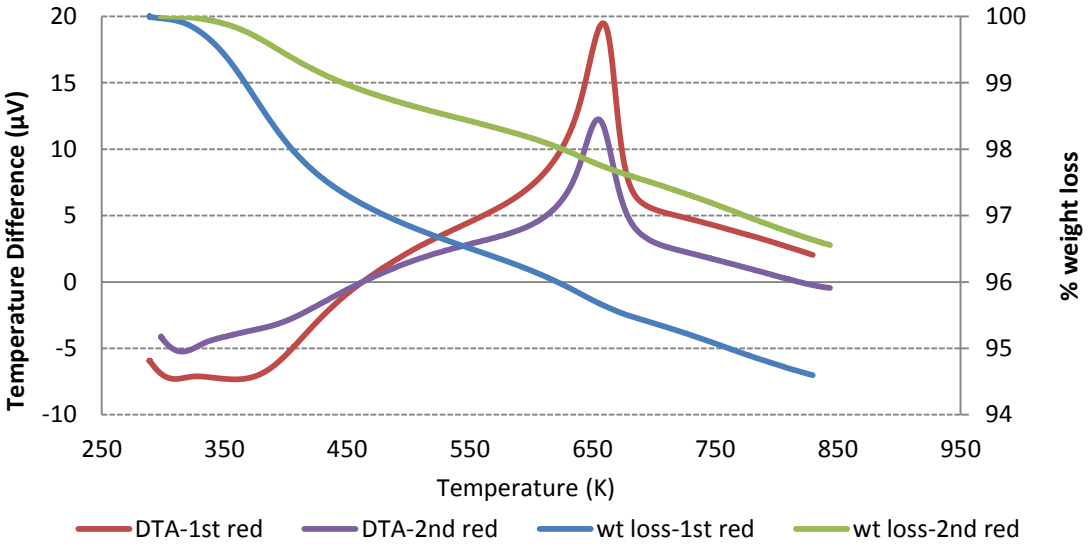

Figure 26: The DTA profile of the catalyst obtained during the TGA-TPR Red-Ox of the CrO_x/Al_2O_3 catalyst

3.2.1.4 Raman analysis

The Raman spectrum of the catalyst is presented Figure 27.The Raman bands observed are assigned to the chromium oxide vibrations. The Raman spectrum reveals bands assigned to chromia at ~380, ~860 and ~990 cm^{-1}. The absence of the band at ~550 cm^{-1} (i.e characteristic of crystalline Cr_2O_3) and ~495 cm^{-1} (i.e characteristics of crystalline CrO_3) shows that the chromium oxide exists as two-dimensional over-layer [77]. A table adapted from Vuurman *et al.*,[78] also adapted from several other sources reveals that the catalyst may exist as both monomer or dimer CrO_4 and Cr_2O_7. The very high frequency band at ~990cm^{-1} is consistent with the symmetric stretching mode of CrO_2, while the band at ~ 860 cm^{-1} is assigned to both the stretching mode of CrO_3 and stretching mode of

bridging Cr-O-Cr. The stretching mode of the CrO_3 may be an indication of amorphous phase as no crystalline diffraction pattern was detected with the XRD, although the detection of the CrO_x diffraction pattern depends on the catalyst loading.

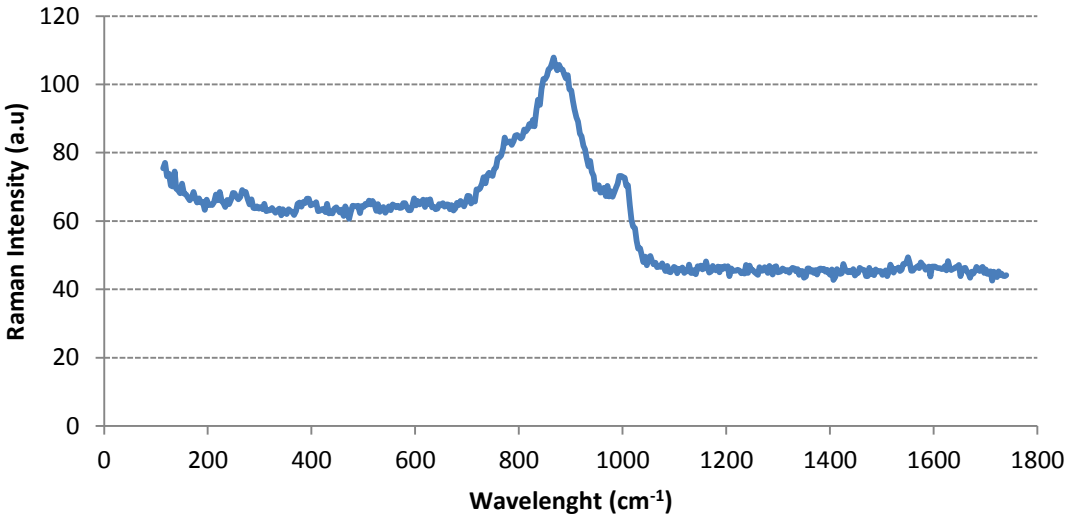

Figure 27: Raman spectrum of the CrO_x/Al_2O_3 catalyst

3.2.1.5 EPR analysis

The EPR profile obtained at various treatment stages of the catalyst preparation are presented in Figure 28. After various treatments of the catalyst, different EPR spectra were observed except for the dried catalyst where no EPR spectrum was seen. The EPR study of the CrO_x/Al_2O_3 catalyst was observed with the purpose of characterizing the Cr^{3+} on the catalyst which produces magnetic chromium species. Resonance effects for chromium oxide catalyst are usually reported to originate from Cr^{3+} subjected to varying degree of the antiferromagnetic exchange forces [79]. All the spectra elucidate different distributions of the Cr^{3+}, and the spectrum obtained for the calcined catalyst may be due to charge transfer absorption of the Cr^{6+} and a lower interaction of the Cr^{3+} ions on the support. The decrease observed in the EPR intensity for the un-calcined and reduced catalyst suggest the transition of $Cr^{6+} \rightarrow Cr^{3+}$ while the broadening could be associated with Cr^{3+} clusters. Also, the shape line across the spectra observed for all the treatment has been thought to arise from small amount of Cr^{5+}[80].

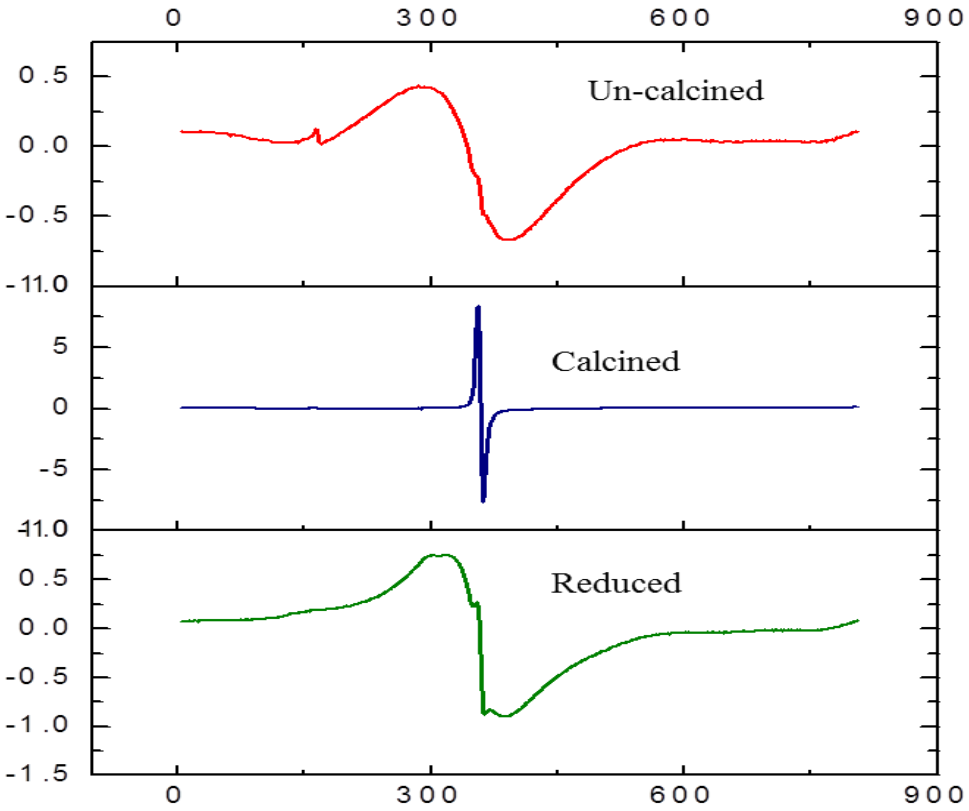

Figure 28: EPR profile obtained during the various CrO_x/Al_2O_3 catalyst treatments

4.2.1.6 AAS and Colorimetric analysis

AAS analysis and colorimetric analysis are presented in Table 11. It is clearly observed that appreciable values for both +3 and +6 oxidation states of Cr are obtained at various treatment stages of the catalyst preparation. The dried catalyst contains a high percentage of Cr^{6+} (3.21% c.f. the total loading 3.32%). While the reduced catalyst, contain the lowest percentage of Cr^{6+} 0.22%, confirming that the catalyst system will still exist as a mixed oxidation state Cr during all the treatment stages but the percentage amount varies.

Table 11: Percentages of the both Cr^{3+} and Cr^{6+} obtained during various catalyst treatments

Sample	Total % Cr	% Cr $^{3+}$ state	% Cr $^{6+}$ state
As prepared* cat	3.32	0.11	3.21
Dried cat	3.21	1.21	2.00
Calcined cat	2.92	1.20	1.72
Reduced cat	3.31	3.09	0.22

* Air dried before the oven overnight drying

3.2.2 Pentane/Hexyne (P/1HY) system

4.2.2.1 Reaction analysis and trans-hydrogenation activity evaluation

The reactant conversions were followed individually and during the mixed trans-hydrogenation reaction. There is observed an increase in the conversion of the pentane at all temperature, with the trans-hydrogenation process compared to the conversions of the pentane dehydrogenation. The dehydrogenation conversions of the pentane run alone is within the calculated equilibrium conversion of n-pentane dehydrogenation. However, ~26% conversion of pentane was obtained at 623 K with trans-hydrogenation, a value higher than the equilibrium conversion of pentane dehydrogenation at this temperature. This increase was also observed with other reaction temperatures (figure 29).

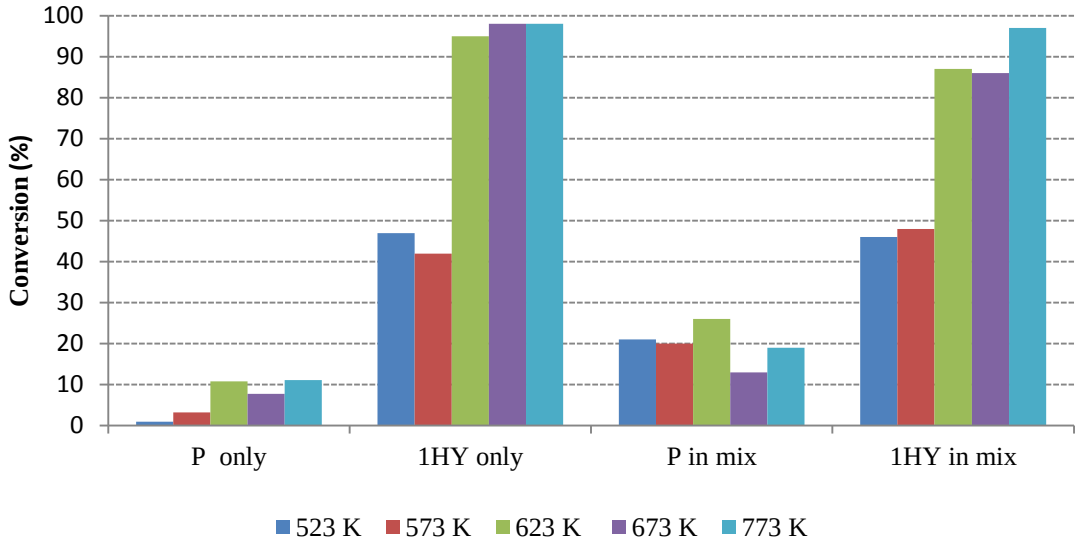

Figure 29: Conversion comparison of P, 1HY and P/1HY mixture using CrO_x/Al_2O_3

The products yields were calculated and are presented in Table 12-16. Most of these products are mostly alkylated and alkylated olefin products obtained with the trans-hydrogenation. The product distribution is pretty much the same with all the reaction temperatures, only the individual yield of the products changes. The yield of the desired products increases with mixed feeds and more valuable products are observed with the trans-hydrogenation process. The (P+H theory) as illustrated in the experimental section, is the yield summation of P and H run individually.

Table 12: Products yield of the trans-hydrogenation over CrO_x/Al_2O_3 at 773K

	P	1HY	P+1HY	P+1HY Theory
	Conversion (%)			
Pentane(P)	11		19	11
Hexyne(1HY)		98	96	98
	Yield (%)			
Iso-pentane	1.01		0.16	1.01
1-Pentene			0.91	0
Trans-2-pentene	8.59			8.59
Hexane		1.57	2.10	1.57
1-Hexene		1.01	0.66	1.01
2-Hexene		0.63	1.64	0.63
3-Hexene		1.56	1.87	1.56
Methyl-2-pentene		3.21	4.16	3.21
3-Methylpentyne		5.18	3.26	5.18
3-Methyl-1-hexene		7.5	5.07	7.50
3-Methylhexane		2.5	5.41	2.51
2-Methyl-1,3-pentadiene		1.35	9.20	1.35
1,4-Hexadiene		13.46	16.92	13.46
2-Methyl-1-hexene		7.37	5.12	7.37
Methylcyclohexane	0.61	8.81	1.60	9.43
Ethylcyclopentane	0.37			0.37

Table 13: Products yield of the trans-hydrogenation over CrO_x/Al_2O_3 at 673K

	P	1HY	P+1HY	P+1HY Theory
	Conversion (%)			
Pentane(P)	08		13	08
Hexyne(1HY)		97	86	97
	Yield (%)			
Iso-pentane	0.46		0.11	0.46
Pentene			0.01	0
Trans-2-Pentene	0.53			0.53
Hexane		0.38	1.95	0.38
1-Hexene			0.27	0
2-Hexene		0.9	6.08	0.9
3-Hexene			0.42	0
Methyl-2-pentene		3.42	4.61	3.42
3-Methylpentyne		7.49	10.28	7.49
3-Methyl-1-hexene		1.67	1.97	1.67
3-Methylhexane		6.17	1.36	6.17
2-Methyl-1,3-pentadiene		7.49	0.27	7.49
1,4-Hexadiene		31.42	25.18	31.42
Methylcyclohexane	3.91	1.8		5.17

Table 14: Products yield of the trans-hydrogenation over CrO_x/Al_2O_3 at 623K

	P	1HY	P+1HY	P+1HY Theory
	Conversion (%)			
Pentane(P)	10		26	10
Hexyne(1HY)		95	87	95
	Yield (%)			
Pentene			0.19	0
Trans-2-Pentene	0.08			0.08
Hexane			0.52	0
1-Hexene		0.33	1.81	0.33
2-Hexene		1.21	2.06	1.21
3-Hexene			1.46	0
Methyl-2-pentene		2.17	2.22	2.17
3-Methylpentyne		11.6	19.24	11.6
3-Methyl-1-hexene		1.29	1.70	1.29
3-Methylhexane		0.55	1.38	0.55
2-Methyl-1,3-pentadiene			2.14	0
1,4-Hexadiene		20.95	19.38	20.95
Methylcyclohexane	5.23	15.19	2.42	20.42
Ethylcyclopentane	1.25	2.77	1.12	3.92

Table 15: Products yield of the trans-hydrogenation over CrO_x/Al_2O_3 at 573K

	P	1HY	P+1HY	P+1HY Theory
	Conversion (%)			
Pentane(P)	04		20	04
Hexyne(1HY)		42	48	42
	Yield (%)			
Iso-pentane			0.05	0
Pentene			0.10	0
Trans-2-Pentene	0.02			0.02
Hexane		0.05	0.88	0.05
1-Hexene		1.07	3.06	1.07
2-Hexene		0.2	3.08	0.2
3-Hexene			3.44	0
Methyl-2-pentene			0.28	0
3-Methylpentyne		6.18	7.75	6.18
3-Methyl-1-hexene		1.13	0.65	1.03
3-Methylhexane		0.45	0.34	0.41
2-Methyl-1,3-pentadiene		0.17	0.66	0.17
1,4-Hexadiene		9.41	5.32	9.41
Methylcyclohexane	0.22	3.87	1.24	3.99
Ethylcyclopentane	0.39	1.36	0.89	1.75

Table 16: Products yield of the trans-hydrogenation over CrO_x/Al_2O_3 at 523K

	P	H	P+H	P+H Theory
	Conversion (%)			
Pentane(P)	0.9		20	0.9
Hexyne(1HY)		47	46	47
	Yield (%)			
Iso-pentane			0	0
Pentene				0
Trans-2-Pentene	0.008			0.008
Hexane		0	0	0
1-Hexene		0.12	0	0.12
2-Hexene		0	0	0
3-Hexene		0	0.09	0
Methyl-2-pentene		0.56	1.45	0.56
3-Methylpentyne		10.55	0	10.55
3-Methyl-1-hexene		1.65	1.81	1.5
3-Methylhexane		0.46	0.31	0.42
2-Methyl-1,3-pentadiene		1.64	1.58	1.64
1,4-Hexadiene		11.51	0.56	11.51
2-Methyl-1-1hexene		1.36	2.24	1.364
Methylcyclohexane		11.18	2.41	11.187

On-going to higher temperature an increase in the total olefin yield was observed as shown in Figure 30. The ratio of olefin to alkylated olefins was about 1:2 at most temperatures. The olefin production is observed to be higher compared to the other valuable products obtained during the trans-hydrogenation as presented in Figure 31. There is also an increase in these valuable products with the reaction temperature (Figure 32)

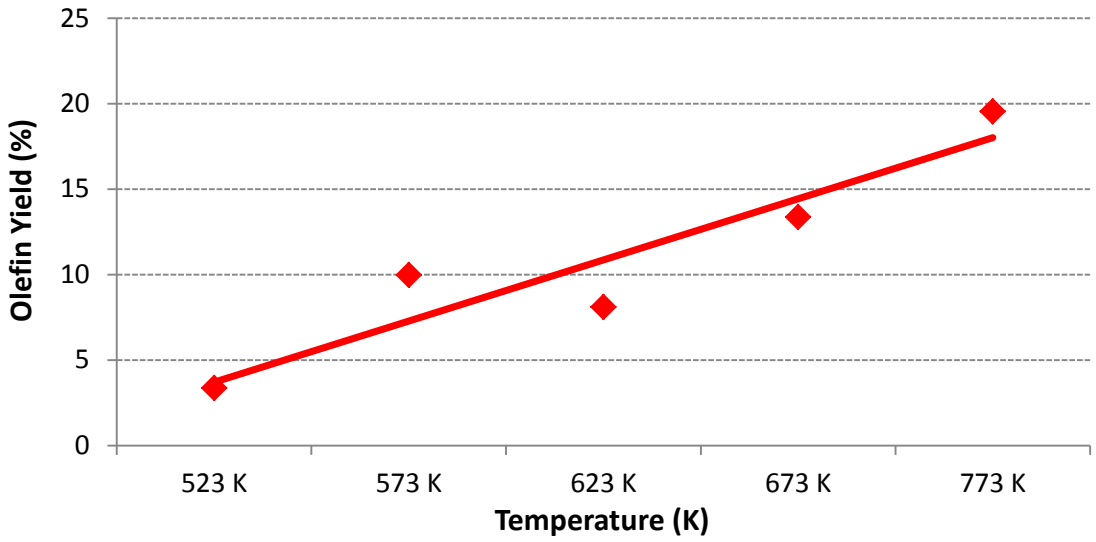

Figure 30: Total olefin yield with temperature over the CrO_x/Al_2O_3 using 1HY system

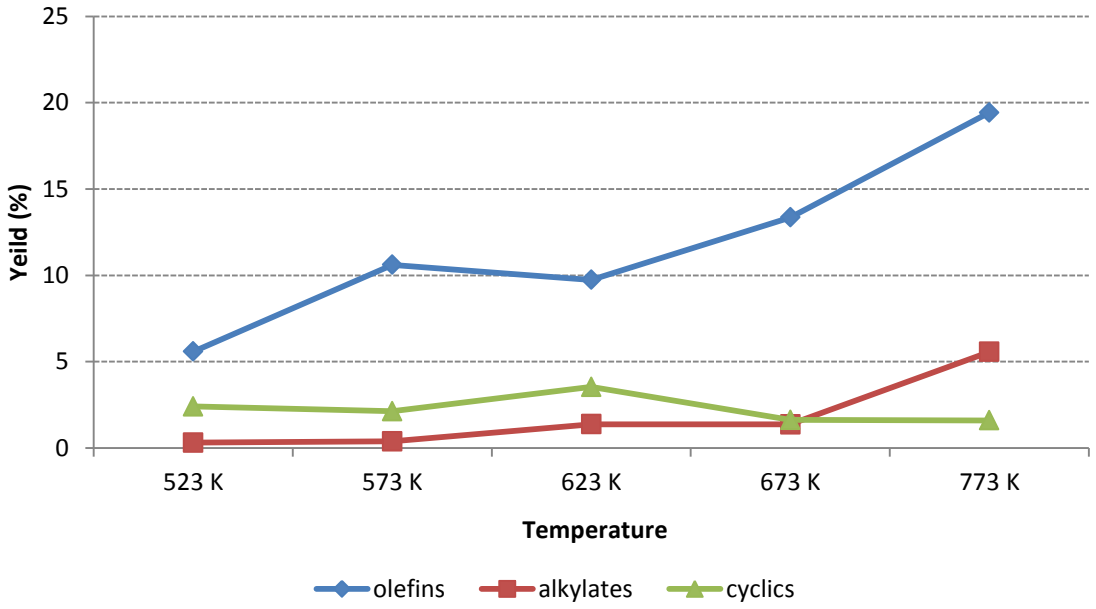

Figure 31: Profile of valuable product in relative to the reaction temperature over CrO_x/Al_2O_3 using 1HY system

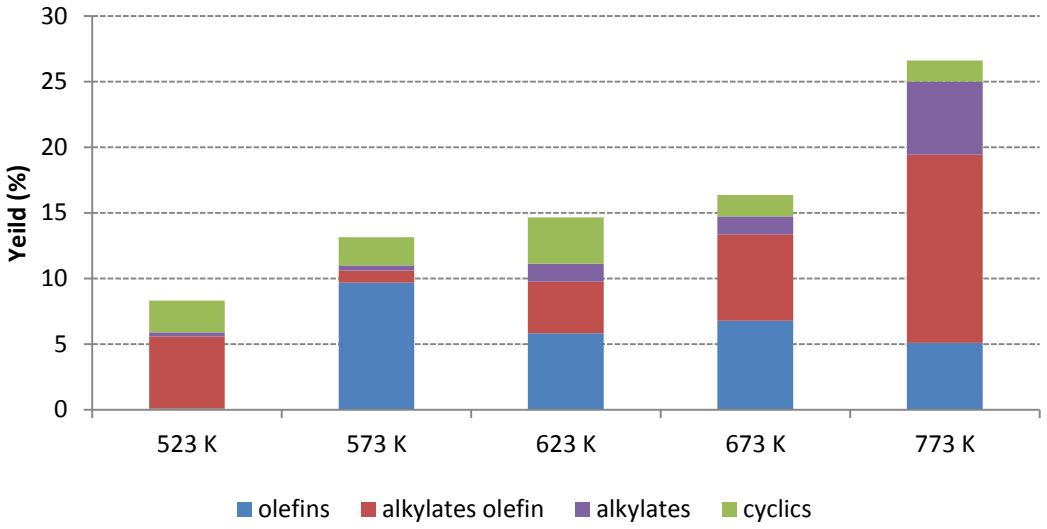

Figure 32: Relationship of the valuable products over CrO_x/Al_2O_3 using 1HY system

The eluent gas products were analysed by on-line mass spectrometry. The evolution of hydrogen was observed from the start of the reaction but later declined at ~ 40 min completely on the stream. CH_4 and C_2H_4 were also evolved at almost the same time when the hydrogen start to decline from the stream and was maintained to the end of the reaction. This same trend was observed with 773-623 K temperatures run while only pulses of these gases were observed with 573 and 523 K temperatures. The result obtained at 773 K is presented in Figure 33

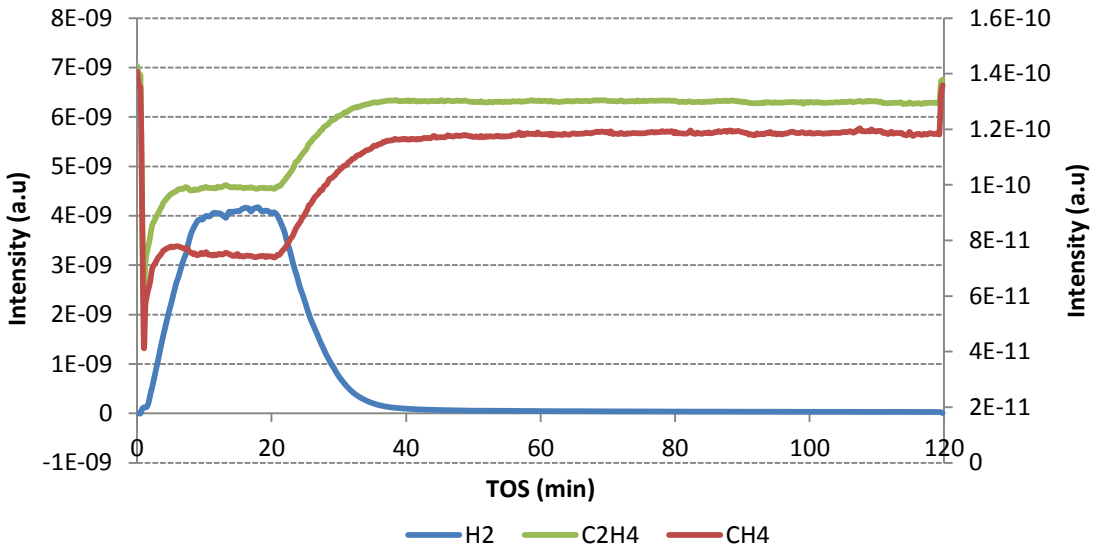

Figure 33: Profile of the evolved gases over CrO_x/Al_2O_3 using P only at 773 K

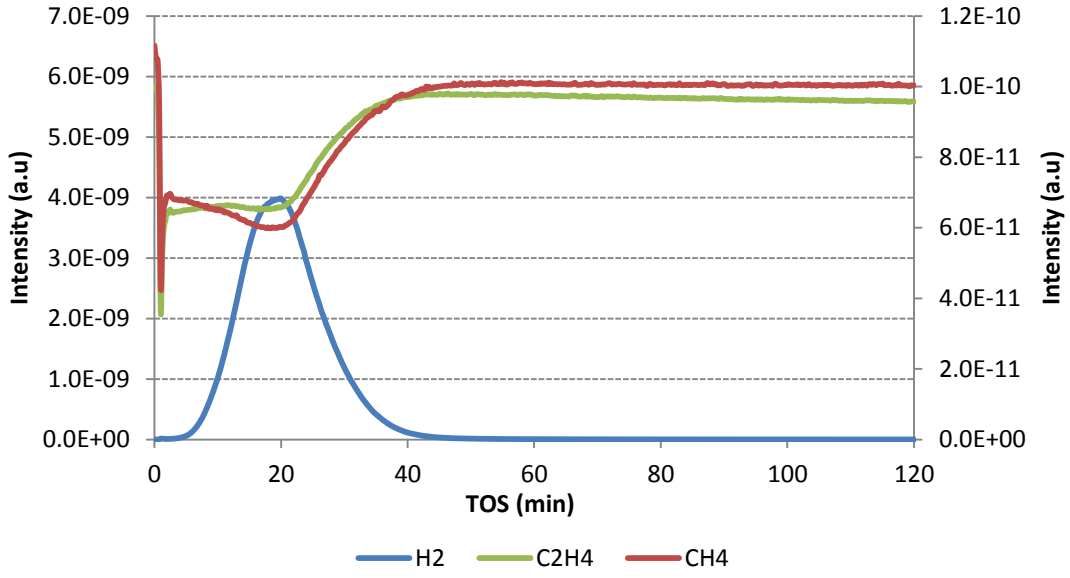

Figure 34: Profile of the evolved gases over CrO_x/Al_2O_3 using 1HY only at 773 K

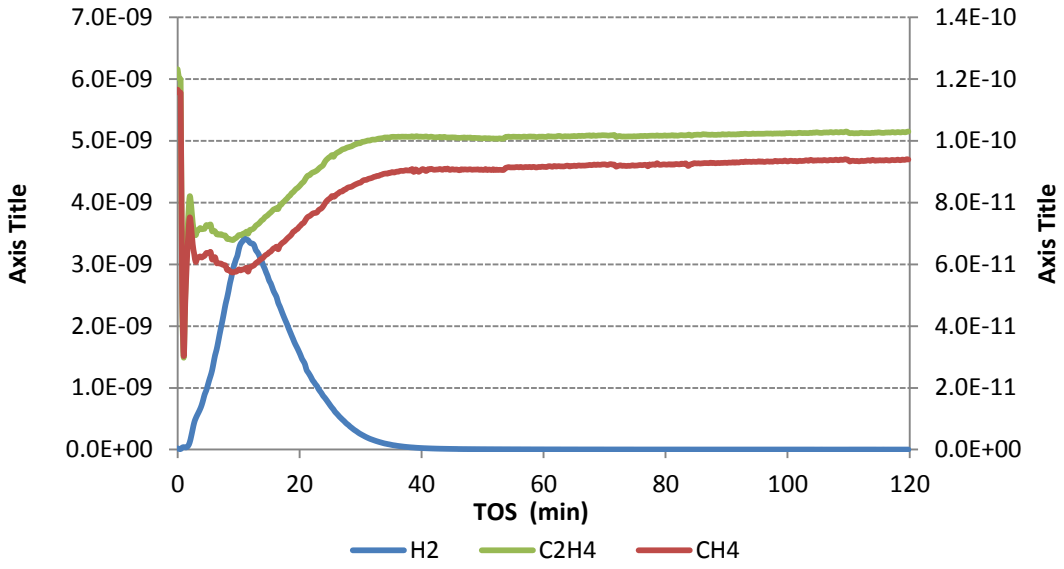

Figure 35: Profile of the evolved gases over CrO_x/Al_2O_3 using P/1HY at 773 K

Table 17: carbon balance for the P/1HY trans-hydrogenation reaction over the CrO_x/Al_2O_3 catalyst

Temperature (K)	Carbon balance (%)				
	Liquid [a] Ptds.	CH4 [b]	C2H4 [b]	Coke [c]	Pdts Non accounted
773	74	3	11	0.60	11
673	83	3	10	0.4	5.01
623	82	3	9	0.19	6.14
573	91	-	-	0.07	4
523	94	-	-	0.02	3

a) Obtained from the GC analysis, b) obtained from the mass spec analysis, c) obtained from the TGA analysis

The hydrogenation reactions of hexyne/hexadiene were also performed to determine the catalyst efficacy on the hydrogenation and compare with the trans-hydrogenation reaction. This was performed using 2% H_2/N_2 in the ratio of 2:1 hexyne or hexadienes/2% H_2/N_2.It is observed that the reaction products and distribution obtained were very similar to that obtained with trans-hydrogenation process. There are also similarities observed in the major products obtained in the two processes, but the hydrogenation process exhibits a higher percentage yield of these products. The reaction obtained at 573K presented the best similarity and the percentage yields of the primary olefin are more significant. The results are presented in Table 18-20. Higher conversions of the reactants were obtained approximately the same with the trans-hydrogenation process at all the tested reaction temperatures.

Table 18: Products yield during the hydrogenation of1HY over the CrOx/Al2O3 at 623K

	Yield (%)		
	1HY + 2% H_2/N_2	P+1HY	P+1HY Theory
Iso-pentane			
Pentene		0.19	0
Trans-2-Pentene			0.08
Hexane	18.46	0.52	0
1-Hexene	3.39	1.81	0.33
2-Hexene	1.07	2.06	1.21
3-Hexene		1.46	0
Methyl-2-pentene	0.74	2.22	2.17
3-Methylpentyne	23.5	19.24	11.6
3-Methyl-1-hexene	1.44	1.70	1.29
3-Methylhexane	0.64	1.38	0.55
2-Methyl-1,3-pentadiene	2.05	2.14	0
1,4-Hexadiene	18.28	19.38	20.95
Methylcyclohexane		2.42	20.42
Ethylcyclopentane		1.12	3.92

Table 19: Products yield during the hydrogenation of 1HY over the CrOx/Al2O3 at 573K

	Yield (%)		
	1HY + 2% H_2/N_2	P+1HY	P+1HY Theory
Iso-pentane		0.05	0
Pentene		0.10	0
Trans-2-Pentene			0.02
Hexane	2.19	0.88	0.05
1-Hexene	2.55	3.06	1.07
2-Hexene	2.61	3.08	0.2
3-Hexene	0.57	3.44	0
Methyl-2-pentene	4.25	0.28	0
3-Methylpentyne	21.84	7.75	6.18
3-Methyl-1-hexene	2.82	0.65	1.03
3-Methylhexane	1.51	0.34	0.41
2-Methyl-1,3-pentadiene	2.98	0.66	0.17
1,4-Hexadiene	19.56	5.32	9.41
Methylcyclohexane	10.69	1.24	3.99
Ethylcyclopentane	0	0.89	1.75

Table 20: Products yield during the hydrogenation of1HY over the CrOx/Al2O3 at 523K

	Yield (%)		
	1HY + 2% H_2/N_2	P+1HY	P+1HY Theory
Iso-pentane		0	0
Pentene			0
Trans-2-Pentene			0.008
Hexane	0.07	0	0
1-Hexene	0.28	0	0.12
2-Hexene	0.23	0	0
3-Hexene	0.22	0.09	0
Methyl-2-pentene	0	1.45	0.56
3-Methylpentyne	17.36	0	10.55
3-Methyl-1-hexene	2.65	1.81	1.5
3-Methylhexane	0.96	0.31	0.42
2-Methyl-1,3-pentadiene	3.28	1.58	1.64
1,4-Hexadiene	26.97	0.56	11.51
Methylcyclohexane	3.81	2.24	1.364
Ethylcyclopentane	10.43	2.41	11.187

3.2.2.2 Post reaction characterization and analysis

The carbonaceous deposit on the spent catalyst was studied using TGA-TPO analysis. The TGA analysis shows a unique weight loss with each type of reactant, and the amount of lost material is seen as a function of the reaction temperatures. The reaction at 773 K reveals the highest weight loss with all the reactants and the 523K reaction the lowest weight loss. The main loss observed with pentane occurs at ~623 - 673 K, while with the hexyne and the mixed feeds the main weight loss occurred at ~ 673 – 823 K. However, a general reduction in

the weight loss was observed using the mixed feed trans-hydrogenation process. The results are presented in Figures 36, 37 and 38.

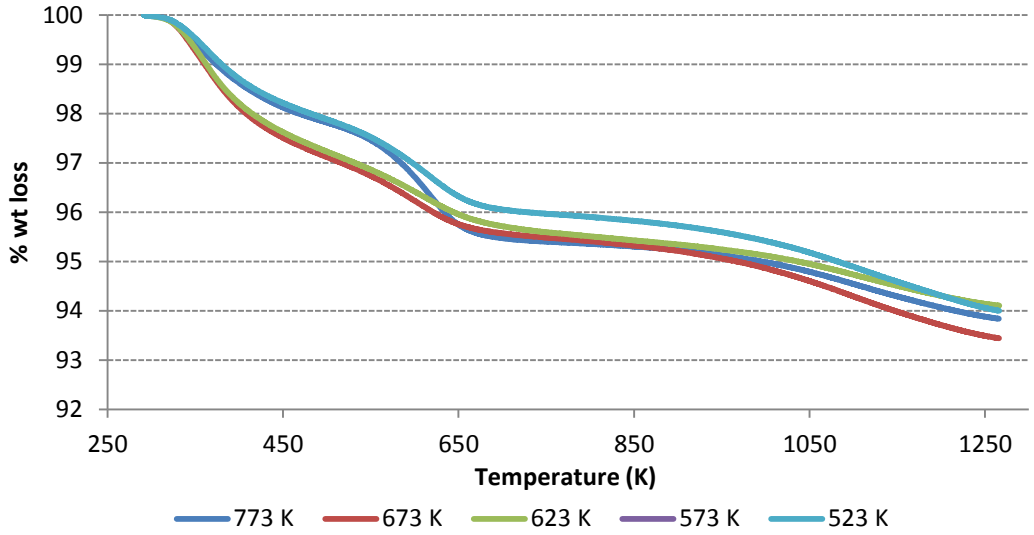

Figure 36 : Weight loss profile of pentane run alone over CrO_x/Al_2O_3 catalyst

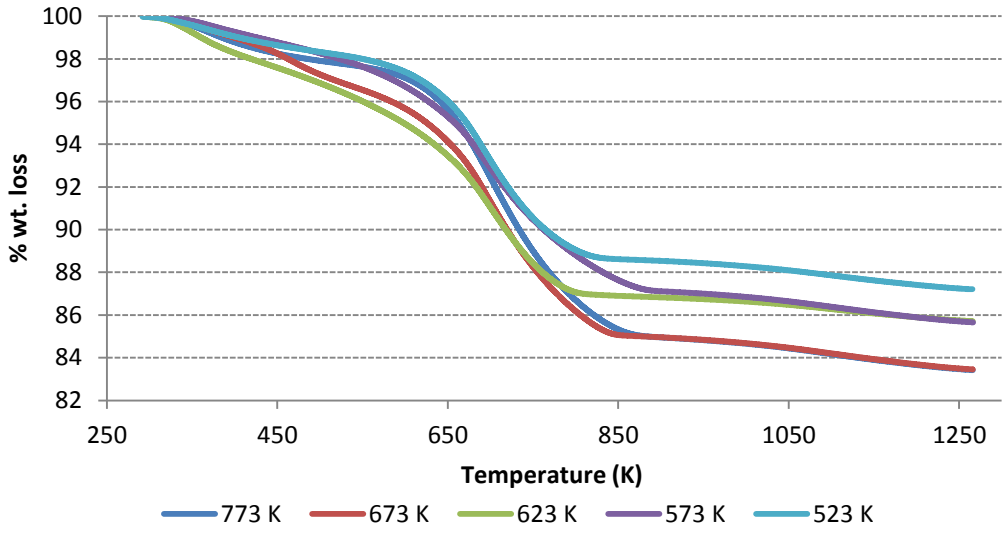

Figure 37: Weight loss profile of hexyne run alone over CrO_x/Al_2O_3 catalyst

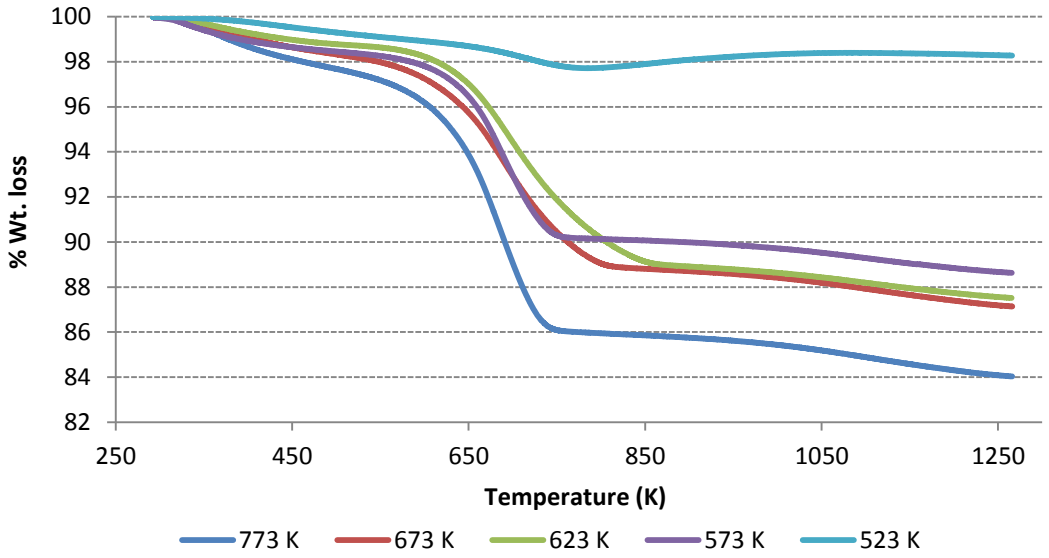

Figure 38: Weight loss profile of the pentane/hexyne mixed feed over CrO_x/Al_2O_3 catalyst

TPO analysis during the TGA revealed carbon dioxide as the main desorption species evolved. This was determined by the mass spectrometer (m/e 44). The results are presented in Figure 39, 40 and 41

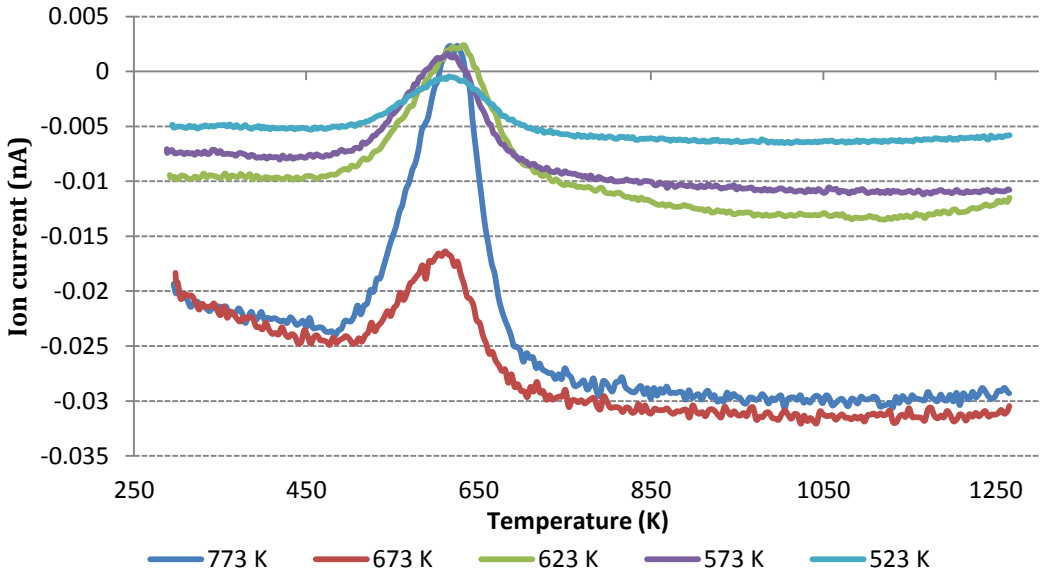

Figure 39: TPO profile of pentane run alone over CrO_x/Al_2O_3 catalyst

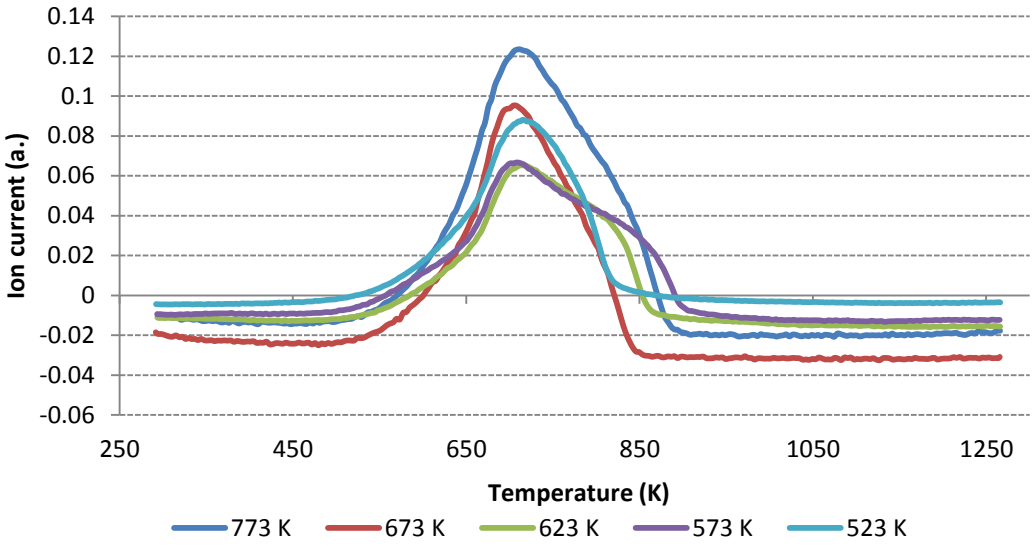

Figure 40: TPO profile of hexyne run alone over CrO_x/Al_2O_3 catalyst

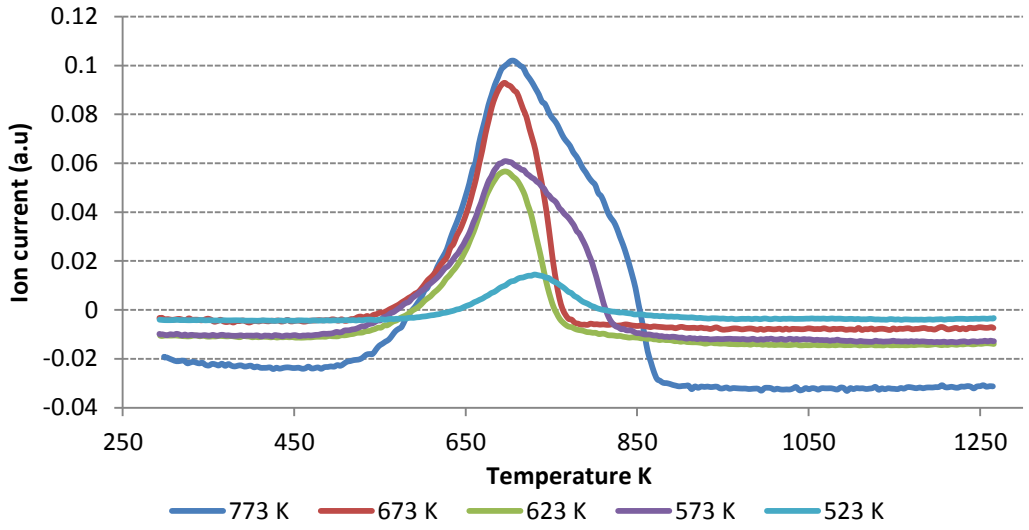

Figure 41: TPO profile of pentane/hexyne mixed feeds over CrO_x/Al_2O_3

The TPO of the spent catalyst obtained after the hydrogenation process is presented in Figure 42. It is observed that at each temperature the CO_2 desorption peak was virtually identical. The TPO of the 523 K run shows a reduced amount of recalcitrant carbon deposit.

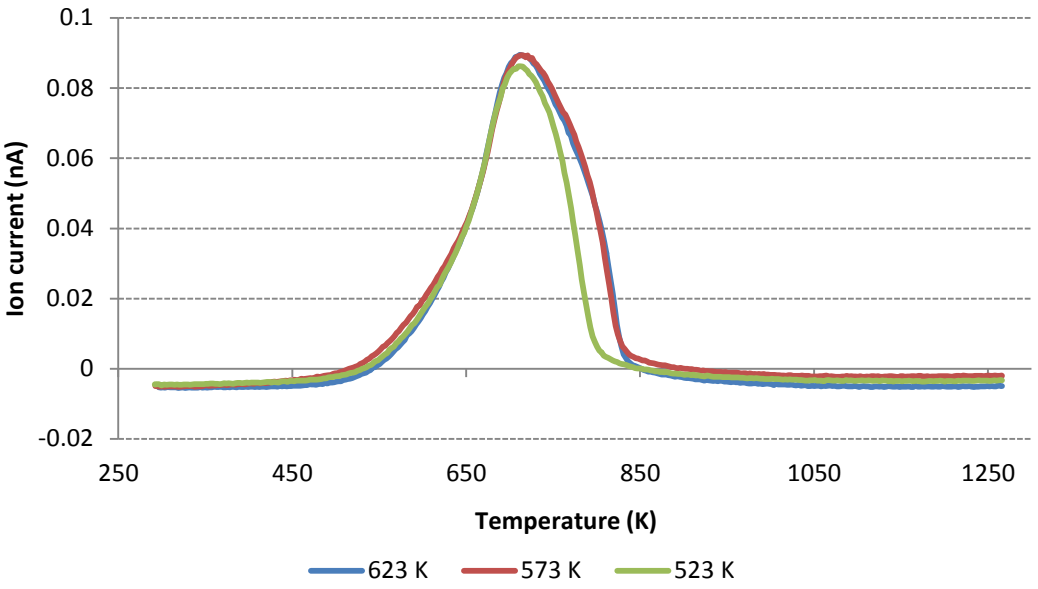

Figure 42: TPO profile of 1HY during hydrogenation over CrO_x/Al_2O_3 catalyst

In addition to this, other masses (m/e 2, 16, 18 and 28) were also monitored. Traces of H_2 CH_4 C_2H_4 and water were also detected in some of the samples. The loss of these species matches the TGA derivative weight loss profile. The result obtained from the spent catalyst used at 773 K is presented in Figure 43. The other masses obtained from the TPO of the catalyst used in the hydrogenation process are shown in Figure 44.

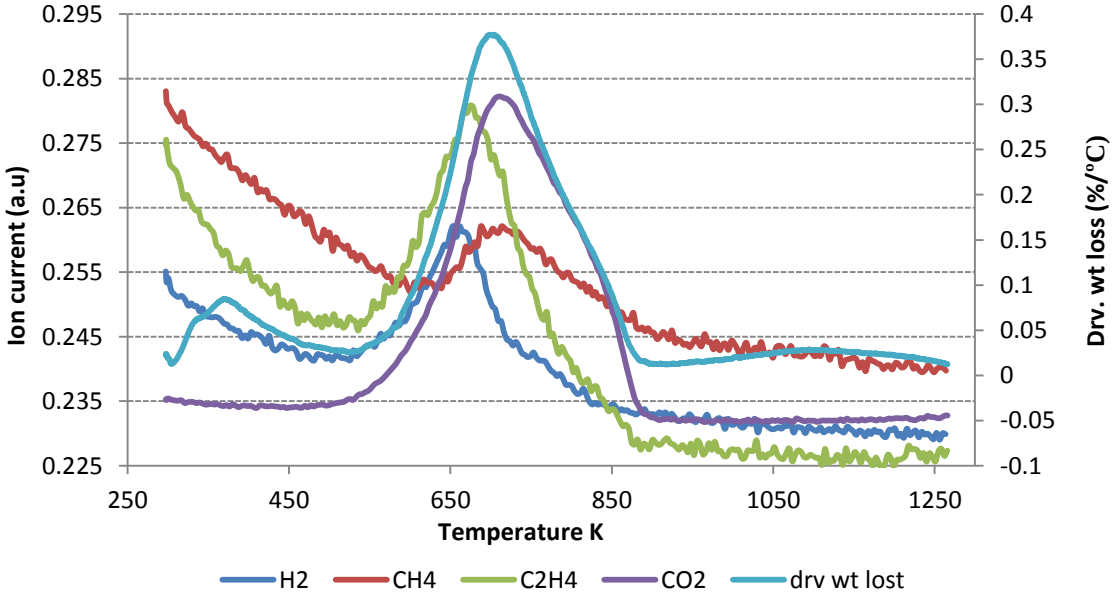

Figure 43: Species obtained during the TPO-MS using hexyne/pentane system with CrO_x/Al_2O_3 catalyst

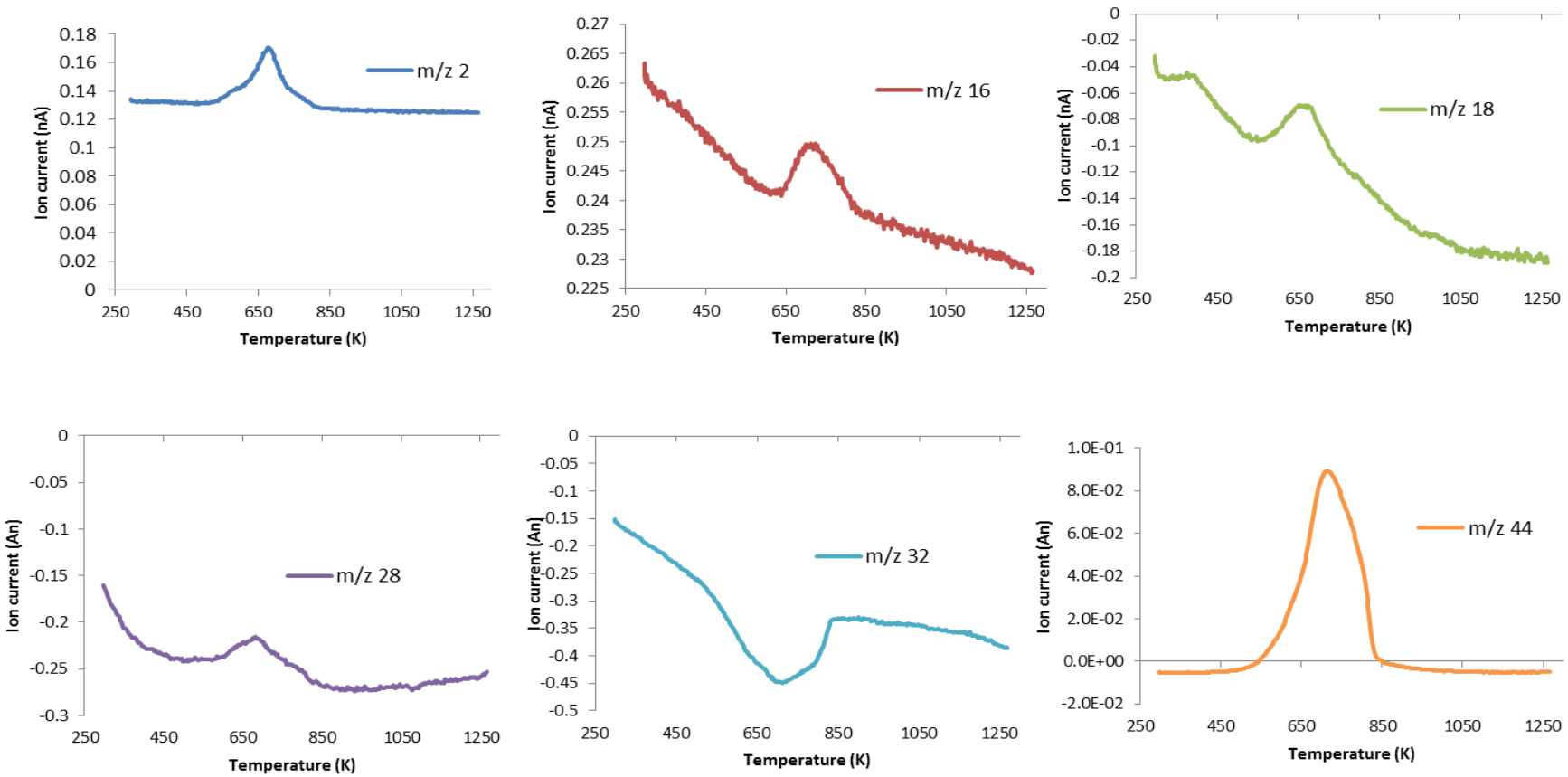

Figure 44: Mass spectra data obtained from TPO during the 1HY hydrogenation over CrO_x/Al_2O_3 catalyst at 623

The amount of carbon species removed from the surface of each catalyst was dependent upon the reaction temperature. The type of reactant used, either fed individually, or as mixed feed trans-hydrogenation process. Samples which had been subjected to only hexyne as the reactant showed the highest amounts of weight loss, but there was a reduction observed in this amount during the trans-hydrogenation process. However, reaction with pentane alone revealed less weight loss compared to hexyne or the mixed feed. The percentage carbon deposit for each run individually alone and as a mixed feed was determined and is presented in Figure 45.

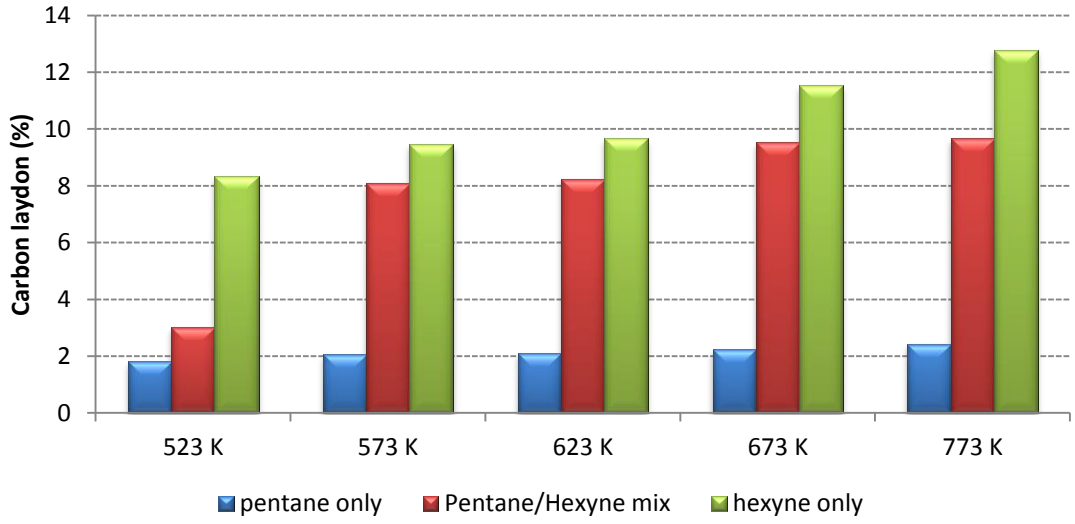

Figure 45: Carbon laydown of the spent CrO_x/Al_2O_3 catalyst over the set temperatures

Table 21: Total amount of carbon deposited on spent CrO_x/Al_2O_3 catalyst at various temperatures

Temperature (K)	Carbon deposited (g/g feed)		
	P	P/1HY	1HY
523	0.0035	0.0047	0.0678
573	0.0040	0.0128	0.0768
623	0.0041	0.0130	0.0787
673	0.0044	0.0150	0.0938
773	0.0048	0.0152	0.1040

The spent catalyst were further analysed using Raman spectroscopy, both UV and visible radiation were used for the studies to analyse the carbon deposit. The UV radiation was used to avoid fluorescence which provides advantages when studying heavily coked material [81-84]. The Raman peaks under UV excitation are enhanced and more intense[85]. When analysing the catalyst with UV radiation, it was observed that only runs with the hexyne and mixed feeds showed Raman bands assigned to coke deposition at ~1380 and 1600 cm^{-1} related to D and G bands respectively. However, the D band was lost using the mixed feed process and only G bands were observed at 523 K and 573 K. Meanwhile, when the same catalysts were analysed with visible radiation, they fluoresced and no clear bands were observed. When UV radiation was used on the spent catalysts that had been used with pentane, they fluoresced but when the same catalysts were analysed with visible radiation, Raman spectra were obtained. The Raman spectra reveals bands assigned to chromia ~880 and ~940 cm^{-1} and G bands assigned to coke deposition at ~1600 cm^{-1}. The G band was only observed with reactions performed at 623, 673 and 773 K. The results are presented in figures 46, 47 and 48

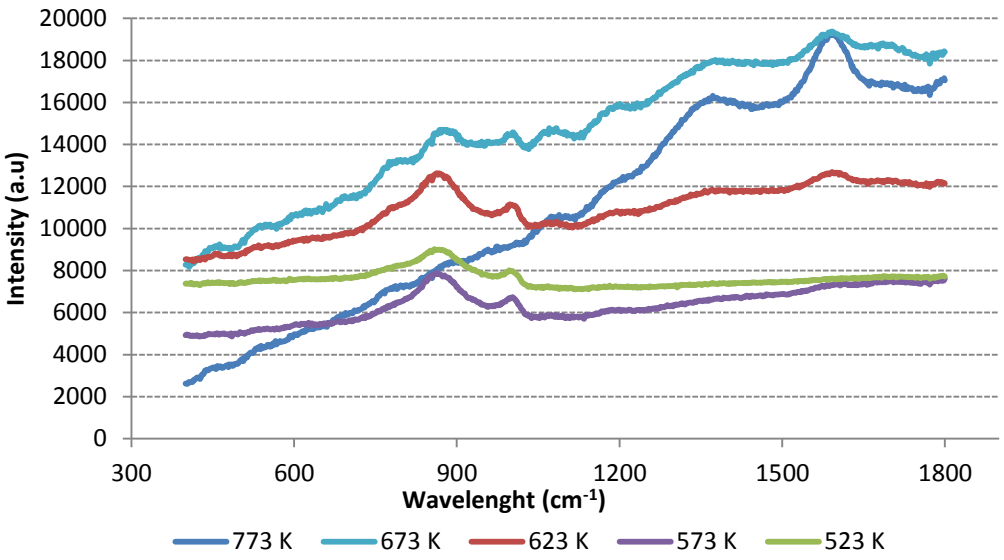

Figure 46: Raman spectra of spent $CrOx/Al_2O_3$ catalyst for sole pentane obtained using the Visible-radiation

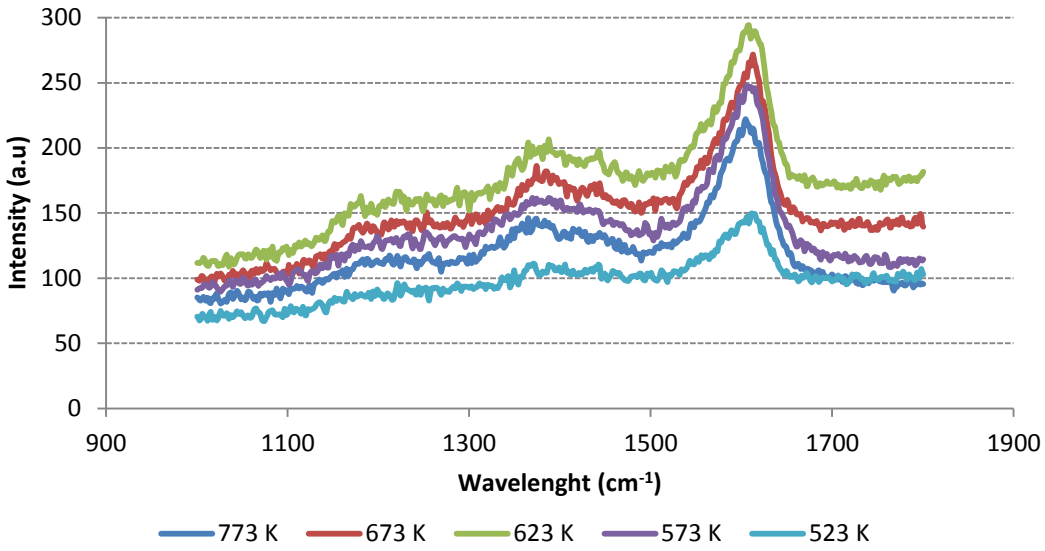

Figure 47: Raman spectra of spent CrOx/Al_2O_3 catalyst for sole 1HY obtained using the UV-radiation

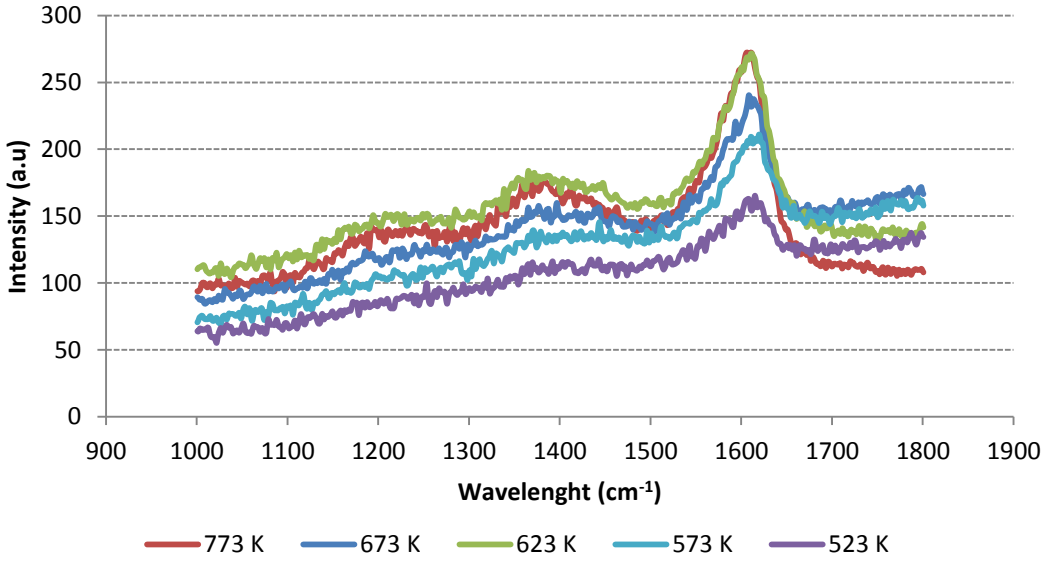

Figure 48: Raman spectra of spent CrOx/Al_2O_3 catalyst for mixed feeds obtained using the UV-radiation

BET analysis was also performed on the spent catalysts; the formation of coke on the catalyst surface decreases the BET surface area and the pore volume. A slight loss in the surface area was observed with all the samples, although samples which had been subjected to pentane alone showed less surface area loss. This reduction is observed as a function of temperature, because the amount of carbon deposited tends to increase with reaction temperature.

Therefore, a plot of S_{BET} vs. Reaction Temperature was obtained .The hexyne reactant exhibited much higher loss while the pentane reactants present the lowest decrease. The results are presented in Figure 49

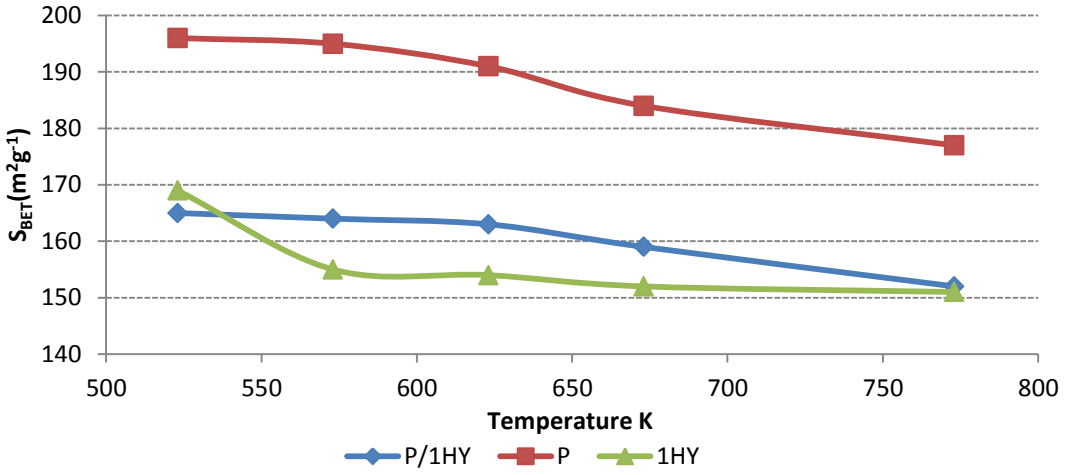

Figure 49: Effect of temperature on the surface area on the spent CrOx/Al2O3 catalyst using 1HY system

The XRD analysis revealed only the diffraction pattern for γ-alumina and there are not any obvious changes observed in the diffraction pattern at any temperature due to these reactions. The fresh catalyst has the same diffraction pattern as the alumina support and there is no evidence for crystalline phases of chromium oxide observed for the studied catalyst due to the percentage loading as reported in previous studies[86]. The result is presented in Figure 50

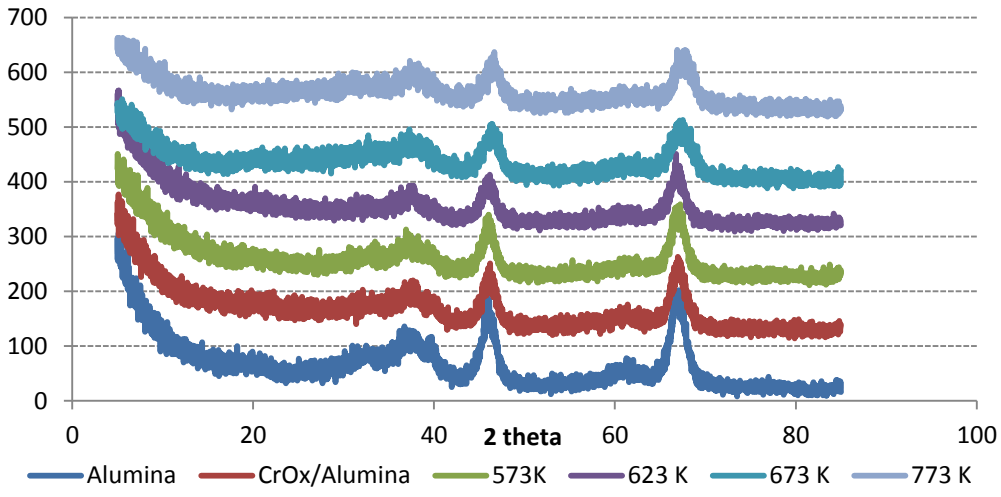

Figure 50: XRD diffraction patterns of the CrOx/Al_2O_3 catalyst pre- and post- reaction

3.2.3 Pentane/1,5-Hexdiene (P/1,5HD) system

3.2.3.1 Reaction analysis and trans-hydrogenation activity evaluation

The reactant conversions were followed individually and during the mixed trans-hydrogenation reaction using the 1,5HD system. There was observed an increase in the conversion of the pentane at all temperatures with the trans-hydrogenation process, compared to the conversions of the pentane dehydrogenation. Conversions higher than what was observed with the 1HY system were obtained here; ~90% was achieved and was observed with nearly all reaction temperatures. These are significantly higher than the equilibrium conversion of pentane dehydrogenation. The result is presented in Figure 51.

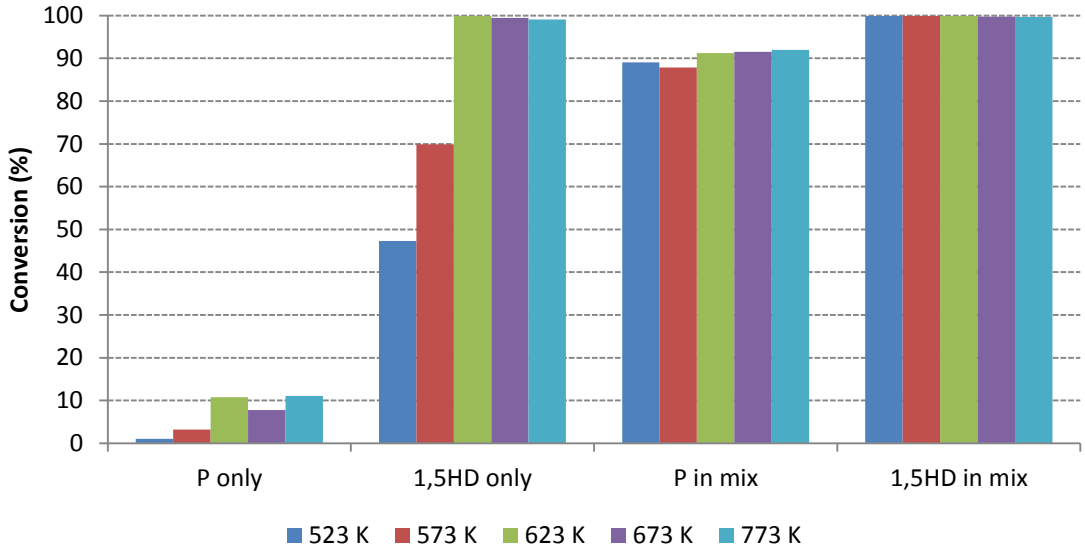

Figure 51: Conversion comparison of P, 1,5HD and P/1,5HD mixture using $CrOx/Al_2O_3$

The product yields were calculated and presented in

Table 22-26. Most of these products are alkylated and alkylated olefin products obtained with the trans-hydrogenation. The product distribution is similar at all the reaction temperatures, only the individual yield of the products changes. The yield of the desired products increases with mixed feeds and more valuable products are observed with the trans-hydrogenation process. Although most of the products were the same with the 1HY system, the % yield were generally higher that those obtained with the 1HY system

Table 22: Product yield of the trans-hydrogenation over 1,5HD system at 773 K

	P	H	P+H	P+H Theory
	Conversion (%)			
Pentane(P)	11		91	11
1,5-hexadiene(1,5HD)		99	99	99
	Yield (%)			
Iso-pentane	1.01		0.23	1.01
1-Pentene			0.15	0
Trans-2-Pentene	8.59			8.59
Hexane		5.47	2.66	5.47
1-Hexene		2.03	1.36	2.03
2-Hexene		1.87	2.55	1.87
3-Hexene		11.75	7.37	11.75
methyl-2-pentene		8.96	13.47	8.96
3-Methylpentyne		0	0.92	
3-Methyl-1-hexene		5.18	20.48	5.18
Benzene		0	4.74	
3-Methylhexane		19.65	10.41	19.65
2-Methyl-1,3-pentadiene		12.57	23.91	12.57
2-Methyl-1-hexene		4.59	4.54	4.59
Methylcyclohexane	0.61	4.64	9.74	5.25
Ethylcyclopentane	0.37	1.38		1.75

Table 23: Product yield of the trans-hydrogenation over 1,5HD system at 673 K

	P	H	P+H	P+H Theory
	Conversion (%)			
Pentane(P)	08		91	91
1,5-hexadiene(1,5HD)		99	99	99
	Yield (%)			
Iso-pentane	0.46		0.21	0.46
1-Pentene				0
Trans-2-Pentene	0.53			0.13
Hexane		1.84	0.47	1.84
1-Hexene		0.79	1.61	0.79
2-Hexene		0.95	1.47	0.95
3-Hexene		2.73	5.41	2.73
Methyl-2-pentene		6.97	8.34	6.97
3-Methylpentyne		0		0
3-Methyl-1-hexene		20.52	19.45	20.52
Benzene		0.62	0.25	0.62
3-Methylhexane		12.28	5.58	12.28
2-Methyl-1,3-pentadiene		19.76	19.36	19.76
2-methyl-1-1hexene		1.66	4.02	1.66
Methylcyclohexane	3.91	1.58	9.49	5.86

Table 24: Product yield of the trans-hydrogenation over 1,5HD system at 623 K

	P	H	P+H	P+H Theory
	Conversion (%)			
Pentane(P)	10		91	91
1,5-hexadiene(1,5HD)		99	99	99
	Yield (%)			
Iso-pentane				0
1-Pentene			0.13	0
Trans-2-Pentene	0.08		0.35	0.08
Hexane		0.89	1.17	0.89
Hexene		0.31	0.39	0.31
2-Hexene		0.91	1.17	0.91
3-Hexene		4.12	4.16	2.12
Methyl-2-pentene		5.01	4.37	5.01
3-Methylpentyne				0
3-Methyl-1-hexene		17.53	16.53	17.53
Benzene			0.34	0
3-Methylhexane		11.56	6.6	11.56
2-Methyl-1,3-pentadiene		19.85	19.84	15.85
2-Methyl-1-1hexene		2.37	3.87	2.37
Methylcyclohexane	5.23	6.49	10.59	11.72
Ethylcyclopentane	1.25			1.25

Table 25: Product yield of the trans-hydrogenation over 1,5HD system at 573 K

	P	H	P+H	P+H Theory
	Conversion (%)			
Pentane(P)	04		87	87.88
1,5-Hexadiene(1,5HD)		99	99	99.81
	Yield (%)			
Iso-pentane				0
1-Pentene				0
Trans-2-Pentene	0.02		0.24	0.02
Hexane		0.53	0.83	0.53
1-Hexene		0	0.23	0
2-Hexene			1.81	0
3-Hexene		4.56	5.37	1.56
methyl-2-pentene		3.26	4.74	3.26
3-Methylpentyne				0
3-methyl-1-hexene		15.83	15.74	13.83
Benzene				0
3-Methylhexane		15.64	7.99	15.64
2-Methyl-1,3-pentadiene		21.17	19.25	21.17
2-Methyl-1-1hexene		3.31	3.48	3.31
Methylcyclohexane	0.22	6.47	12.34	6.47
Ethylcyclopentane	0.39			0.39

Table 26: Product yield of the trans-hydrogenation over 1,5HD system at 523 K

	P	H	P+H	P+H Theory
	Conversion (%)			
Pentane(P)	0.9		89	0.9
1,5-Hexadiene(1,5HD)		98	99.71	98
	Yield (%)			
Iso-pentane			0.006	0
1-Pentene				0
2-Pentene	0.008		0.21	0.008
Hexane		6.58	0.54	6.58
1-Hexene		0	0.15	0
2-Hexene		0.16	0.56	0.16
3-Hexene		2.36	4.17	0.36
Methyl-2-pentene		5.21	5.73	5.21
3-Methylpentyne			0	0
3-Methyl-1-hexene		28.45	7.67	28.45
Benzene		0.42	0	0.42
3-Methylhexane		8.82	3.83	8.82
2-Methyl-1,3-pentadiene		22.5	16.58	22.5
2-Methyl-1-1hexene		4.5	9.15	1.5
Methylcyclohexane		4.07	21.94	4.07

There is an increase in the yield of the total olefins with increasing reaction temperature; ~50 % total olefin is obtained at 773 K. The total olefin comprises also the alkylated olefins, and the olefin to alkylated olefins ratio is about 1:4 at most temperatures. However, the total valuable product which is the summation of both the olefins, alkylated olefins and alkylated products is ~60% using the 1,5HD system at 773 K. Higher yield of the valuable products were predominantly observed at higher temperatures as presented in Figure 52. The olefin production is observed to be higher than the other valuable as presented in Figure 53. There is also an increase in these valuable products with the reaction temperature (Figure 54)

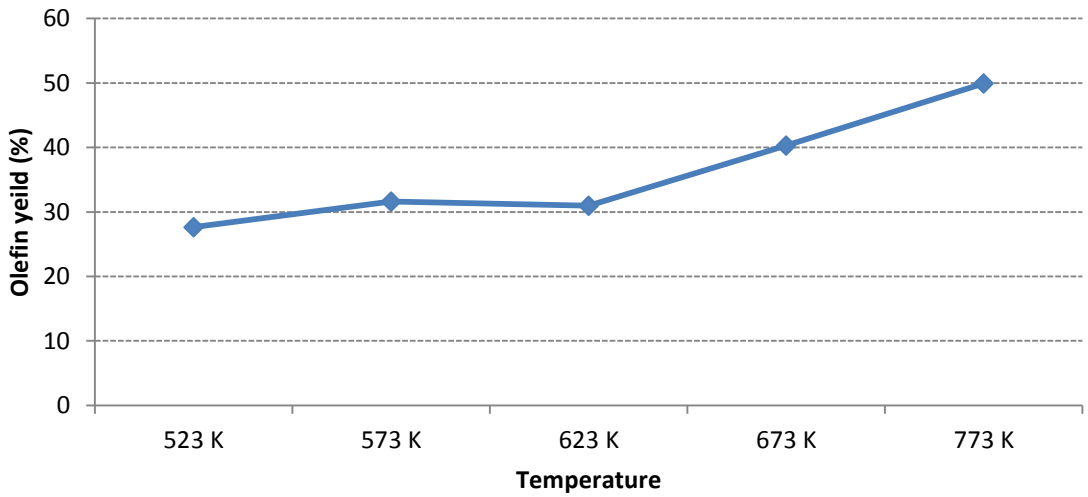

Figure 52: Total olefin yield with temperature over the $CrOx/Al_2O_3$ using 1,5HD system

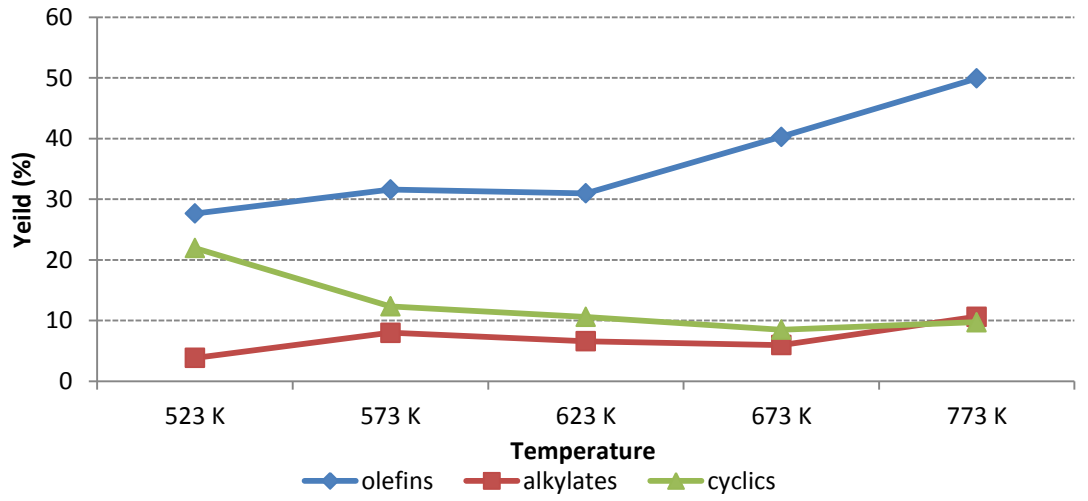

Figure 53: Profile of valuable product relative to the reaction temperature over $CrOx/Al_2O_3$ using 1,5HD system

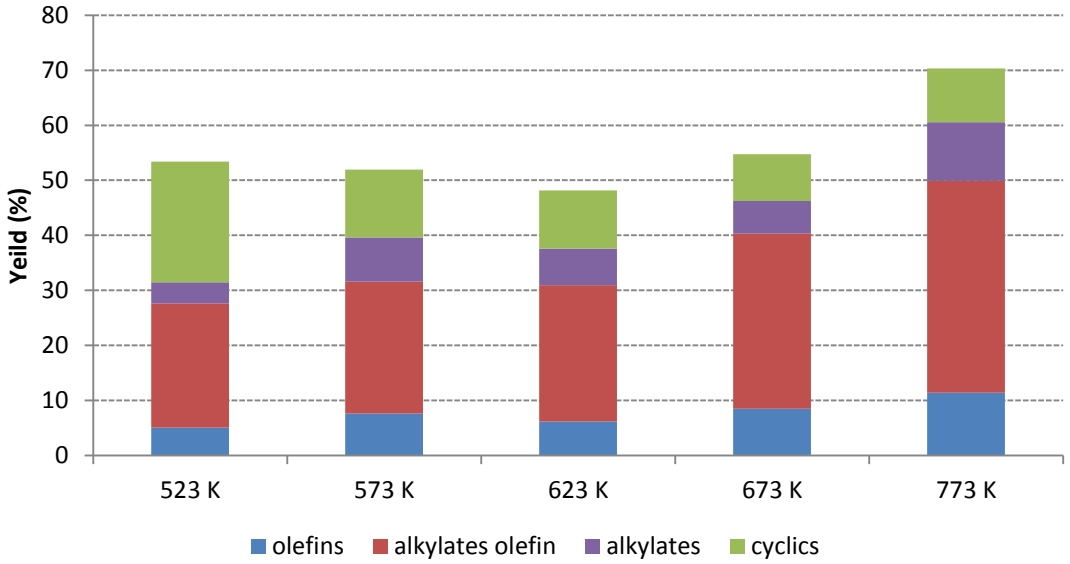

Figure 54: Relationship of the valuable products over $CrOx/Al_2O_3$ using 1,5HD system

The eluent gas products analysis using this system also confirms the evolution of hydrogen from the start of the reaction. Unlike the 1HY system, the hydrogen evolution here gradually declined but was maintained in the reaction stream. There is a significant reduction of the hydrogen at ~20 min before the gradual decline. However, at this very period of time, there was evolution of C_3H_6 and C_4H_8 which increased over the reaction period. C_3H_8 and C_4H_8 were evolved in this system confirming that the 1,5HD behaves differently to the 1HY on the catalyst surface. Although they have the same molecular formula (C_6H_{10}) they are of different configuration. This same gas evolution trend was observed at 773-623 K reaction temperatures while only pulses of gas were observed with the 573 K and 523 K. The result obtained at 723 K is presented in Figure 55 and 56

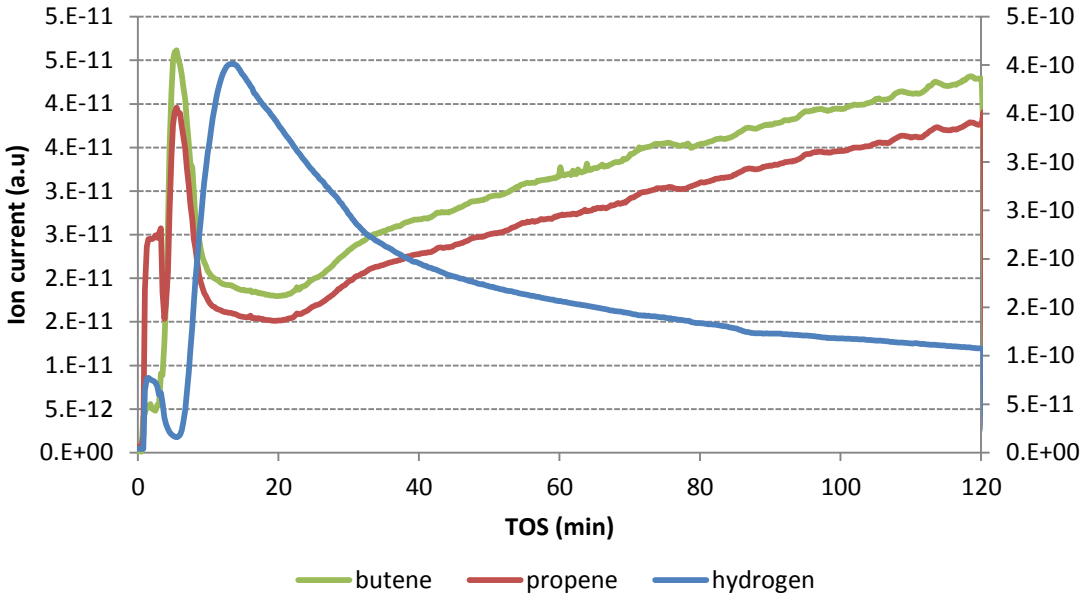

Figure 55: Profile of the evolved gases over $CrOx/Al_2O_3$ using 1,5HD only at 723 K

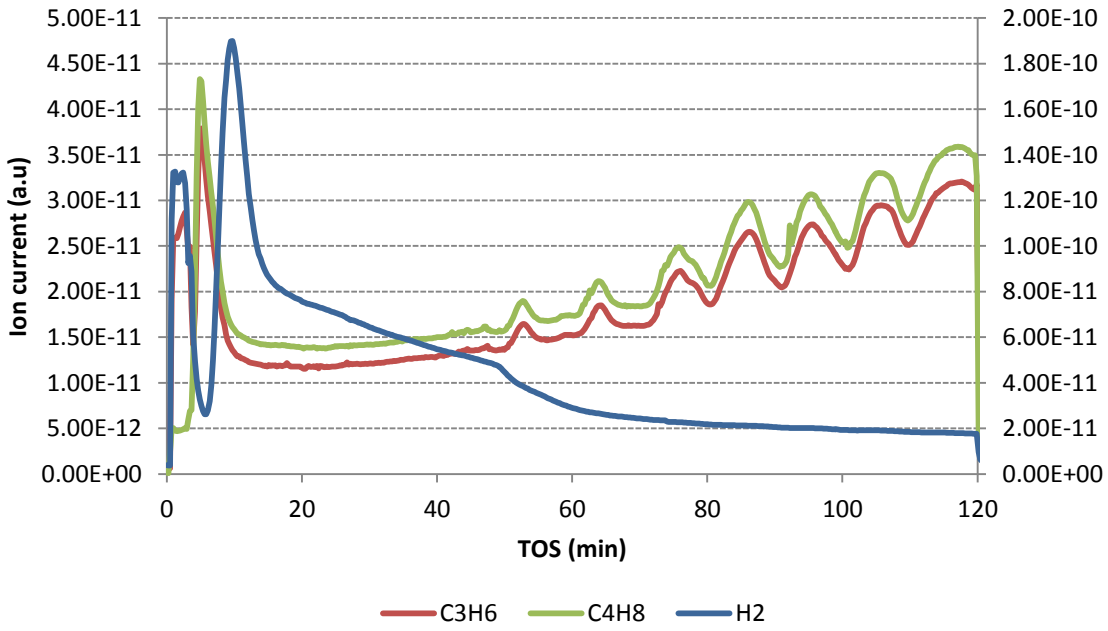

Figure 56: Profile of the evolved gases over $CrOx/Al_2O_3$ using P/1,5HD at 723K

Table 27: carbon balance for the trans-hydrogenation reaction over the $CrOx/Al_2O_3$ catalyst

Temperature (K)	Carbon balance (%)				
	Liquid [a] Ptds.	**C3H6 [b]**	**C4H8 [b]**	**Coke [c]**	**Pdts un-accounted**
773	**81**	**1.78**	**0.89**	**0.061**	**16.2**
673	**84**	**1.45**	**0.84**	**0.061**	**13.6**
623	**83**	**1.13**	**0.67**	**0.065**	**14.7**
573	**89**	**-**	**-**	**0.052**	**10.9**
523	**91**	**-**	**-**	**0.054**	**9.9**

a) Obtained from the GC analysis, b) obtained from the mass spec analysis, c) obtained from the TGA analysis

The hydrogenation reaction of 1,5-hexadiene also show similar reaction products and distribution obtained during trans-hydrogenation. There are also similarities observed in the major products obtained in the two processes, but the hydrogenation process exhibits a higher percentage yield of these products and there is general increase in the olefin products. However, it is clearly observed that there is observed trans-hydrogenation comparing the two processes together. The results are presented in Table 28-30. Higher conversions of the reactants were obtained approximately the same with the trans-hydrogenation process at all the tested reaction temperatures.

Table 28: Products yield during the hydrogenation of 1,5HD over $CrOx/Al_2O_3$ at 623 K

	1,5HD + 2% H_2/N_2	P+1,5HD	P+15HD Theory
Iso-pentane			0
Pentene		0.13	0
Trans-2-Pentene		0.35	0.08
Hexane	0.75	1.17	0.89
Hexene	5.77	0.39	0.31
2-Hexene	0.75	1.17	0.91
3-Hexene	3.4	4.16	2.12
Methyl-2-pentene	4.76	4.37	5.01
3-Methylpentyne			0
3-Methyl-1-hexene	30.59	16.53	17.53
Benzene		0.34	0
3-Methylhexane	3.99	6.6	11.56
2-Methyl-1,3-pentadiene	15.27	19.84	15.85
2-Methyl-1-1hexene	5.86	3.87	2.37
Methylcyclohexane	16.25	10.59	11.72
Ethylcyclopentane			1.25

Table 29: Products yield during the hydrogenation of 1,5HD over $CrOx/Al_2O_3$ at 573 K

	1,5HD + 2% H_2/N_2	P+1,5HD	P+15HD Theory
Iso-pentane			0
Pentene			0
Trans-2-Pentene		0.24	0.02
Hexane	0.74	0.83	0.53
Hexene	42.33	0.23	0
2-Hexene	0.79	1.81	0
3-Hexene	2.53	5.37	1.56
Methyl-2-pentene	1.57	4.74	3.26
3-Methylpentyne	0		0
3-Methyl-1-hexene	18.75	15.74	13.83
Benzene	0		0
3-Methylhexane	1.22	7.99	15.64
2-Methyl-1,3-pentadiene	11.82	19.25	21.17
2-Methyl-1-1hexene	2.45	3.48	3.31
Methylcyclohexane		12.34	6.47
Ethylcyclopentane			0.39

Table 30: Products yield during the hydrogenation of 1,5HD over $CrOx/Al_2O_3$ at 523 K

	1,5HD +2% H_2/N_2	P+1,5HD	P+15HD Theory
Iso-pentane		0.006	0
Pentene			0
Trans-2-Pentene		0.21	0.008
Hexane	5.58	0.54	6.58
Hexene	17.05	0.15	0
2-Hexene	0.31	0.56	0.16
3-Hexene	1.62	4.17	0.36
Methyl-2-pentene	2.14	5.73	5.21
3-Methylpentyne		0	0
3-Methyl-1-hexene	19.86	7.67	28.45
Benzene		0	0.42
3-Methylhexane	1.74	3.83	8.82
2-Methyl-1,3-pentadiene	8.3	16.58	22.5
2-Methyl-1-1hexene	4.6	9.15	1.5
Methylcyclohexane	6.25	21.94	4.07

4.2.3.2 Post reaction characterization and analysis

The TGA- weight loss analysis of the spent catalyst reveals a similar trend in the weight loss just like the 1HY system, where the amount of the loss material is observed as a function of the reaction temperature. The reaction at 773 K reveals a high loss with both the 1,5HD run alone and P/1,5HD trans-hydrogenation, and the catalyst run at 523 K reveals the lowest loss. The main loss occurred at ~ 530 – 710 K. However, general reduction in the weight loss was observed using the mixed feed trans-hydrogenation process as observed with 1HY

system, but there is general reduction in loss material compared with the 1HY system. The results are presented in Figure 57 and 58.

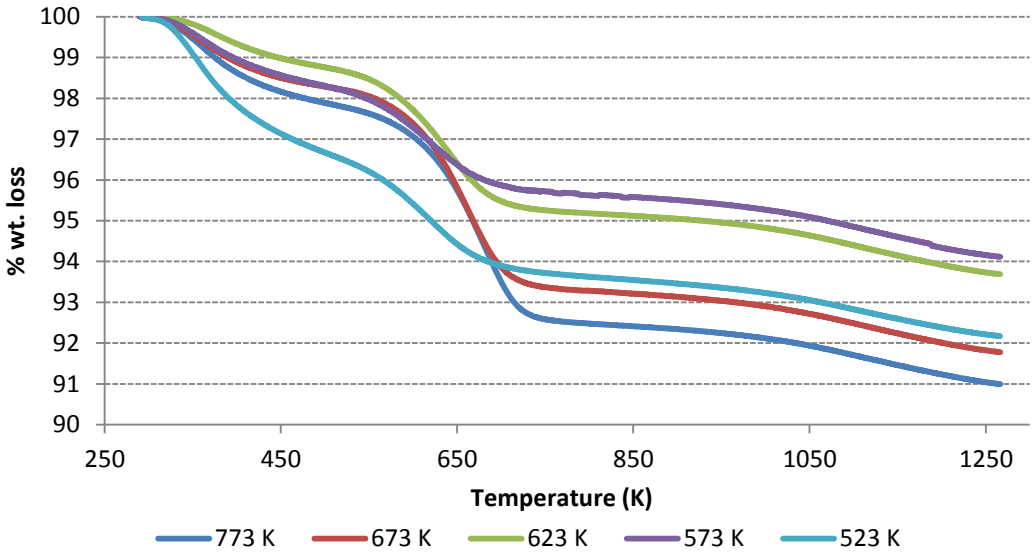

Figure 57: Weight loss profile of 1,5HD run alone over $CrOx/Al_2O_3$ catalyst

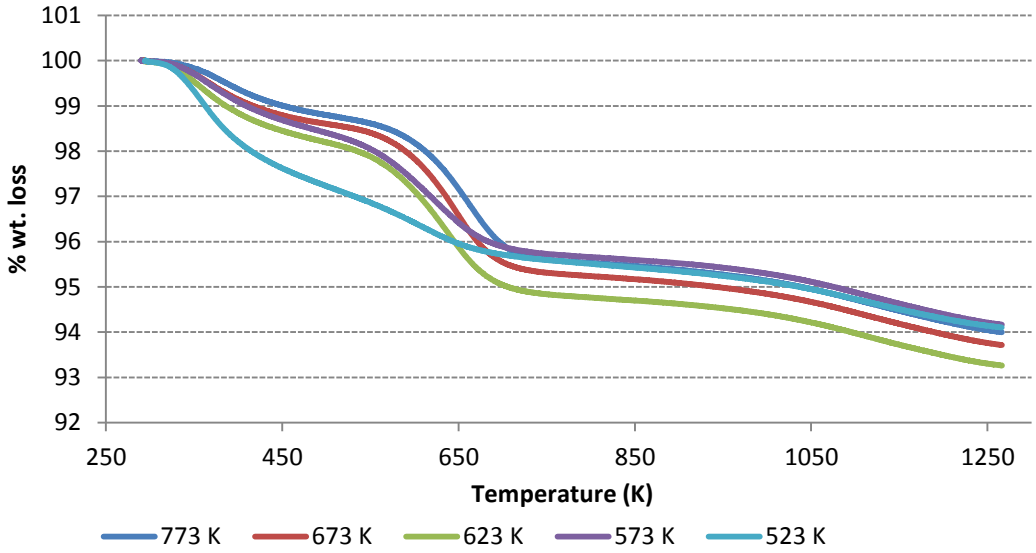

Figure 58: Weight loss profile of P/1,5HD mixed feed over $CrOx/Al_2O_3$ catalyst

The TPO analysis during the TGA confirmed that the weight loss was due to the combustion of surface carbon. This was determined by the mass spectrometer (m/e 44). However, in addition to this, fragments (m/e 2, 16, 18 and 28) were also monitored. Unlike the 1HY system only traces of water was detected in some of the samples. There was also observed a shift in the CO_2 desorption peak

with reaction temperature using this system. The results are presented in Figure 59 and 60. A similar effect of the shift in the CO_2 evolution with the reaction temperature was observed with the hydrogenation spent catalyst. The results are presented in Figure 61.

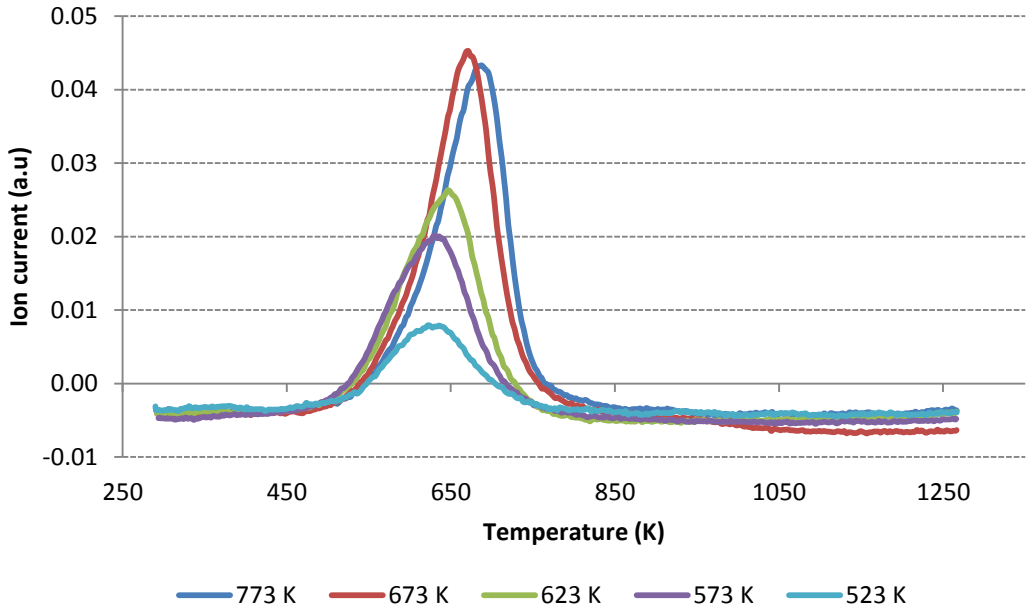

Figure 59: TPO profile of 1,5HD run alone over CrO_x/Al_2O_3 catalyst

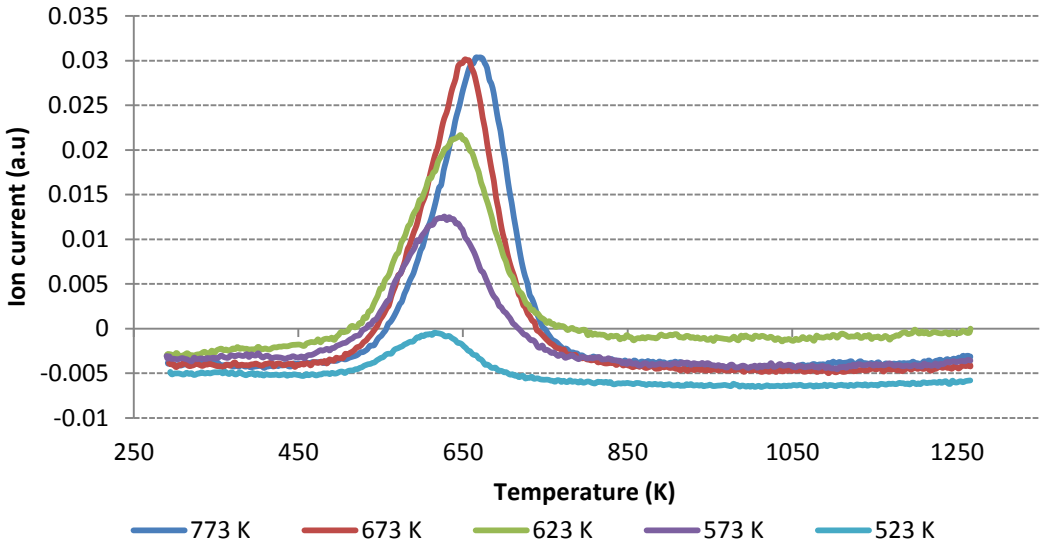

Figure 60: TPO profile of P/1,5HD mixed feed over CrO_x/Al_2O_3 catalyst

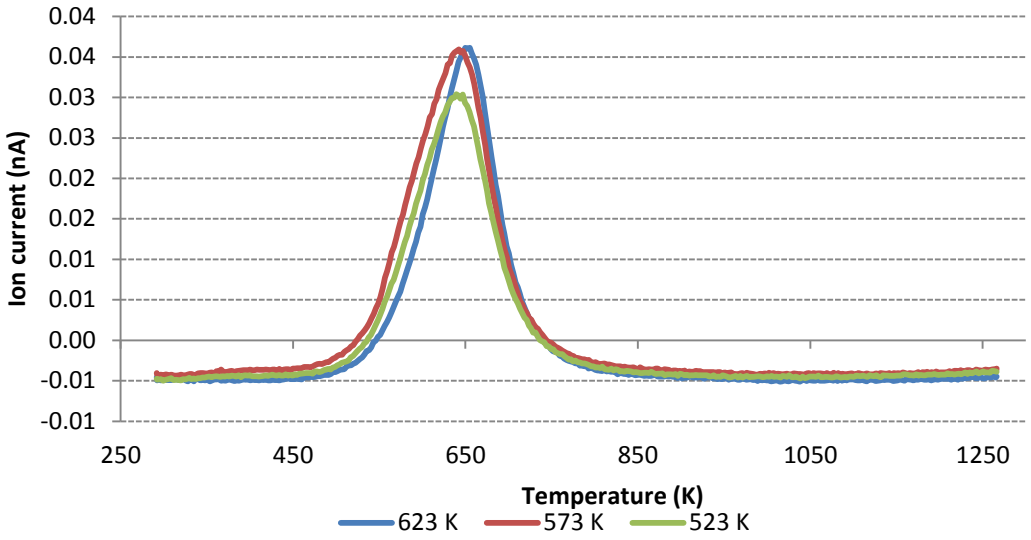

Figure 61: TPO profile during 1,5HD hydrogenation over CrO_x/Al_2O_3 catalyst

The loss of these species matches the TGA derivative weight loss profile and their evolution masses and loss can be assigned to CO_2. The result obtained at 723 K is presented in Figure 62. m/e 2 was detectable in the eluant of the hydrogenation spent catalyst. The result is presented in Figure 63.

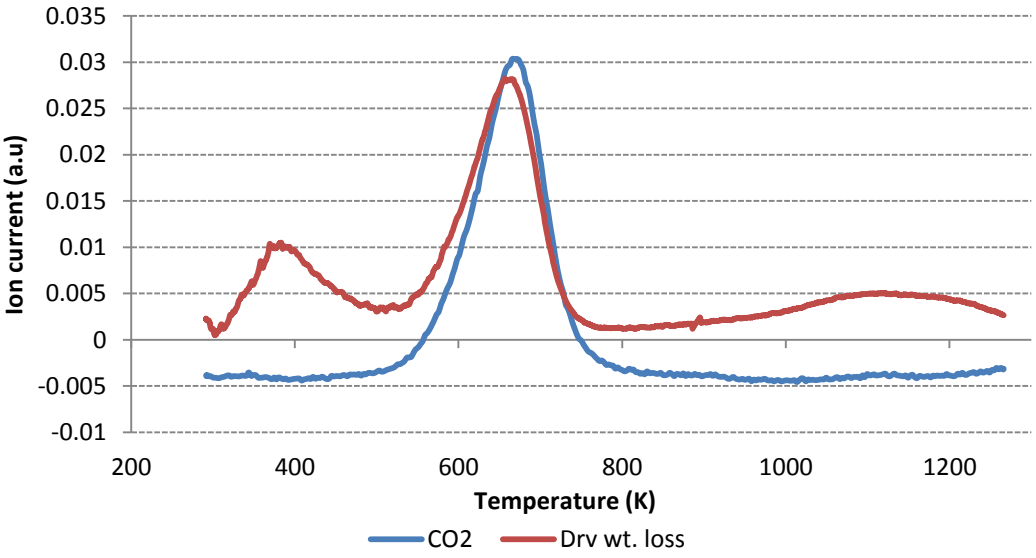

Figure 62: Species obtained during the TPO-MS using 1,5 HD system with CrO_x/Al_2O_3 catalyst

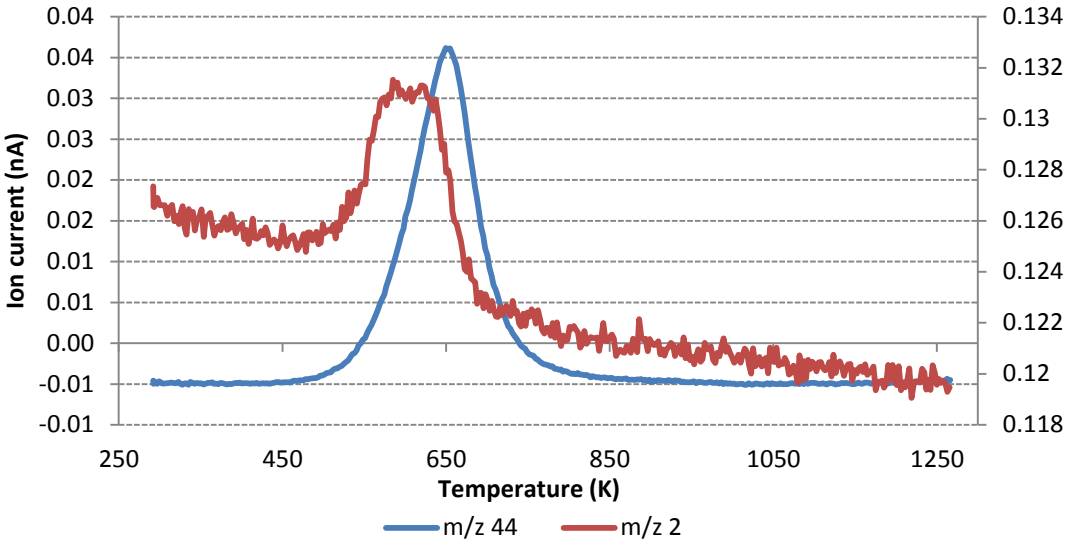

Figure 63: Mass spectra data obtained from TPO during the 1,5HD hydrogenation over $CrOx/Al_2O_3$ catalyst at 623 K

There are also changes observed in the amount of the carbon species desorbed from the surface of each catalyst over the reaction temperatures range using the 1,5HD system. The amount of the carbon species desorbed depends on whether the 1,5HD was fed individually or as mixed feed trans-hydrogenation process. There is also general reduction in the amount of the carbon compare to the 1HY system. Samples, which have been subjected to 1,5HD reactant only, show higher amount of weight loss, but there is a reduction observed in this amount during the trans-hydrogenation process observed with temperature 773-623 K. There is no obvious change observed at lower temperature (573-523 K) and the amount of this material is almost the same fed individually or as mixed feed. The percentage carbon deposit for each run individually and as a mixed feed is determined and presented in Figure 64

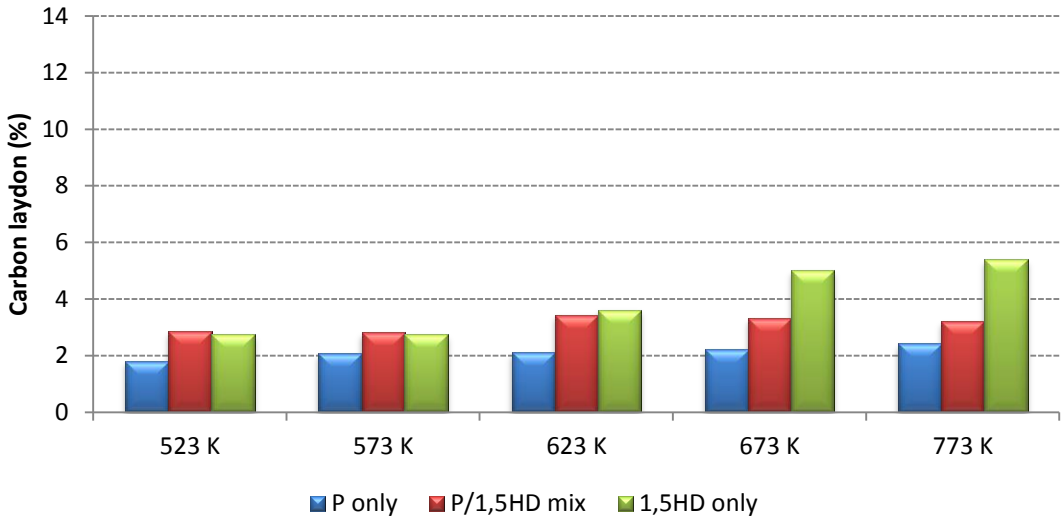

Figure 64: Carbon laydown of the spent CrO_x/Al_2O_3 catalyst over the set temperatures

The amount of carbon formed related to the reactant feed were summarized and presented in Table 31. It is observed that there is clear reduction of the carbon formation with the trans-hydrogenation system.

Table 31: Total amount of carbon deposited on spent CrO_x/Al_2O_3 catalyst at various temperatures using 1,5HD system

Temperature (K)	Carbon deposited (g/g feed)		
	P	P/1,5HD	1,5HD
523 K	0.0035	0.0045	0.0054
573 K	0.0040	0.0044	0.0054
623 K	0.0041	0.0054	0.0071
673 K	0.0044	0.0052	0.0098
773 K	0.0048	0.0051	0.0105

The Raman spectroscopic analysis of the spent catalysts was obtained using UV radiation for the studies of the carbon deposit similar to the 1HY system. The Raman spectrum shows Raman bands assigned to coke deposition at ~1380 and 1600 cm^{-1} related to D and G bands respectively this was only observed with 1,5HD feed at 773 K, only G bands were observed at low temperature (573-523 K) as there is no clear evidence for the D bands. The D band was lost using the

mixed feed process and only G bands are observed at all the reaction temperatures. This behaviour is similar to the 1HY system. The results are presented in Figure 65 and 66

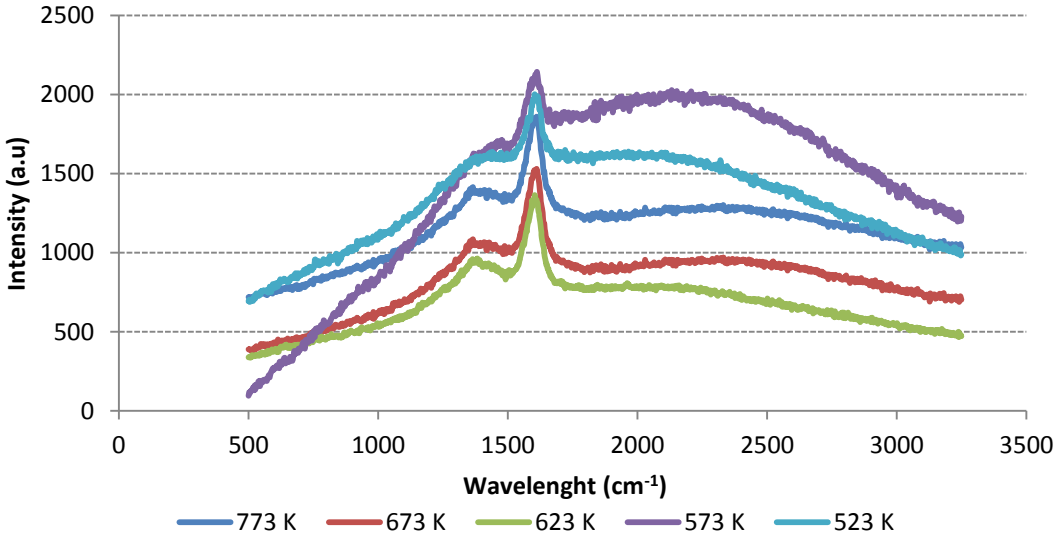

Figure 65: Raman spectra of spent CrO_x/Al_2O_3 catalyst for sole 1,5HD obtained using the UV-radiation

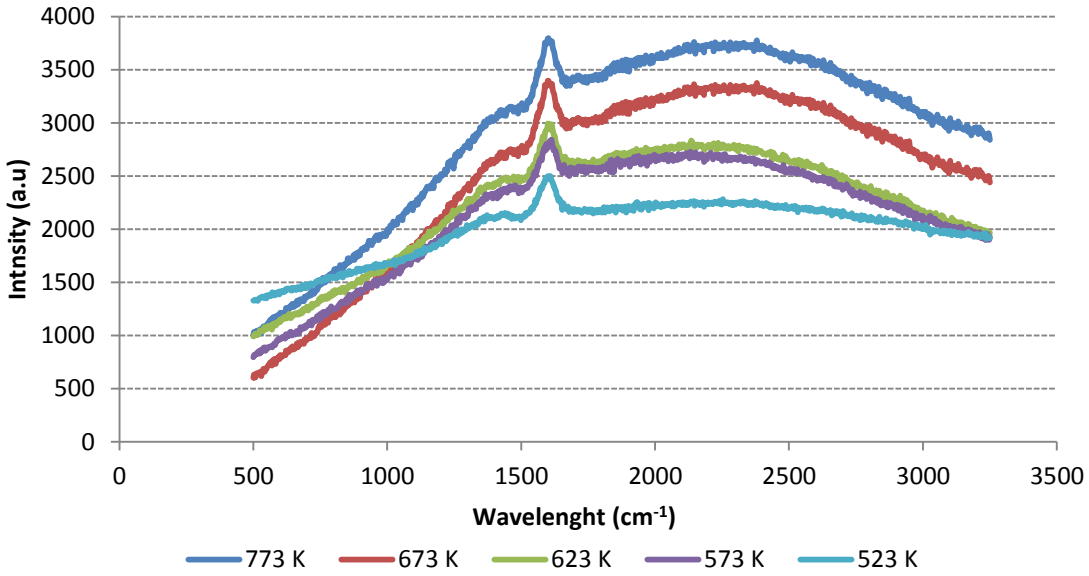

Figure 66: Raman spectra of spent CrO_x/Al_2O_3 catalyst for mixed feeds obtained using the UV-radiation

The BET analysis performed on the spent catalyst also suggests that the formation of coke on the catalyst surface decreases the S_{BET} and the pore

volume. Significant loss in the S_{BET} observed with all the samples, just like with the 1HY system. Samples which had been subjected to the pentane run showed less surface area loss compared to the 1,5HD and the mixed feed. The S_{BET} reduction is observed as a function of temperature the losses are more significant at high reaction temperature. A plot of S_{BET} vs. reaction temperature was obtained to relate the effect of reaction temperature on the catalyst BET surface area. However, the 1HY system exhibit much higher loss compared to the 1,5HD system at all reaction temperatures. The result is presented in Figure 67

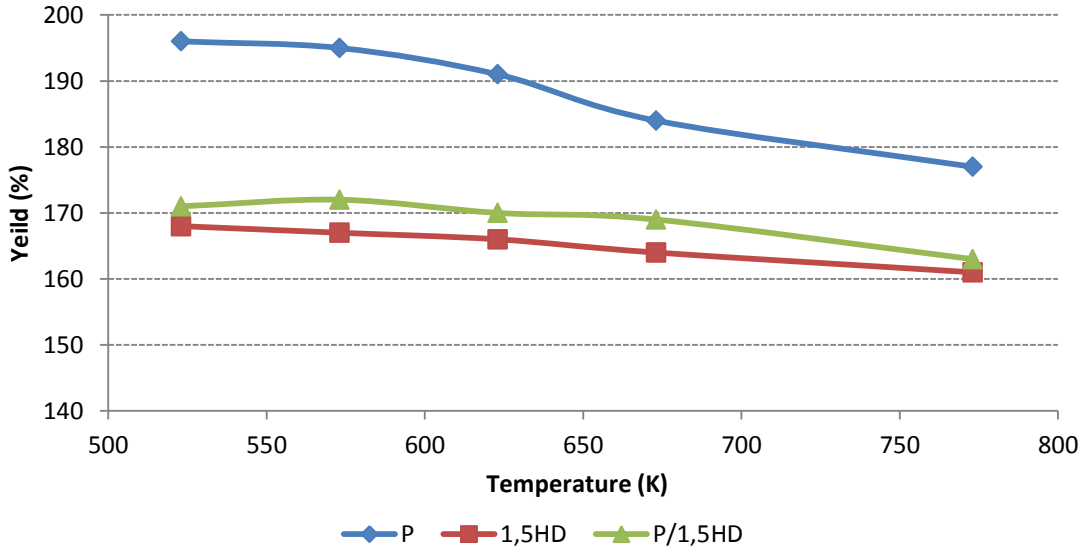

Figure 67: Effect of temperature on the surface area on the spent CrO_x/Al_2O_3 catalyst using 1,5HD system

The XRD analysis of the spent catalyst using the 1,5HD system also revealed only the diffraction pattern for γ-alumina

3.2.4 Pentane/2,4-Hexadiene (P/2,4HD) system

3.2.4.1 Reaction analysis and trans-hydrogenation activity evaluation

Reactant conversions were followed individually and during the mixed trans-hydrogenation reaction using the 2,4HD system. The conversion of pentane was poorer, and conversions lower than when pentane was run individually except at 623 K. Slightly higher conversion (~17 %) was obtained compared to when pentane was run individually (~10 %). The trans-hydrogenation process does not improve the conversion of the pentane dehydrogenation and there is no significant increase in the equilibrium conversion of pentane dehydrogenation unlike with the 1HY and 1,5HD systems. This is consistent with the thermodynamic limitation as explained in (section 3.1), reaction with 2,4-HD is not expected to lift this limitation. The result is presented in Figure 68

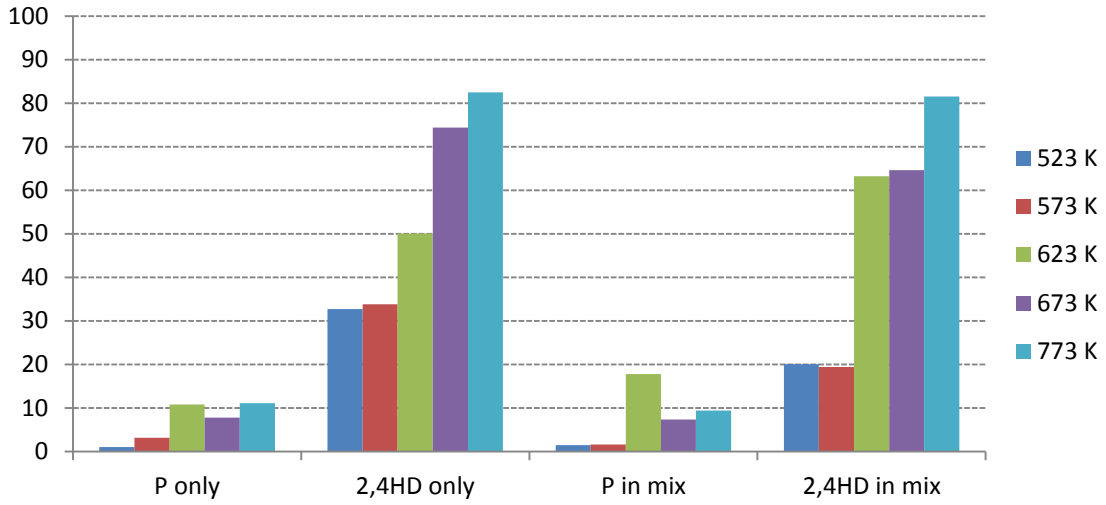

Figure 68: Conversion comparison of P, 2,4HD and P/2,4HD mixture using $CrOx/Al_2O_3$

The reaction using 2,4HD was performed with 2:1 cis/trans mixture. It is observed that the both forms of the 2,4HD react differently during the trans-hydrogenation and when fed alone. The trans-2,4HD reacted faster than the cis-2,4HD and higher conversions of the trans-2,4HD were obtained at all reaction temperatures compare to the cis-2,4HD. There is a general decrease in the conversions of both cis/trans during the trans-hydrogenation and cis presented zero conversion at lower temperature (573-523 K). The result is in Figure 69

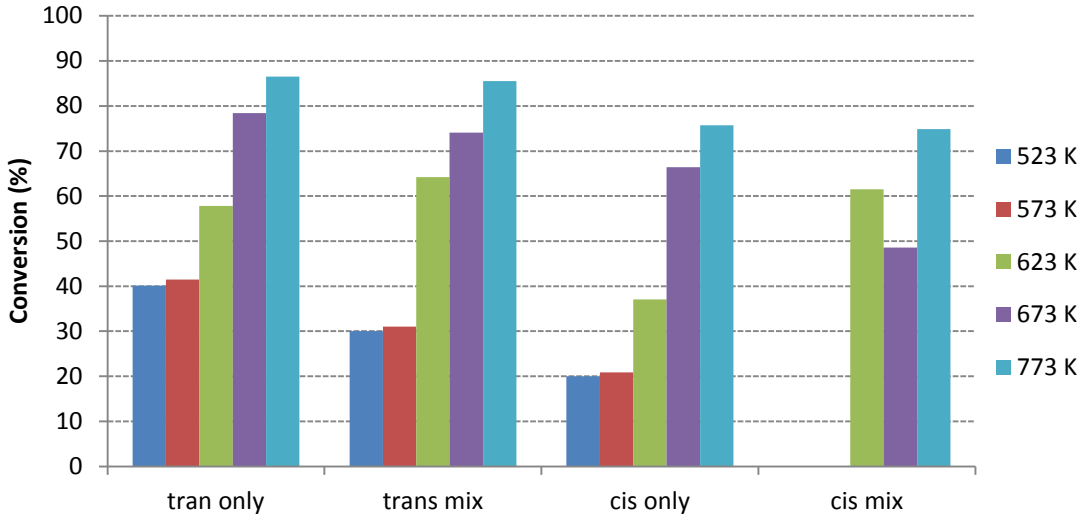

Figure 69: Conversion comparison of cis/trans 2,4HD using CrO_x/Al_2O_3

The products yields were calculated and presented in Table 32-36. Low percentage yield of the valuable products obtained with this system. Most of the reaction products observed with the other two systems were seen here. However, the product distribution is similar at all the reaction temperatures just like the other reaction systems, only the individual yield of the products changes.

Table 32: Products yield of the trans-hydrogenation over CrO_x/Al_2O_3 using 2,4HD system at 773 K

	P	H	P+H	P+H Theory
	Conversion (%)			
Pentane(P)	11		9.4	11
2,4-Hexadiene(2,4HD)		82	81	82
Cis-2,4HD		75	74	
Trans-2,4HD		86	85	
	Yield (%)			
Iso-pentane	1.01			1.01
Pentene			0.03	0
Trans-2-Pentene	8.59		0.1	8.59
Hexane		1.99	2.55	1.99
1-Hexene		0.42	0.23	0.42
2-Hexene		0.93	0.53	0.93
3-Hexene		2.53	3.65	2.53
Methyl-2-pentene		6.89	7.11	6.89
Benzene		2.25		2.25
2-Methyl-1,3-pentadiene		22.5	5.58	22.5
Methylcyclohexane	0.61	12.64	12.33	13.25
Ethylcyclopentane	0.37			0.37

Table 33: Products yield of the trans-hydrogenation over CrO_x/Al_2O_3 using 2,4HD system at 673 K

	P	H	P+H	P+H Theory
	Conversion (%)			
Pentane(P)	08		07	08
2,4-Hexadiene(2,4HD)		74	64	74
Cis-2,4HD		74	48	
Trans-2,4HD		78	66	
	Yield (%)			
Iso-pentane	0.46			0.46
Pentene			0.09	0
Trans-2-Pentene	0.53			0.13
Hexane		1.92	0.86	0.92
1-Hexene		0.3	0.26	0.3
2-Hexene		0.87	2.6	0.87
3-Hexene		2.35	2.17	2.35
Methyl-2-pentene		4.18	5.97	4.18
2-Methyl-1,3-pentadiene		21.52	10.58	21.52
Methylcyclohexane	3.91	11.87	10.12	15.78

Table 34: Products yield of the trans-hydrogenation over CrO_x/Al_2O_3 using 2,4HD system at 623 K

	P	H	P+H	P+H Theory
	Conversion (%)			
Pentane(P)	10		17	10
2,4-Hexadiene (2,4HD)		50	63	50
Cis-2,4HD		64	61	
Trans-2,4HD		57	37	
	Yield (%)			
Iso-pentane			0.41	
Pentene			0.12	0
Trans-2-Pentene	0.08			0.08
Hexane		2.4	1.18	0.4
1-Hexene		0.14	0	0.14
2-Hexene		0.45	0.21	0.45
3-Hexene		1.4	2.43	1.4
Methyl-2-pentene		4.03	6.21	4.03
2-Methyl-1,3-pentadiene		18.52	7.14	21.52
Methylcyclohexane	5.23	10.87	9.21	16.10
Ethylcyclopentane	1.25			1.25

Table 35: Products yield of the trans-hydrogenation over CrO_x/Al_2O_3 using 2,4HD system at 573 K

	P	H	P+H	P+H Theory
	Conversion (%)			
Pentane(P)	4		1.6	4
2,4-Hexadiene(2,4HD)		34	20	34
Cis-2,4HD		31	0	
Trans-2,4HD		41	21	
	Yield (%)			
Iso-pentane			0.04	0
Pentene			0.12	0
Trans-2-Pentene	0.02			0.02
Hexane		1.07	0.4	0.07
1-Hexene		0	0.14	0
2-Hexene		0.15	0.49	0.15
3-Hexene		0.48	1.56	0.48
Methyl-2-pentene		5.89	6.95	6.89
3-Methylhexane			2.2	0.41
2-Methyl-1,3-pentadiene		8.52	0	**8.52**
Methylcyclohexane	0.22	5.76	5.45	5.98
Ethylcyclopentane	0.39			0.39

Table 36: Products yield of the trans-hydrogenation over CrO_x/Al_2O_3 using 2,4HD system at 523 K

	P	H	P+H	P+H Theory
	Conversion (%)			
Pentane(P)	1		1.5	1
2,4-Hexadiene(2,4HD)		32	20	32
Cis-2,4HD		30	0	
Trans-2,4HD		40	20	
	Yield (%)			
Iso-pentane			0.01	0
Pentene				0
Trans-2-Pentene	0.008			0.008
Hexane		1.18	0.09	0.18
1-Hexene		0.04	0	0.04
2-Hexene		0.22	0.13	0.22
3-Hexene		0.73	1.48	0.73
Methyl-2-pentene		4.2	4.54	4.2
3-Methylhexane		3.82	4.08	3.82
2-Methyl-1,3-pentadiene		7.69	0	7.69
Methylcyclohexane		4.55	3.83	4.55

The total olefin yield obtained with the 2,4HD system is very low (~13%) at 773 K, compared with the other two systems. The result is presented in Figure 70. There is no clear difference in the olefin production compared to the other valuable products as presented in Figure 71 but there is an increase in these valuable products with the reaction temperature (Figure 72)

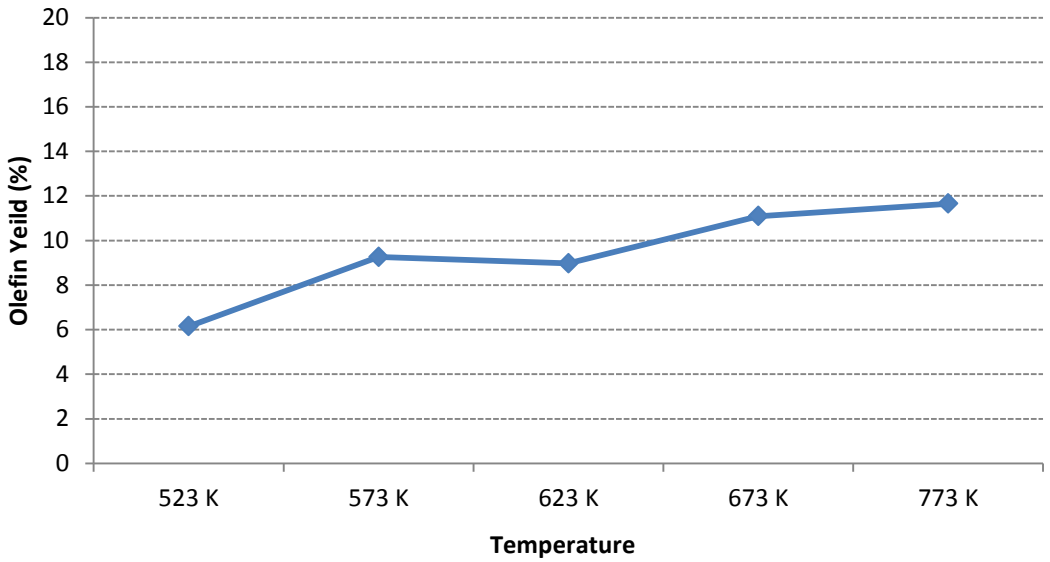

Figure 70: Total olefin yield with temperature over the CrO_x/Al_2O_3 using 2,4HD system

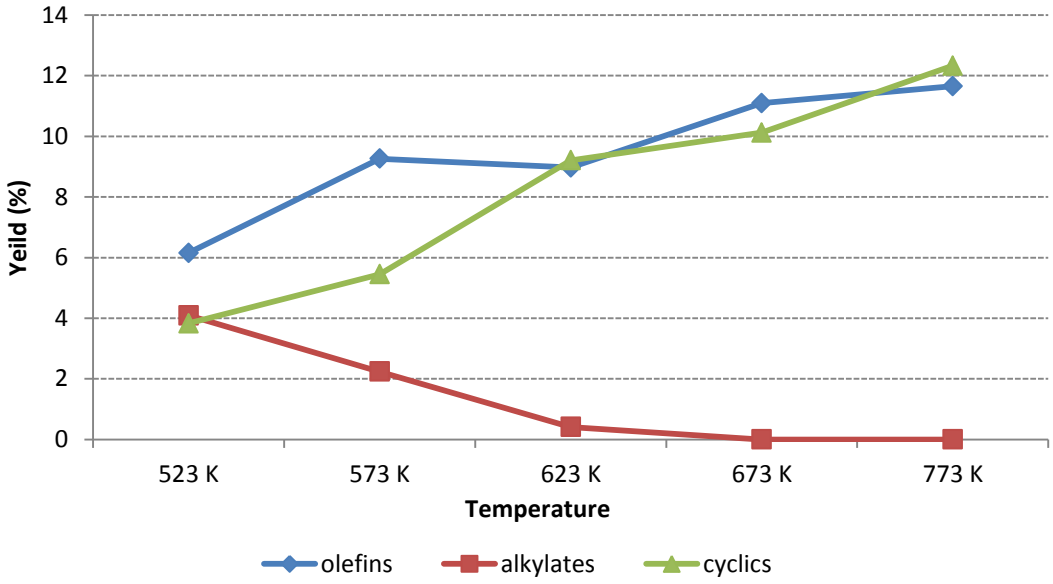

Figure 71: Profile of valuable product relative to the reaction temperature over CrO_x/Al_2O_3 using 2,4HD system

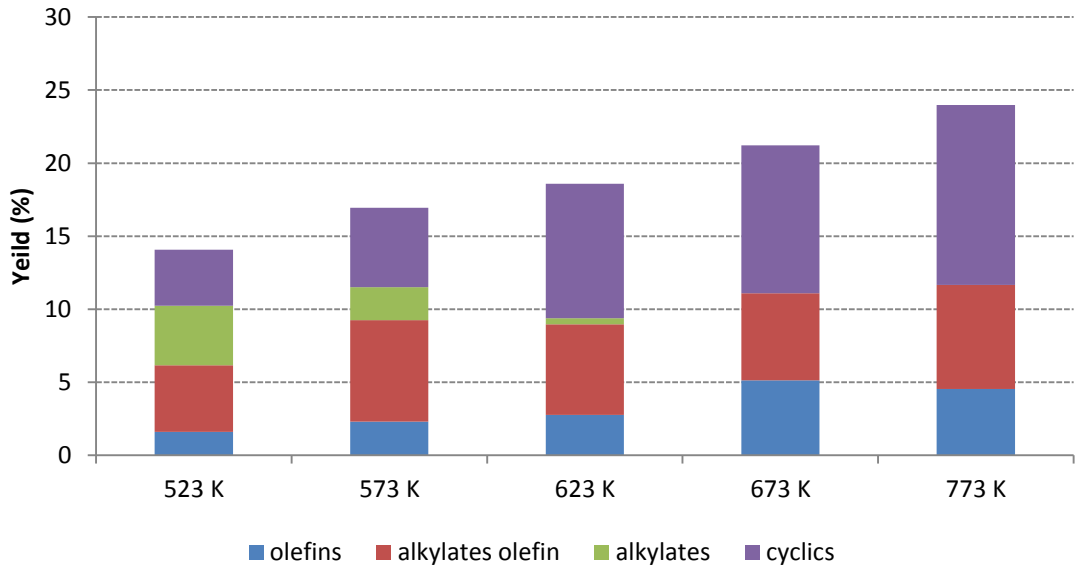

Figure 72: Relationship of the valuable products over CrO_x/Al_2O_3 using 2,4HD system

The eluent gas products analysis using 2,4 HD system also confirm the evolution of hydrogen from the start of the reaction. The hydrogen evolution also gradually declined but was maintained in the reaction stream similar to the 1,5HD system. There is a significant reduction of the hydrogen at ~20 min before the gradual decline. C_3H_6 and C_4H_8 evolution were observed also with this system, and increased and maintained on stream for the reaction period after the hydrogen declined from the reaction stream. C_3H_8 and C_4H_8 were evolved, which shows similar fragmentation with 1,5HD on the catalyst surface.

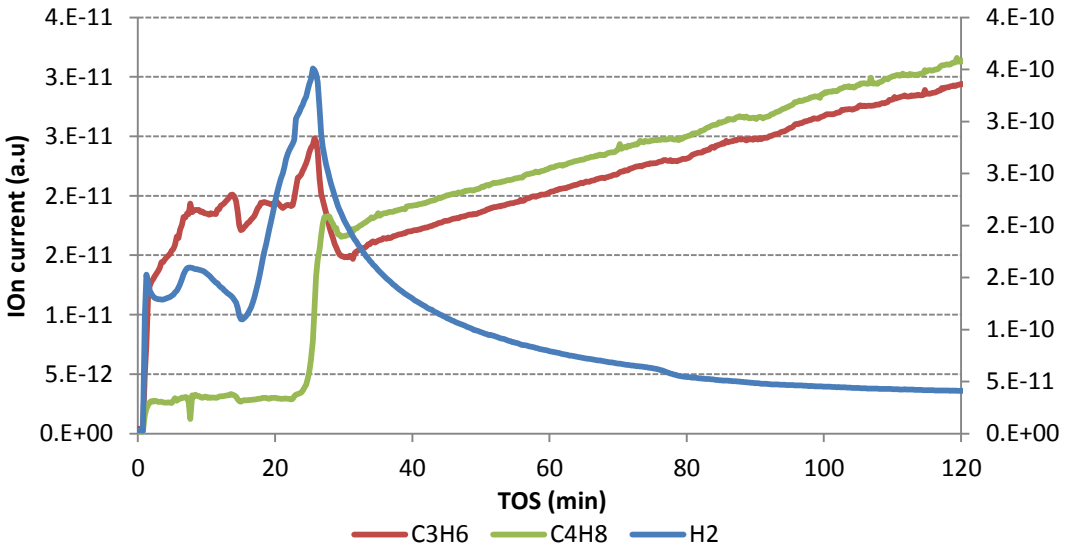

Figure 73: Profile of the evolved gases over CrO_x/Al_2O_3 using 2,4HD only at 723 K

2,4HD and 1,5HD are of the same class hexadiene but only that the arrangement of the two double bonds is different, so there is high tendency they might fragmented in the same way. The result obtained at 723 K is presented in Figure 73 and 74

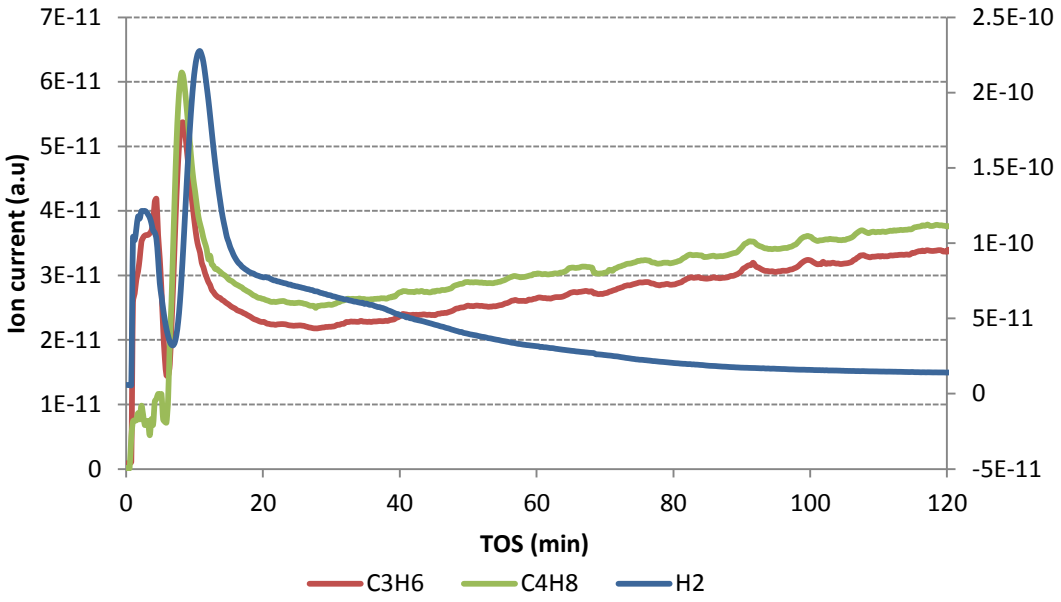

Figure 74: Profile of the evolved gases over CrO_x/Al_2O_3 using P/2,4HD mixed feed at 723 K

Table 37: carbon balance for the trans-hydrogenation reaction over the CrO_x/Al_2O_3 catalyst

Temperature (K)	Carbon balance (%)				
	Liquid [a] Ptds.	**C3H6 [b]**	**C4H8 [b]**	**Coke [c]**	**Pdts un-accounted**
773	**86**	**0.66**	**0.76**	**0.048**	**12.5**
673	**87**	**0.61**	**0.81**	**0.053**	**11.3**
623	**86**	**0.65**	**0.69**	**0.040**	**12.6**
573	**90**	**-**	**-**	**0.038**	**9.9**
523	**94**	**-**	**-**	**0.034**	**6.9**

a) Obtained from the GC analysis, b) obtained from the mass spec analysis, c) obtained from the TGA analysis

Table 38: Products yield during the hydrogenation of 2,4HD over CrO_x/Al_2O_3 at 623 K

	2,4HD + 2% H_2/N_2	P+H	P+H Theory
	Conversion (%)		
2,4-Hexadiene (2,4HD)	69	63	50
	Yield (%)		
Iso-pentane		0.41	
Pentene		0.12	0
Cis-2-Pentene	1.21		
Trans-2-Pentene			0.08
Hexane	1.25	1.18	0.4
1-Hexene	3.45	0	0.14
2-Hexene		0.21	0.45
3-Hexene	2.53	2.43	1.4
Methyl-2-pentene	4.34	6.21	4.03
2-Methyl-1,3-pentadiene	20.52	7.14	21.52
Methylcyclohexane	14.82	9.21	16.1
Ethylcyclopentane			1.25

Table 39: Products yield during the hydrogenation of 2,4HD over CrO_x/Al_2O_3 at 573 K

	2,4HD + 2% H_2/N_2	**P+H**	**P+H Theory**
	Conversion (%)		
2,4-hexadiene(2,4HD)	64	20	34
	Yield (%)		
Iso-pentane		0.04	0
Pentene		0.12	0
cis-2-Pentene			
Trans-2-Pentene	1.26		0.02
Hexane	2.01	0.4	0.07
1-Hexene	1.54	0.14	0
2-Hexene	1.15	0.49	0.15
3-Hexene	4.81	1.56	0.48
methyl-2-pentene	6.29	6.95	6.89
3-Methylhexane		2.2	0.41
2-Methyl-1,3-pentadiene	18.52	0	8.52
Methylcyclohexane	12.76	5.45	5.98
Ethylcyclopentane			0.39

Table 40: Products yield during the hydrogenation of 2,4HD over CrO_x/Al_2O_3 at 523 K

	2,4HD + 2% H_2/N_2	P+H	P+H Theory
	Conversion (%)		
2,4-Hexadiene(2,4HD)	51	20	32
	Yield (%)		
Iso-pentane		0.01	0
Pentene			0
Cis-2-Pentene	0.32		
Trans-2-Pentene			0.008
Hexane	2.18	0.09	0.18
1-Hexene	1.04	0	0.04
2-Hexene	1.22	0.13	0.22
3-Hexene	3.63	1.48	0.73
Methyl-2-pentene	4.83	4.54	4.2
3-Methylhexane	3.88	4.08	3.82
2-Methyl-1,3-pentadiene	9.72	0	7.69
Methylcyclohexane	10.53	3.83	4.55

4.2.4.2 Post reaction characterization and analysis

The TGA weight loss analysis of the spent catalyst shows a weight loss with the 2,4HD system, and the amount of lost material is also a function of the reaction temperature. There is also difference in the material loss across the reaction temperatures when the 2,4HD was fed individually compared to trans-hydrogenation where all the reaction temperatures exhibit similar weight loss. The reaction at 773 K present high loss with both the 2,4HD run alone and P/2,4HD trans-hydrogenation: the 523 K presents the lowest loss. The main loss of 2,4HD and the mixed feeds occurred at ~ 530 – 710 K. There is also evidence for another weight loss at higher temperature with some of the reaction temperatures. However, there is no clear reduction in the weight loss observed using the mixed feed trans-hydrogenation process as observed with both 1HY and 1,5HD systems, but there is general reduction in the amount of deposited material. The results are presented in Figure 75 and 76

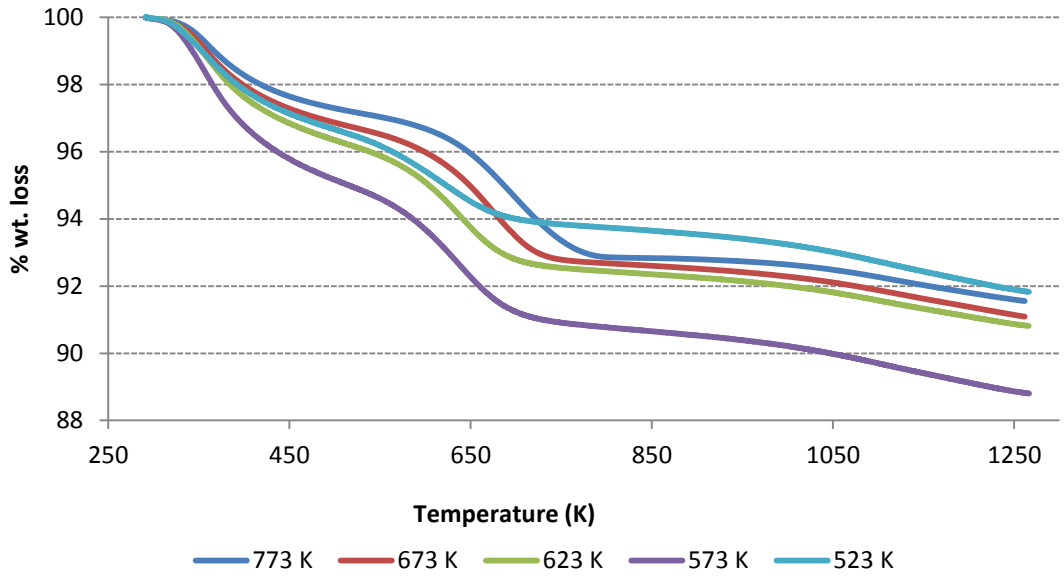

Figure 75: Weight loss profile of 2,4HD run alone over CrO_x/Al_2O_3 catalyst

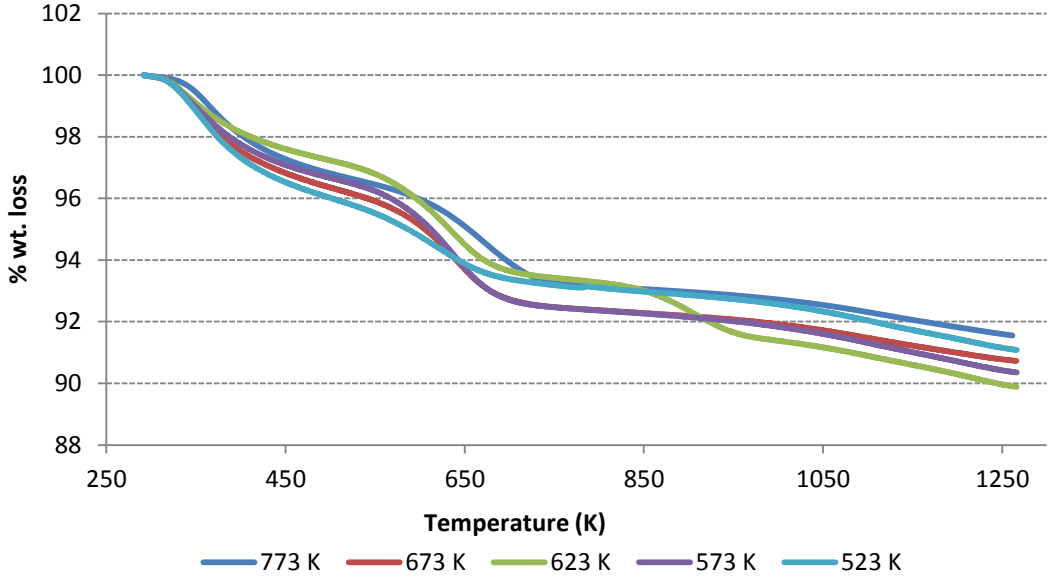

Figure 76: Weight loss profile of P/2,4HD mixed feed over CrO_x/Al_2O_3 catalyst

2,4HD desorption is similar to that of 1,5HD except for the evidence of additional desorbed species at higher temperature. However, the DTA analysis obtained the catalysts used at all reaction temperatures are the same with those obtained with the 1,5HD system and there is no peak associated with the higher temperature desorption species suggesting very minimal desorption. The DTA result exhibit one exothermic peak at ~673 K and one endothermic peak at ~420

K observed with both 1,5HD and 2,4 HD systems. The 1HY system exhibit an endothermic peak at ~523 K temperature. These two peaks were the main features observed with the whole three systems. The result is presented in Figure 77

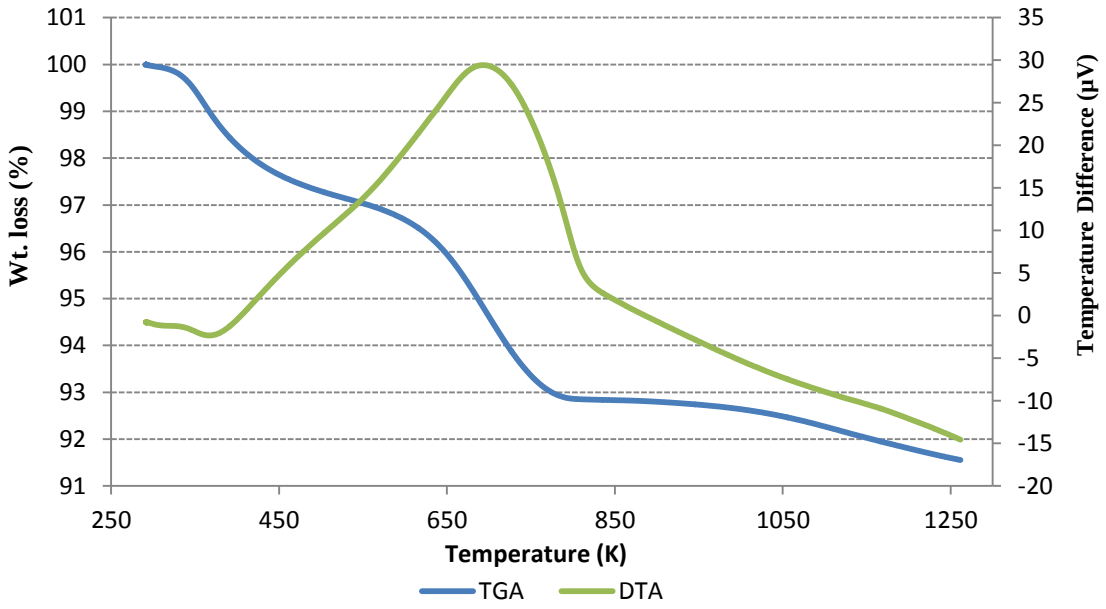

Figure 77: TGA/DTA profile of 2,4HD system over CrOx/Al2O3 catalyst

The TPO analysis during the TGA revealed carbon dioxide as the main desorption species evolved with the 2,4HD system. This was determined by mass spectrometry (m/e 44). However, in addition to this, fragments (m/e 2, 16, 18 and 28) were also monitored and like the 1,5HD system, only traces of water was detected in some of the samples. Unlike the 1,5HD system there is an observed shift in the CO_2 desorption peak with reaction temperature between the 773 K temperature and the other reaction temperatures. There is observed another evolution CO_2 at a higher temperature with 623-523 K reaction temperatures. The results are presented in Figure 78 and79. Similar TPO profiles were obtained during the hydrogenation process (Figure 80).

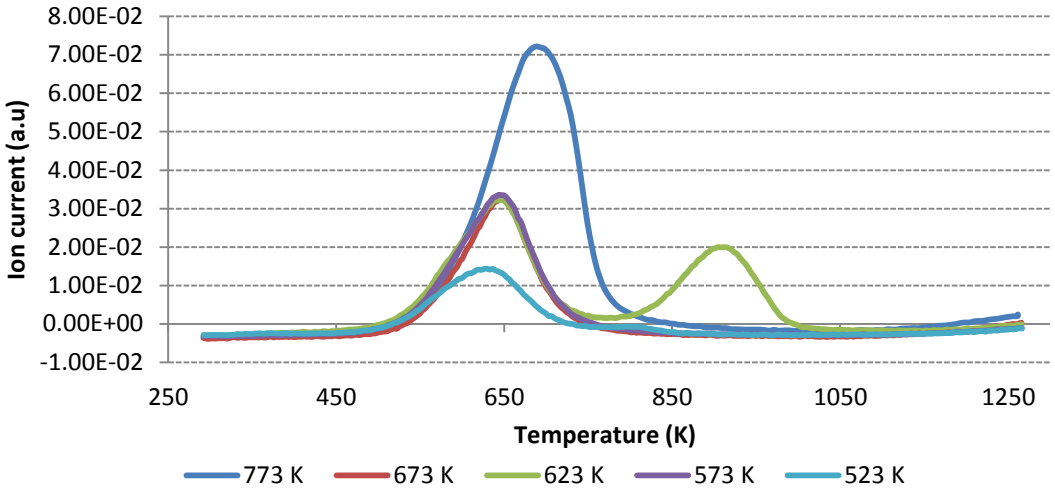

Figure 78: TPO profile of P/2,4HD mixed feed over CrO_x/Al_2O_3 catalyst

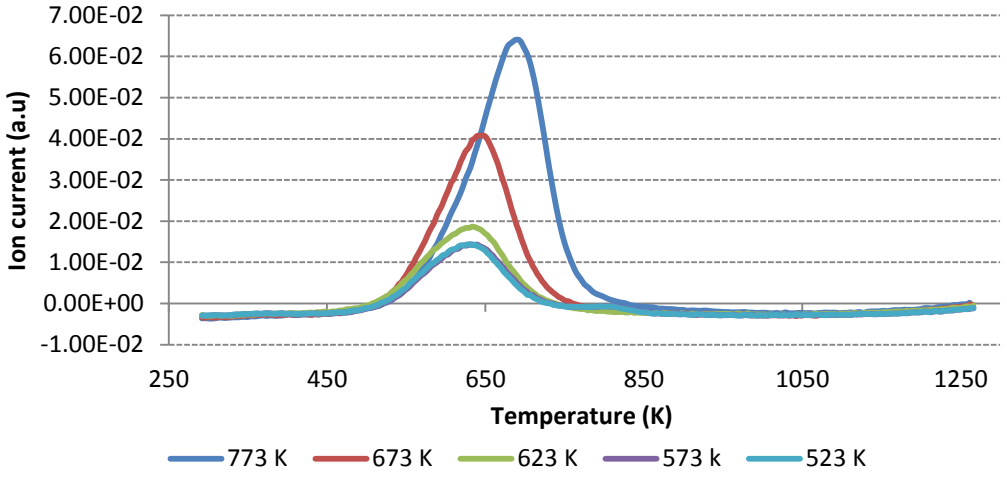

Figure 79: TPO profile of 2,4HD run alone over CrO_x/Al_2O_3 catalyst

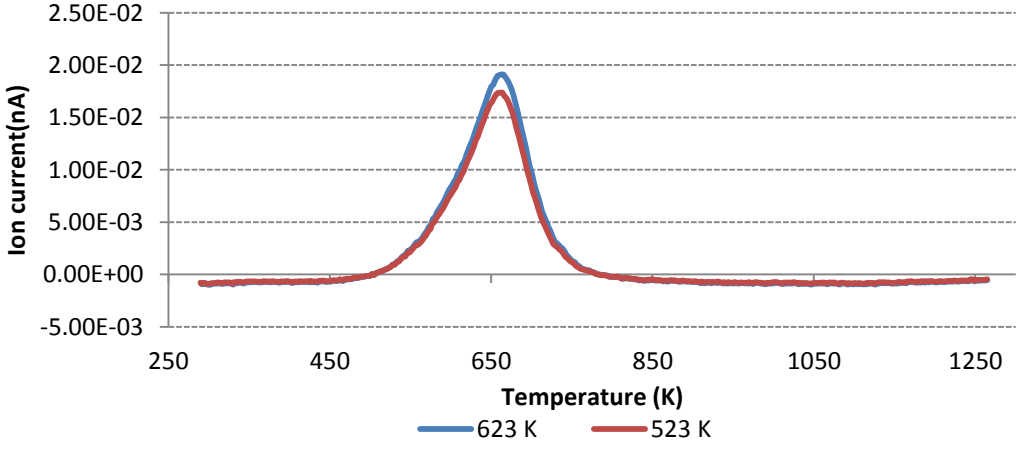

Figure 80: TPO profile of 2,4HD during hydrogenation over CrO_x/Al_2O_3 catalyst

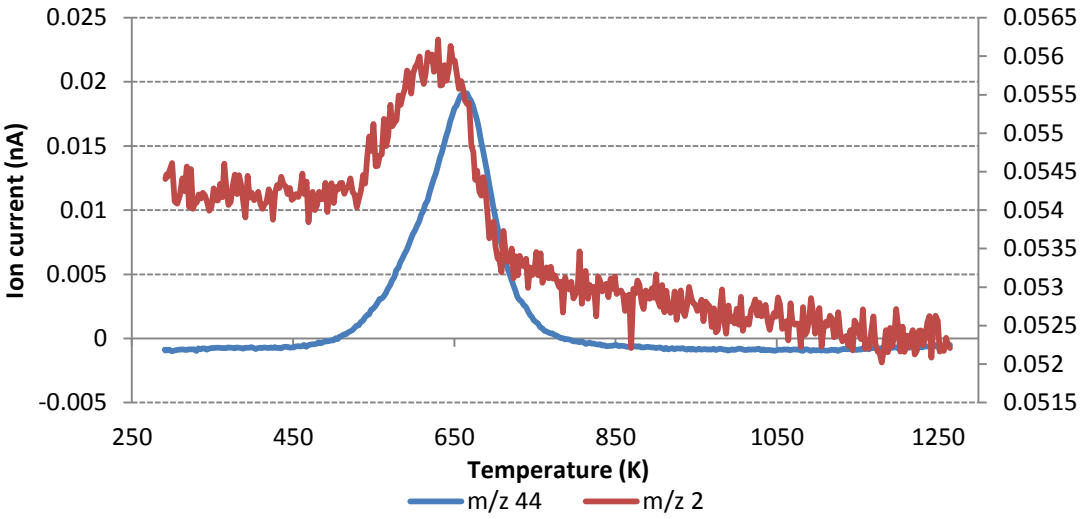

Figure 81: Mass spectra data obtained from TPO during the 2,4HD hydrogenation over CrO_x/Al_2O_3 catalyst at 623 K

2,4HD exhibited no clear changes in the amount of the carbon species deposited on the surface of the catalyst, over the reaction temperatures range. The amount of the carbon species desorbed is less than what was observed with both 1HY and 1,5HD systems and there are no clear changes in the amount of weight loss during the trans-hydrogenation process and when reactants are fed individually. The percentage carbon deposit for each run individually and as a mixed feed is determined and presented in Figure 82

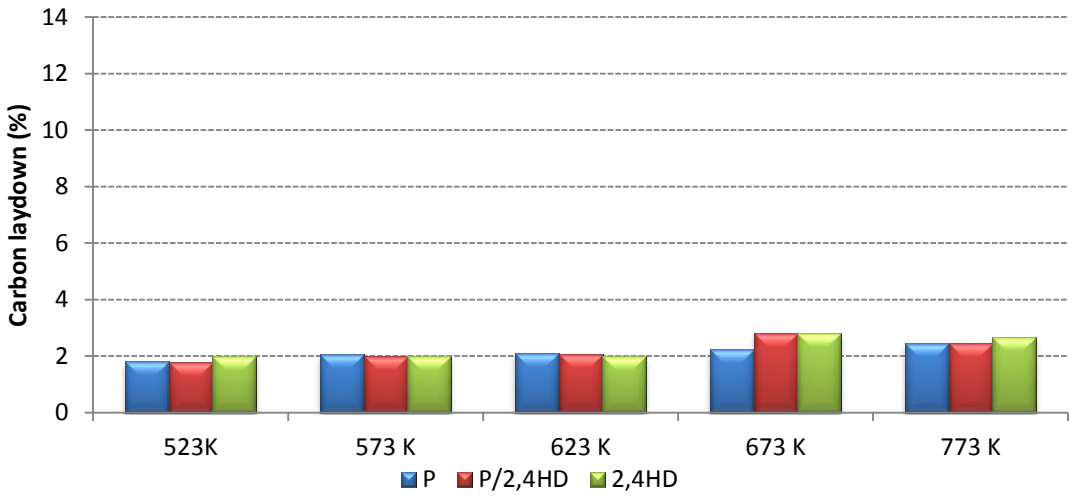

Figure 82: Carbon laydown of the spent CrO_x/Al_2O_3 catalyst over the set temperatures

The amount of the carbon formed related to the reactant feed is summarized and presented in Table 41. Although there are no clear changes obtained in the % deposition of the carbon during both the trans-hydrogenation and when fed alone, it is observed that there is clear reduction of the carbon formation with the trans-hydrogenation system related to amount of the reactant fed.

Table 41: Total amount of carbon deposited on spent CrO_x/Al_2O_3 catalyst at various temperatures using 2,4HD system

Temperature (K)	Carbon deposited (μmol/g)		
	P	P/2,4HD	2,4HD
523	0.0035	0.0028	0.016
573	0.0040	0.0032	0.016
623	0.0041	0.0033	0.016
673	0.0044	0.0044	0.023
773	0.0048	0.0040	0.022

The Raman spectroscopic analysis of the spent catalysts was obtained using UV radiation for the studies of the carbon deposit in a manner similar to that used with the 1HY and 1,5HD systems. The Raman spectra reveal Raman bands assigned to coke deposition at ~1380 and 1600 cm^{-1} related to D and G bands respectively this was only observed with 2,4HD feed at all reaction temperatures. This was also observed during the trans-hydrogenation system but there is no any Raman band obtained at low temperature between (573-523 K). The results are presented in Figure 83 and 84

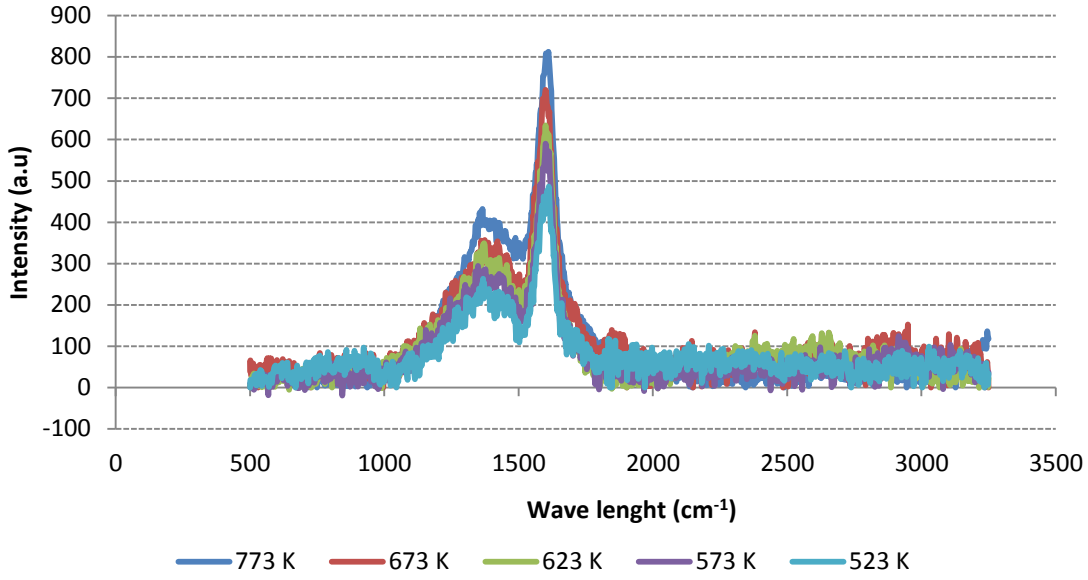

Figure 83: Raman spectra of spent CrO_x/Al_2O_3 catalyst for sole 2,4HD obtained using the UV-radiation

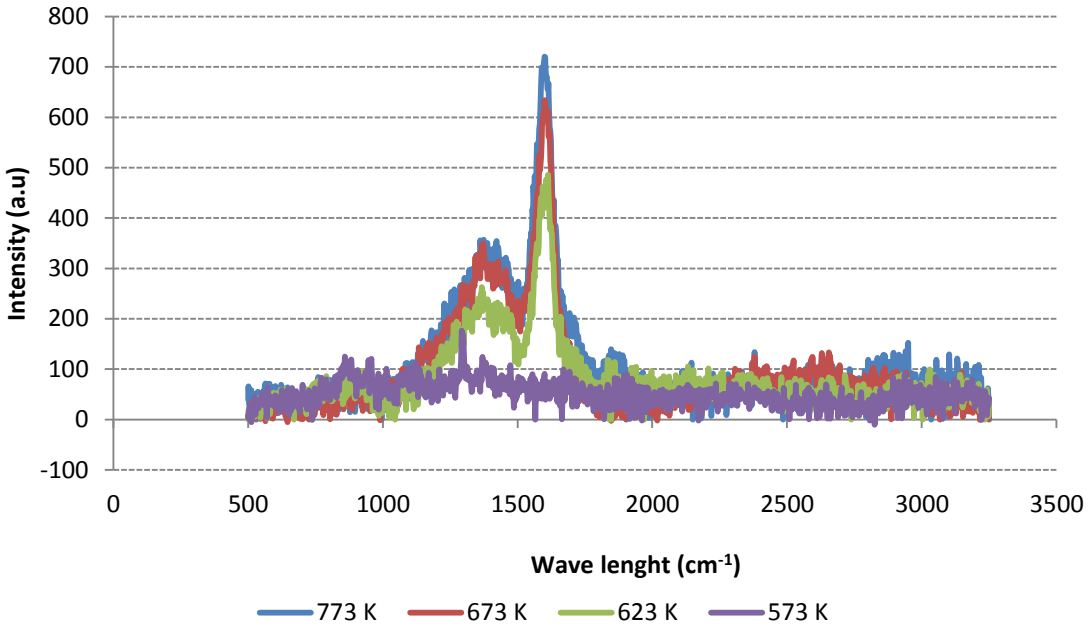

Figure 84: Raman spectra of spent CrO_x/Al_2O_3 catalyst for 2,4HD mixed feeds obtained using the UV-radiation

The BET analysis performed on the spent catalysts also suggest that the formation of coke on the catalyst surface using 2,4HD system also decreases the BET surface area and the pore volume. A significant loss in the S_{BET} was observed

with all the samples. Although, the results were very similar to 1,5HD system, there is slightly smaller decrease in the S_{BET} with the 2,4HD.

The XRD analysis of the spent catalyst using the 2,4HD system also revealed only the diffraction pattern for γ-alumina and there was not any obvious changes observed in the diffraction pattern of the spent catalyst at all temperatures due to these reactions.

The CHN analysis obtained over the chromia catalyst with three reaction systems is presented in Table 42

Table 42: Elemental analysis over chromia catalyst with the three reaction systems

	wt. % C	**Wt. % H**	**wt. % C**	**Wt. % H**	**wt. % C**	**Wt. % H**
	1HY		1,5HD		2,4HD	
773 K	7.91	1.55	2.55	0.66	2.55	0.74
673 K	9.49	1.82	2.91	0.71	2.21	0.61
623 K	9.51	1.71	3.21	0.69	1.91	0.46
573 K	11.1	1.95	5.11	1.05	3.11	0.74
523 K	12.01	1.62	5.94	1.42	2.94	0.61

3.3 K-CrO_x/Al_2O_3 catalyst

3.3.1 Pre-reaction catalyst characterisation

3.3.1.1 BET surface area and pore volume determination

The summary of the parameters extracted from the BET analysis result indicated that the S_{BET} and the pore volume of the chromia catalyst further decreased upon impregnation of the doping metal precursor as presented in Table 43

Table 43: b S_{BET}, pore volume and pore diameter of the support and K-CrO_x/Al_2O_3 catalyst

	S_{BET} (m^2/g)	V_p(cm^3g^{-1})	D_p(Å)
Y-Al2O3	208	0.52	100
CrOx/Al2O3	203	0.46	91
K- CrOx/Al2O3	151	0.36	93

The adsorption isotherm for the catalyst is the type II model. The result is presented in Figure 85

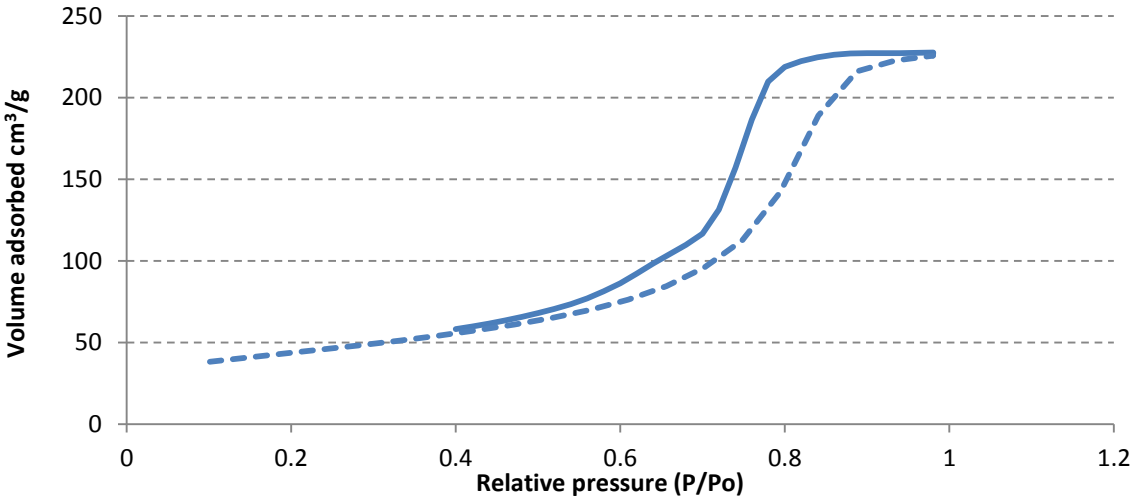

Figure 85: Nitrogen adsorption isotherm at 78 K for the support and the K-CrO_x/Al_2O_3 catalyst

Figure 86 illustrated the pore volume distribution as measured in the mesopore range for the support. It presents a uniform distribution but there is no clear

decrease in the pore volume of the chromia catalyst upon impregnation of the doped alkali but there is observed a slight shift in the pore diameter after impregnation, suggesting that the small pores are filled with the potassium salt.

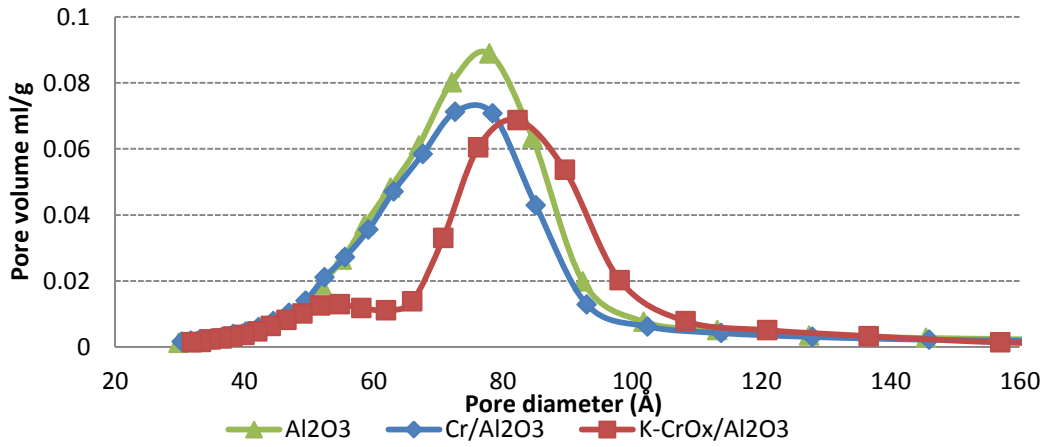

Figure 86: Pore volume distribution of the support and the K-CrO_x/Al_2O_3 catalyst

3.3.1.2 XRD analysis

The XRD analysis of the catalyst revealed additional diffraction pattern upon loading of the potassium, associated with both α-K_2O and ß-K_2O crystalline phases. No evidence of the chromium oxide crystalline phase is observed; instead the diffraction pattern for the starting γ-alumina support is retained. This is expected as was previously explained with the chromia catalyst. The result is presented in Figure 87

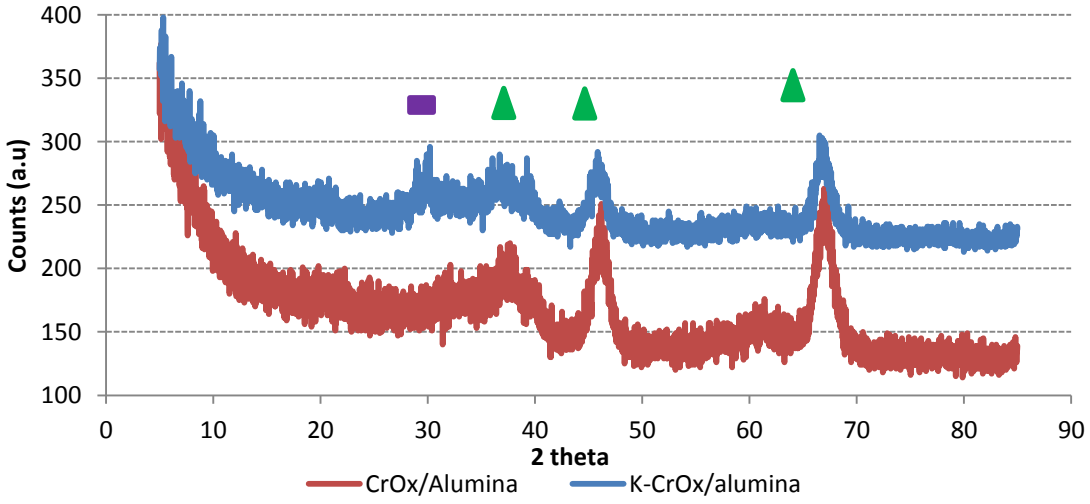

Figure 87: XRD diffraction pattern of the CrO_x/Al_2O_3 and the K-CrO_x/Al_2O_3 catalyst

3.3.1.3 Thermogravimetric analysis

The standard TGA-TPR obtained from ambient temperature to 1273 K showed three distinct weight losses at, ~540, ~760, and ~1050 K. the weight losses at ~540 and ~760 K were found to be consistent with the Red-Ox cycles.

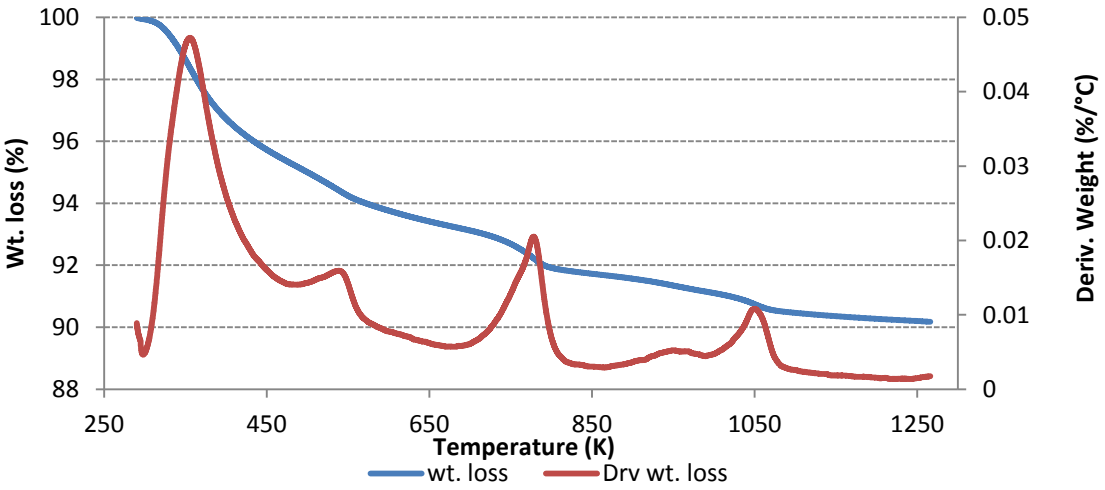

Figure 88: The standard TGA-TPR profile of the K-CrO_x/Al_2O_3 catalyst

All the three weight losses presented in Figure 88 were due to hydrogen uptakes as confirmed by the mass spec data (m/e 2) presented in Figure 89. This is indicative of multiple reduction stages observed with the doped chromia catalyst compared to the chromia catalyst where only a single reduction process was observed.

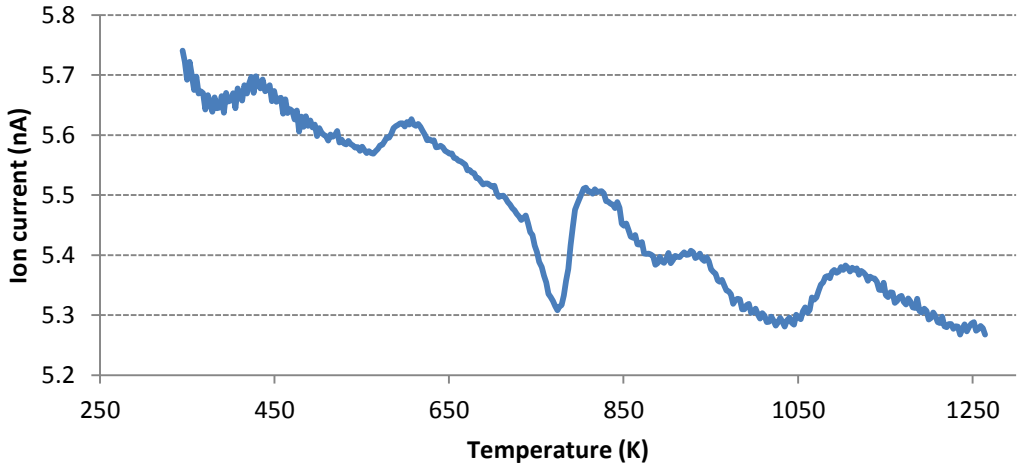

Figure 89: mass spectra data (m/e 2) obtained during the standard TGA-TPR

The first weight loss at ~ 540 K is a single event that uses hydrogen. It could be that KOH interacting with the alumina support or the decomposition of the K_2O species. This is because the oxide of potassium decomposes at ~ 623 K. the weight loss at ~760 K could be assigned to the reductive stage of the chromia, this is similar to what was observed with the chromia catalyst except that this is shifted to a higher temperature suggesting that the presence of the potassium may have had an effect on the reduction stage of the chromia. The weight loss at ~ 1050 K corresponding to ~ 2% could be assigned to the loss of volatile potassium due to high temperature effect, the melting point of potassium is ~1033 K and is about the same temperature the loss was observed.

The Red-Ox profile presented in Figure 90 shows two peaks during the 1st cycle ~540 K and ~760 K, and only loss at ~760 K was observed during the 2nd cycle. The peak observed with both cycles corresponding to ~ 2% weight loss in both cases is associated with hydrogen consumption which would suggest an indicative reduction of the chromia and its reproducibility. If the weight loss of ~2% was due to loss of oxygen; ~0.36 mg of the 26.59 mg of the catalyst was lost. This corresponds to ~1.49: 1 Cr: O lost, which shows that for about every one atom of the chromium, ~0.66 atoms of oxygen is removed. This is very similar to what was observed with the chromia catalyst. This as explained previously could be a reduction step of the chromium oxide between Cr^{6+} and Cr^{3+}.The peak at ~ 540 K corresponding to ~2 %, is observed only with the 1st cycle suggesting a decomposition stage of the K_2O plus a partial reduction stage of the K_2O. The first peak obtained at ~373 K is associated to desorption of physisorbed H_2O absorbed on the catalyst from atmosphere. There is slight endothermic effect observed at ~540 K due to ~2 % weight loss during the 1st cycle; ~ 0.38 mg of the 26.59 mg of the catalyst was lost. This correspond to ~ 2.8:1 K:O lost, which shows that for every one atom of the potassium ~0.35 atom of the oxygen is lost. This could be reduction process of the potassium oxide to peroxides and super oxide and leading to the decomposition process. The result is presented in Figure 90

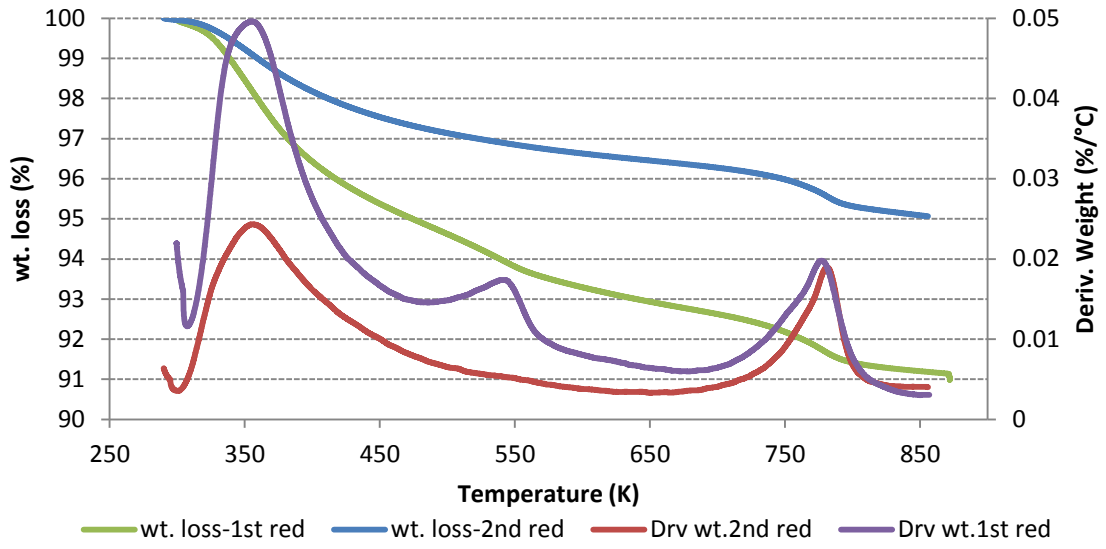

Figure 90: The TGA-TPR profile of the K-CrO_x/Al_2O_3 during the Red-Ox cycles

From the TGA-TPR-MS result (m/e 2), the hydrogen consumption perfectly matched the reduction peak at ~760 K observed with both cycles. There is no obvious consumption observed for the peak at -540 K during the first cycle. The result is presented in Figure 91

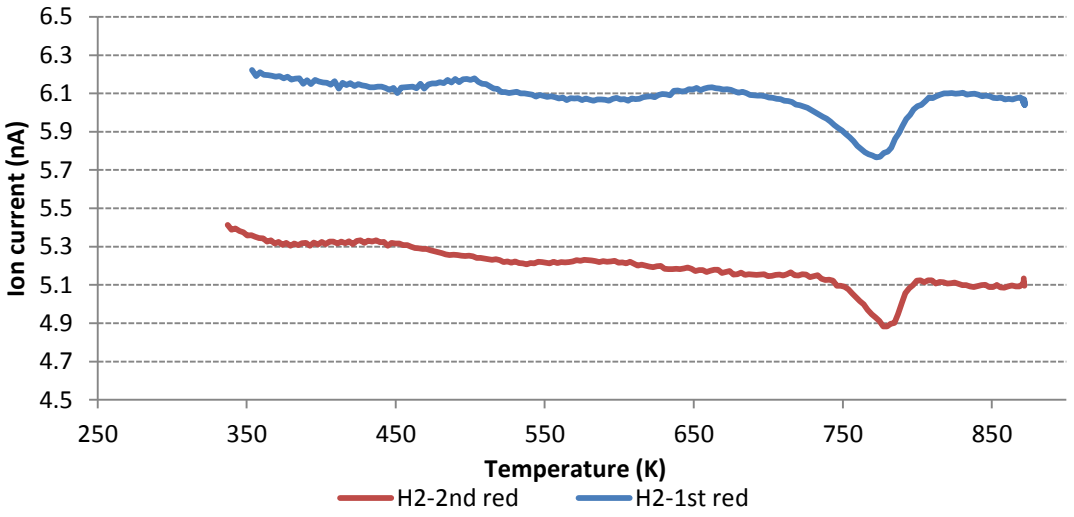

Figure 91: mass spectra data obtained during the TGA-TPR Ox-Red cycle

The DTA profile of both 1st and 2nd reduction cycles shows an exothermic peak at ~ 760 K. The results between the two cycles were consistent with the other TGA results shown above. The result is presented in Figure 92

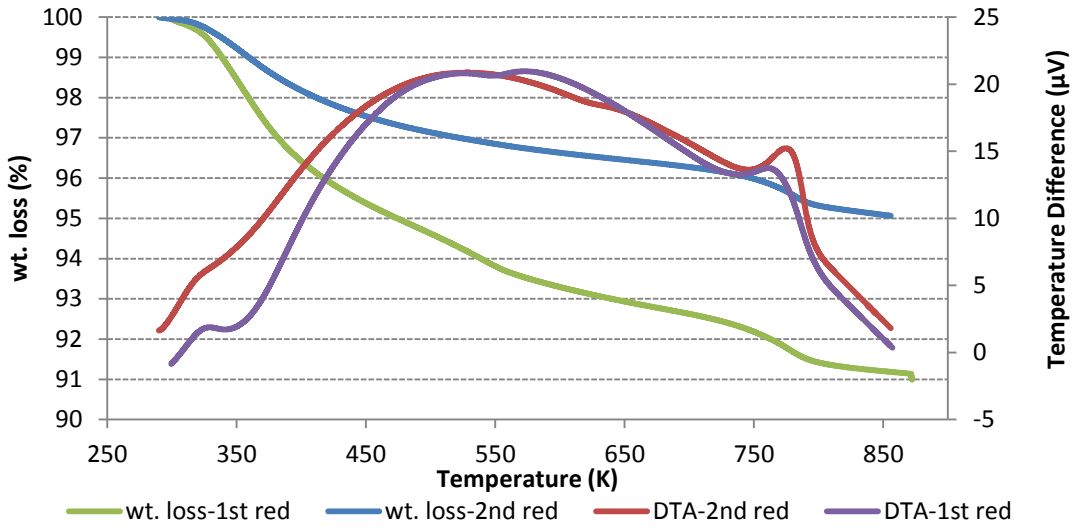

Figure 92: The DTA profile of the K-CrOx/Al2O3 catalyst obtained during the TGA-TPR Red-Ox cycle

4.3.3.4 Raman analysis

The Raman spectrum of the catalyst is presented in figure? The Raman bands observed are assigned to chromium oxide vibrations. The Raman spectrum reveals bands assigned to chromia at 348, 383, 850, 870 and 904 cm^{-1}. The alumina support does not show any Raman feature in the region studied and no feature for the potassium species is observed, thus, the loading of potassium salt onto the catalyst had no effect on the Raman spectra of the chromia. The result is presented in Figure 93

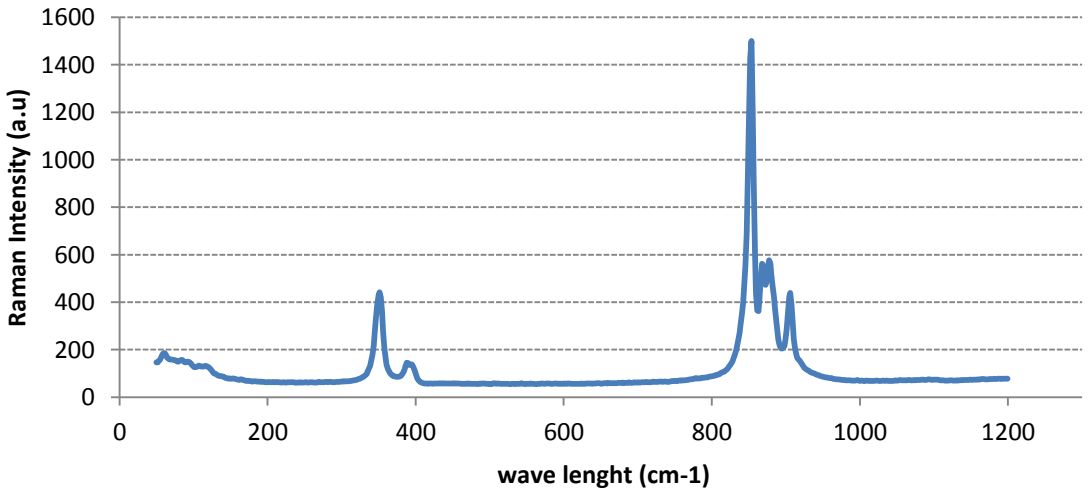

Figure 93: Raman spectrum of the K-CrO_x/Al_2O_3 catalyst

3.3.2 Pentane/Hexyne (P/1HY) system

3.3.2.1 Reaction analysis and trans-hydrogenation activity evaluation

Increased conversions were obtained on using the doped chromia catalyst. When pentane was run individually at all temperatures, conversions above the calculated equilibrium conversion for pentane dehydrogenation were obtained (~35 % conversion observed above ~11 % at 723K). More significantly, during the trans-hydrogenation processes, higher conversions were obtained at all the reaction temperatures compared to ones obtained with the chromia catalyst. About ~90 % conversion was obtained at 723 K. The results are presented in Figure 94

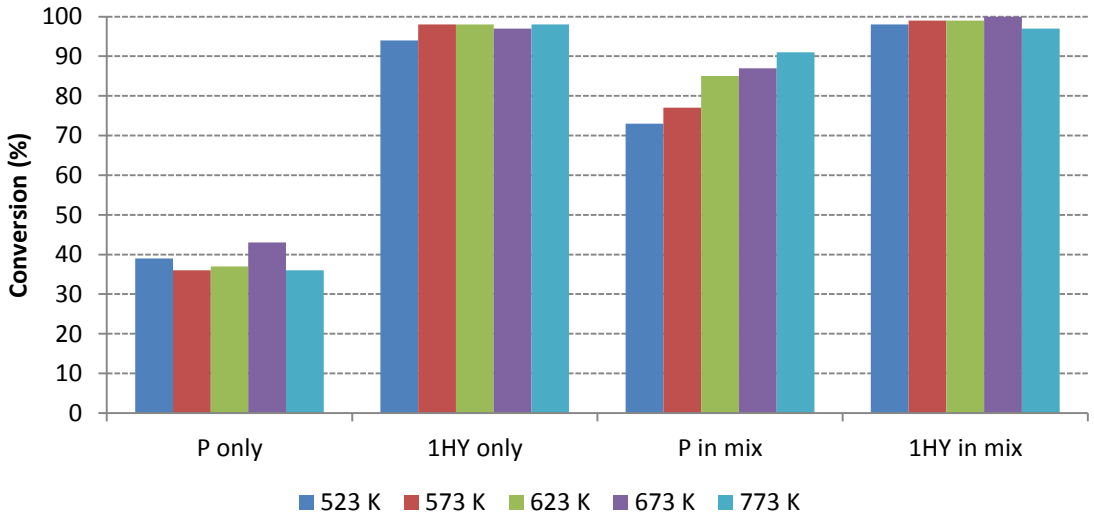

Figure 94: Conversion comparison of P, 1HY and P/1HY mixed feeds over K-CrO_x/Al_2O_3

The product distributions obtained with the doped catalyst are almost the same as the chromia catalyst. However, one of the major products with chromia catalyst (3MPY) was not observed with this catalyst and instead, an increase in the yield of (3MH1) and traces of (B) were observed. Like the CrO_x/Al_2O_3 catalyst, the distribution of the products changes with temperature and the % yield observed for individual product changes across the reaction temperatures. The results are presented in Table 44-49

Table 44: Products yield of the trans-hydrogenation over K-CrOx/Al_2O_3 at 773K

	P	H	P+H	P+H Theory
	Conversion (%)			
Pentane(P)	35.7		91	35.7
Hexyne(1HY)		98	97	98
	Yield (%)			
Iso-pentane	10.48		0.21	0.48
Pentene			1.81	0
Trans-2-Pentene	0.2			0.2
4-Methylpentene		0.03		0.03
Hexane		0.77	0.66	0.77
1-Hexene		2.58	1.60	2.58
2-Hexene		0.9	3.56	0.9
3-Hexene		3.24	4.04	3.24
Methyl-2-pentene		10.65	8.58	10.65
3-Methyl-1-hexene		21.06	15.29	21.06
Benzene		4.09	2.86	4.09
3-Methylhexane		6.27	4.59	6.27
2-Methyl-1,3-pentadiene		23.3	17.05	23.3
methylcyclohexane	17.69	6.20	18.94	23.89

Table 45: Products yield of the trans-hydrogenation over K-CrO_x/Al_2O_3 at 673K

	P	H	P+H	P+H Theory
	Conversion (%)			
Pentane(P)	43.58		87	43.58
Hexyne(1HY)		97	100	97
	Yield (%)			
Iso-pentane			0.04	0
Pentene	22.82			22.82
Trans-2-Pentene	0.22			0.22
Cis-2-pentene	0.57			0.57
Hexane		0.4	10.76	0.4
1-Hexene		1.3	2.72	1.3
2-Hexene		0.22	5.29	0.22
3-Hexene		1.23	12.35	1.23
Methyl-2-pentene		9.89	1.26	9.89
3-Methyl-1-hexene		28.16	14.64	28.16
Benzene		1.45	0.52	1.45
3-Methylhexane		6.88	1.28	6.88
2-Methyl-1,3-pentadiene		27.7	4.96	27.7
Methylcyclohexane	11.6	2.58	14.06	14.18

Table 46: Products yield of the trans-hydrogenation over K-CrO_x/Al_2O_3 at 623K

	P	H	P+H	P+H Theory
	Conversion (%)			
Pentane(P)	37.58		85	85
Hexyne(1HY)		97	99	99
	Yield (%)			
Iso-pentane	10.38		0.07	10.38
Pentene			0.27	0
Trans-2-Pentene	0.46		0.42	0.46
Cis-2-pentene	0.33		0.14	0.33
Hexane		0.75	0.34	0.75
1-Hexene			0.49	0
2-Hexene			5.17	0
3-Hexene			0.72	0
Methyl-2-pentene		3.55	5.58	3.55
3-Methyl-1-hexene		17.32	16.17	17.32
Benzene		1.45	1.03	1.45
3-Methylhexane		4.86	3.28	0
2-Methyl-1,3-pentadiene		6.8	15.00	6.8
1,4-Hexadiene		31.67		31.67
Methylcyclohexane	11.76	10.95	16.45	22.71

Table 47: Products yield of the trans-hydrogenation over K-CrO_x/Al_2O_3 at 573K

	P	H	P+H	P+H Theory
	Conversion (%)			
Pentane(P)	36.59		77	36.59
Hexyne(1HY)		98	99	98
	Yield (%)			
Iso-pentane	10.38		0.18	10.38
Pentene			0.10	0
Trans-2-Pentene	0.42			0.42
Cis-2-pentene	0.71			0.71
Hexane			0.80	0
1-Hexene			0.13	0
2-Hexene			3.17	0
3-Hexene		0.4	0.63	0.4
Methyl-2-pentene		4.47	2.35	4.47
3-Methyl-1-hexene		18.5	17.05	18.5
Benzene		5.3	0	5.3
3-Methylhexane			2.03	0
2-Methyl-1,3-pentadiene		16.13	9.07	16.13
2-Methyl-1-1hexene			0.89	0
1,4-Hexadiene		35.56	0	35.56
Methylcyclohexane	13.37	12.54	14.87	15.91

Table 48: Products yield of the trans-hydrogenation over K-CrOx/Al_2O_3 at 523K

	P	H	P+H	P+H Theory
	Conversion (%)			
Pentane(P)	38.22		73	38.22
Hexyne(1HY)		94	98	94
	Yield (%)			
Iso-pentane	**26.74**			**26.74**
Pentene	**8.12**		0.06	**8.12**
Trans-2-Pentene			0.26	**0**
Cis-2-pentene			0.42	**0**
Hexane			0.29	**0**
1-Hexene			0.20	**0**
2-Hexene			0.07	**0**
3-Hexene			0.27	**0**
Methyl-2-pentene		6.23	6.25	**6.23**
3-Methylpentyne		33.42		**33.42**
3-Methyl-1-hexene			19.36	**0**
3-Methylhexane		3.91	3.16	**3.91**
2-Methyl-1,3-pentadiene		25.89	16.43	**25.89**
Methylcyclohexane	3.72	11.86	13.19	3.7236

There is also an increase in the yield of the valuable products observed with the K-CrO_x/Al_2O_3 compared to the CrO_x/Al_2O_3 catalyst; ~35 % total olefin is obtained at 723 K but the ratio of the olefin to alkylated olefins is ~1:4 at most temperatures. The total valuable products are summed up to ~50% which includes other alkylated products. The result is presented in Figure 95. The olefin production is also observed to be higher compared to the other valuable products obtained during the trans-hydrogenation over the K-CrO_x/Al_2O_3 as presented in Figure 96. There is also an increase in these valuable products with the reaction temperature Figure 97

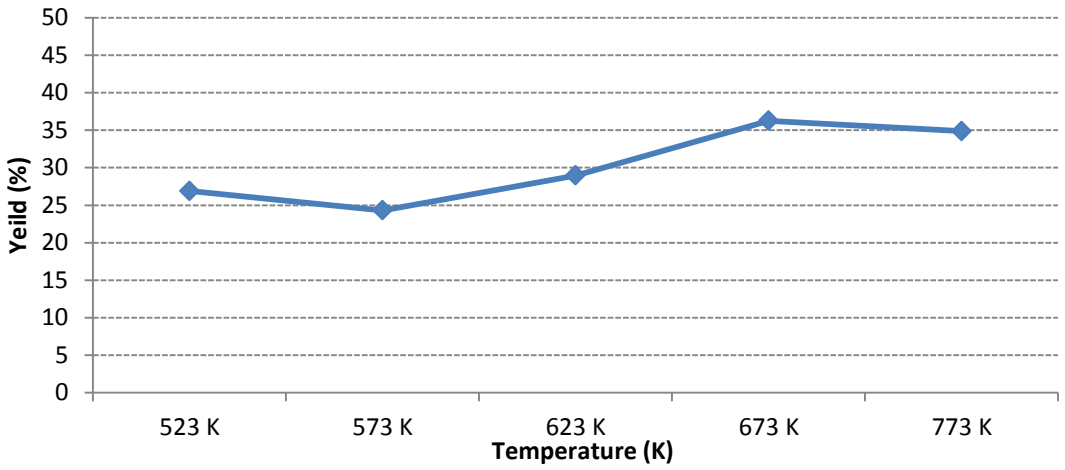

Figure 95: Total olefin yield with temperature over the K-CrO_x/Al_2O_3

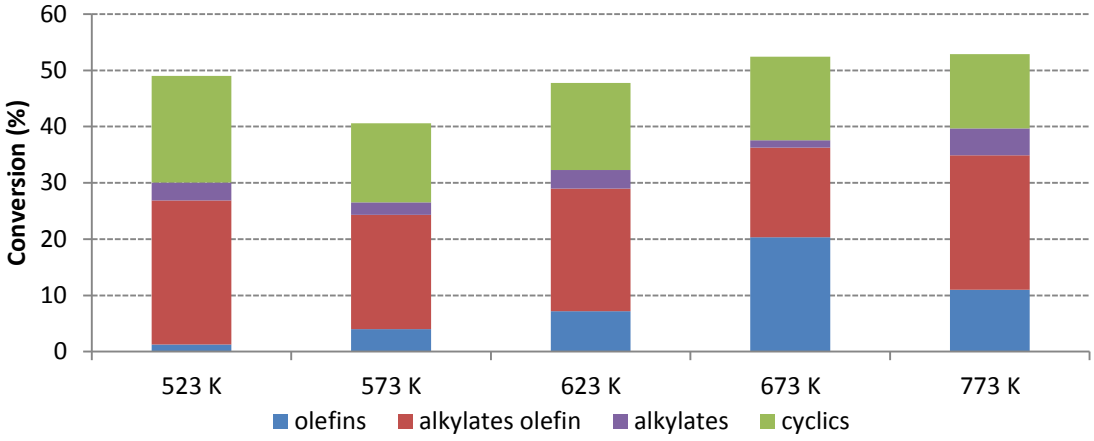

Figure 96: Profile of valuable product in relative to the reaction temperature over K-CrO_x/Al_2O_3

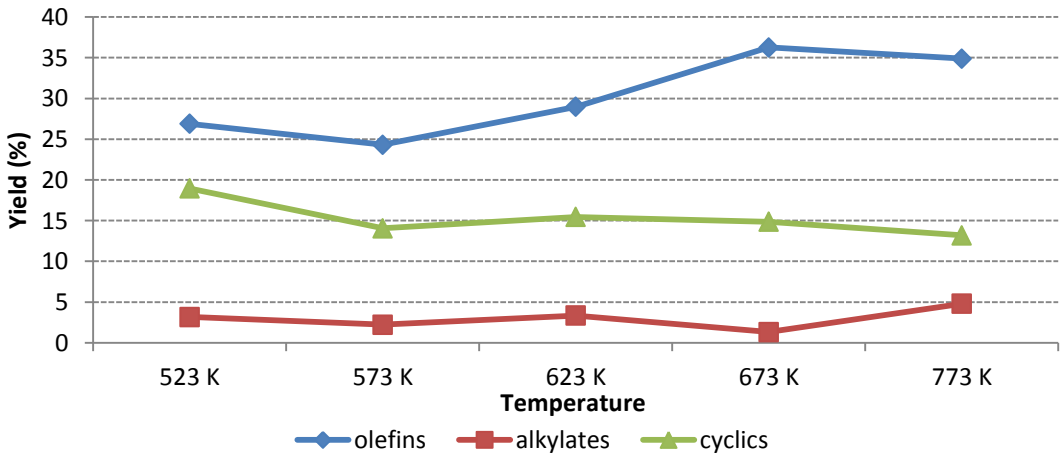

Figure 97: Relationship of the valuable products over the K-CrO_x/Al_2O_3

The evolved gases observed with the doped catalyst are the same (H_2, CH_4 and C_2H_4) with the evolved ones observed with the chromia catalyst. However, CH_4 and C_2H_4 were initially observed at ~10 min of the reaction on stream, but later completely declined at ~ 30 min, showing less cracking activity compared to the chromia catalyst. Pulse of hydrogen was only observed at the beginning of the reaction, the hydrogen then evolved back again at ~15 min and decline gradually through the reaction period time on stream. The result at 723 K is presented in figures 98, 99 and 100

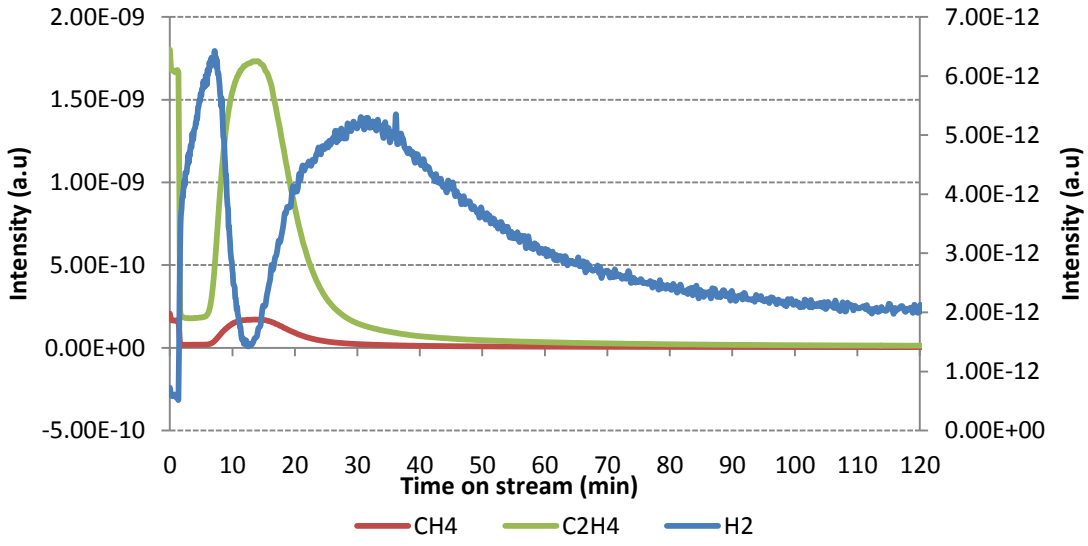

Figure 98: Profile of the evolved gases over K-CrOx/Al_2O_3 using P only at 723 K

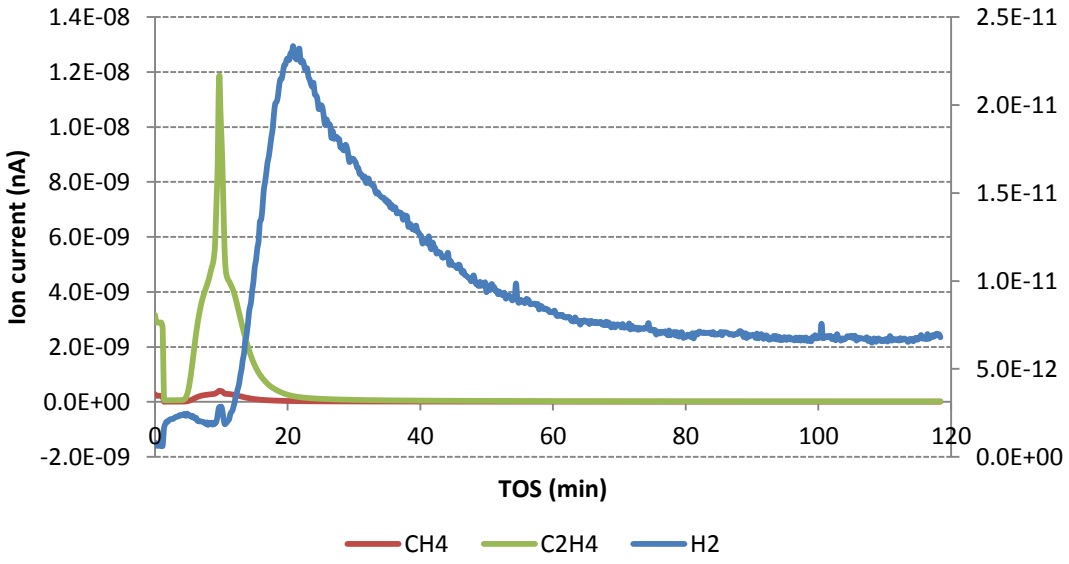

Figure 99: profile of the evolved gases over K-CrOx/Al_2O_3 using 1HY only at 723 K

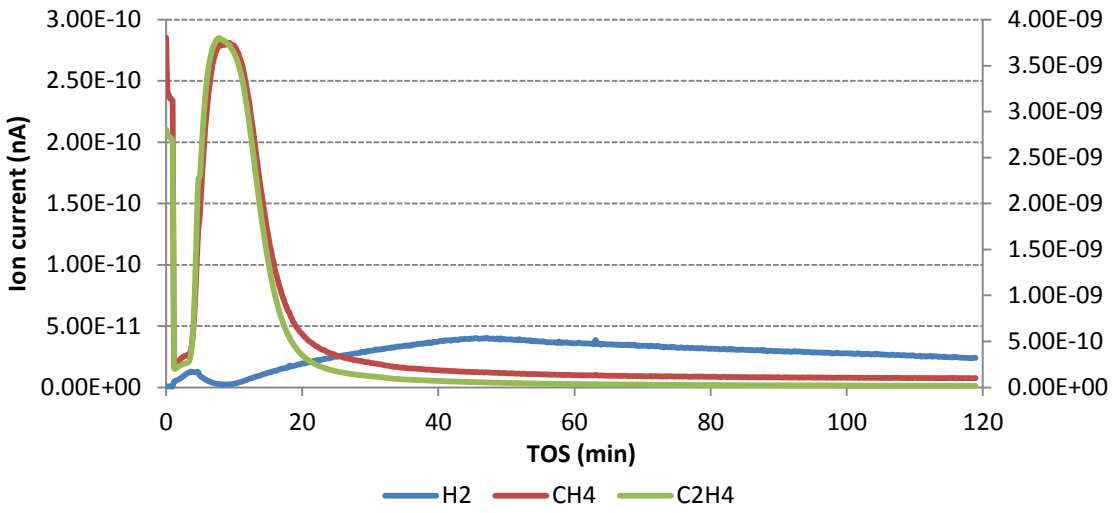

Figure 100: profile of the evolved gases over K-CrOx/Al_2O_3 using P/1HY at 723 K

Table 49: carbon balance for the trans-hydrogenation reaction over the K-CrO_x/Al_2O_3 catalyst

Temperature (K)	Carbon balance (%)				
	Liquid[a] Ptds.	CH4[b]	C2H6[b]	coke[c]	Pdts un-accounted
773	78	2.86	17.38	0.43	
673	77	2.74	7.77	0.36	
623	76	2.66	10.16	0.15	
573	82	-	-	0.01	10
523	84	-	-	0.003	11

a) Obtained from the GC analysis, b) obtained from the mass spec analysis, c) obtained from the TGA analysis: Pdts = products

4.2.2.2 Post reaction characterization and analysis

The catalysts were analysed after use by TGA. The weight losses for the doped catalysts were less than those observed with the chromia catalyst. The main loss observed with the catalyst used for pentane dehydrogenation occurs at ~673 K. Unlike the chromia catalyst, there are differences observed with the hexyne and mixed feed reactants. The main loss using both feeds occurs ~573 K, but the mixed feed has extended loss to ~ 723 K, while the hexyne feeds has extended loss to ~773 K. the results are presented in figures 101, 102 and 103

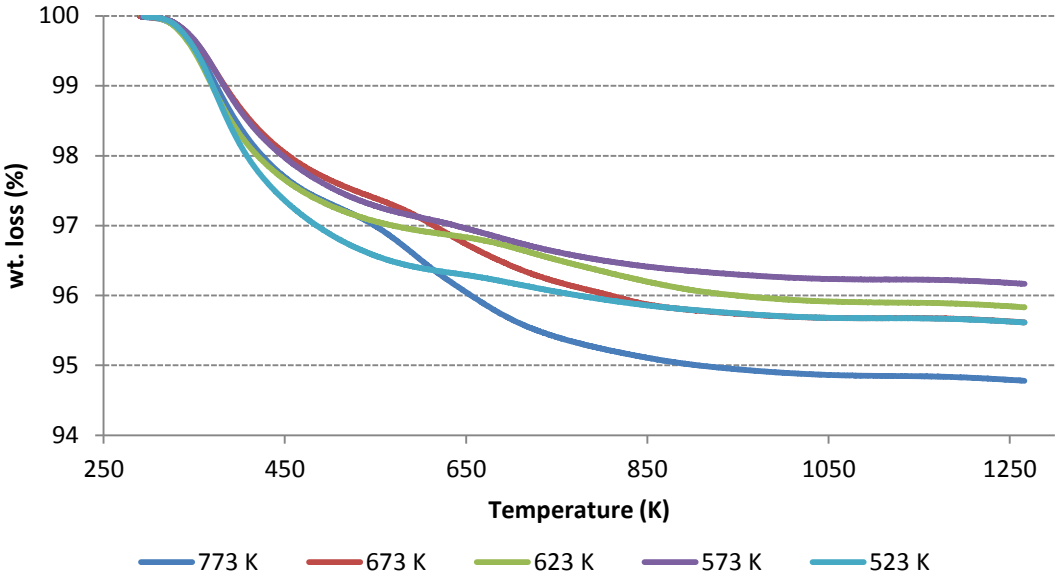

Figure 101: Weight loss profile of pentane run alone over K-CrO_x/Al_2O_3 catalyst

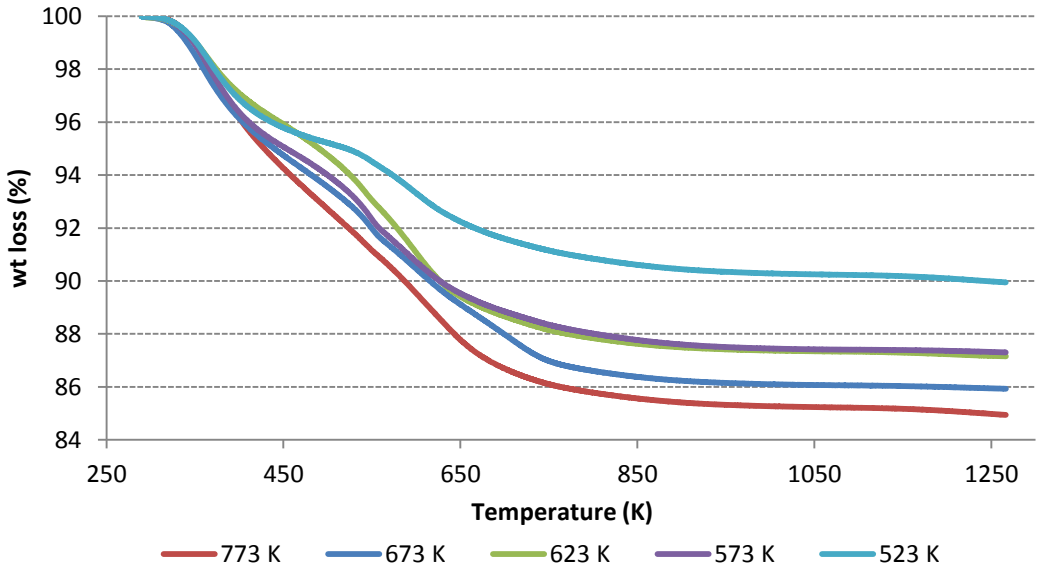

Figure 102: Weight loss profile of hexyne alone over K-CrO_x/Al_2O_3 catalyst

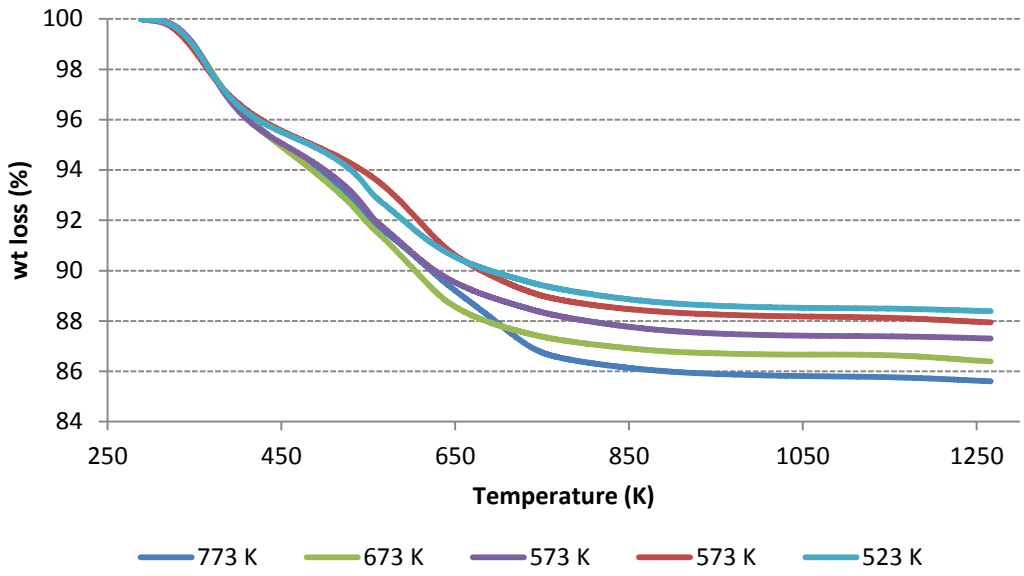

Figure 103: Weight loss profile of the mixed feeds over CrO_x/Al_2O_3 catalyst

The derivative weight analysis plot is observed to be the same for all reaction temperatures for each reactant, three different weight losses were observed with the K-chromia catalyst suggesting three different carbon species when the catalyst was subjected to either the hexyne or mixed feeds. The results are presented in Figure 104 and 105

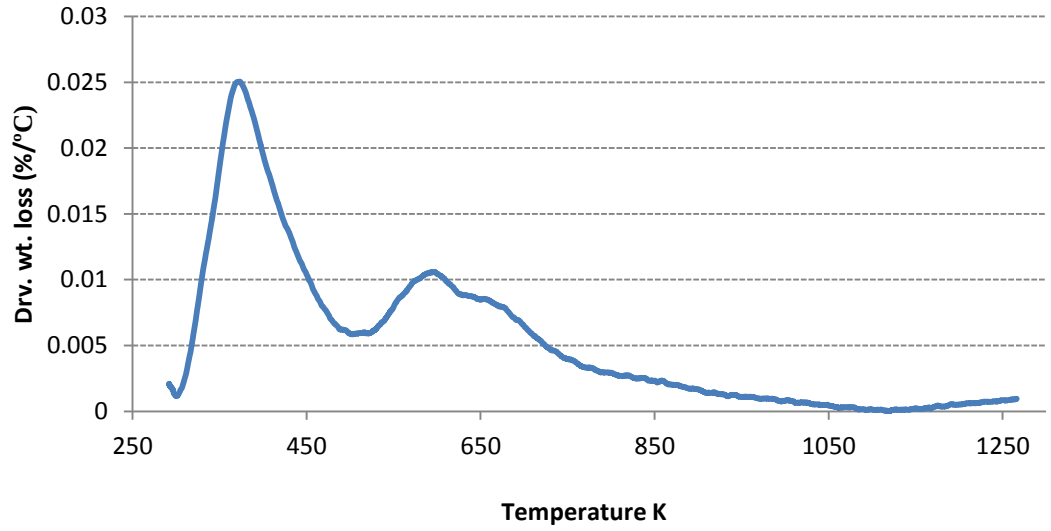

Figure 104: Derivative weight loss profile pentane over K-CrO_x/Al_2O_3 catalyst

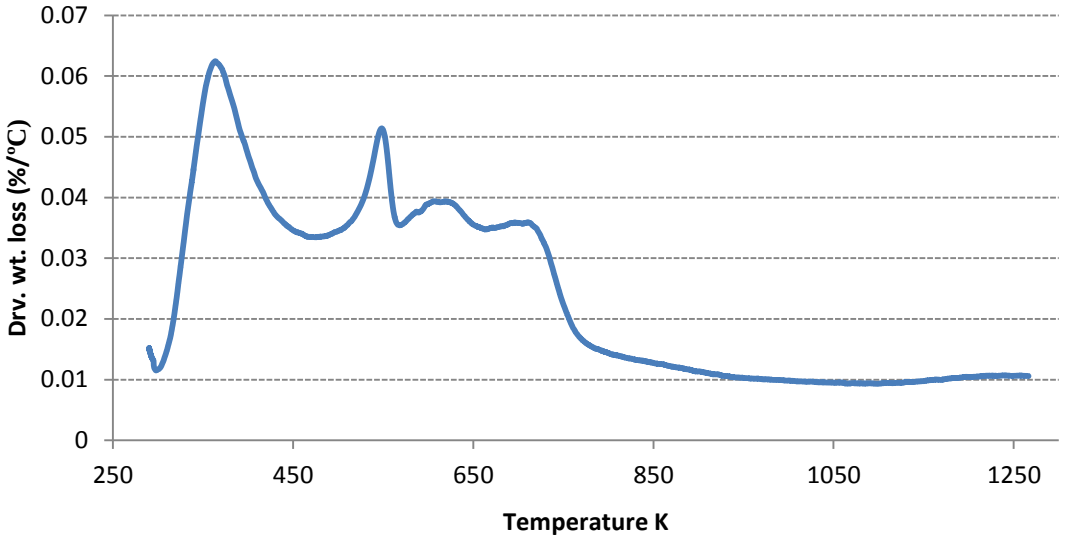

Figure 105: Derivative weight loss profile of hexyne and the mixed feeds over K-CrO_x/Al_2O_3 catalyst

The TPO analysis also revealed carbon dioxide as the main desorption species evolved at all temperatures. However, only trace of water was detected in some of the samples when other (m/e 2, 16 and 28) were monitored. All the profiles show three main evolutions of CO_2 suggesting three different carbonaceous deposits. However, this is not observed with the mixed feed apart from the 723 K, instead a broader peak was observed. Meanwhile, there is almost no desorption using the pentane. This could be due to less significant weight loss observed with the pentane reactants. The results are presented in Figure 106 and 107

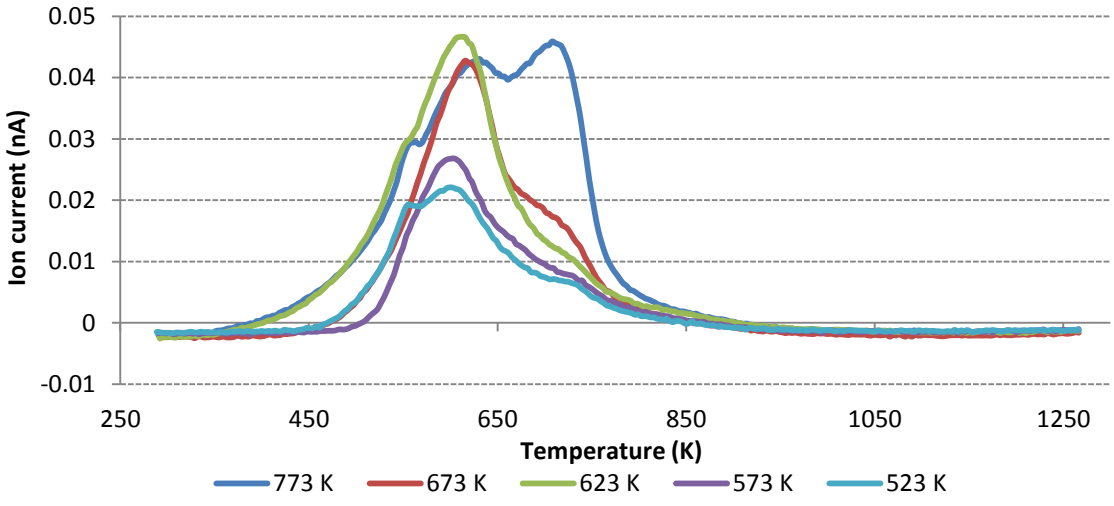

Figure 106: TPO profile of hexyne run alone over K-CrO_x/Al_2O_3 catalyst

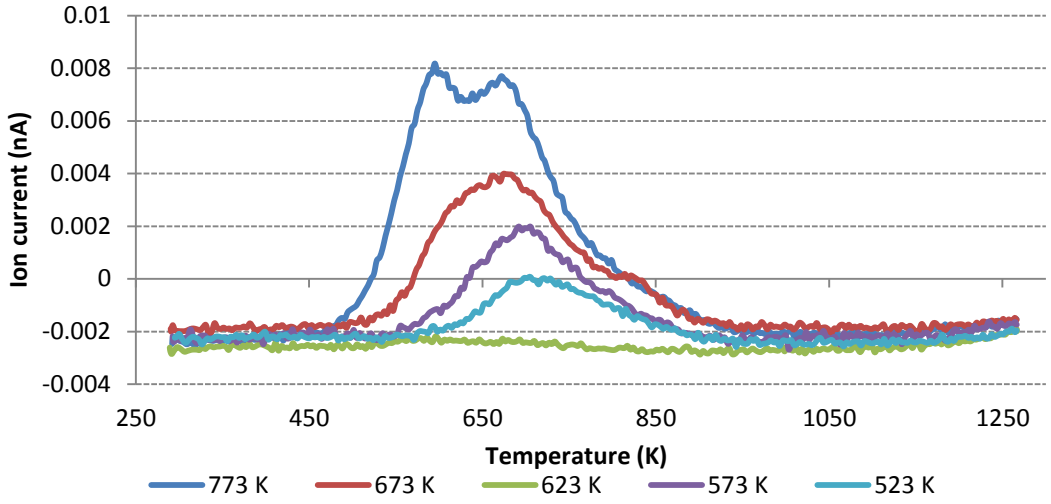

Figure 107: TPO profile of pentane/hexyne mixed feeds over K-CrO_x/Al_2O_3 catalyst

The losses of both the CO_2 and H_2O, matches the TGA derivative weight loss profile of the sample. The result is presented in Figure 108

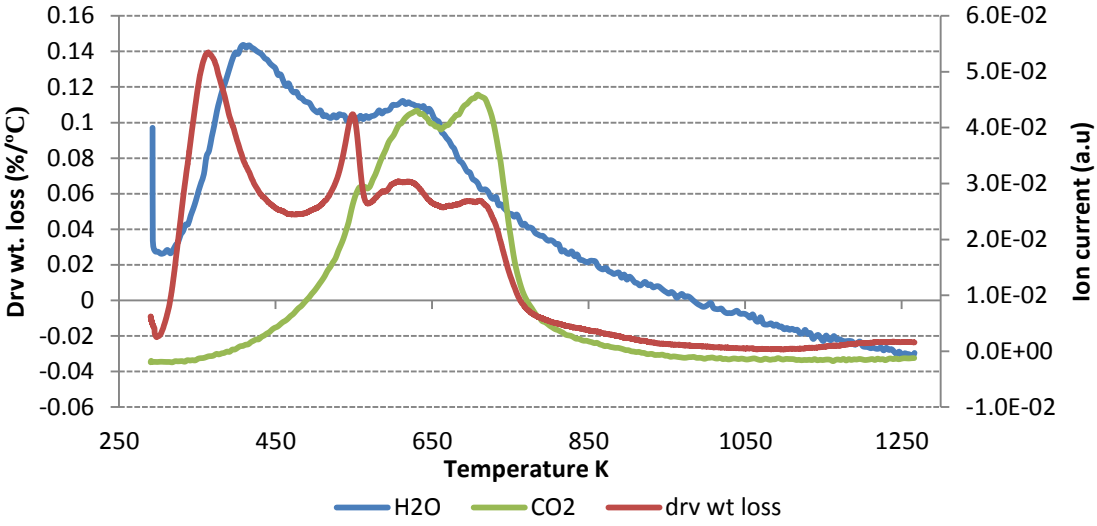

Figure 108: Species obtained during the TPO-MS using hexyne/pentane system with K-CrOx/Al_2O_3 catalyst

There is not much difference to the amount the carbon material deposited during the mixed feed trans-hydrogenation and the hexyne single feed unlike with the chromia catalyst. Meanwhile, there is a general reduction in the amount of the carbon desorption observed with this catalyst compared to the chromia catalyst at all the temperatures,~ 4% reduction observed at 723 K

between the two catalysts. The pentane reactant presents almost no deposition of carbon material, with ~1 % laydown at 723 K. The result is shown in Figure 109

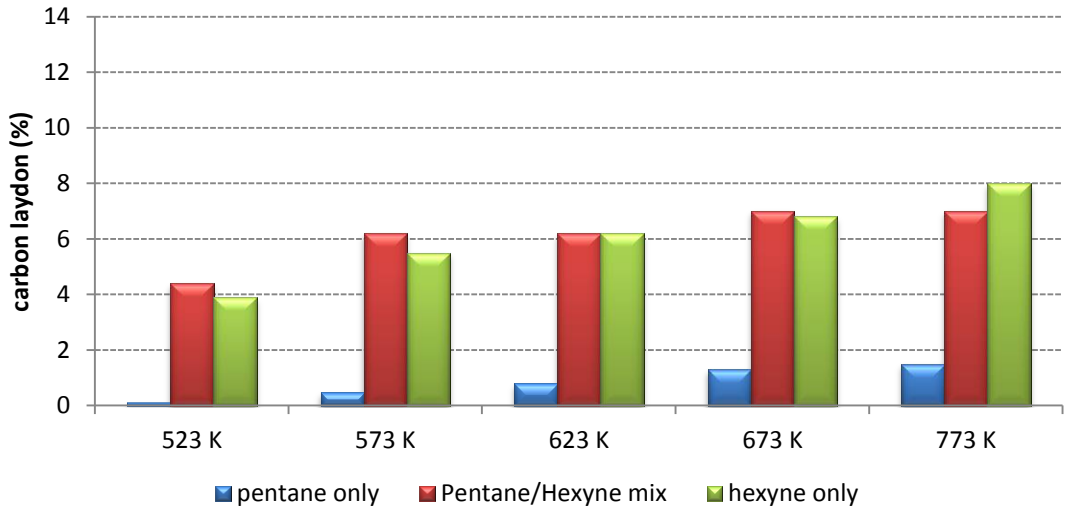

Figure 109: Carbon laydown on spent K-CrOx/Al_2O_3 catalyst

Table 50: Total amount of carbon deposited on spent K-CrO_x/Al_2O_3 catalyst at various temperatures

Temperature (K)	Amount of carbon deposited (g/g feed)		
	P	P/1HY	1HY
523	0.0002	0.007	0.032
573	0.0009	0.010	0.045
623	0.0016	0.010	0.050
673	0.0025	0.011	0.055
773	0.0029	0.011	0.065

The Raman spectra obtained with K-CrO_x/Al_2O_3, reveals only a G-band mode with the hexyne reactant using the visible radiation source, no evidence for D bands were observed. Meanwhile, the bands obtained at from catalysts run at 573 and 523K reaction temperatures with hexyne as the feed were very noisy. Also, the pentane run shows very noisy spectra using both the UV and Visible radiation sources. The results are presented in figures 110, 111 and 112

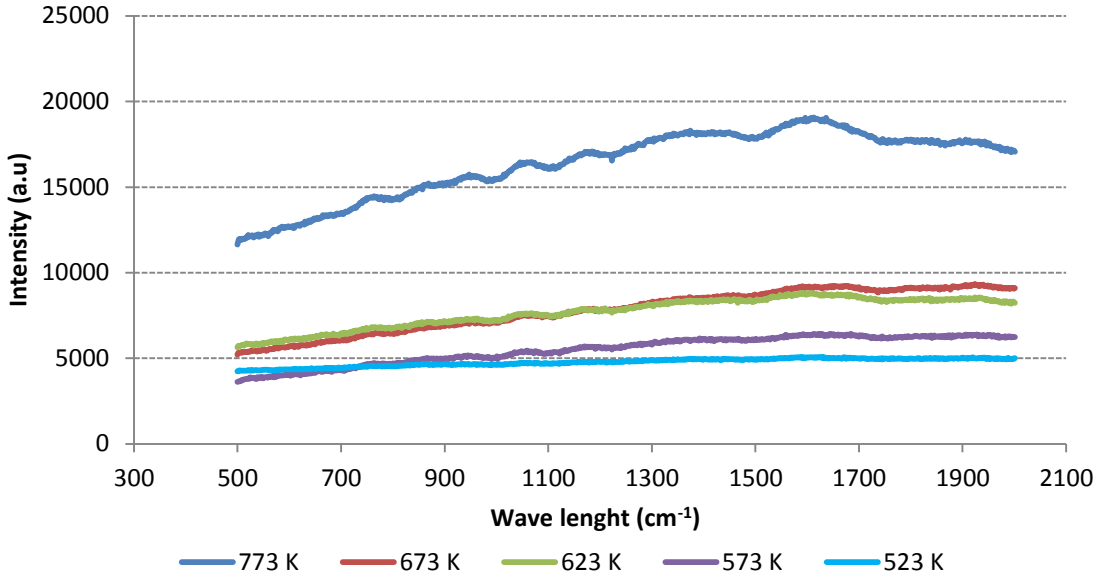

Figure 110: Raman spectra of spent K-CrO_x/Al_2O_3 catalyst for sole pentane obtained using the Vis-radiation

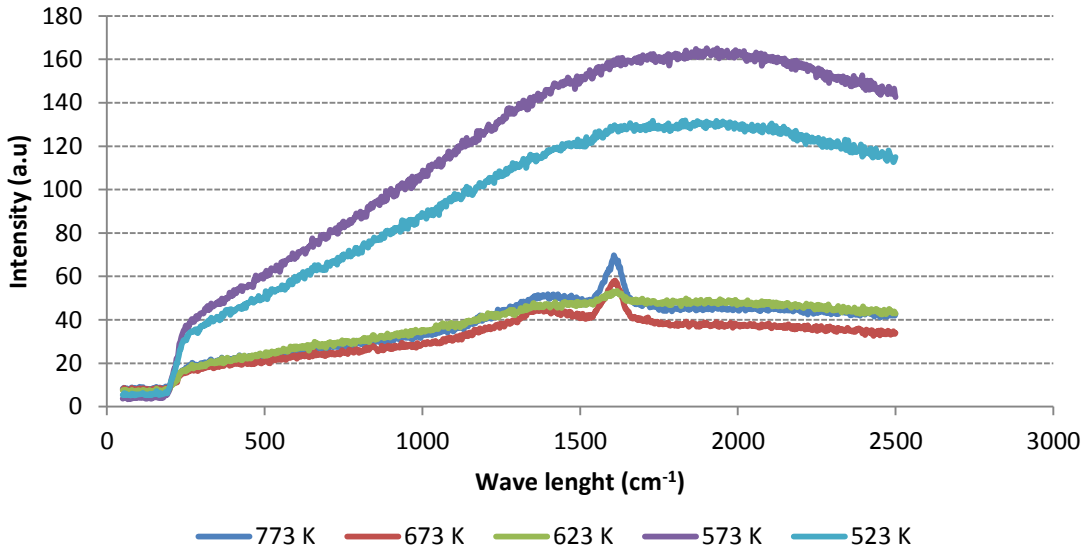

Figure 111: Raman spectra of spent K-CrO_x/Al_2O_3 catalyst for sole hexyne obtained using the UV-radiation

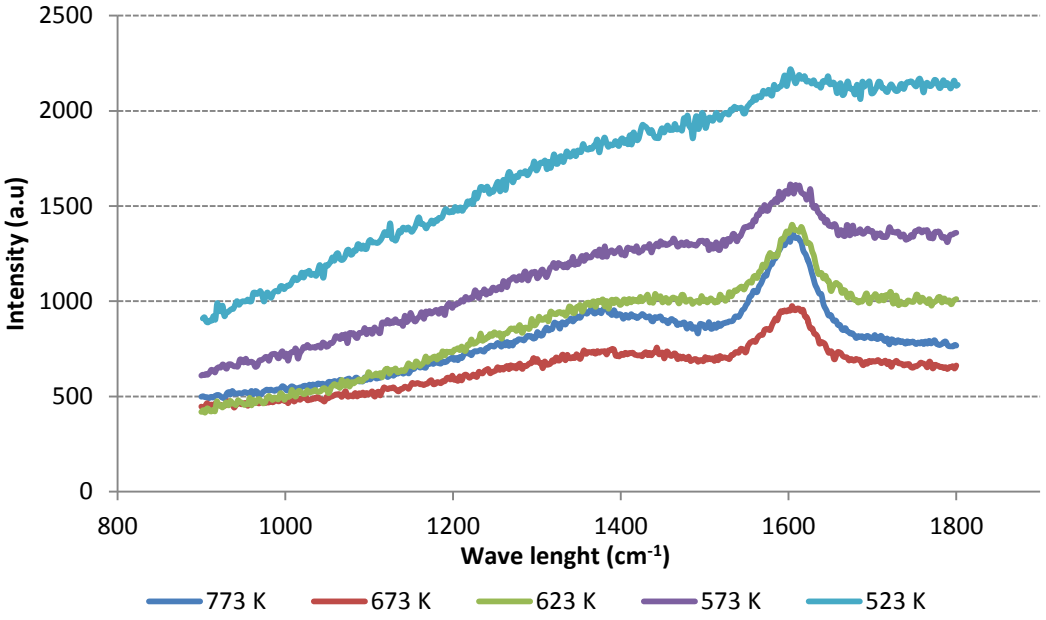

Figure 112: Raman spectra of spent CrO_x/Al_2O_3 catalyst for mixed feeds obtained using the UV-radiation

The S_{BET} analysis performed on the spent catalyst shows that, the reaction after pentane dehydrogenation a loss of BET surface area from ~151 m^2/g to ~23 m^2/g was measured. However, when hexyne was present as a reactant alone or used as the co-reactant, only a small decrease in the surface area was observed (~133 m^2/g).

3.3.3. Pentane/1,5-Hexdiene (P/1,5HD) system

3.3.3.1 Reaction analysis and trans-hydrogenation activity evaluation

Similar conversions were obtained on using the potassium-doped chromia catalyst with the P/1,5HD system as had been observed with the non-doped catalyst. There is a significant increase in the conversion of pentane during the trans-hydrogenation. The results are presented in Figure 113

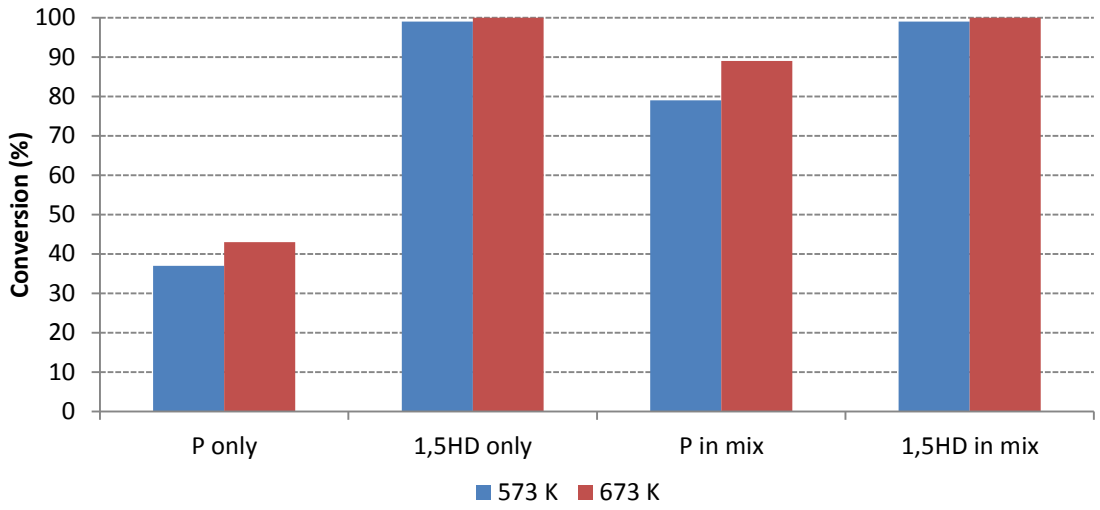

Figure 113: Conversion comparison of P, 1,5HD and P/1,5HD mixture using K-CrO_x/Al_2O_3

The product distributions obtained with the doped catalyst are the same with chromia catalyst using this system. However, there are more shifts to the production of valuable products here. The results are presented in Table 51 and 52

Table 51: Products yield of the trans-hydrogenation over K-CrO_x/Al_2O_3 using 1,5HD system at 673K

	P	H	P+H	P+H Theory
	Conversion (%)			
Pentane(P)	43		89	43
1,5-Hexadiene (1,5HD)		100	100	100
	Yield (%)			
Iso-pentane			31.15	0
Pentene	22.82		4.06	22.82
Trans-2-Pentene	0.22			0.22
Cis-2-pentene	0.57			0.57
Hexane		1.93	0.72	1.93
1-Hexene		1.32	2.25	1.32
2-Hexene				0
3-Hexene		2.01		2.01
Methyl-2-pentene		9.79	2.41	9.79
3-Methyl-1-hexene		19.62	14.98	19.62
Benzene		1.08		1.08
3-Methylhexane		4.81	1.08	4.81
2-Methyl-1,3-pentadiene		19.49	4.85	19.49
2-Methyl-1-1hexene		6	2.98	6
Methylcyclohexane	11.6	13.53	10.08	25.13

Table 52: Products yield of the trans-hydrogenation over K-CrO_x/Al_2O_3 using 1,5HD system at 573K

	P	H	P+H	P+H Theory
	Conversion (%)			
Pentane(P)	37.58		82	85
Hexyne(H)		99	99	99
	Yield (%)			
Iso-pentane	10.38	0.41	6.14	10.79
Pentene			1.81	0
Trans-2-Pentene	0.42			0.42
Cis-2-pentene	0.71			0.71
Hexane		0.92	1.35	0.92
1-Hexene			2.23	0
2-Hexene		0.27		0.27
3-Hexene		0.61	5.43	0.61
Methyl-2-pentene		7.55	14.95	7.55
3-Methyl-1-hexene		15.95	17.55	15.95
Benzene				0
3-Methylhexane			1.48	0
2-Methyl-1,3-pentadiene		37.67	14.93	37.67
2-methyl-1-1hexene		2.24	4.72	2.24
Methylcyclohexane	13.37	13.53	9.1	26.90

3.3.3.2 Post reaction characterization and analysis

The doped catalyst revealed less weight loss than the non-doped catalyst. There is evidence for changes in the losses with the trans-hydrogenation process and a reduction in the weight loss is observed with reduced temperature. This is consistent with previous results. The results are presented in Figure 114 and 115

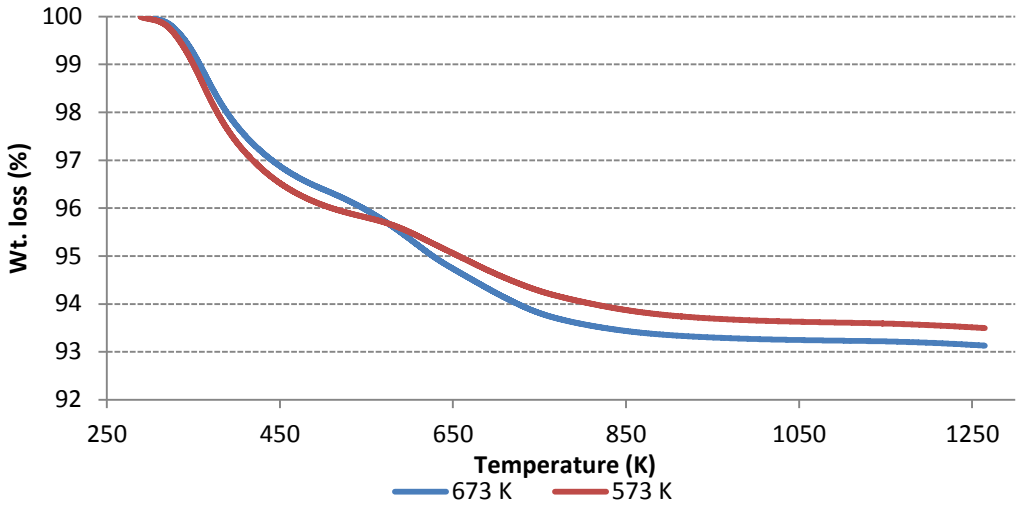

Figure 114: Weight loss profile of 1,5HD run alone over K-CrO_x/Al_2O_3 catalyst

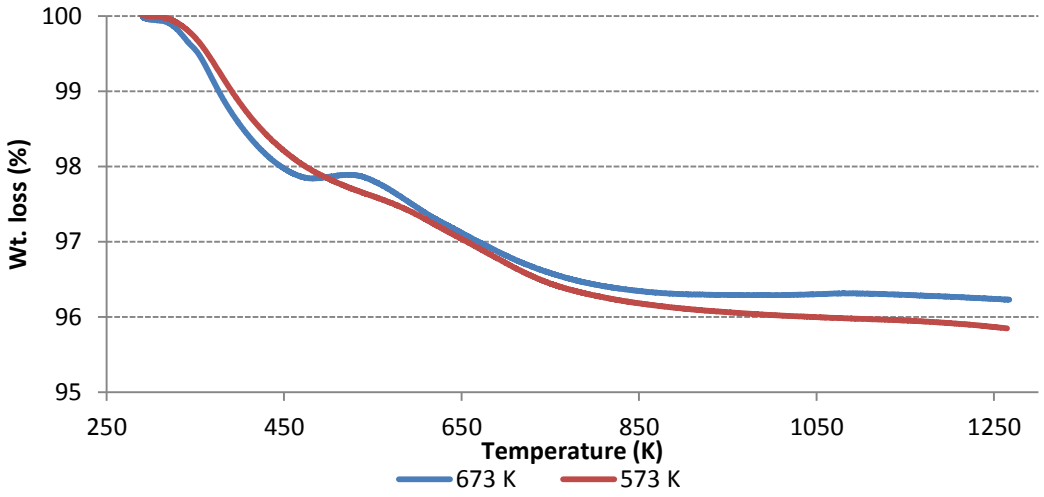

Figure 115: Weight loss profile of P/1,5HD mixed feed over K-CrO_x/Al_2O_3 catalyst

The TPO analysis of the catalysts used for pentane dehydrogenation, 1,5HD reaction and transhydrogenation revealed carbon dioxide as the main desorption species evolved at all the run temperatures. The TPO profiles show two main weight losses, unlike the three observed with the 1HY system. All the losses are associated with CO_2 and are from different carbonaceous deposits. Meanwhile, there is almost no evolution of carbon dioxide from the catalyst used for pentane dehydrogenation. However, there are observed changes in the temperature of the carbon dioxide evolution with changes in the reaction temperature. This shows that temperature the formation of the carbonaceous

deposits could be influential. The evolution at ~608 K is more predominant when the catalyst has been run under high temperature conditions while the evolution at ~700 K is more predominant when the catalyst has been run under low temperature conditions with the 608 K evolution almost vanishing. This is the opposite case observed with the 1HY system (Figure 116 and 117)

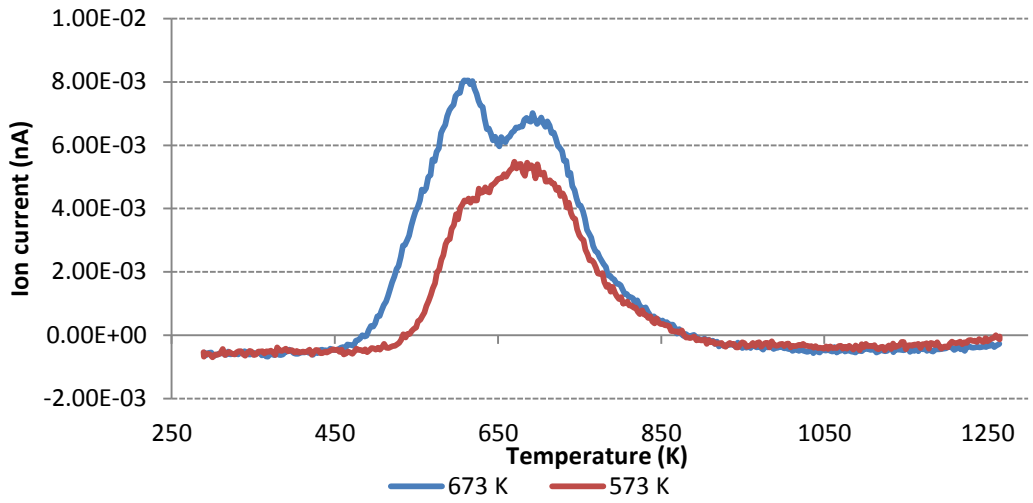

Figure 116 TPO profile of 2,4HD run alone over K-CrO_x/Al_2O_3 catalyst

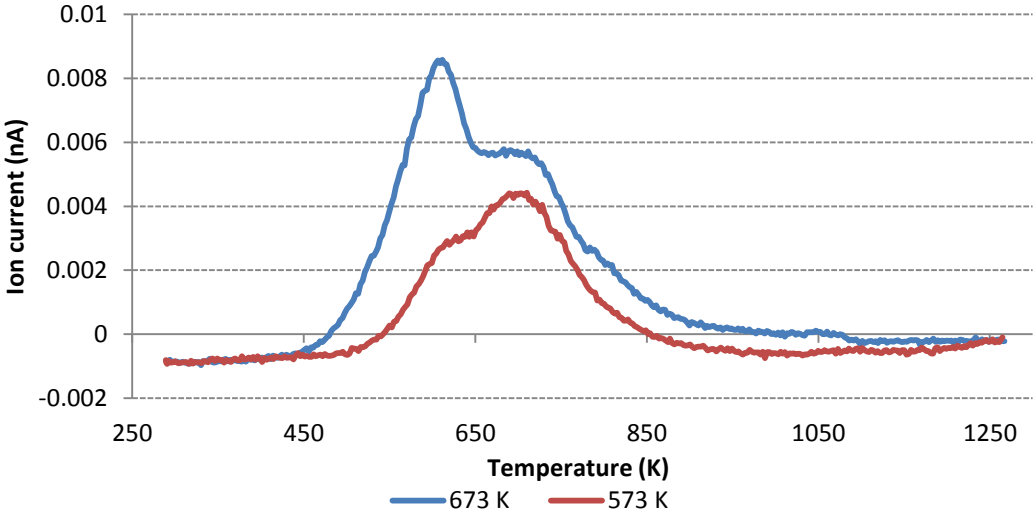

Figure 117: TPO profile of P/2,4HD mixed feed over K-CrO_x/Al_2O_3 catalyst

There is less carbon formation on the surface of the doped catalyst compared to the chromia catalyst, with an ~2% reduction. The Raman spectra confirm the deposition of carbon on the spent catalyst; the spectra reveals only G-band mode: no evidence for the D bands were observed

3.3.4 Pentane/2,4-Hexadiene (P/2,4HD) system

3.3.4.1 Reaction analysis and trans-hydrogenation activity evaluation

The conversion of pentane was poorer, during the trans-hydrogenation with this catalyst. This shows that the doping of the catalyst does not improve the activity of the catalyst. This is consistent with the thermodynamic limitation as mentioned above. Reaction with the 2,4-HD does not seems to influence the lifting of this limitations. The result is presented in Figure 118

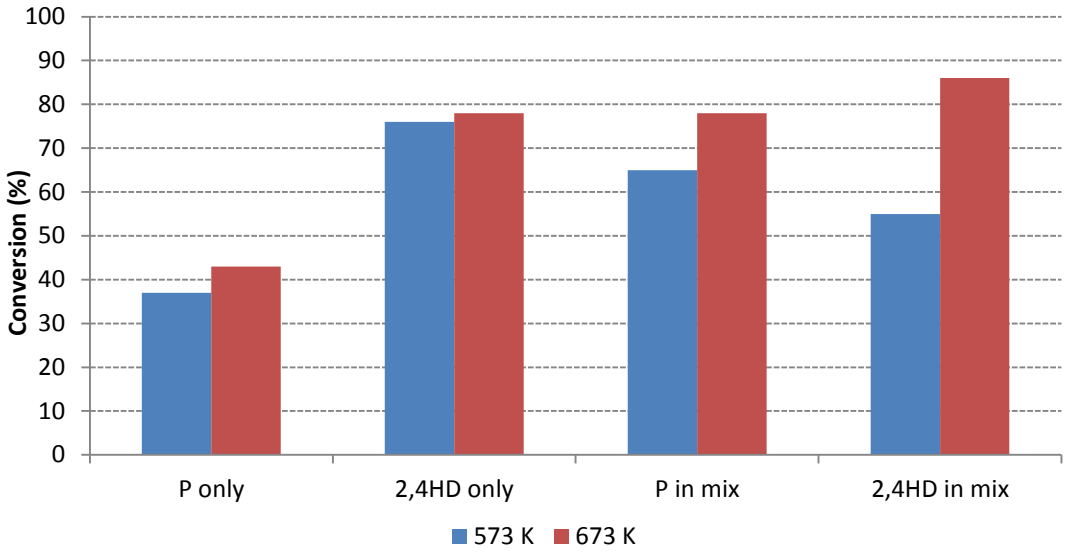

Figure 118: Conversion comparison of P, 2,4HD and P/2,4HD mixture using K-CrO_x/Al_2O_3

The product distribution is similar to what was observed with the chromia catalyst. However, there is a little improvement in the yield of the products on using the doped catalyst. The result are presented in Table 53 and 54

Table 53: Products yield of the trans-hydrogenation over K-CrO_x/Al_2O_3 using 2,4HD system at 673 K

	P	H	P+H	P+H Theory
	Conversion (%)			
Pentane(P)	43		11	43
2,4-Hexadiene (2,4HD)		68	76	76
	Yield (%)			
Iso-pentane				0
Pentene	22.82			22.82
Trans-2-Pentene	0.22			0.22
Cis-2-pentene	0.57			
Hexane				0
1-Hexene				0
2-Hexene				0
3-Hexene		2.88	3.87	2.88
1,3-Hexadiene				0
methyl-2-pentene		7.93	2.05	7.93
3-Methylhexane		2.02	11.4	2.02
2-Methyl-1,3-pentadiene		18.03	10.42	18.03
Methylcyclohexane	11.6	19.31	18.15	19.31

Table 54: Products yield of the trans-hydrogenation over K-CrO_x/Al_2O_3 using 2,4HD system at 573 K

	P	H	P+H	P+H Theory
	Conversion (%)			
Pentane(P)	38		15	38
2,4-Hexadiene (2,4HD)		66	45	66
	Yield (%)			
iso-pentane	10.38			0.38
Pentene				0
Trans-2-Pentene	0.42			0
Cis-2-pentene	0.71			
Hexane				0
1-Hexene				0
2-Hexene				0
3-Hexene		0.22	2.91	0.22
1,3-Hexadiene				0
methyl-2-pentene		3.45	5.94	3.45
3-Methylhexane		2.21	3.75	2.21
2-Methyl-1,3-pentadiene		10.85		10.85
2-methyl-1-1hexene		13.63	12.33	13.63
Methylcyclohexane	13.37	13.21	12.78	13.21

3.3.4.2 Post reaction characterization and analysis

The doped catalyst presents less weight loss with the 2,4HD system. The weight losses are very similar those observed with 1,5H system when the doped catalyst was used. There is also evidence for changes in these losses with the trans-hydrogenation process and a reduction in the weight loss is observed with a lower reaction temperature. This is consistent with previous results. The results are presented in Figure 119 and 120

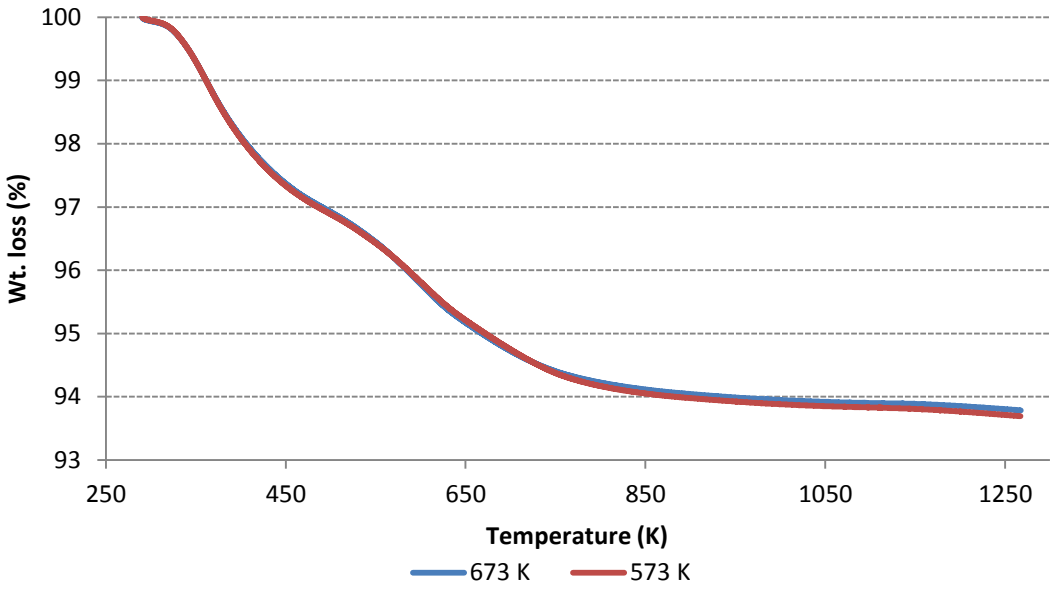

Figure 119: Weight loss profile of 2,4HD run alone over K-CrO_x/Al_2O_3 catalyst

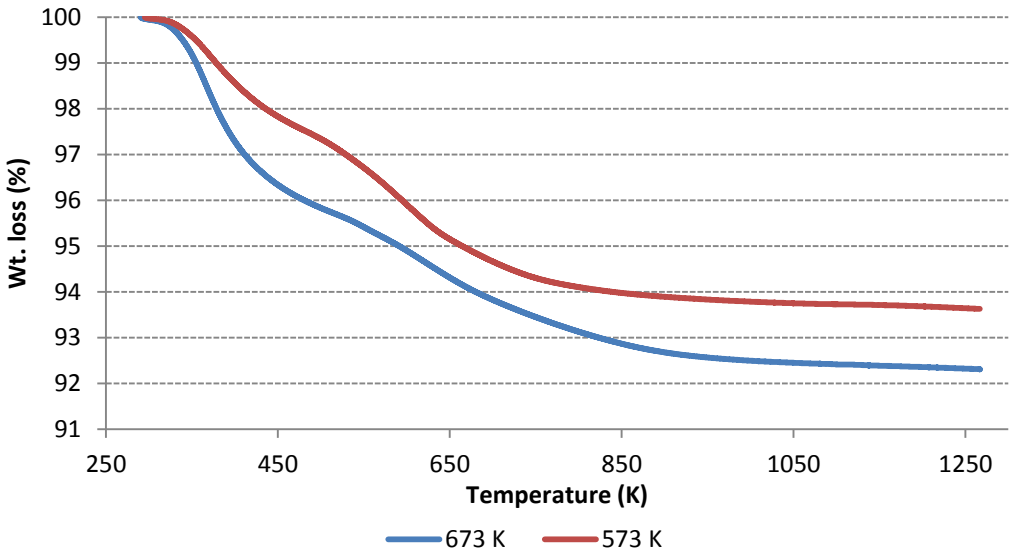

Figure 120: Weight loss profile of P/2,4HD mixed feed over K-CrO_x/Al_2O_3 catalyst

The TPO analysis here also revealed carbon dioxide as the main desorption species evolved at all the run temperatures. The TPO profiles reveal two main weight losses similar to the 1,5HD feed. All the losses are associated with the CO_2 but may be from different carbonaceous deposits. The peak ~608 K is more predominant at all reaction temperatures while the peak at ~700 K starts to disappear during the trans-hydrogenation and completely disappears at low reaction temperatures. The results are presented in Figure 121 and 122

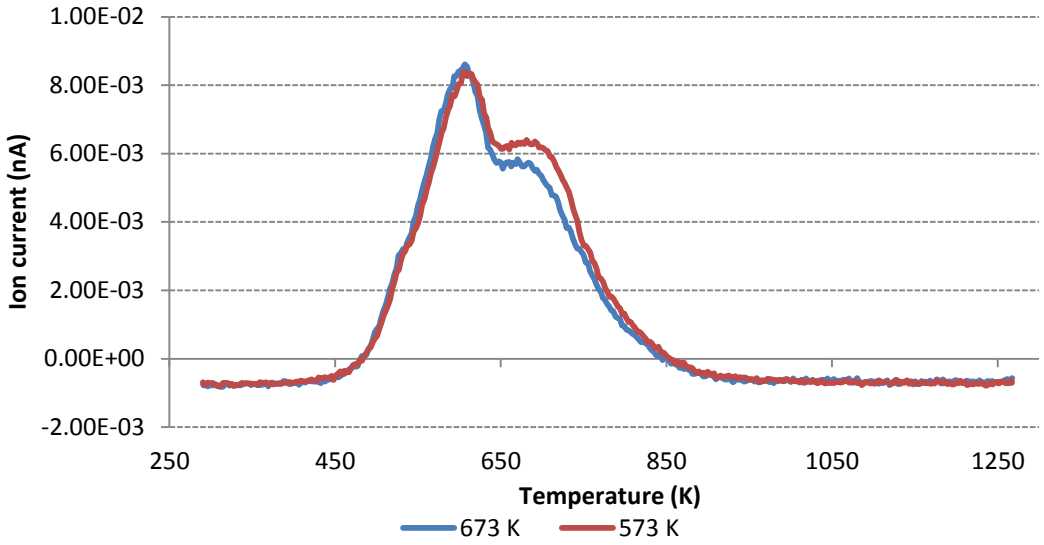

Figure 121: TPO profile of 2,4HD run alone over K-CrO_x/Al_2O_3 catalyst

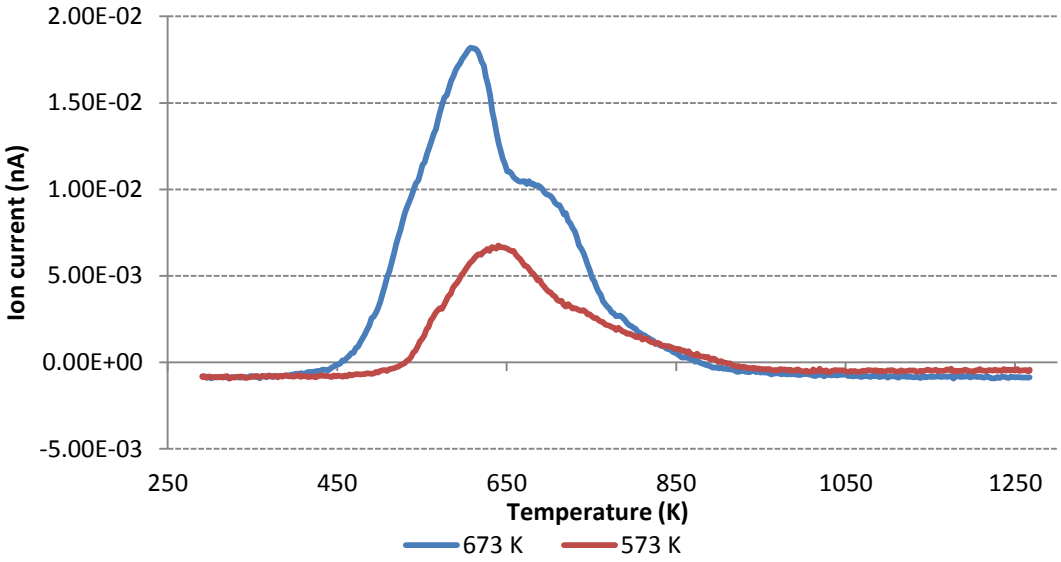

Figure 122: TPO profile of P/2,4HD mixed feed over CrO_x/Al_2O_3 catalyst

There is less carbon formation on the surface of the catalyst compared to the chromia catalyst. The Raman spectra also confirm the deposition of carbon on the spent catalyst; the spectra reveal only G-band mode and no evidence for the D bands were observed

3.4 Pt/Al_2O_3 catalyst

3.4.1 Pre-reaction catalyst characterisation

3.4.1.1 BET surface area and pore volume determination

The Pt/Al_2O_3 catalyst used in this work was a commercial 1wt. % supplied by Johnson Matthey (ref no: 1074).

Table 55 shows the summary of the parameters extracted from the BET analysis. The table result indicated the S_{BET}, pore volume and the pore diameter of the catalyst

Table 55: S_{BET}, pore volume and average pore diameter of the Pt/Al_2O_3 catalyst

	S_{BET} (m^2 g^{-1})	V_p(cm^3g^{-1})	D_p(Å)
Pt/Y-Al2O3	119	0.49	154

The adsorption isotherm for the catalyst was found to obey the type II model. The result is presented in Figure 123

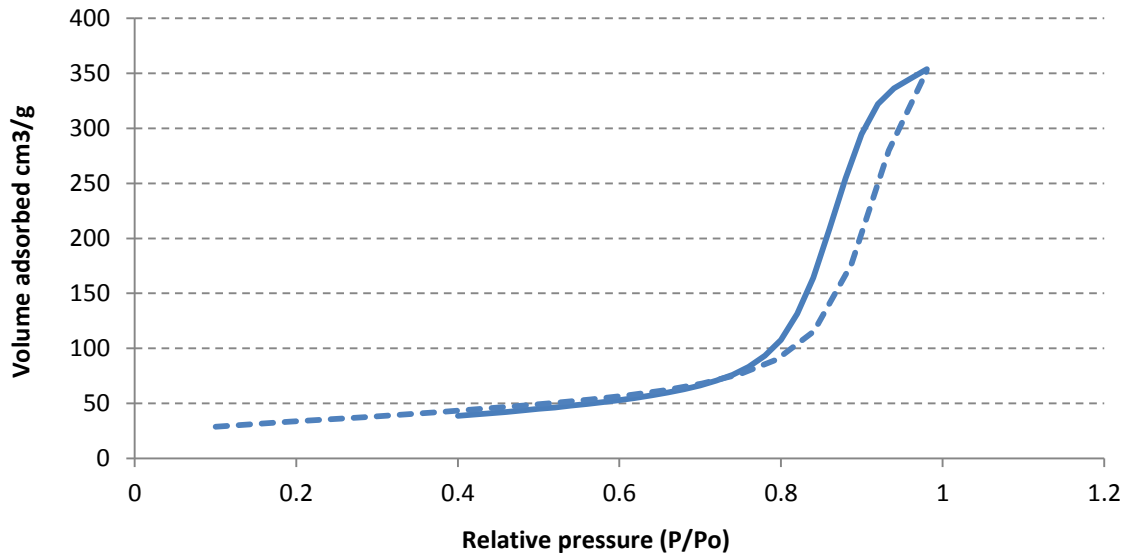

Figure 123: Nitrogen adsorption isotherm at 78 K for the support and the Pt/Al_2O_3 catalyst

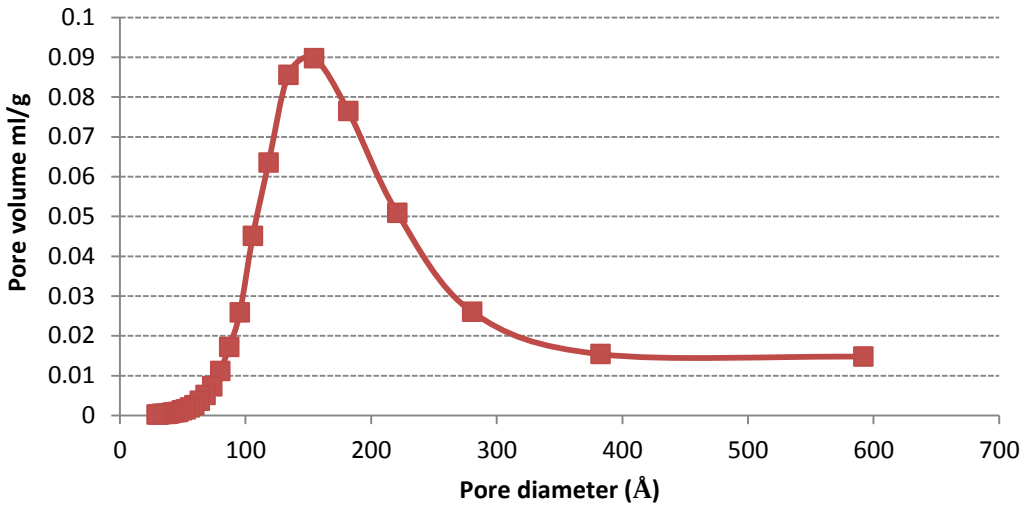

Figure 124: Pore volume distribution of the support and the Pt/Al_2O_3 catalyst

The pore volume distribution as measured in the mesopores range for the support is presented in Figure 124.

4.4.1.2 XRD analysis

The XRD analysis of the catalyst revealed a diffraction pattern associated with mixed theta and gamma alumina and no evidence was observed for the crystalline phase of the PtO, due to the low metal loading[87, 88]. The result is presented in Figure 125

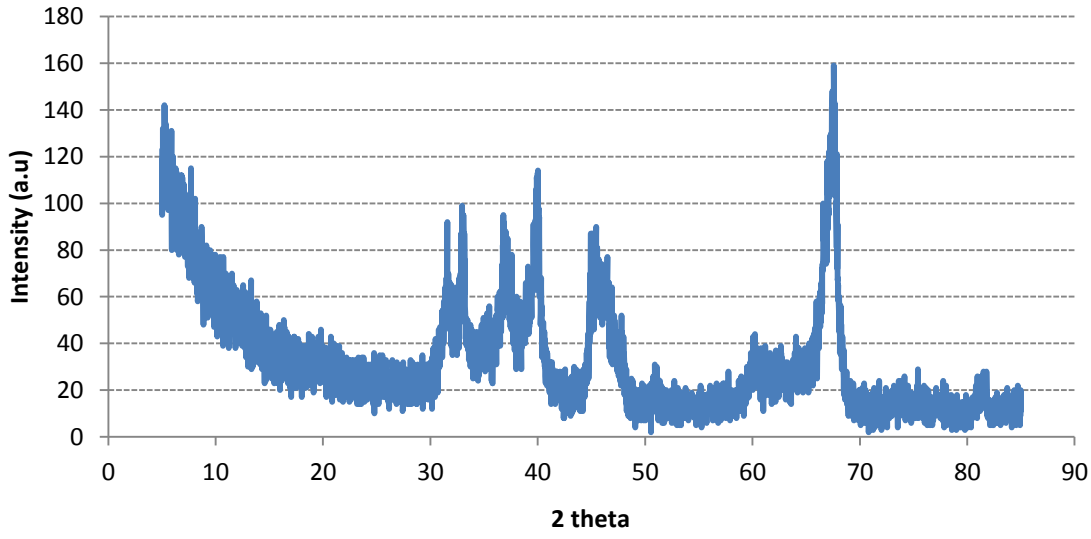

Figure 125: XRD diffraction pattern of the Pt/Al_2O_3 catalyst

4.4.1.3 Thermogravimetric analysis

The standard TGA-TPR obtained from ambient temperature to 1273 K is found to be consistent with the Ox-Red cycles and the reduction peak observed at ~473 K and ~510 K perfectly matches ones obtained with the reduction cycles. The result is presented in Figure 126

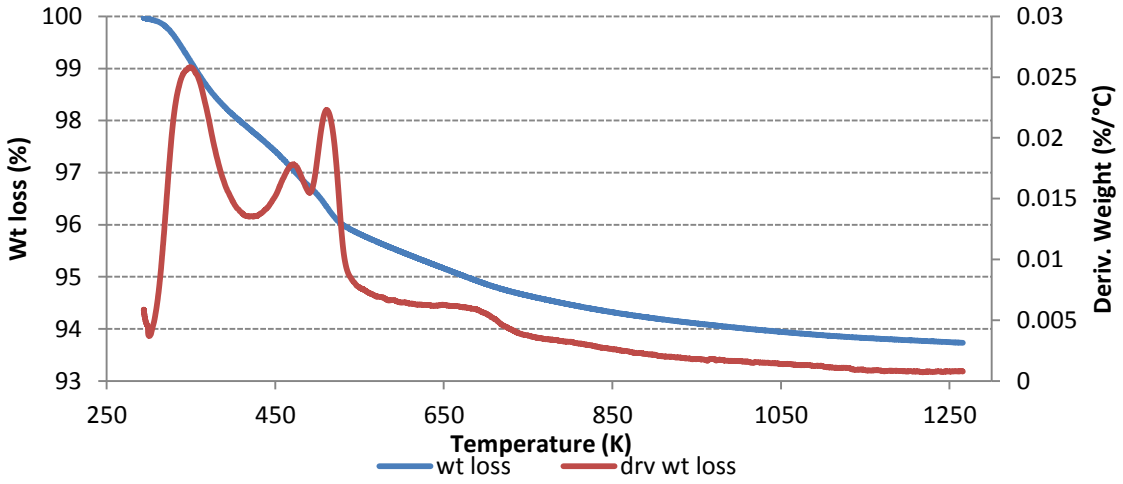

Figure 126: The standard TGA-TPR profile of the Pt/Al2O3 catalyst

The TGA-TPR obtained during the Ox-Red cycles showed two shouldered peaks at ~473 K and ~510 K obtained during the 1st cycle. It is not clear if the two peaks are associated with H_2 consumption, because the 2nd cycle presented no peaks. The first peak obtained at ~373 K is associated to desorption of physiosorbed H_2O from atmosphere. The result is presented in Figure 127.

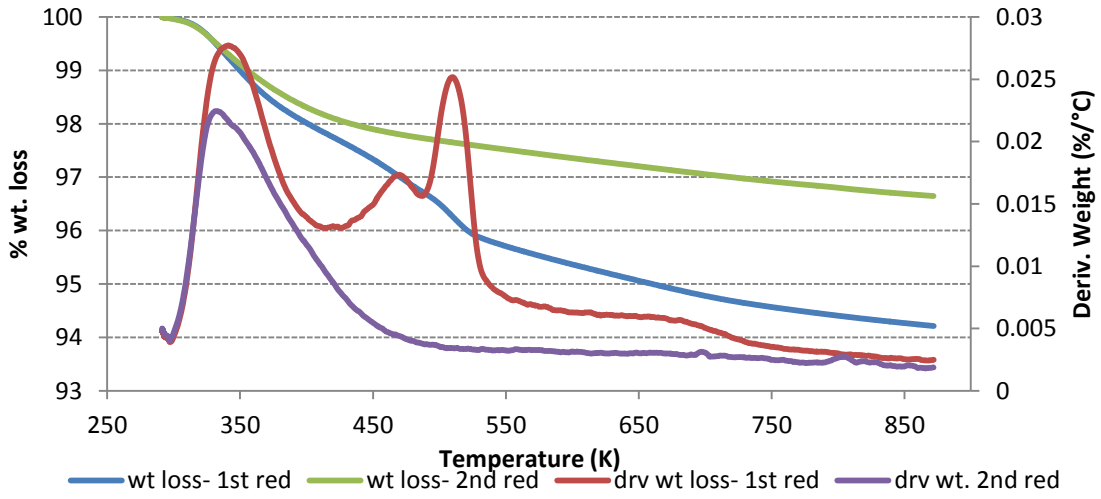

Figure 127: The TGA-TPR profile during the Red-OX cycles of the Pt/Al_2O_3 catalyst

The DTA of the reduction 1st and 2nd cycles shows one endothermic effect in the temperature ~373 K ascribed to the removal of physiosorbed water corresponding to moisture lost mainly from the alumina support and the weight loss is ~2% and ~1% respectively. An endothermic peak was also observed at ~ 510 K corresponding to weight loss of ~4% and was not observed during the second cycle. This confirms that there is uptake of heat energy due to the loss and therefore the weight loss can be predominantly assigned to the thermal decomposition of the platinum complex, and obviously a small hydrogen uptake for the reduction process. The result is presented in Figure 128

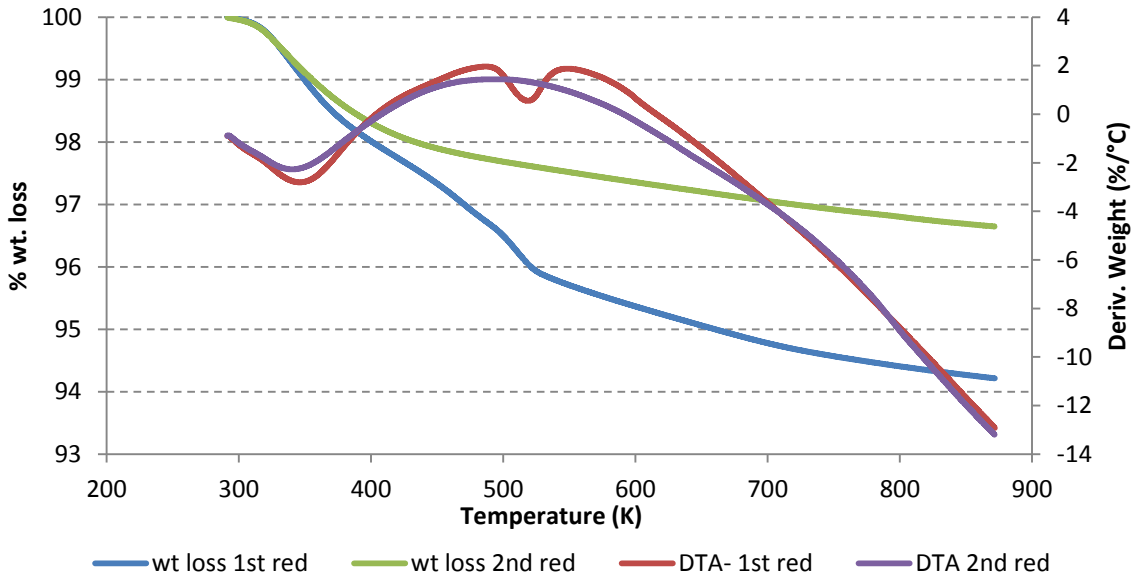

Figure 128: The DTA profile of the catalyst obtained during the TGA-TPR Ox-Red cycle of the Pt/Al2O3 catalyst

4.4.3.4 Raman analysis

The Raman spectrum obtained from the Pt/γ-Al_2O_3 catalyst is presented in Figure 129. The Raman spectrum contained a broad band at ~600 cm^{-1} assigned to an amorphous platinum oxide vibration, similar to the one obtained with EUROPT-1 [89]. The alumina support does not show any Raman feature in the region studied. However, the sharp band at ~300 cm^{-1} may have arisen due to residual Cl which may be present in the Pt/γ-Al_2O_3 catalyst. The chlorine could be from the precursor salt during the catalyst preparation as argued by Graham *et al*. [90]

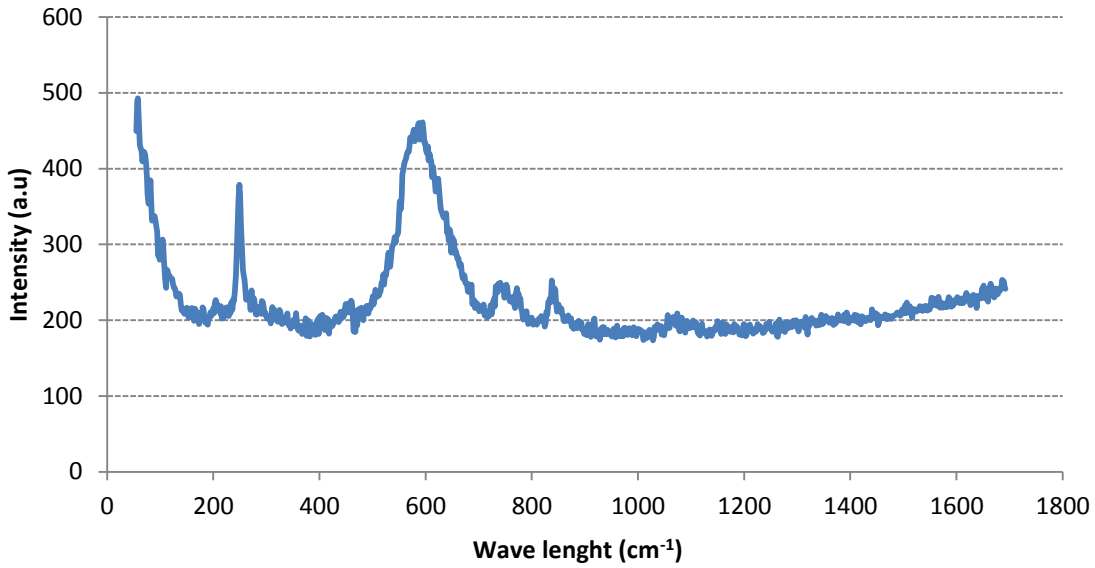

Figure 129: Raman spectrum of the Pt/Al_2O_3 catalyst

3.4.2 Pentane/Hexyne (P/1HY) system

3.4.2.1 Reaction analysis and trans-hydrogenation activity evaluation

The reactant conversions were followed individually and during the mixed trans-hydrogenation reaction, as in previous reactions with the chromia catalyst. There is an observed increase in the conversion of the pentane at all temperatures in the trans-hydrogenation process. There is a 10% increase on average, for dehydrogenation conversions of the pentane, when run alone with the platinum catalyst compared to chromia catalyst. This value is also higher than the equilibrium conversion of n-pentane dehydrogenation (~14 %). However, the ratio in the conversions of the pentane obtained during the dehydrogenation with that obtained during the trans-hydrogenation using the platinum is about the same as with the chromia catalyst (~1:2). The result is presented in Figure 130.

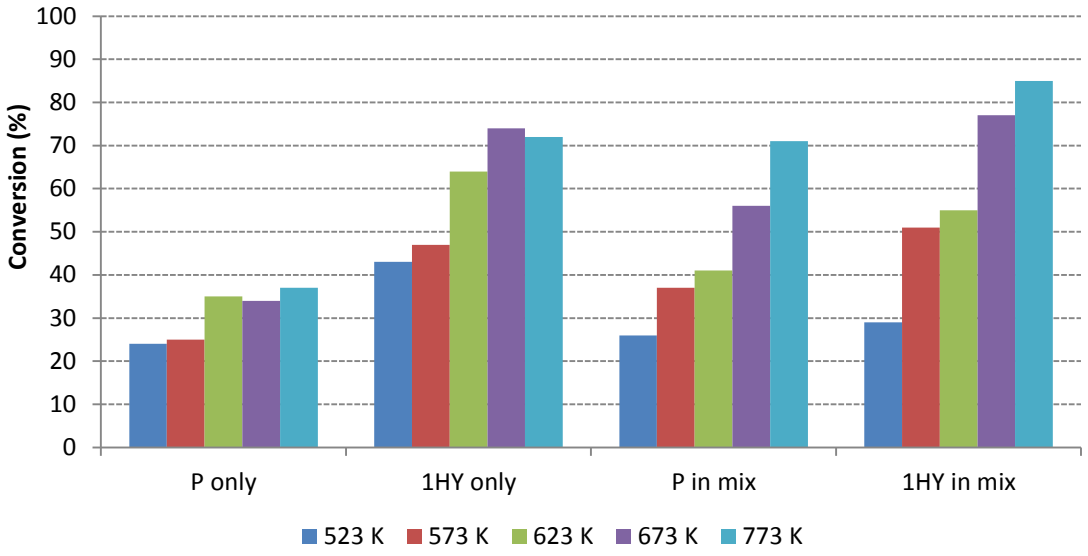

Figure 130: Conversion comparison of P, 1HY and P/1HY mixture using Pt/Al_2O_3

The products yields are presented in Table 56-60. Most of these products are alkylated and alkylated olefin products obtained with the trans-hydrogenation. The product distribution is similar at all the reaction temperatures, only the individual yield of the products changes. There is similarity here with the chromia catalyst. However, the individual yields were observed to either increase or decrease across the temperature range. The pentane dehydrogenation presented more valuable products, but lower hydrocarbon products were observed with hexyne run alone at higher temperature. The yield of the desired products increases with mixed feeds and more valuable products are observed with the trans-hydrogenation process.

Table 56: Products yield of the trans-hydrogenation over Pt/Al_2O_3 at 773 K

	P	H	P+H	P+H Theory
	Conversion (%)			
Pentane(P)	37		71	37
1-Hexyne(1HY)		71	85	71
	Yield (%)			
Iso-pentane	1.67	0.23	0.23	1.9
Pentene	4.01		0.36	4.01
Trans-2-Pentene	5.27	8.03	3.15	13.3
Cis-2-pentene	2.64		0.18	2.64
4-methylpentene	0.52			0.52
hexane		0.31	0.3	0.31
1-Hexene		1.18	2.79	1.18
2-Hexene		0.61	0.36	0.61
3-Hexene		0.6	2.25	0.6
Methyl-2-pentene		10.31	3.3	10.31
3-Methylpentyne		27.53	30.98	27.53
3-Methyl-1-hexene			8.68	0
Benzene			0.9	0
3-Methylhexane		2.5	1.44	2.5
2-Methyl-1,3-pentadiene		0.46	5.98	0.46
Methylcyclohexane	17.03	14.62	9.32	31.65

Table 57: Products yield of the trans-hydrogenation over Pt/Al_2O_3 at 673 K

	P	H	P+H	P+H Theory
	Conversion (%)			
Pentane(P)	34		56	34
1-Hexyne(1HY)		74	77	74
	Yield (%)			
Iso-pentane	1.18	1.22	2.21	2.4
Pentene	2.59	0.33		2.92
Trans-2-Pentene	1.92	0.2		2.12
Cis-2-pentene	1.93	2.87		3.8
4-Methylpentene		5.38		5.38
Hexane		0.98		0.98
1-Hexene		3.67	3.06	3.67
2-Hexene		1.58	1.11	1.58
3-Hexene		4.83	4.02	4.83
Methyl-2-pentene		7.77	10.99	7.77
3-Methylpentyne		1.97	13.54	1.97
3-Methyl-1-hexene		9.52	1.11	9.52
Benzene		6.95		6.95
3-Methylhexane		3.21		3.21
2-Methyl-1,3-pentadiene		13.25	16.99	13.25
Methylcyclohexane	17.03	3.06	9.44	20.09

Table 58: Products yield of the trans-hydrogenation over Pt/Al2O3 at 623 K

	P	H	P+H	P+H Theory
	Conversion (%)			
Pentane(P)	35		41	35
1Hexyne(1HY)		64	55	64
	Yield (%)			
Iso-pentane	1.27	13.93	0.86	15.2
Pentene	0.16			0.16
Trans-2-Pentene	3.45			3.45
Cis-2-pentene	1.56			1.56
Hexane		0.17		0.17
1-Hexene		0.74	3.06	0.74
2-Hexene		0.39	1.84	0.39
3-Hexene		0.67	1.38	0.67
Methyl-2-pentene		6.61	11.52	6.61
3-Methylpentyne		18.41	14.54	18.41
3-methyl-1-hexene		2.39		2.39
Benzene				0
3-Methylhexane		0.71		0.71
2-Methyl-1,3-pentadiene		8.95	12.55	8.95
Methylcyclohexane	14.83	2.82	10.65	17.65

Table 59: Products yield of the trans-hydrogenation over Pt/Al_2O_3 at 573 K

	P	H	P+H	P+H Theory
	Conversion (%)			
Pentane(P)	25		37	25
1-Hexyne(1HY)		47	51	47
	Yield (%)			
Iso-pentane	1.51		0.22	1.51
Pentene	0.11		0.31	0.11
Trans-2-Pentene	0.69		0.2	0.69
Cis-2-pentene	0.23			0.23
Hexane			0.33	0
1-Hexene		1.29	3.64	1.29
2-Hexene		0.39	1.91	0.39
3-Hexene		0.5	4.29	0.5
Methyl-2-pentene			1.04	0
3-Methylpentyne		12.67	13.99	12.67
3-Methyl-1-hexene			8.09	0
Benzene				0
3-Methylhexane		0.71	1.30	0.71
2-Methyl-1,3-pentadiene		0.47	19.7	0.47
Methylcyclohexane	14.83	4.85	12.51	9.68

Table 60: Products yield of the trans-hydrogenation over Pt/Al_2O_3 at 523 K

	P	H	P+H	P+H Theory
	Conversion (%)			
Pentane(P)	25		26	25
1-Hexyne(1HY)		37	29	37
	Yield (%)			
Iso-pentane	**1.08**		**2.01**	**1.08**
Pentene	**0.01**			**0.01**
Trans-2-Pentene	**2.04**			**2.04**
Cis-2-pentene	**0.01**			**0.01**
Hexane		0.11		**0.11**
1-Hexene		**0.52**	**0.15**	**0.52**
2-Hexene		0.13		**0.13**
3-Hexene		**1.28**		**1.28**
Methyl-2-pentene		**0.61**	4.21	**0.61**
3-Methylpentyne				**0**
3-Methyl-1-hexene		**1.84**	1.71	**1.84**
Benzene				**0**
3-Methylhexane		**0.38**		**0.38**
2-Methyl-1,3-pentadiene		1.64	0.59	**1.64**
Methylcyclohexane	12.21	11.59	11.99	**23.8**

The total olefin yield is shown in Figure 131. The yield ~20% at 773 K obtained using the Pt/Al_2O_3 catalyst was similar to that found with the chromia catalyst. The ratio of olefin to alkylated olefins was about 1:1.5 at most temperatures. The olefin production was observed to be higher compared to the other valuable products obtained during the trans-hydrogenation as presented in Figure 132. There was also an increase in these valuable products with the reaction temperature (Figure 133)

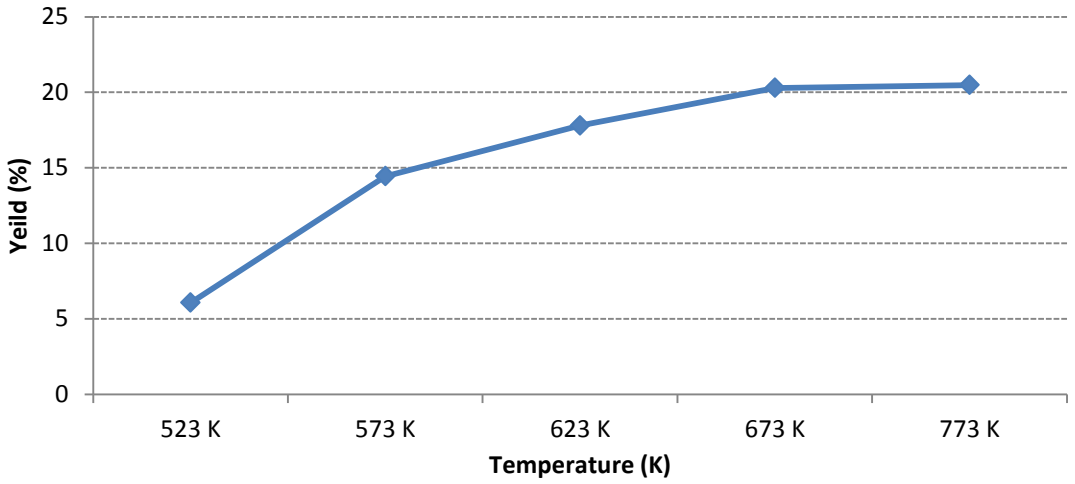

Figure 131: Total olefin yield with temperature over the Pt/Al_2O_3 using 1HY system

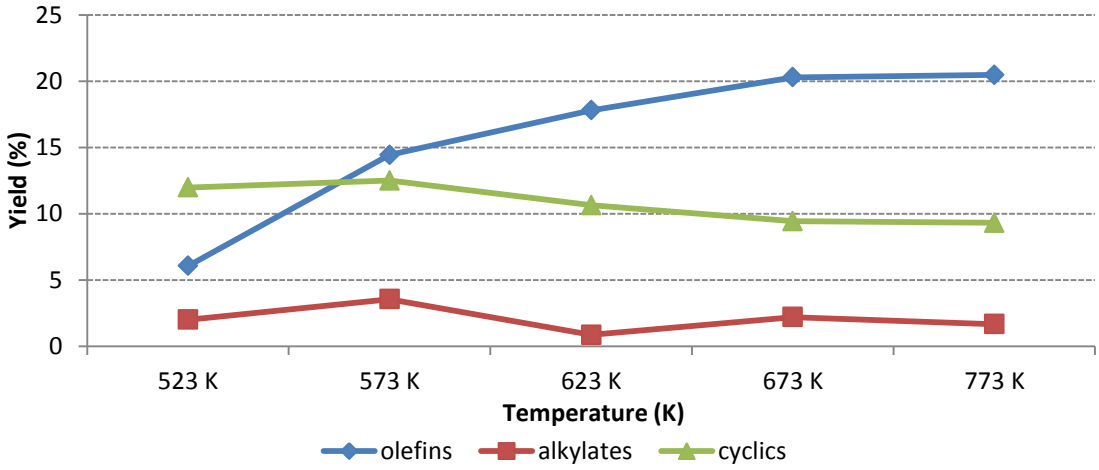

Figure 132: Profile of valuable product in relative to the reaction temperature over Pt/Al_2O_3 using 1HY system

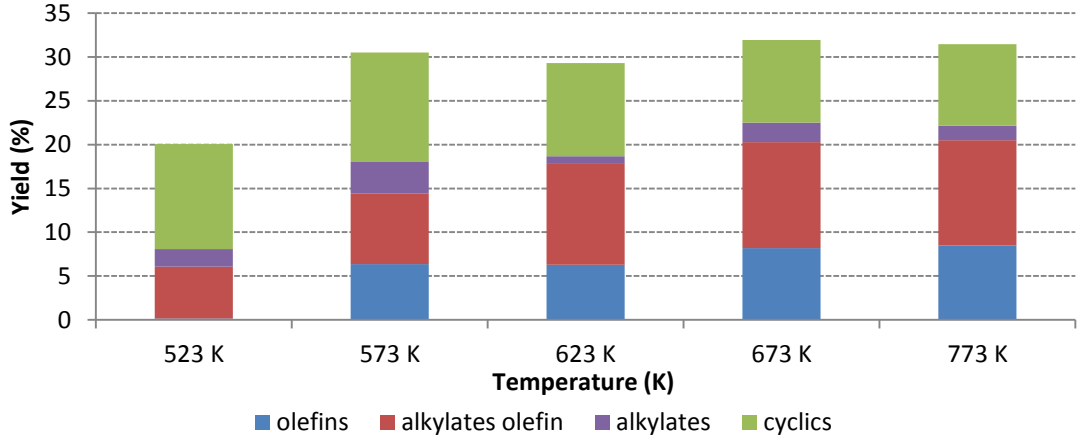

Figure 133: Relationship of the valuable products over Pt/Al_2O_3 using 1HY system

The analysis of the eluent gas products during pentane dehydrogenation confirms the evolution of H_2, CH_4 and C_2H_4. Evolution of hydrogen was observed from the start of the reaction and maintained for the reaction period. Pulses of CH_4 and C_2H_4 were also evolved but completely declined by ~20 min. The result obtained at 773 K is presented in Figure 134. Only pulses of hydrogen, methane and ethene were observed during the hexyne run (Figure 135). Whilst during the trans-hydrogenation, there hydrogen was still observed at all times on stream but it was gradually consumed in the process (Figure 136)

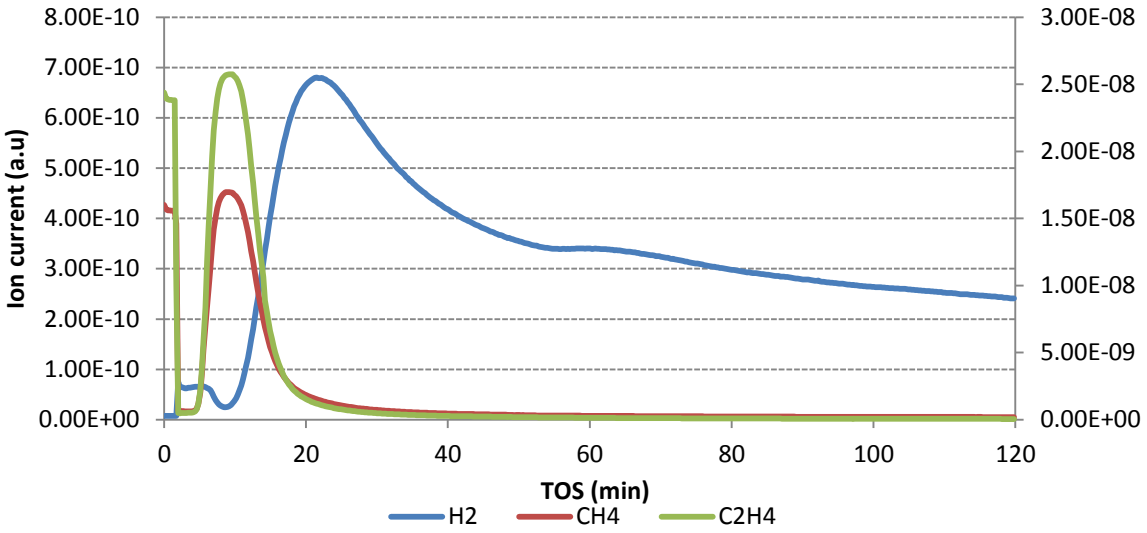

Figure 134: Profile of the evolved gases over Pt/Al_2O_3 using P only at 773 K

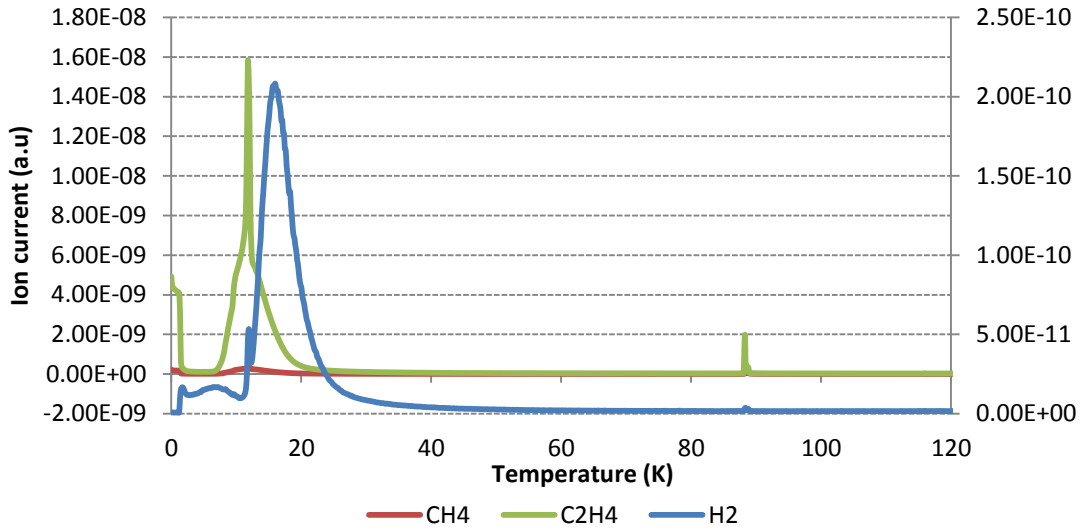

Figure 135: Profile of the evolved gases over Pt/Al_2O_3 using 1HY only at 773 K

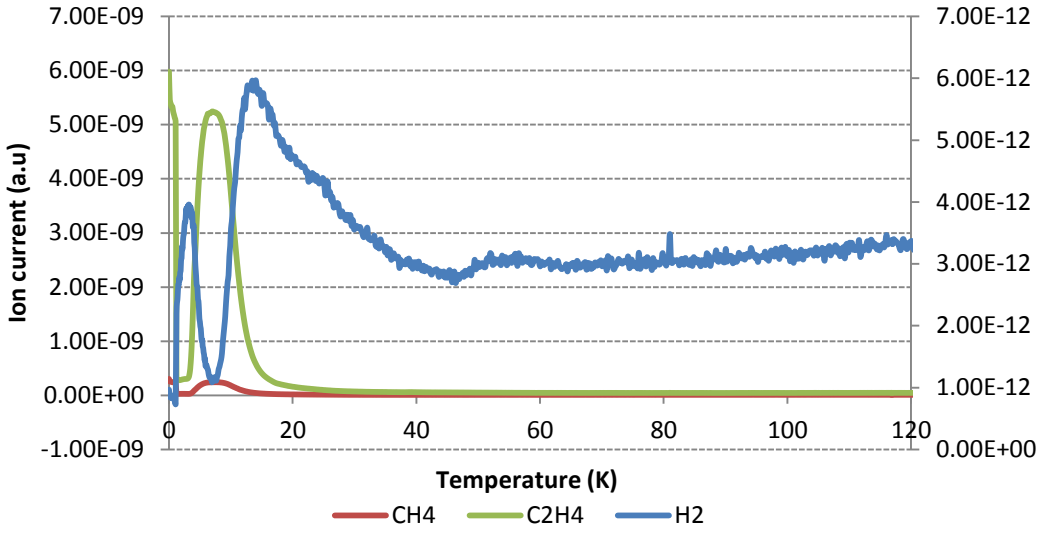

Figure 136: Profile of the evolved gases over Pt/Al_2O_3 using P/1HY at 773 K

Table 61: carbon balance for the P/1HY trans-hydrogenation reaction over the Pt/Al_2O_3 catalyst

Temperature (K)	Carbon balance (%)				
	Liquid Ptds.	CH4	C2H4	coke	Pdts Non accounted
773	89	-	-	0.31	10.69
673	90	-	-	0.29	9.08
623	93	-	-	0.26	6.74
573	92	-	-	0.11	7.89
523	94	-	-	0.09	5.91

The hydrogenation reactions were performed over the 623-523 K temperature. The reaction products and distribution obtained were observed to be similar to that obtained with trans-hydrogenation process but the hydrogenation process exhibits a higher percentage yield of these products. Unlike the chromia catalyst, there is also increase in the conversion of the hexyne during the hydrogenation process. Although there are similarities, but the hydrogenation process exhibited higher olefinic products and more value added products were obtained than with the chromia catalyst. The results are presented in Tables 62,

63 and 64. There hydrogenation results presented higher olefins value but these values were observed to have increase during the trans-hydrogenation compared to when the hexyne is run alone.

Table 62: Products yield during the hydrogenation of1HY over the Pt/Al_2O_3 at 623 K

	1HY	P+H	P+H Theory
1-Hexyne(1HY)	**Conversion (%)**		
	76	55	64
	Yield (%)		
Iso-pentane	6.73	0.86	15.2
Pentene			0.16
Trans-2-Pentene			3.45
Cis-2-pentene			1.56
Hexane	1.37		0.17
1-Hexene	16.86	3.06	0.74
2-Hexene	3.12	1.84	0.39
3-Hexene	2.41	1.38	0.67
Methyl-2-pentene	3.63	11.52	6.61
3-Methylpentyne	4.46	14.54	18.41
3-Methyl-1-hexene	0.6		2.39
Benzene			0
3-Methylhexane			0.71
2-Methyl-1,3-pentadiene	3.24	12.55	8.95
Methylcyclohexane	8.69	10.65	17.65

Table 63: Products yield during the hydrogenation of1HY over the Pt/Al_2O_3 at 573 K

	1HY	P+H	P+H Theory
	Conversion (%)		
1-Hexyne(1HY)	68	51	47
	Yield (%)		
Iso-pentane		0.22	1.51
Pentene		0.31	0.11
Trans-2-Pentene		0.2	0.69
Cis-2-pentene			0.23
Hexane	4.01	0.33	0
Hexene	14.09	3.64	1.29
2-Hexene	4.21	1.91	0.39
3-Hexene	6.42	4.29	0.5
Methyl-2-pentene	1.38	1.04	0
3-Methylpentyne		13.99	12.67
3-Methyl-1-hexene	1.2	8.09	0
Benzene			0
3-Methylhexane		1.3	0.71
2-Methyl-1,3-pentadiene	3.42	19.7	0.47
Methylcyclohexane	14.81	12.51	9.68

Table 64: Products yield during the hydrogenation of1HY over the Pt/Al_2O_3 at 523 K

	1HY	P+H	P+H Theory
	Conversion (%)		
1-Hexyne(1HY)	69	29	37
	Yield (%)		
Iso-pentane	4.7	2.01	1.08
Pentene			0.01
Trans-2-Pentene			2.04
Cis-2-pentene			0.01
Hexane	3.7		0.11
1-Hexene	12.05	0.15	0.52
2-Hexene	3.31		0.13
3-Hexene	3.74		1.28
Methyl-2-pentene	0.82	4.21	0.61
3-Methylpentyne			0
3-Methyl-1-hexene	0.71	1.71	1.84
Benzene			0
3-Methylhexane	0.38		0.38
2-Methyl-1,3-pentadiene	3.12	0.59	1.64
Methylcyclohexane	23.64	11.99	23.8

The TGA analysis of the spent catalyst shows a unique weight loss with each type of reactant using the platinum catalyst with variation in the amount of the loss with lower temperature. The amount of lost material is also observed to vary as a function of the reaction temperatures. The pentane run presented very small differences across the temperature range. The reaction at 773 K, 673 K and 623 K during the hexnye run revealed about the same weight loss while reaction at 573 K and 523 K revealed a similar weight loss, there is also a very significant difference in the weight loss between the two temperature groups. The main loss observed with pentane was observed at ~373 K and there was no obvious loss after that. Whilst with hexyne and the mixed feeds there were two distinct main weight losses, the first occurred at ~ 375 – 480 K and the second loss

occurred at ~510-800 K. However, a general reduction in the weight loss was observed using the mixed feed trans-hydrogenation process. The results are presented in figures 137, 138 and 139

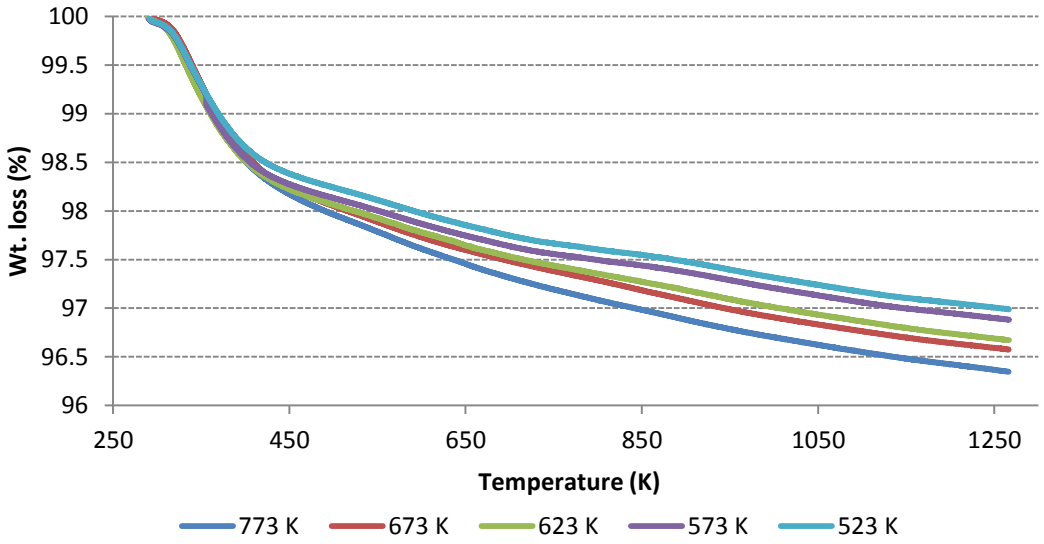

Figure 137: Weight loss profile of pentane run alone over Pt/Al_2O_3 catalyst

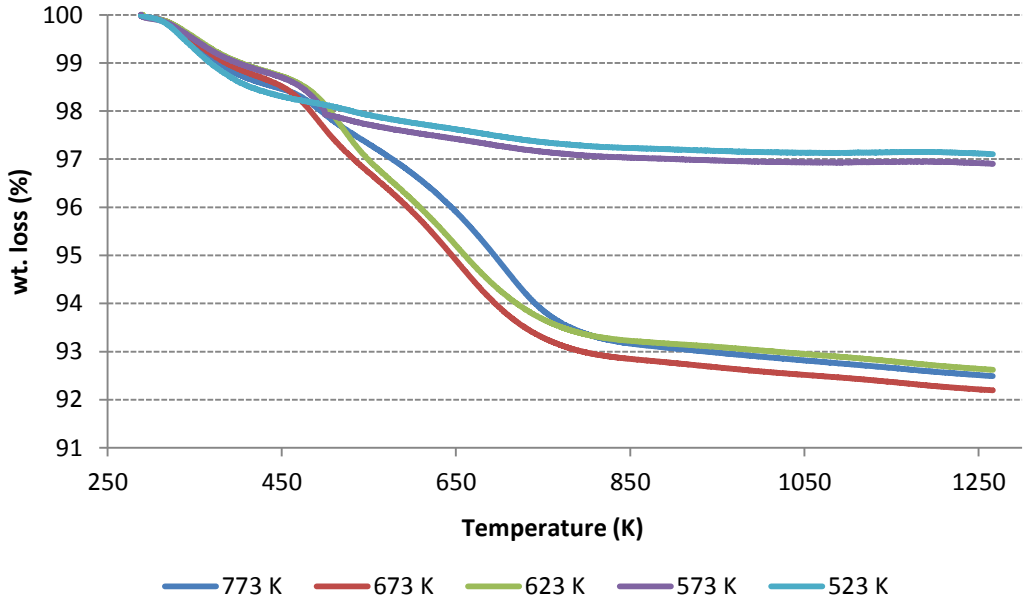

Figure 138: Weight loss profile of hexyne run alone over Pt/Al_2O_3 catalyst

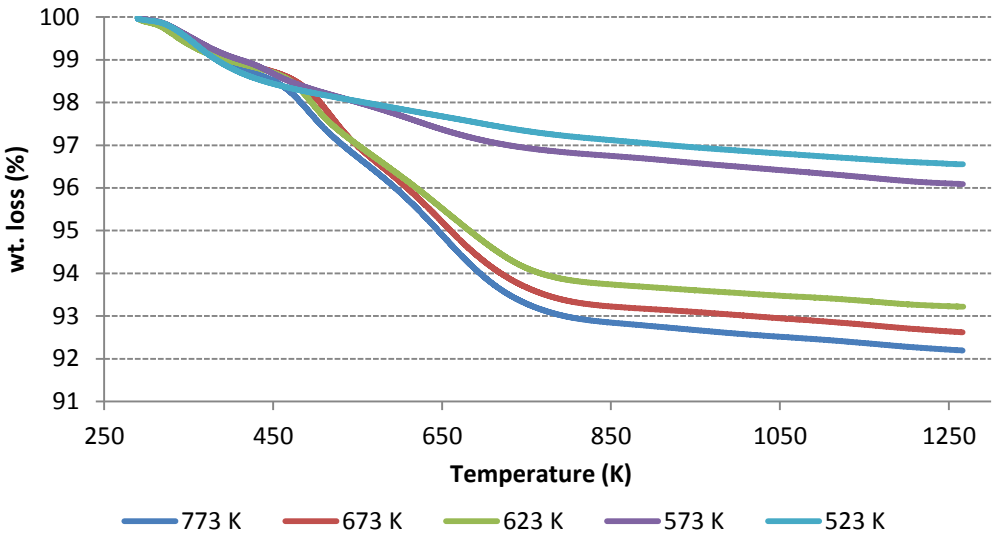

Figure 139: Weight loss profile of P/1HY mixed feed over Pt/Al_2O_3 catalyst

TPO analysis of the spent catalyst during the TGA revealed carbon dioxide as the main desorption species evolved with all the reactions. However, there was no clear and obvious evidence for this during the pentane run. There is also confirmed two different carbon species during the trans-hydrogenation and the hexyne run, with observed changes during the two processes. This was determined by the mass spectrometer (m/e 44). The results are presented in figure 140, 141 and 142

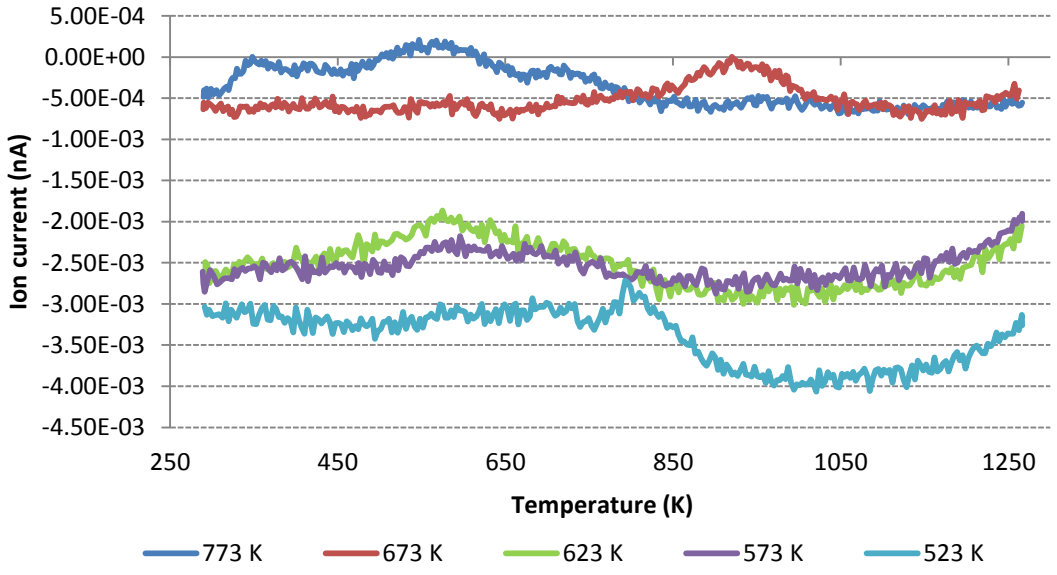

Figure 140: TPO profile of pentane over Pt/Al_2O_3 catalyst

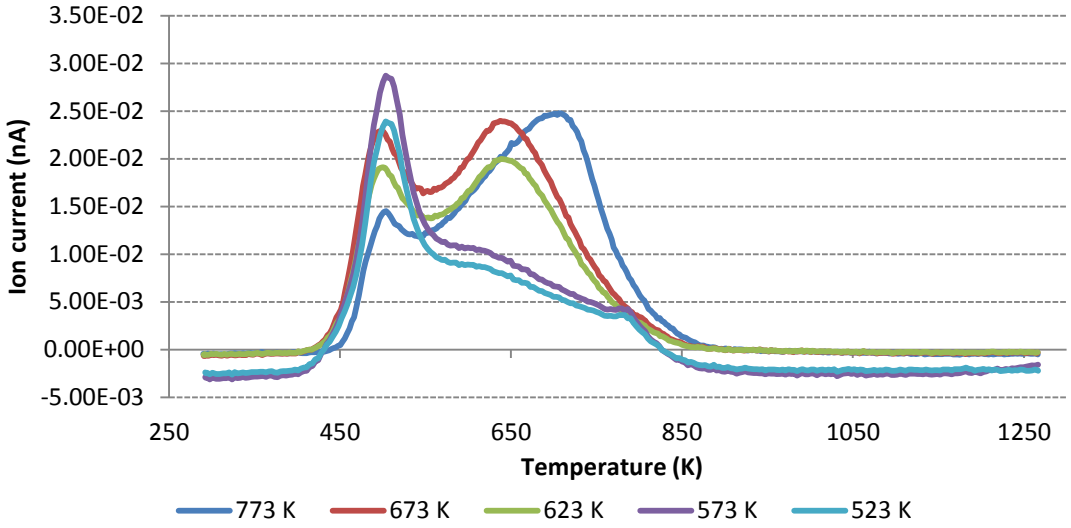

Figure 141: TPO profile of hexyne over Pt/Al_2O_3 catalyst

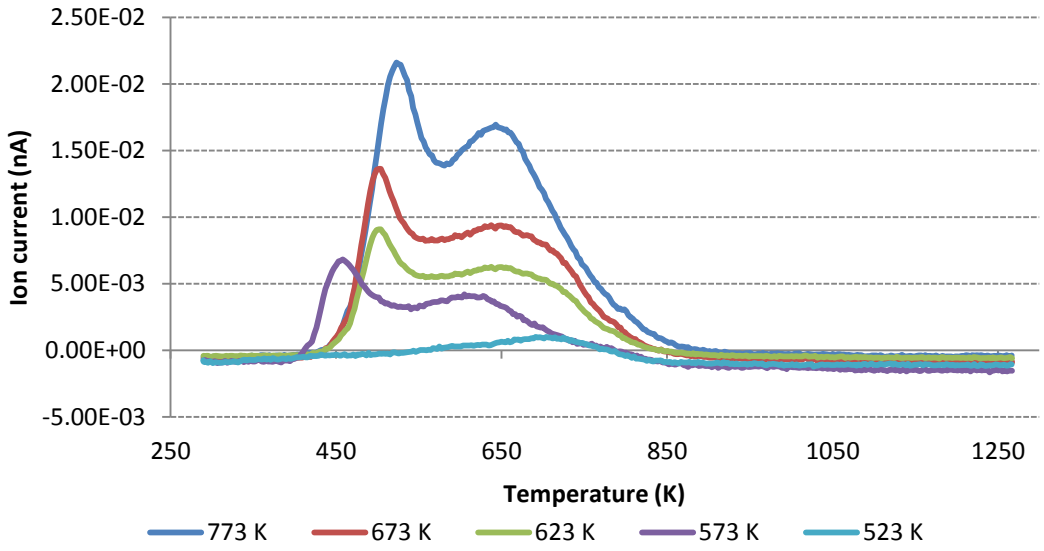

Figure 142: TPO profile of P/1HY mixed feed over Pt/Al_2O_3 catalyst

Meanwhile, The TPO of the spent catalyst obtained during the hydrogenation process is presented in Figure 143. It reveals a profile similar to that obtained during the trans-hydrogenation.

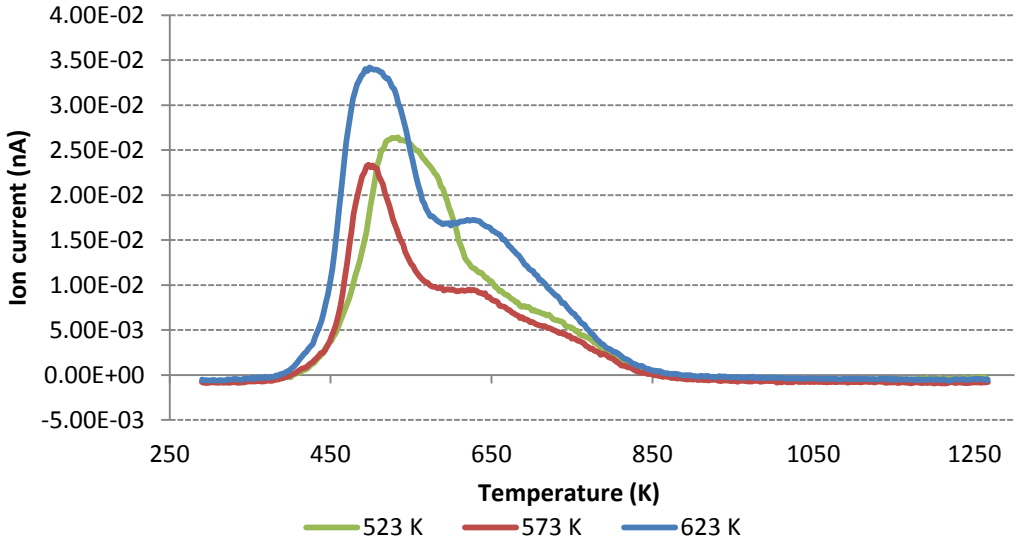

Figure 143: TPO profile during 1HY hydrogenation over Pt/Al_2O_3 catalyst

In addition to this, fragments (m/e 2, 16, 18 and 28) were also monitored. However, apart from the CO_2 only trace levels of CO were detected in some of the samples. The evolution of the CO species matches the two peaks observed with the TGA derivative weight loss profile and could be a fragmentation species of the CO_2 desorption. The result obtained from the hydrogenation process also presented same type of species

The carbon laydown analysis is presented in Figure 144. It is observed that the extent of carbon deposition was only half of that observed with the CrO_x/Al_2O_3. However, unlike the CrO_x/Al_2O_3 system, only a slight reduction from the catalysts run at 773-623 K in carbon laydown was observed during the mixed feed trans-hydrogenation, whilst slightly higher laydowns were obtained from the catalysts run at 573 and 523 K. Samples which had been subjected to hexyne reactant only showed higher amounts of weight loss except for the reactions at 573 and 523 K. Reaction with pentane alone revealed less weight loss compared to hexyne or the mixed feed. There was observed significant reduction in carbon deposition compared to when hexyne and the mixed feed were used, only ~0.3% was obtained at 773 K. This is also significantly less compared to what was obtained with the chromia catalyst (~2.4%). The percentage carbon deposit for each run individually and as a mixed feed is determined and presented in Figure 144

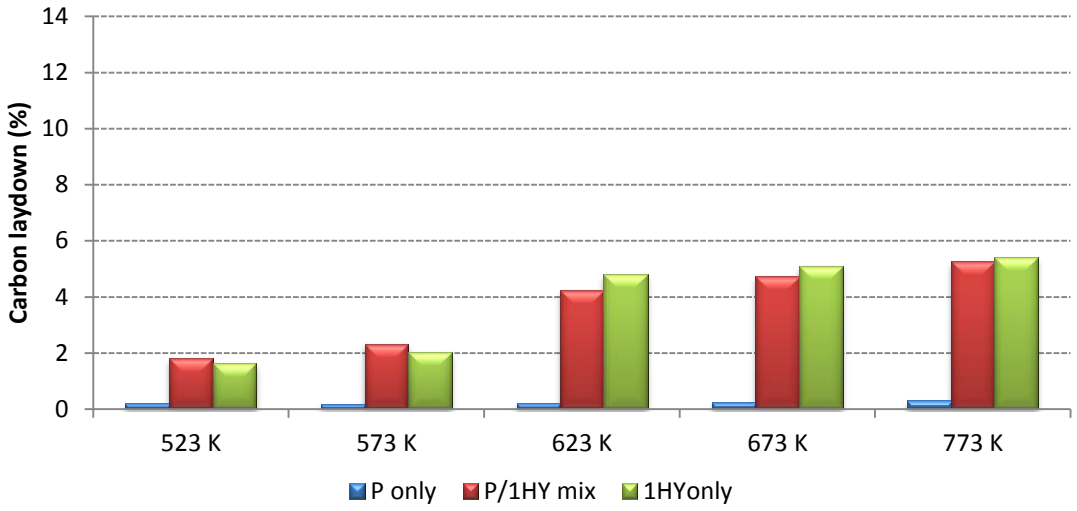

Figure 144: Carbon laydown of the spent Pt/Al_2O_3 catalyst over the set temperatures using P/1HY system

Table 65: Total amount of carbon deposited on spent Pt/Al_2O_3 catalyst at various temperatures

Temperature (K)	Carbon deposited (g/g feed)		
	P	P/1HY	1HY
523	0.00039	0.0029	0.0132
573	0.00035	0.0037	0.0166
623	0.00041	0.0067	0.0391
673	0.00045	0.0074	0.0416
773	0.00061	0.0083	0.0440

The analysis of the spent catalyst using Raman spectroscopy was performed using both UV and visible radiation to study the carbon deposit. The UV radiation has been used to avoid fluorescence which provides advantages to study heavily coke material as previously explained [81, 82] and has also been successfully used to study either fresh or heavily coke material in this regards,[83, 84] because the Raman peaks under UV excitation are enhanced and more intense [85]. We were unable to detect any Raman band with the spent platinum catalyst from either the pentane or hexyne runs or their mixed feed with the visible radiation. However, analysing the spent catalyst from the pentane experiments with UV radiation bands were observed at all the temperature run

except for the 773 K presenting a slightly more intense G-band at ~1600 cm^{-1} associated with carbon deposit. Raman bands assigned to coke deposition at ~1380 and 1600 cm^{-1} related to D and G bands respectively were observed with the hexyne runs and the mixed feed. However, the D band was lost in the spectra obtained from the catalysts used at 523 and 573 K with hexyne feed, whilst the D-band was observed only with the catalyst run at 773 K using the mixed feed trans-hydrogenation process. Meanwhile, when the catalysts were analysed with visible radiation, they fluoresced and no clear bands were observed. There were no Raman spectra bands assigned to Platinum observed with the spent catalyst. The results are presented in figures 145, 146 and 147

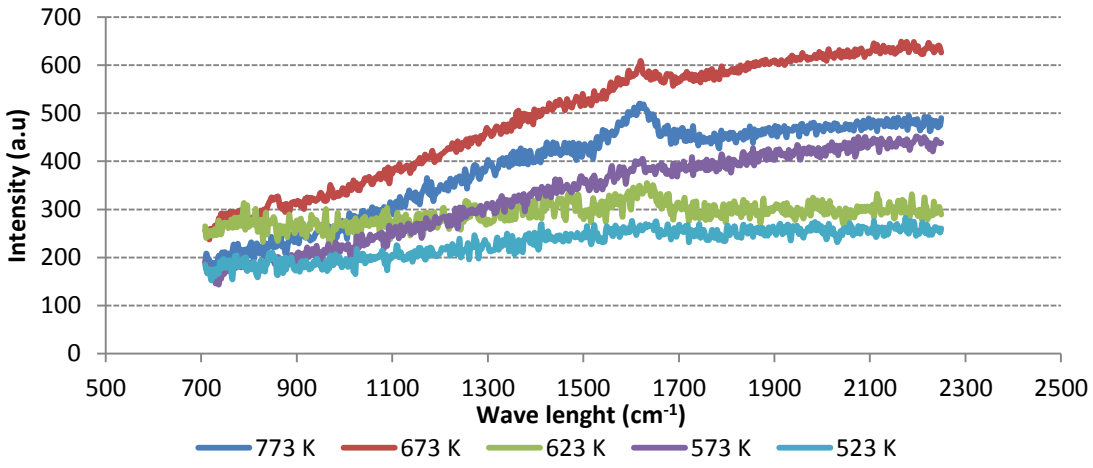

Figure 145: Raman spectra of spent Pt/Al_2O_3 catalyst for sole pentane obtained using the UV-radiation

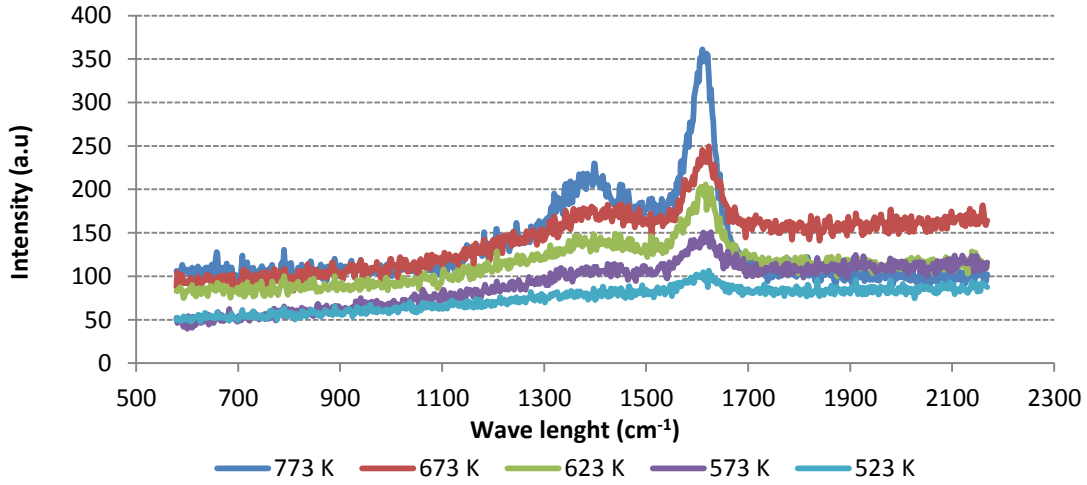

Figure 146: Raman spectra of spent Pt/Al_2O_3 catalyst for sole hexyne obtained using the UV-radiation

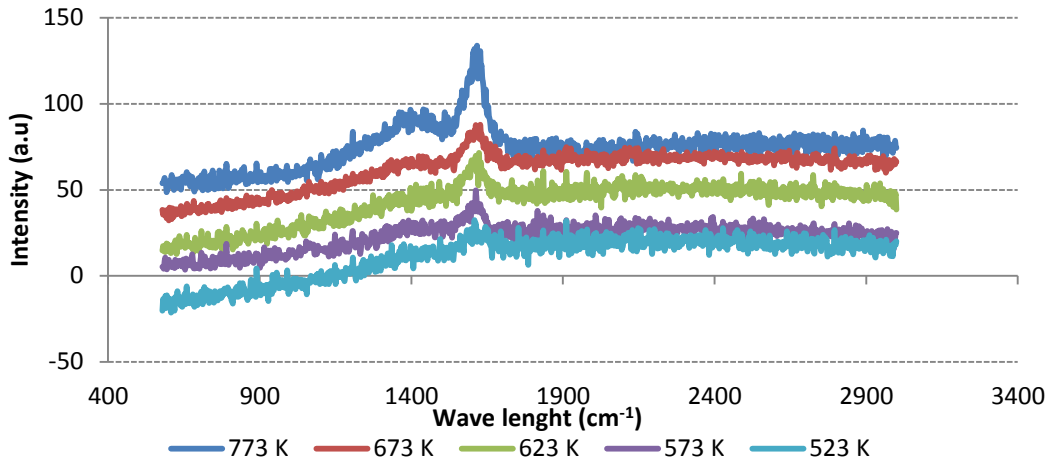

Figure 147: Raman spectra of spent Pt/Al_2O_3 catalyst for mixed feeds obtained using the UV-radiation

The BET analysis performed on the spent catalyst reveals no clear changes in the surface area of the spent catalyst after the reaction at all temperature. Unlike the chromia catalyst where a slight reduction in surface area as a function of temperature was observed, the platinum catalyst still maintains its initial surface area after the reaction with ~±5 $m^2 g^{-1}$ which is within the variability of the measurement. The formation of coke on the platinum catalyst does not show effects on the S_{BET} area and the pore volume, although only a small carbon deposit was observed with the platinum compared to the chromia catalyst.

The XRD analysis of the spent catalyst revealed only the diffraction pattern for γ-alumina and there was not any obvious changes observed in the diffraction pattern at any temperature due to these reactions (Figure 148)

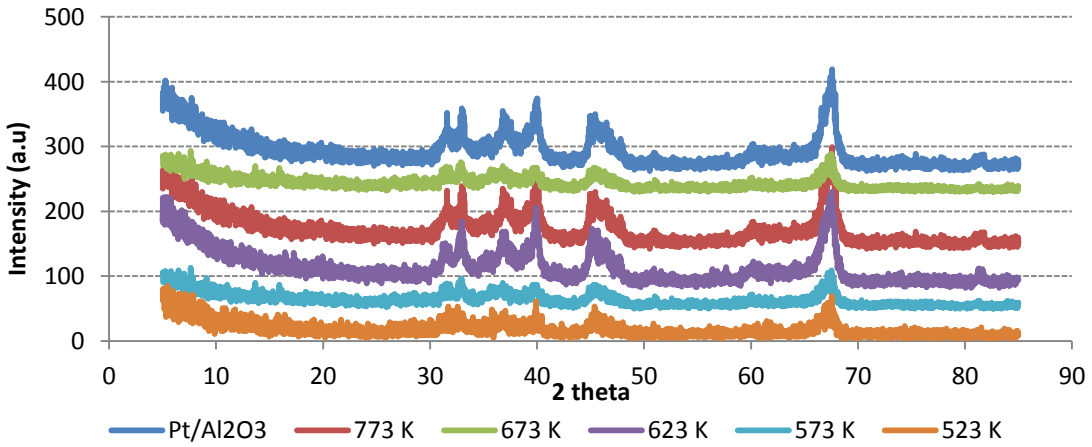

Figure 148: XRD diffraction patterns of the Pt/Al_2O_3 catalyst pre- and post- reaction

3.4.3 Pentane/1,5-Hexdiene (P/1,5HD) system

3.4.3.1 Reaction analysis and trans-hydrogenation activity evaluation

The reactant conversions were followed individually and during the mixed trans-hydrogenation reaction also here using the 1,5HD system. There is observed an increase in the conversion of pentane at all temperatures (except for 523 K), with the trans-hydrogenation process compared to the conversions of the pentane dehydrogenation. However, conversion lower than what was observed with the chromia catalyst were obtained, ~60% at 773 K compared to ~90% obtained with the chromia catalyst. The result is presented in Figure 149.

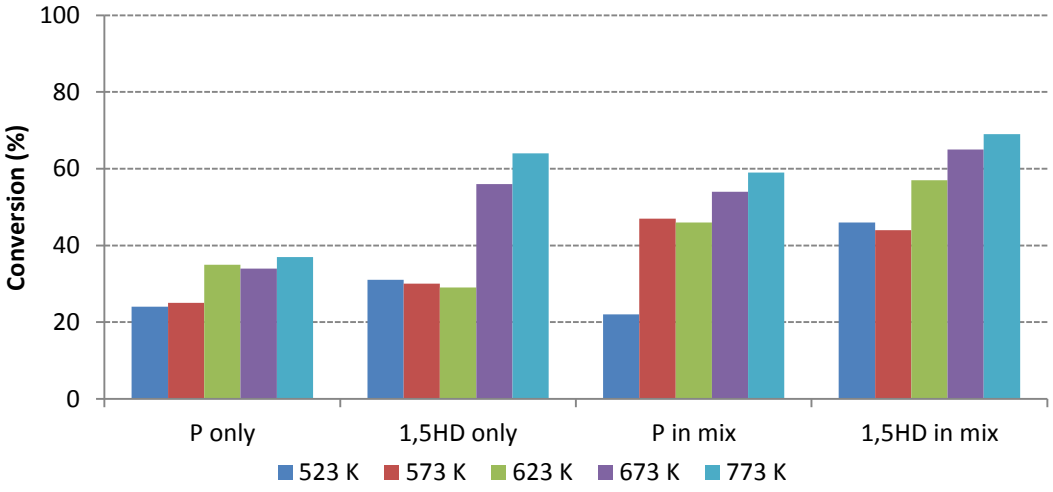

Figure 149: Conversion comparison of P, 1,5HD and P/1,5HD mixture using Pt/Al_2O_3

The product yields were calculated and presented in Table 66-70. Most of these products are also alkylated and alkylated olefin products obtained with trans-hydrogenation similar to the chromia catalyst. The product distribution is the same across the temperature range, but the individual yield of the products changes with the temperature. The yield of the desired products increases with mixed feeds and more valuable products are observed during the trans-hydrogenation process. Although most of the products were the same as the 1HY system, except for 3-methylpentyne which is not observed here, there are also similarities with the chromia catalyst.

Table 66: Products yield of the trans-hydrogenation over 1,5HD system at 773 K using Pt/Al_2O_3

	P	H	P+H	P+H Theory
	Conversion (%)			
Pentane(P)	37		59	37
1,5-Hexadiene(1,5HD)		64	69	64
	Yield (%)			
Iso-pentane	1.67		2.51	1.67
Pentene	4.01		0.01	4.01
Trans-2-Pentene	5.27		2.02	5.27
Cis-2-pentene	2.64	0.07	2.08	2.71
2-Methyl-2-butene	0.52	0.16	0.01	0.68
4-Methylpentene	1.67	0.02		1.69
Hexane			1.95	0
1-Hexene		0.27	1.05	0.27
2-Hexene		0.09		0.09
3-Hexene		2.89	7.8	2.89
Methyl-2-pentene		3.64	3.8	3.64
3-Methyl-1-hexene		5.8	5.24	5.8
Benzene		0.84	0.26	0.84
3-Methylhexane		1.86	1.31	1.86
2-Methyl-1,3-pentadiene		3.9	2.23	3.9
2-Methyl-1-1hexene		0.45		0.45
Methylcyclohexane	17.03	12.75	19.75	29.78

Table 67: Products yield of the trans-hydrogenation over 1,5HD system at 673 K using Pt/Al_2O_3

	P	H	P+H	P+H Theory
	Conversion (%)			
Pentane(P)	34		54	34
1,5-hexadiene (1,5HD)		56	65	56
	Yield (%)			
Iso-pentane	1.18		1.03	1.18
Pentene	2.59			2.59
Trans-2-Pentene	1.92			1.92
Cis-2-pentene	1.93	0.05		1.98
2-Methyl-2-butene	1.18	0.12	0.01	1.30
Hexane		1.18	3.1	1.18
1-Hexene		1.77	2.31	1.77
2-Hexene		1.27	1.13	1.27
3-Hexene		5.16	6.35	5.16
Methyl-2-pentene		2.51	1.59	2.51
3-Methyl-1-hexene		4.76	4.61	4.76
Benzene		0.43		0.43
3-Methylhexane		2.12	3.45	2.12
2-Methyl-1,3-pentadiene		6.57	4.71	6.57
2-Methyl-1-1hexene		2.56		2.56
Methylcyclohexane	17.03	14.76	15.61	32.64

Table 68: Products yield of the trans-hydrogenation over 1,5HD system at 623 K using Pt/Al_2O_3

	P	H	P+H	P+H Theory
	Conversion (%)			
Pentane(P)	35		46	35
1,5-hexadiene (1,5HD)		29	57	29
	Yield (%)			
Iso-pentane	1.27		1.03	1.27
Pentene	0.16			0.16
Trans-2-Pentene	3.45			3.45
Cis-2-pentene	1.56			1.56
2-Methyl-2-butene		0.13	0.04	0.13
Hexane		0.43	0.1	0.43
1-Hexene		1.74	2.65	1.74
2-Hexene		0.79	0.25	0.79
3-Hexene		3.36	6.36	3.36
Methyl-2-pentene		1.41	1.11	1.41
3-Methyl-1-hexene		3.08	4.62	3.08
Benzene			0.23	0
3-Methylhexane		0.98	2.91	0.98
2-Methyl-1,3-pentadiene		3.19	3.57	3.19
2-Methyl-1-1hexene		0.54	2.67	0.54
Methylcyclohexane	14.83	4.51	17.21	19.34

Table 69: Products yield of the trans-hydrogenation over 1,5HD system at 573 K using Pt/Al_2O_3

	P	H	P+H	P+H Theory
	Conversion (%)			
Pentane(P)	25		47	25
1,5-hexadiene (1,5HD)		30	44	30
	Yield (%)			
Iso-pentane	1.51		1.03	
Pentene	0.11		2.01	1.51
Trans-2-Pentene	0.69			0.11
Cis-2-pentene	0.23			0.69
2-Methyl-2-butene				0.23
Hexane		0.22		0.22
1-Hexene		0.98	1.1	0.98
2-Hexene		1.39		1.39
3-Hexene		2.51	5.3	2.51
Methyl-2-pentene		0.53	0.2	0.53
3-Methyl-1-hexene		3.85	4.68	3.85
3-Methylhexane		1.38	2.65	1.38
2-Methyl-1,3-pentadiene		3.72	3.62	3.72
2-Methyl-1-1hexene		1.54	2.76	1.54
Methylcyclohexane	14.83	4.96	14.1	19.79

Table 70: Products yield of the trans-hydrogenation over 1,5HD system at 523 K using Pt/Al_2O_3

	P	H	P+H	P+H Theory
	Conversion (%)			
Pentane(P)	24		22	24
1,5-hexadiene (1,5HD)		31	46	31
	Yield (%)			
Iso-pentane	1.08		2.01	1.08
Pentene	0.01			0.01
Trans-2-Pentene	2.04			2.04
Cis-2-pentene	0.01			0.01
Hexane		0.11		0.11
1-Hexene		1.52	2.15	1.52
2-Hexene		1.13		1.13
3-Hexene		3.28	3.79	3.28
Methyl-2-pentene		0.61	0.21	0.61
3-Methyl-1-hexene		2.84	2.71	2.84
3-Methylhexane		1.38	2.84	1.38
2-Methyl-1,3-pentadiene		1.64	1.59	1.64
2-Methyl-1-hexene		2.65	3.46	2.65
Methylcyclohexane	12.21	6.59	11.99	18.80

There was an increase in the yield of the total olefin with increasing reaction temperature; ~22 % total olefin was obtained at 723 K which is ~25% lower than the chromia catalyst. The total olefin comprises also the alkylated olefins, and the olefin to alkylated olefins ratio is about 1:1 at most temperatures. However, the total valuable product which is the summation of both the olefins, alkylated olefins and alkylated products is ~45% using the 1,5HD system at 773 K which is less than the chromia catalyst. Higher yield of the valuable products were predominantly observed at higher temperatures as presented in Figure 150. The olefin production is observed to be higher than the other valuable as presented in Figure 151. There is also an increase in these valuable products with the reaction temperature (Figure 152)

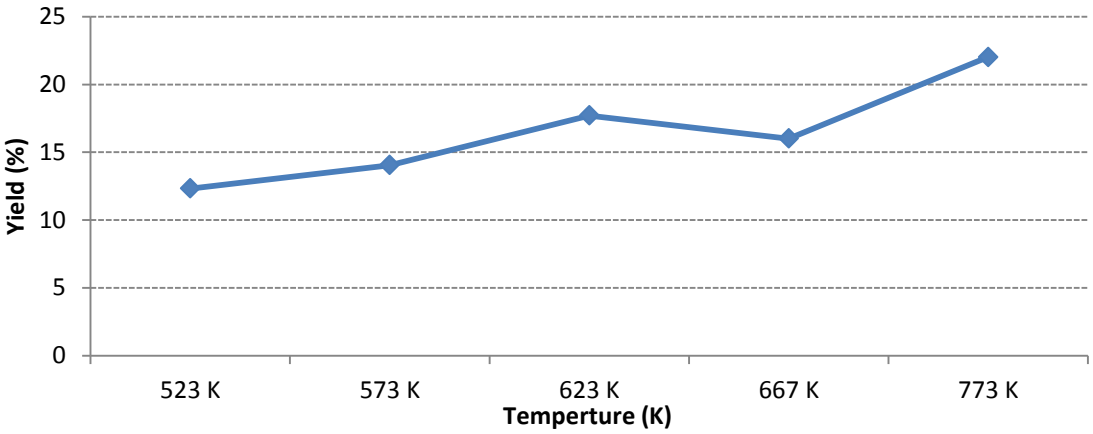

Figure 150: Total olefin yield with temperature over the Pt/Al_2O_3 using 1,5HD system

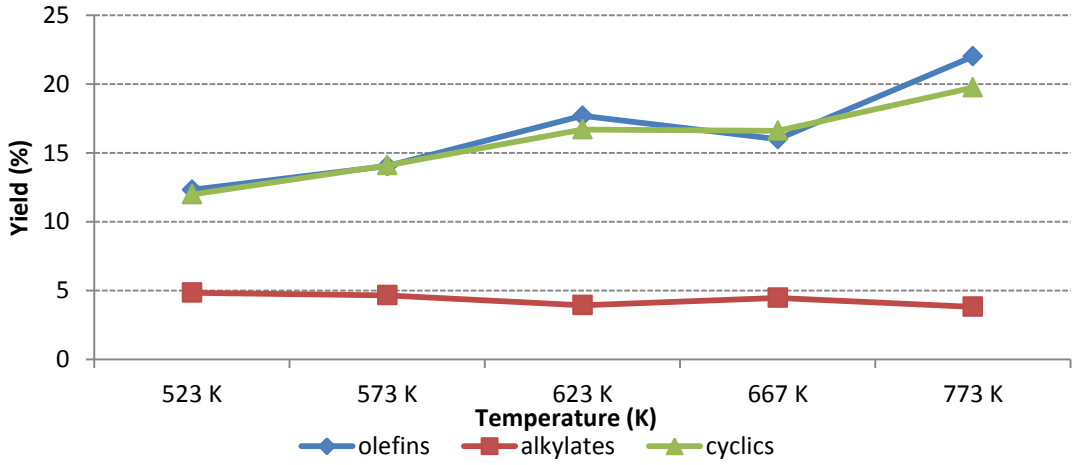

Figure 151: Profile of valuable product relative to the reaction temperature over Pt/Al_2O_3 using 1,5HD system

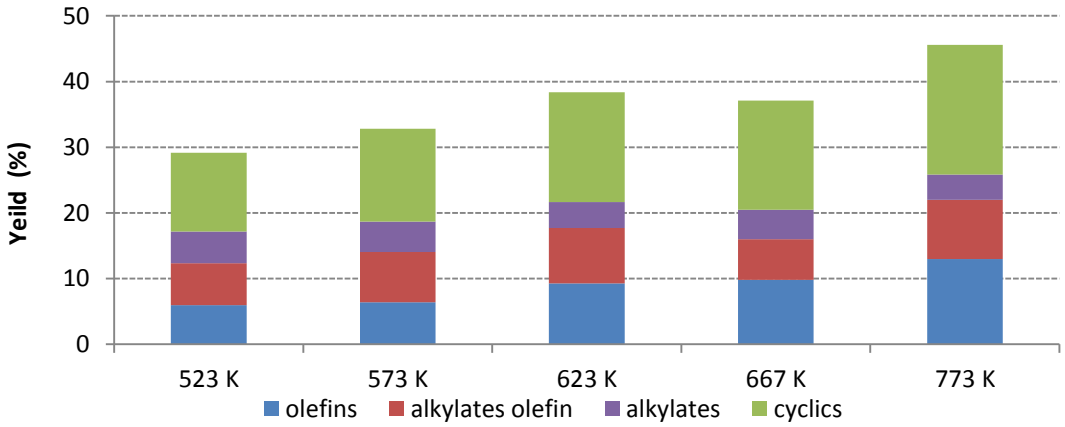

Figure 152: Relationship of the valuable products over Pt/Al_2O_3 using 1,5HD system

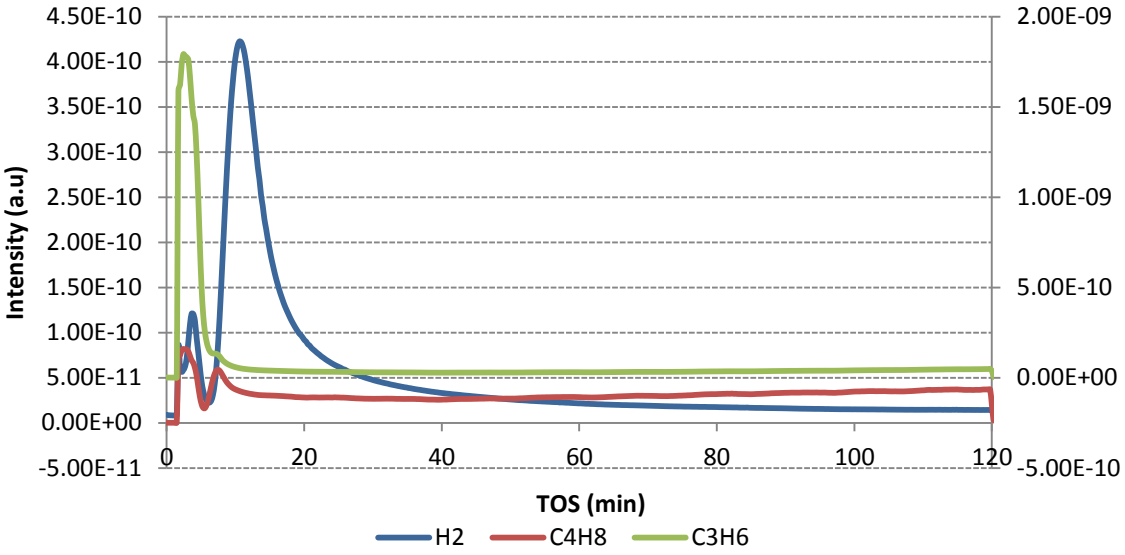

Figure 153: Profile of the evolved gases over Pt/Al_2O_3 using 1,5HD only at 773 K

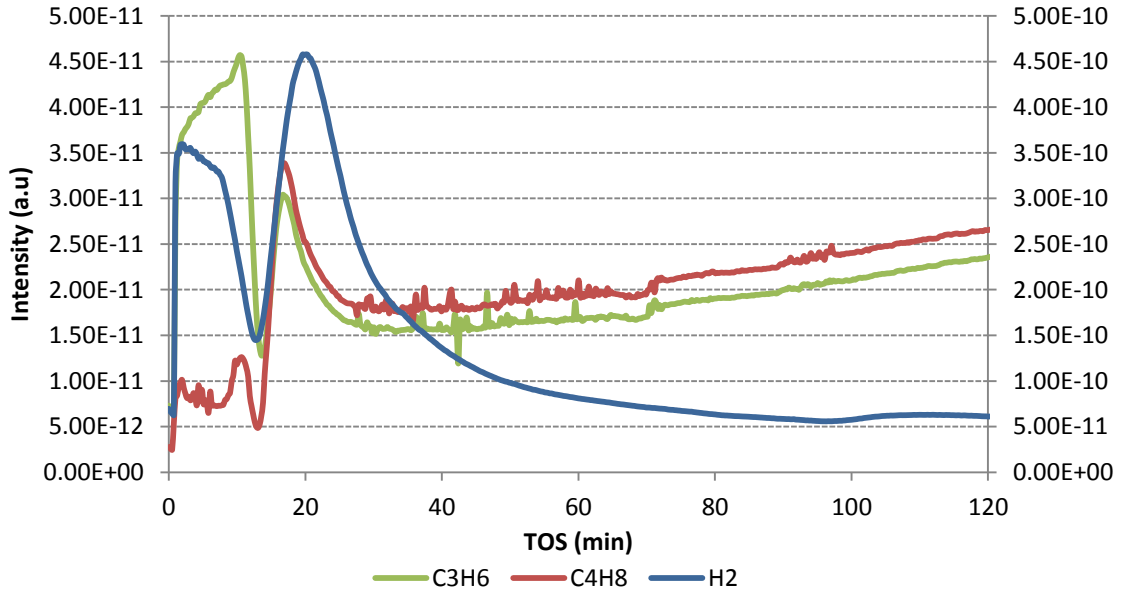

Figure 154: Profile of the evolved gases over Pt/Al_2O_3 using P/1,5HD at 773 K

The eluent gas analysis using this system also confirms the evolution of hydrogen from the start of the reaction during the trans-hydrogenation. The hydrogen evolution here was gradually declining but was maintained in the reaction stream. There was evolution of C_3H_6 and C_4H_8 which increased and maintained on stream for the reaction period. C_3H_8 and C_4H_8 were evolved using this system confirming that the 1,5HD behaved differently to the 1HY on the catalyst

surface; this same trend was also observed with the chromia catalyst. There are only pulses of these gases observed with the 1,5HD run only and there was no evidence that these are maintained in the reaction stream. The result obtained at 723 K is presented in Figure 153 and 154

Table 71: carbon balance for the P/1HY trans-hydrogenation reaction over the Pt/Al_2O_3 catalyst

Temperature (K)	Carbon balance (%)				
	Liquid Ptds.	C_3H_6	C_4H_8	coke	Pdts Non accounted
773	88	1.81	1.03	0.09	9.07
673	87	1.68	0.98	0.08	10.26
623	90	1.24	0.86	0.08	7.82
573	91	1.35	0.71	0.079	6.15
523	93	-	-	0.071	6.29

The hydrogenation reactions were performed over the 623-523 K temperature range. The result are presented in Table 71-73

Table 72: Products yield during the hydrogenation of 1,5HD over the Pt/Al_2O_3 at 623 K

	H	P+H	P+H Theory
	Conversion (%)		
1,5-Hexadiene (1,5HD)	73	57	29
	Yield (%)		
Iso-pentane	2.55	1.03	1.27
Pentene			0.16
Trans-2-Pentene			3.45
Cis-2-pentene			1.56
2-Methyl-2-butene		0.04	0.13
Hexane	3.23	0.1	0.43
1-Hexene	10.72	2.65	1.74
2-Hexene	3.96	0.25	0.79
3-Hexene	9.6	6.36	3.36
Methyl-2-pentene	2.55	1.11	1.41
3-Methyl-1-hexene	0.68	4.62	3.08
Benzene		0.23	0
3-Methylhexane		2.91	0.98
2-Methyl-1,3-pentadiene	8.12	3.57	3.19
2-Methyl-1-1hexene		2.67	0.54
Methylcyclohexane	18.16	17.21	19.34

Table 73: Products yield during the hydrogenation of 1,5HD over the Pt/Al_2O_3 at 573 K

	H	P+H	P+H Theory
	Conversion (%)		
1,5 Hexadiene (1,5HD)	61	44	30
	Yield (%)		
Iso-pentane	8.12	2.01	1.51
Pentene			0.11
Trans-2-Pentene			0.69
Cis-2-pentene			0.23
Hexane	3.46		0.22
1-Hexene	7.92	1.1	0.98
2-Hexene	2.41		1.39
3-Hexene	6.5	5.3	2.51
Methyl-2-pentene	0.61	0.2	0.53
3-Methyl-1-hexene	2.38	4.68	3.85
3-Methylhexane		2.65	1.38
2-Methyl-1,3-pentadiene	5.24	3.62	3.72
2-Methyl-1-1hexene		2.76	1.54
Methylcyclohexane	12.24	14.1	19.79

Table 74: Products yield during the hydrogenation of 1,5HD over the Pt/Al_2O_3 at 523 K

	H	P+H	P+H Theory
	Conversion (%)		
1,5 Hexadiene (1,5HD)	62	46	31
	Yield (%)		
Iso-pentane	19.54	2.01	1.08
Pentene			0.01
Trans-2-Pentene			2.04
Cis-2-pentene			0.01
Hexane	2.68		0.11
1-Hexene	1.76	2.15	1.52
2-Hexene	3.13		1.13
3-Hexene	6.41	3.79	3.28
Methyl-2-pentene	0.27	0.21	0.61
3-Methyl-1-hexene	2.53	2.71	2.84
3-Methylhexane		2.84	1.38
2-Methyl-1,3-pentadiene	1.4	1.59	1.64
2-Methyl-1-1hexene		3.46	2.65
Methylcyclohexane	12	11.99	18.8

4.4.3.2 Post reaction characterization and analysis

The TGA- weight loss analysis of the spent catalyst shows the amount of lost material is a function of the reaction temperatures, but there is not much difference in the weight loss across the temperature range. This is the same trend observed both with the 1,5HD run alone and P/1,5HD trans-hydrogenation. Although the catalyst used at 523 K presented the lowest loss there is not much difference with the 773 K experiment. The main weight loss from the catalysts used with 1,5HD and the mixed feeds occurred at ~ 530 – 811 K, the peak extended to higher temperature when compare to the equivalent chromia catalyst (530-710 K). The results are presented in Figure 155 and 156

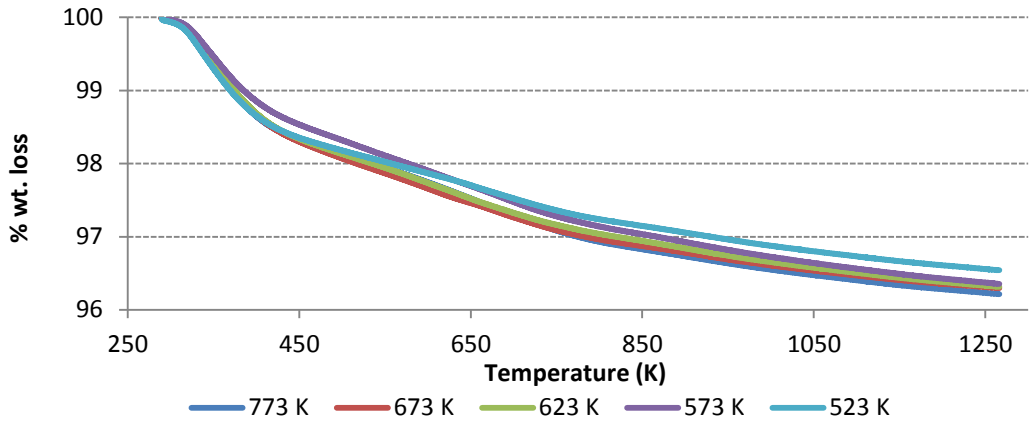

Figure 155: Weight loss profile of 1,5HD run alone over Pt/Al_2O_3 catalyst

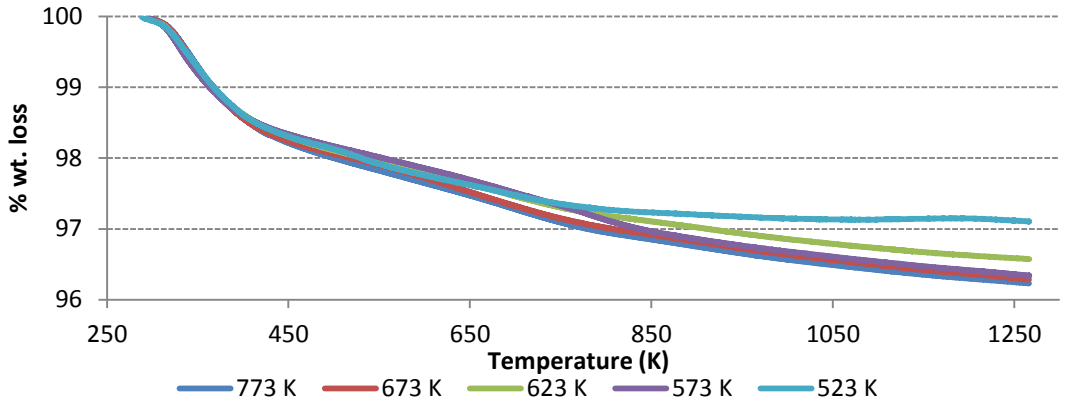

Figure 156: Weight loss profile of P/1,5HD mixed feed over Pt/Al_2O_3 catalyst

The derivative weight analysis plot is observed to show almost no difference between the 1,5HD run only, and the trans-hydrogenation process (Figure 157)

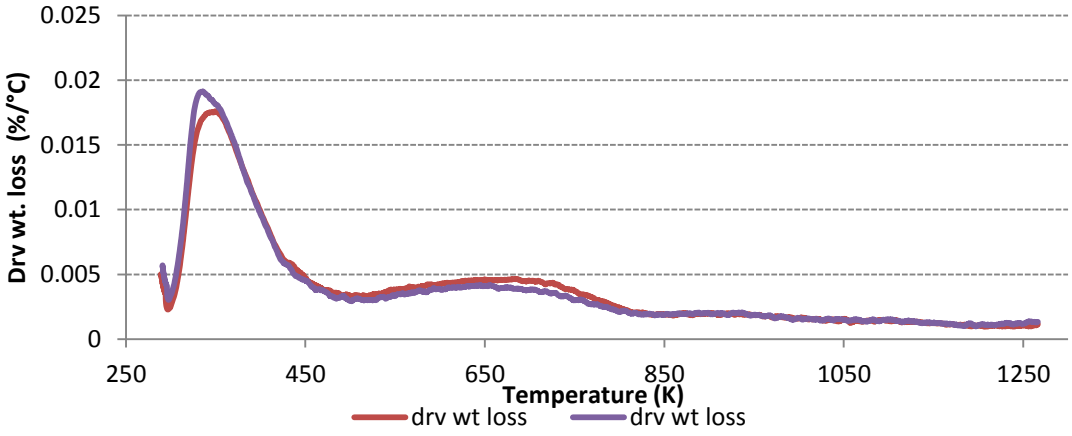

Figure 157: Derivative wt. loss profile of 1,5HD and the mixed feeds over Pt/Al_2O_3 catalyst

The TPO analysis during the TGA revealed carbon dioxide as the main desorption species evolved with the 1,5HD system using the platinum catalyst. This was determined by the mass spectrometer (m/e 44). However, in addition to this, fragments (m/e 2, 16, 18 and 28) were also monitored. There were no traces of any of these fragments detected in the samples. There is observed evidence for possibly two forms of surface carbon with this reaction system, one ~400 K and predominantly at 570-861 K during the trans-hydrogenation, there is no clear distinction between the two evolutions instead an extended CO_2 peak is observed (400-860 K) The results are presented in Figure 158 and 159

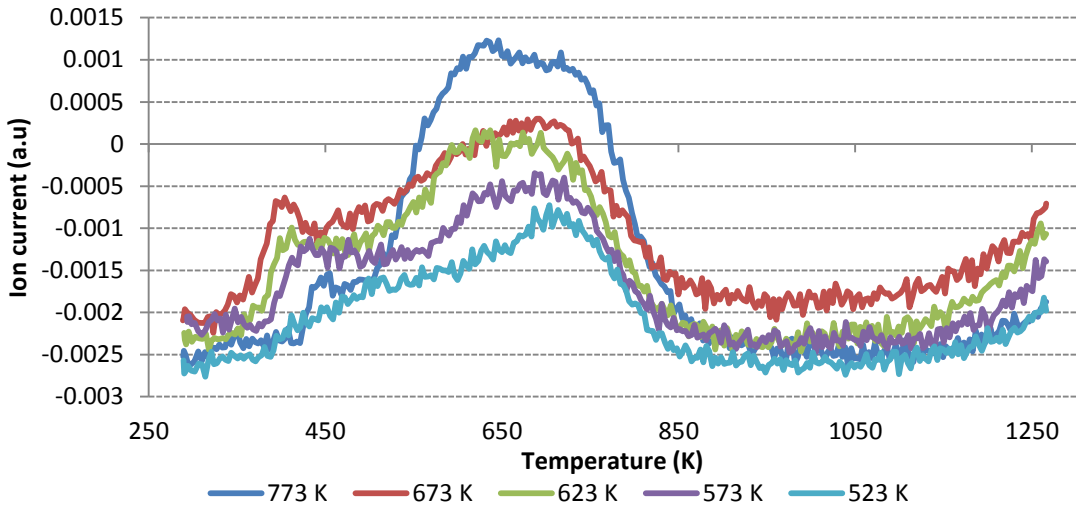

Figure 158: TPO profile of 1,5HD run alone over Pt/Al_2O_3 catalyst

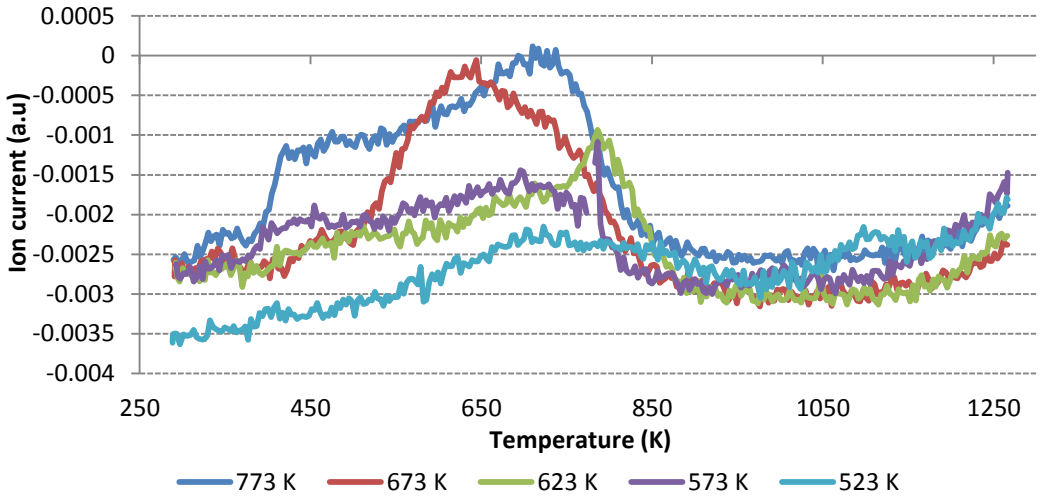

Figure 159: TPO profile of P/1,5HD mixed feed over Pt/Al_2O_3 catalyst

The TPO of the catalysts after use in the 1,5HD hydrogenation shows two/three peaks associated with CO_2 evolution. This profile is different to what was observed during trans-hydrogenation but the evolution starts at about the same temperature. The result is presented in Figure 160

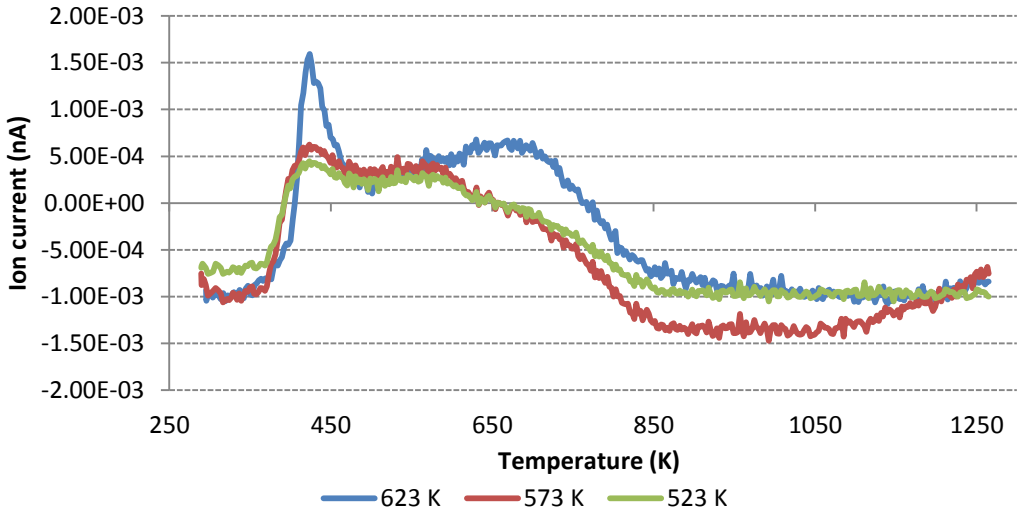

Figure 160: TPO profile of catalysts after 1,5HD hydrogenation over Pt/Al_2O_3 catalyst

The carbon dioxide TPO profile matches the TGA derivative weight loss profile confirming the weight loss occurred from retained carbon combustion. The result obtained at 723 K is presented in Figure 161

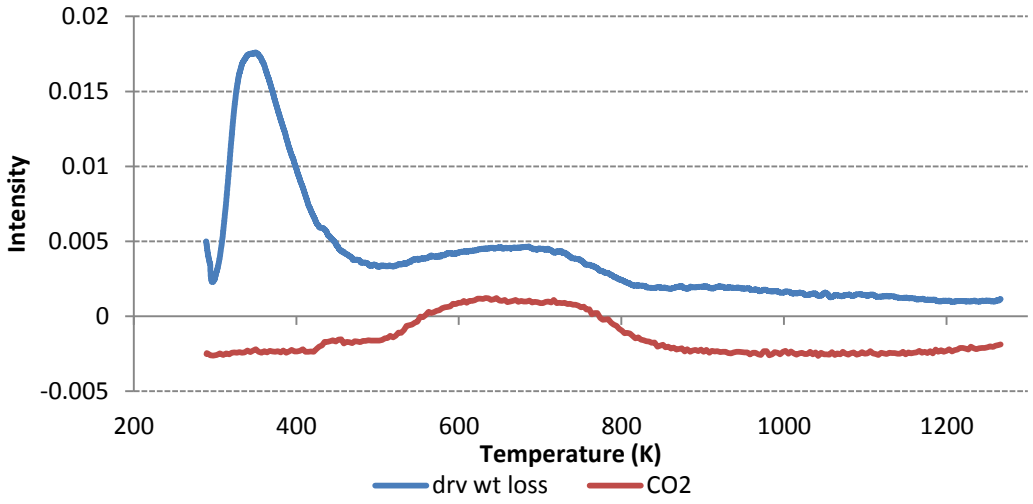

Figure 161: Comparison of derivative weight loss and carbon dioxide evolution obtained from the TPO-MS using P/1,5HD system with the Pt/Al_2O_3 catalyst

There is little change observed in the amount of the carbon species desorbed from the surface of each catalyst over the reaction temperatures range using the 1,5HD system over the platinum catalyst. There is no dependency in the amount of the carbon species desorbed when either the 1,5HD was fed individually or as mixed feed trans-hydrogenation process: the % carbon laydown is almost the same. However, there is a significant reduction in the amount of carbon deposited compared to the 1HY system. The % laydown is <3% with all the reaction temperatures 773-523 K and is about 65% less than the 1HY system. The percentage carbon deposit for each run was determined and is presented in Figure 162

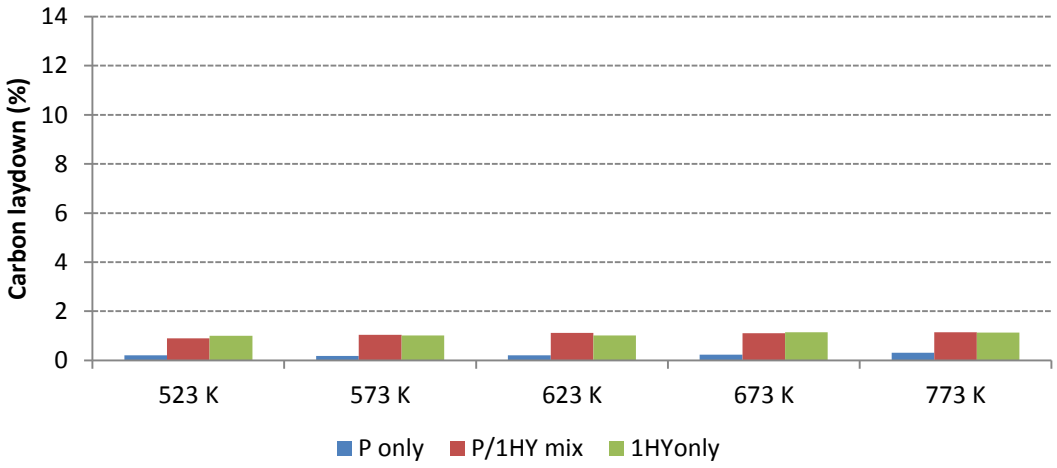

Figure 162: Carbon laydown of the spent Pt/Al_2O_3 catalyst over the set temperatures

Table 75: Total amount of carbon deposited on spent Pt/Al_2O_3 catalyst at various temperatures

Temperature (K)	Carbon deposited (g/g feed)		
	P	P/1,5HD	1,5HD
523	0.00039	0.00142	0.00813
573	0.00035	0.00164	0.00821
623	0.00041	0.00176	0.00821
673	0.00045	0.00175	0.00927
773	0.00061	0.00180	0.00919

The amount of the carbon formed related to the reactant feed is summarized and presented in table. It is observed that there is clear reduction of the carbon formation with the trans-hydrogenation system.

The Raman spectroscopic analysis of the spent catalysts was obtained using UV radiation for the studies of the carbon deposit. The Raman spectra show Raman bands assigned to coke deposition at ~1380 and 1600 cm^{-1} related to D and G bands respectively. This was observed with 1,5HD feed for all the reaction temperatures except 523 K and 573 K, where only G band was observed. G-band was only observed with the P/1,5HD trans-hydrogenation at all reaction temperatures except 773 K where both D and G bands were observed. The D band was lost using the mixed feed process and only G bands are observed at most reaction temperatures. The results are presented in Figure 163 and 164

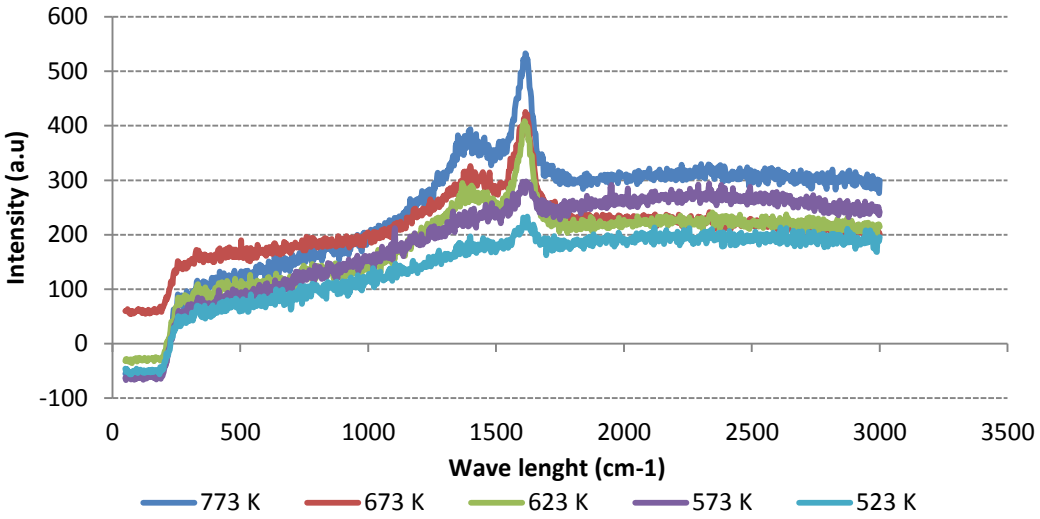

Figure 163: Raman spectra of spent Pt/Al_2O_3 catalyst for sole 1,5HD obtained using the UV-radiation

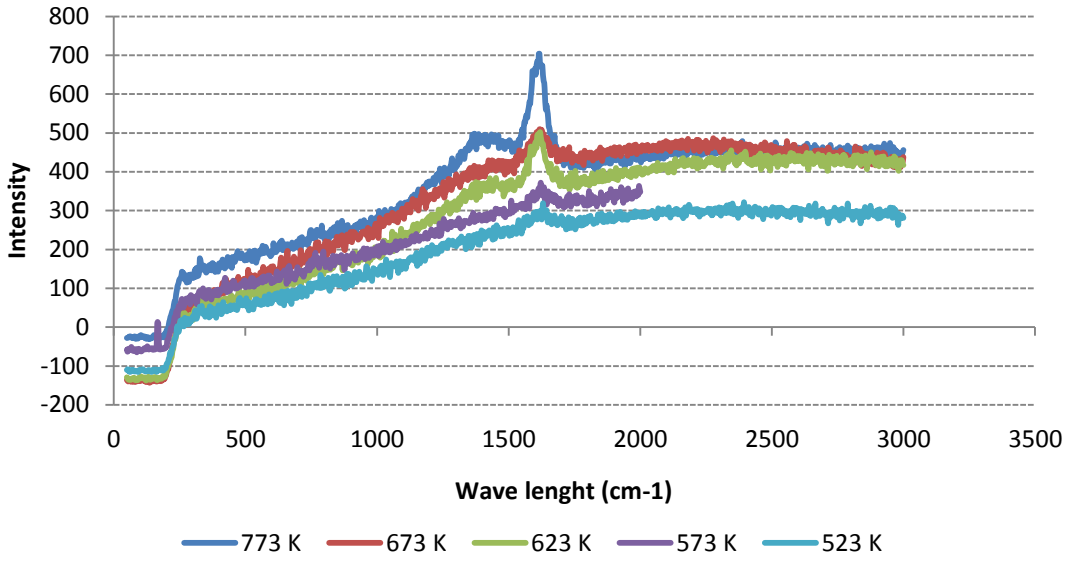

Figure 164: Raman spectra of spent Pt/Al2O3 catalyst for mixed feeds obtained using the UV-radiation

The BET analysis performed on the spent catalysts also suggests that the formation of coke on the catalyst has no effect on the BET surface area and the pore volume. There is no significant loss in the S_{BET}, only small changes were observed. This is very similar to P/1HY system. The 1HY system exhibit much higher carbon deposit compared to the 1,5HD system at all reaction temperatures but neither reaction showed any change in the S_{BET}.

The XRD analysis of the spent catalyst using the 1,5HD system also revealed only the diffraction pattern for γ-alumina

3.4.4 Pentane/2,4-Hexadiene (P/2,4HD) system

3.4.4.1 Reaction analysis and trans-hydrogenation activity evaluation

The reactant conversions were followed individually and during the mixed trans-hydrogenation reaction using the 2,4HD system over the platinum catalyst. The conversion of pentane was only ~1-2 % increase observed during the trans-hydrogenation compared to the pentane dehydrogenation except for 773 K reaction temperature. Slightly higher conversion ~46% was obtained compared to ~37% when pentane was run individually. Only ~1-2 % values are within the experimental error so it can be assumed that the trans-hydrogenation process does not really improve the conversion of the pentane dehydrogenation compared to 1HY and 1,5HD systems. This is similar to what was observed with the chromia catalyst and is consistent with the thermodynamic suggestion with this 2,4HD reactant as explained in section 3.1. The result is presented in Figure 165

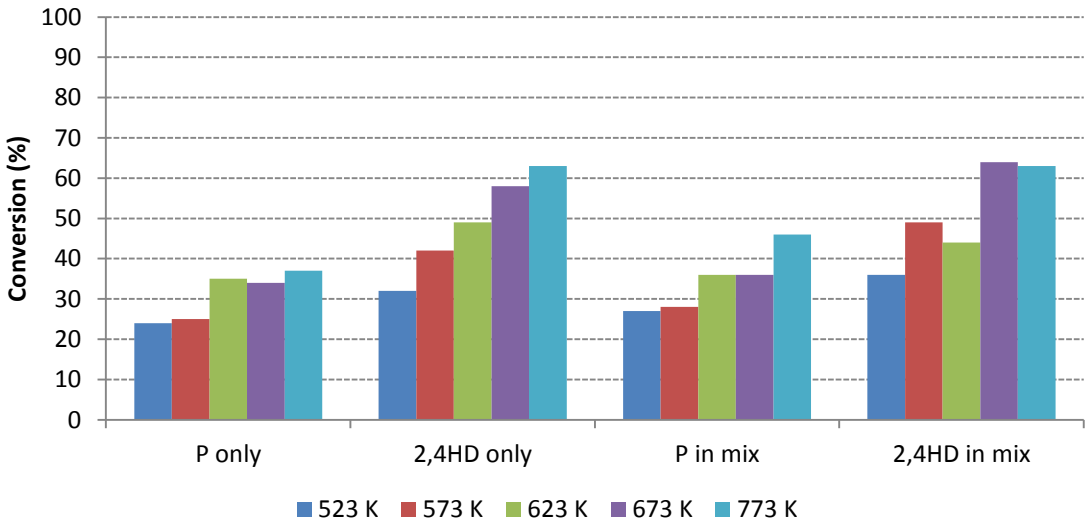

Figure 165: Conversion comparison of P, 2,4HD and P/2,4HD mixture using $PtAl_2O_3$

The products yields were calculated and presented in Table 75-79. Low percentage yields of the valuable products were obtained with this system compared with to the other systems. The product distribution is pretty much the same with all the reaction temperatures just like the other reaction systems, but only the individual yield of the products changes.

Table 76: Products yield of the trans-hydrogenation over 2,4HD system at 773 K using Pt/Al_2O_3

	P	H	P+H	P+H Theory
	Conversion (%)			
Pentane(P)	37		46	37
2,4-Hexadiene (2,4HD)		63	63	63
	Yield (%)			
Iso-pentane	1.67		20.7	1.67
Pentene	4.01		1.49	4.01
Trans-2-Pentene	5.27		0.44	5.27
Cis-2-pentene	2.64			2.64
2-Methyl-2-butene	0.52			0.52
4-Methylpentene	1.67			1.67
hexane		5.94	3.78	5.94
Methyl-2-pentene		14.26	4.04	14.26
Benzene			5.21	0
3-Methylhexane		5.76		5.76
2-Methyl-1,3-pentadiene		6.19	7.21	6.19
Methylcyclohexane	17.03	18.57	13.03	35.60

Table 77: Products yield of the trans-hydrogenation over 2,4HD system at 673 K using Pt/Al_2O_3

	P	H	P+H	P+H Theory
	Conversion (%)			
Pentane(P)	34		36	34
2,4-Hexadiene (2,4HD)		58	64	58
	Yield (%)			
Iso-pentane	1.18		4.76	1.18
Pentene	2.59			2.59
Trans-2-Pentene	1.92			1.92
Cis-2-pentene	1.93		0.43	1.93
2-methyl-2-butene	1.18			1.18
Hexane			2.91	
3-Hexene		2.88		2.88
Methyl-2-pentene		10.93	4.05	10.93
3-Methylhexane		4.31	5.69	4.31
2-Methyl-1,3-pentadiene		4.03	9.05	4.03
Methylcyclohexane	17.03	16.02	12.40	33.05

Table 78: Products yield of the trans-hydrogenation over 2,4HD system at 623K using Pt/Al_2O_3

	P	H	P+H	P+H Theory
	Conversion (%)			
Pentane(P)	35		36	56
2,4-Hexadiene (2,4HD)		49	44	52
	Yield (%)			
Iso-pentane	1.27		4.25	1.27
Pentene	0.16			0.16
Trans-2-Pentene	3.45			3.45
Cis-2-pentene	1.56			1.56
2-methyl-2-butene		3.68		3.68
Hexane		2.33		2.33
3-Hexene		7.89	4.81	7.89
Methyl-2-pentene			3.51	
3-Methylhexane		2.13	8.18	2.13
2-Methyl-1,3-pentadiene		4.94		4.94
Methylcyclohexane	14.83	19.11	8.94	33.94

Table 79: Products yield of the trans-hydrogenation over 2,4HD system at 573K using Pt/Al_2O_3

	P	H	P+H	P+H Theory
	Conversion (%)			
Pentane(P)	25		28	25
2,4-Hexadiene (2,4HD)		42	49	42
	Yield (%)			
Iso-pentane	1.51		8.97	1.51
Pentene	0.11			0.11
Trans-2-Pentene	0.69			0.69
Cis-2-pentene	0.23			0.23
Hexane		10.93	3.3	10.93
Methyl-2-pentene		4.28	5.18	4.28
3-Methylhexane			1.14	0
2-Methyl-1,3-pentadiene			10.93	0
2-Methyl-1-1hexene		3.21		3.21
Methylcyclohexane	14.83	14.55	7.61	29.38

Table 80: Products yield of the trans-hydrogenation over 2,4HD system at 523 K using Pt/Al_2O_3

	P	H	P+H	P+H Theory
	Conversion (%)			
Pentane(P)	24		27	24
2,4-Hexadiene (2,4HD)		32	36	32
	Yield (%)			
Iso-pentane	1.08	0.66		1.74
Pentene	0.01			1.08
Trans-2-Pentene	2.04			0.01
Cis-2-pentene	0.01			2.04
Hexane		1.03	3.4	1.03
1-Hexene		0.41		0.41
2-Hexene		0.4		0.4
3-Hexene		1.85		1.85
Methyl-2-pentene		4.06	5.98	4.06
3-Methylhexane		1.92	1.76	1.92
2-Methyl-1,3-pentadiene		0.97	11.98	0.97
Methylcyclohexane	12.21	12.52	8	7.73

The total olefin yield obtained with the 2,4HD system is very low (~6%) at 773 K, this is a value lower that the chromia catalyst and lower compared with the values obtained over the platinum catalyst with the other two systems. The result is presented in Figure 166. The olefin production is lower than the other valuable products as presented in Figure 167, but there is an increase in these valuable products with the reaction temperature (Figure 168)

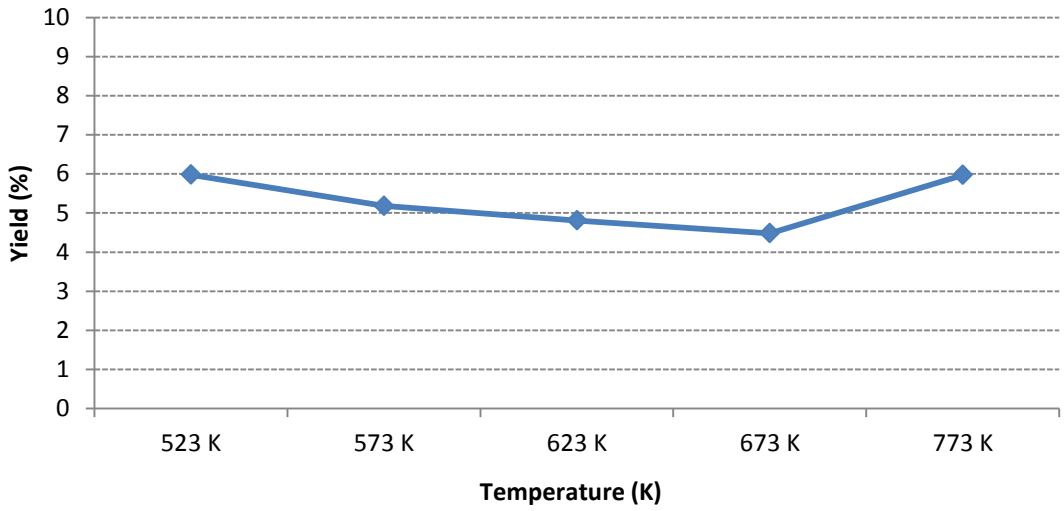

Figure 166: Total olefin yield with temperature over the Pt/Al_2O_3 using 2,4HD system

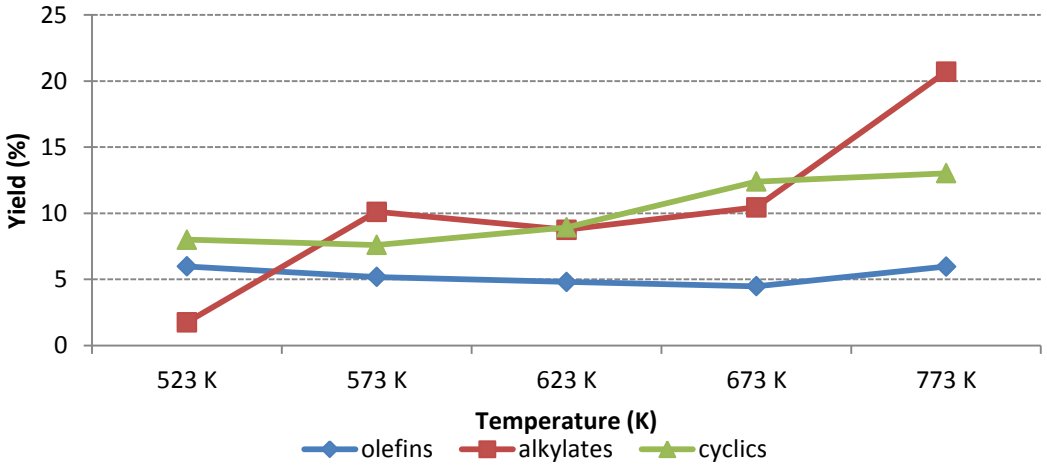

Figure 167: Profile of valuable product relative to the reaction temperature over Pt/Al_2O_3 using 2,4HD system

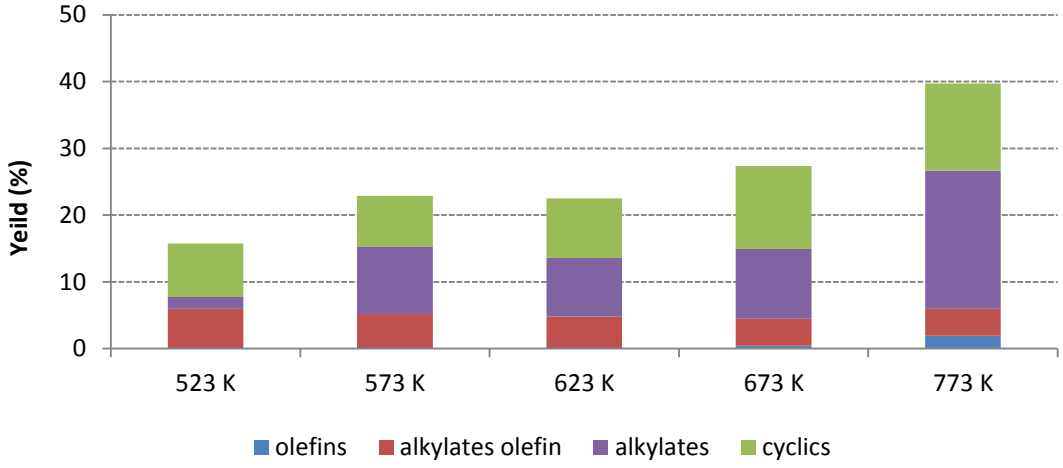

Figure 168: Relationship of the valuable products over Pt/Al_2O_3 using 2,4HD system

The eluent gas products analysis using 2,4 HD system also shows pulses of H_2, C_3H_6 and C_4H_8 from the start of the reaction. The hydrogen evolution here was slightly maintained in the reaction stream but gradually declined with the 2,4HD run. There is a significant reduction of the hydrogen at ~30 min during the trans-hydrogenation. C_3H_8 and C_4H_8 were evolved using this system which shows similar fragmentation with 1,5HD using the platinum catalyst. This is also the same eluent gases observed using the chromia catalyst. The result obtained at 723 K is presented in Figure 169 and 170

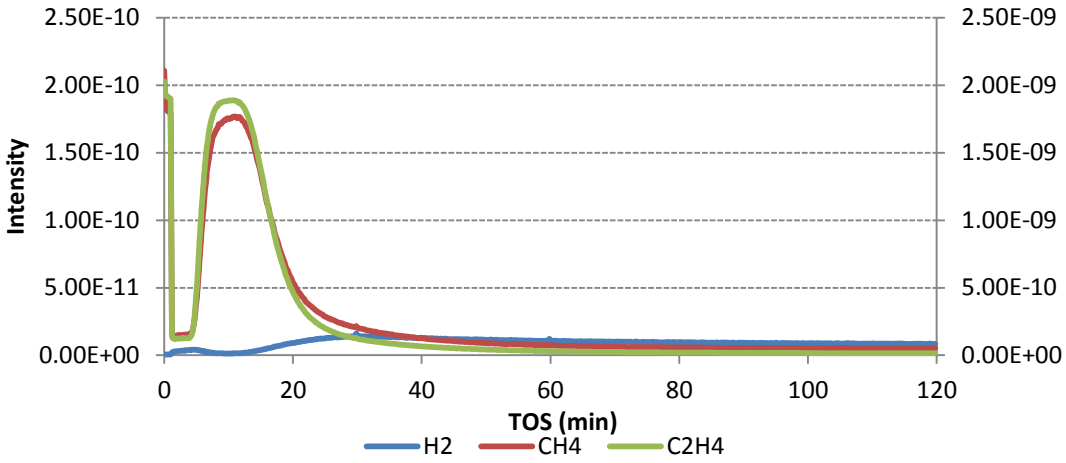

Figure 169: Profile of the evolved gases over Pt/Al_2O_3 using 2,4HD only at 723 K

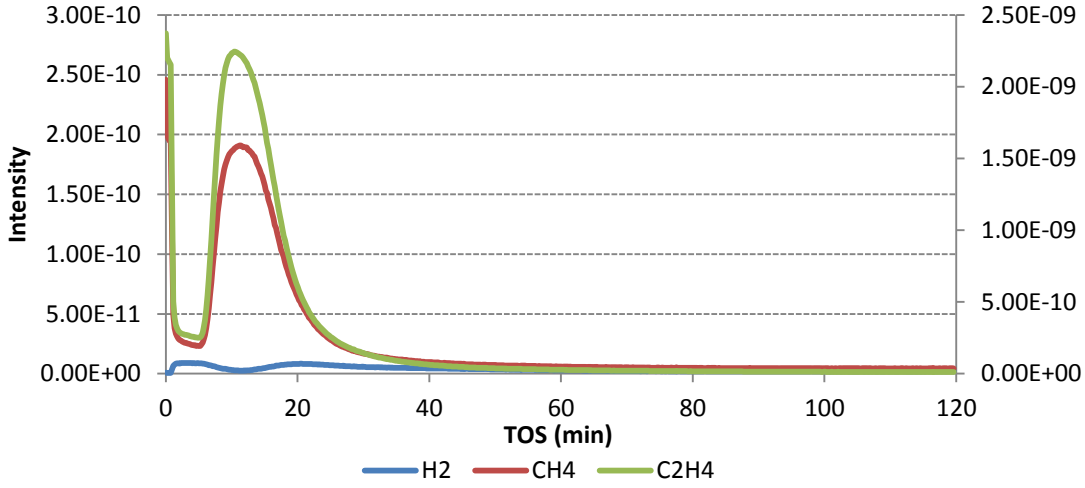

Figure 170: Profile of the evolved gases over Pt/Al_2O_3 using P/2,4HD mixed feed at 723 K

The hydrogenation reaction processes were performed over the 623-523 K temperature. The result are presented in 80-82

Table 81: Products yield during the hydrogenation of 2,4HD over the Pt/Al2O3 at 623 K

	2,4HD +2% H_2/N_2	P+H	P+H Theory
	Conversion (%)		
2,4-Hexadiene (2,4HD)	63	44	52
	Yield (%)		
Iso-pentane		4.25	1.27
Pentene			0.16
Trans-2-Pentene			3.45
Cis-2-pentene			1.56
Cexane	9.85		3.68
1-Hexene	3.47		
2-Hexene	5.72		
3-Hexene	9.86		2.33
Methyl-2-pentene	1.85	4.81	7.89
3-Methylhexane	1.42	3.51	
3-Methyl-1-hexene	0.24		
2-Methyl-1,3-pentadiene		8.18	2.13
2-Methyl-1-1hexene			4.94
Methylcyclohexane	5.26	8.94	33.94

Table 82: Products yield during the hydrogenation of 2,4HD over the Pt/Al_2O_3 at 573 K

	2,4HD +2% H_2/N_2	P+H	P+H Theory
	Conversion (%)		
2,4-Hexadiene (2,4HD)	60	49	42
	Yield (%)		
Iso-pentane		8.97	1.51
Pentene			0.11
Trans-2-Pentene			0.69
Cis-2-pentene			0.23
Hexane	12.49	3.3	10.93
1-Hexene	5.01		
2-Hexene	8.24		
3-Hexene	13.16		
methyl-2-pentene	1.23	5.18	4.28
3-Methylhexane	1.32	1.14	0
2-Methyl-1,3-pentadiene	0.23	10.93	0
2-Methyl-1-1hexene			3.21
Methylcyclohexane	11.16	7.61	29.38

Table 83: Products yield during the hydrogenation of 2,4HD over the Pt/Al_2O_3 at 523 K

	2,4HD +2% H_2/N_2	P+H	P+H Theory
	Conversion (%)		
2,4hexadiene (2,4HD)	62	36	32
	Yield (%)		
Iso-pentane			1.74
Pentene			1.08
Trans-2-Pentene			0.01
Cis-2-pentene			2.04
Hexane	10.59	3.4	1.03
1-Hexene	5.31		0.41
2-Hexene	8.04		0.4
3-Hexene	15.21		1.85
Methyl-2-pentene	1.64	5.98	4.06
3-Methylhexane	1.93	1.76	1.92
2-Methyl-1,3-pentadiene	0.32	11.98	0.97
Methylcyclohexane	13.45	8	7.73

4.2.4.2 Post reaction characterization and analysis

The TGA- weight loss analysis of the spent catalyst shows a weight loss with all 2,4HD systems, with the amount of weight lost increasing as a function of the reaction temperatures. Although there are only small differences in the amount of material lost across the reaction temperature range. The catalyst used at a reaction temperature of 773 K presents the highest loss with both the 2,4HD run alone and P/2,4HD trans-hydrogenation, and the catalyst used at a reaction temperature of 523 K presented the lowest loss. Two weight losses were observed in both processes, first loss occurred at ~ 390 – 500 K while the second loss occurred at ~505-840 K. The results are presented in Figure 171 and 172

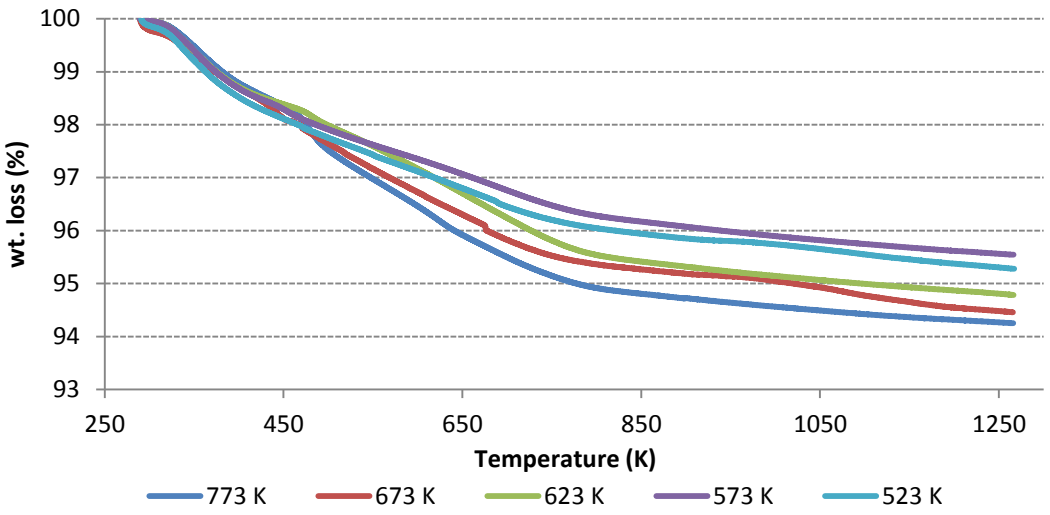

Figure 171: Weight loss profile of 2,4HD run alone over $Pt/A_{l2}O_3$ catalyst

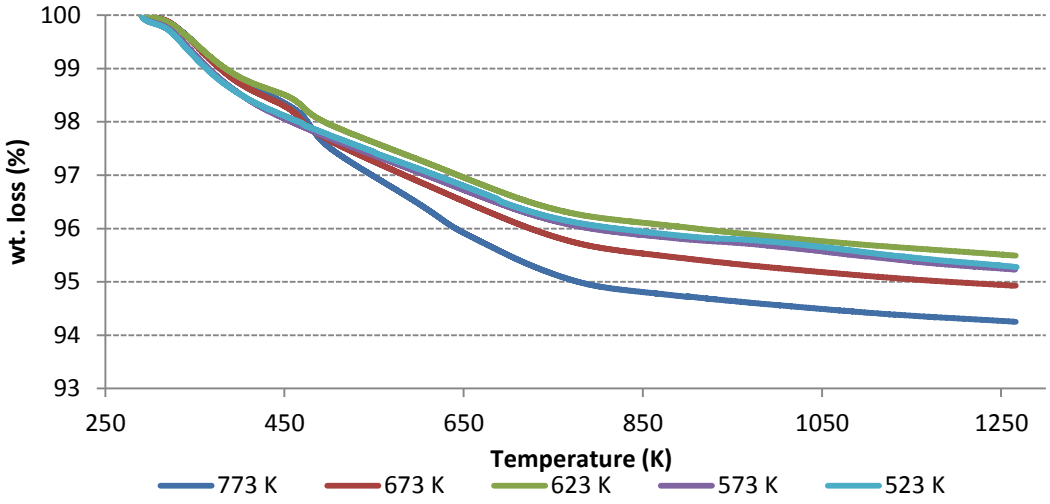

Figure 172: Weight loss profile of P/2,4HD mixed feed over $Pt/A_{l2}O_3$ catalyst

The derivative weight analysis plots show that the two process presented different profiles. Nevertheless evidence for two types of surface deposit was observed with both processes. During the trans-hydrogenation, the intensity of the first peak is higher than the second peak and the second peak is broader, whereas the two peaks have about the same intensities during the 2,4HD run alone. Evidence for three desorption peaks could also be argued with the 2,4 HD run, but this is only observed with the 773 K run. The results are presented in Figure 173 and 174

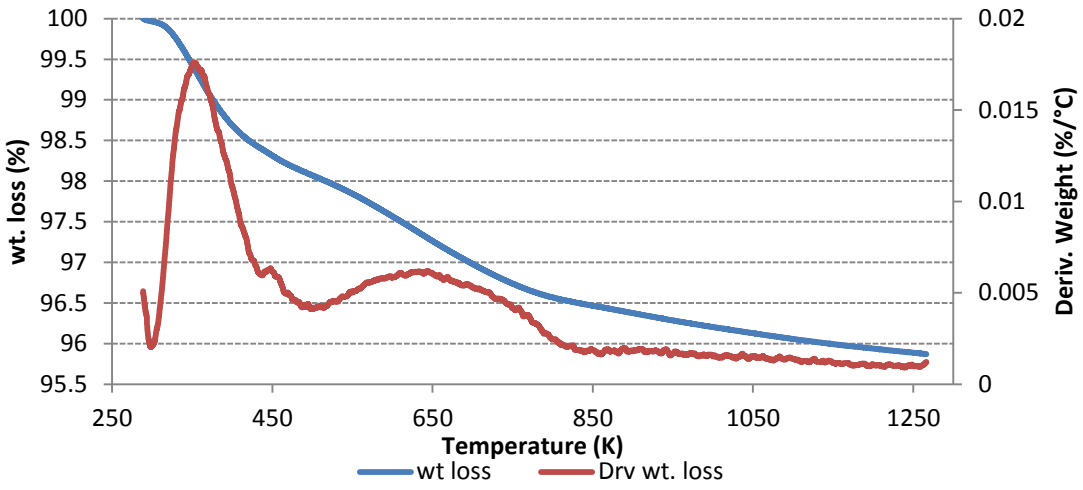

Figure 173: Derivative weight loss profile of 2,4HD feeds over $Pt/A_{l2}O_3$ catalyst at 773 K

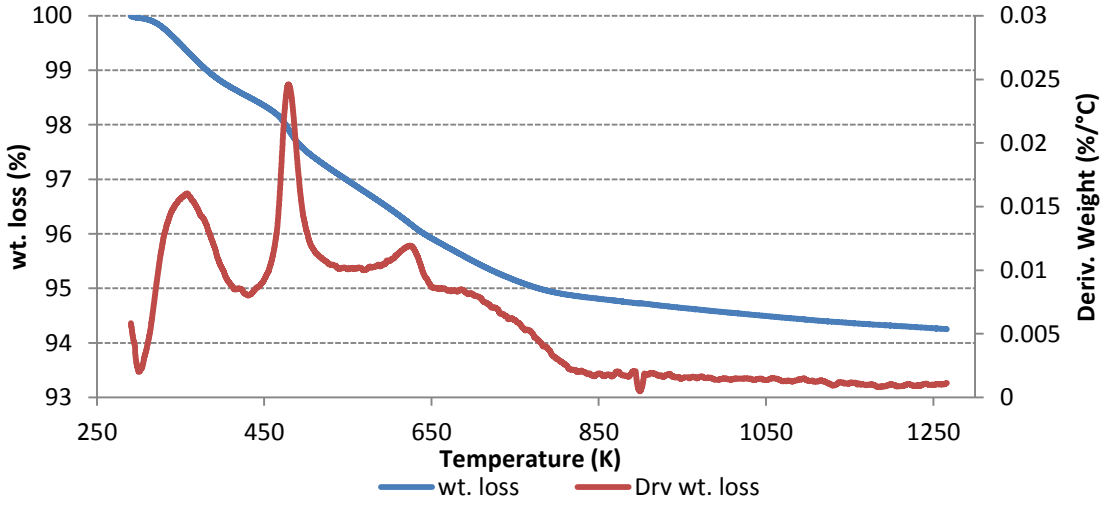

Figure 174: Derivative wt. loss profile of 2,4HD mixed feeds over $Pt/A_{l2}O_3$ catalyst at 773 K

The TPO analysis during the TGA for the P/2,4HD spent catalyst also revealed carbon dioxide as the main desorption species evolved for both peaks. This was determined by the mass spectrometer (m/e 44). However, in addition to this, fragments (m/e 2, 16, 18 and 28) were also monitored and like the 1,5HD system, traces of only CO was also detected in some of the samples. Two CO_2 peaks were observed here with both of the reactions processes, a sharped peak at ~480 K with a slight shift with reaction temperature and a broad peak at ~490-800 K. Unlike the 1,5HD system there is an observed shift in the CO_2 desorption peak to a slightly higher temperature with higher reaction temperature, this was only observed with the first CO_2 peaks with both reaction

processes. The results are presented in Fig 175 and 176. A different TPO profile was obtained from the catalyst used in the hydrogenation process (Fig177).

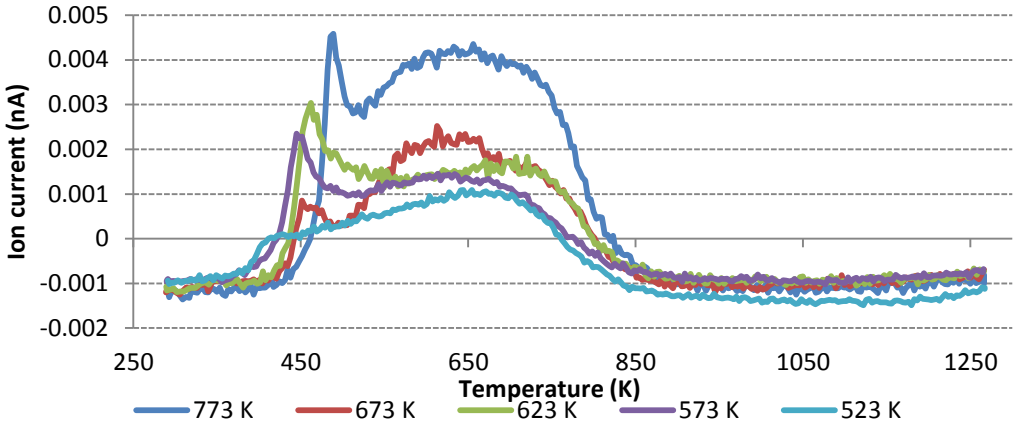

Figure 175: TPO profile of 2,4HD run alone over $Pt/A_{l2}O_3$ catalyst

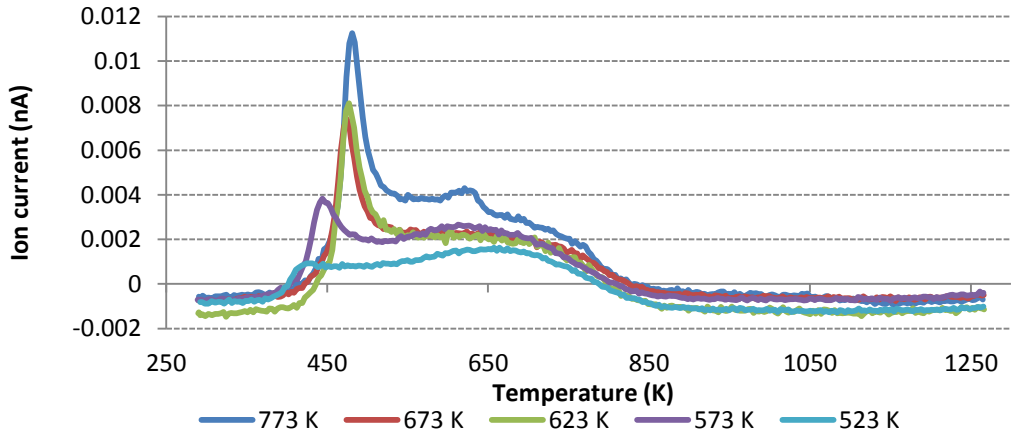

Figure 176: TPO profile of P/2,4HD mixed feed over $Pt/A_{l2}O_3$ catalyst

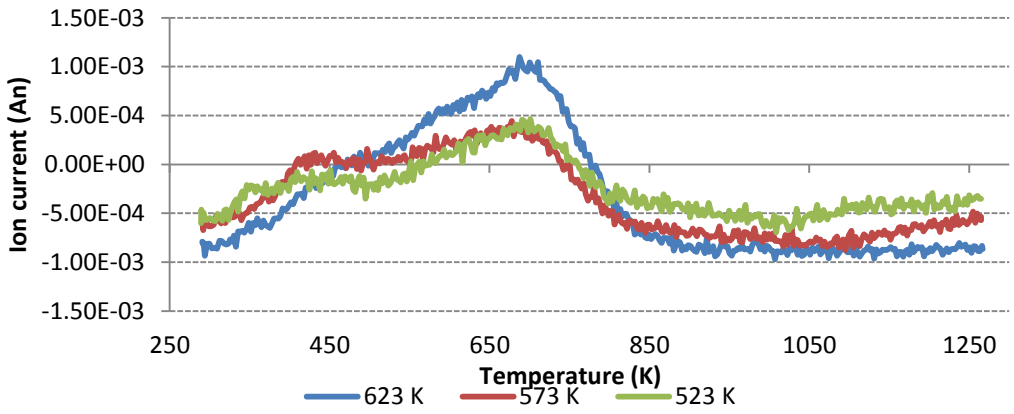

Figure 177: TPO profile during 2,4HD hydrogenation over $Pt/A_{l2}O_3$ catalyst

Compared with the 1,5 HD system, the 2,4HD exhibited a higher amount of carbon species deposited on the surface of the spent catalyst. The amount of the carbon laydown is less than what was observed with 1HY systems. At the higher reaction temperatures there is observed a slight reduction in the amount of carbon laydown during the trans-hydrogenation process compared to the 2,4HD run alone. The result is presented in Figure 178

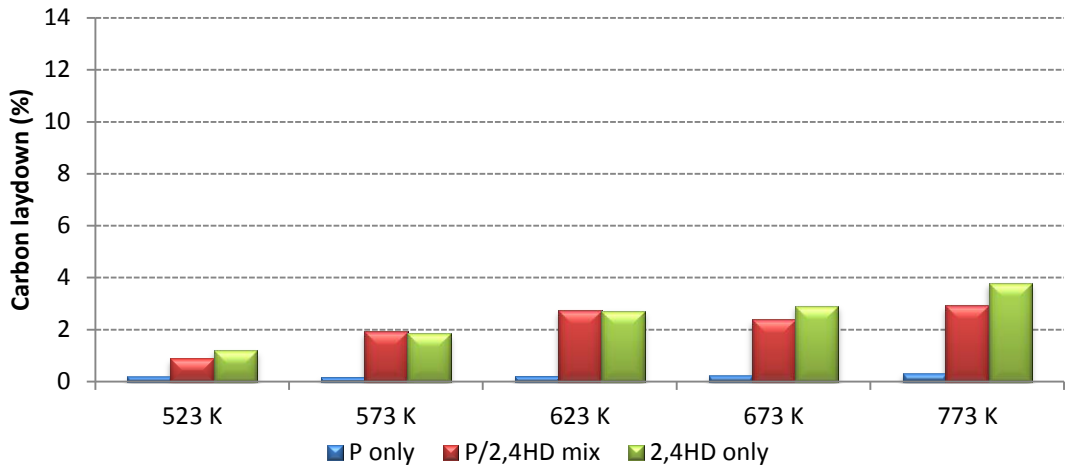

Figure 178: Carbon laydown of the spent $Pt/A_{l2}O_3$ catalyst over the set temperatures

The amount of the carbon formed relative to the reactant feed is summarized and presented in Table 84. Lower carbon deposition was obtained during the trans-hydrogenation and there is a clear reduction of the carbon formation with the trans-hydrogenation system relative to the amount of the reactant fed.

Table 84: Total amount of carbon deposited on spent $Pt/A_{l2}O_3$ catalyst at various temperatures using 2,4HD system

Temperature (K)	Carbon deposited (µmol/g)		
	P	P/2,4HD	2,4HD
523	0.0035	0.0014	0.0098
573	0.0040	0.0030	0.0151
623	0.0041	0.0043	0.0221
673	0.0044	0.0038	0.0236
773	0.0048	0.0046	0.0308

The Raman spectroscopic analysis of the spent catalysts for the two processes was obtained using UV radiation. The Raman spectra reveals bands assigned to coke deposition predominantly at ~ 1600 cm^{-1} related to G bands, except for the catalyst used for the 2,4HD alone run at 773 K, where a ~1300 cm^{-1} band was assigned as a D-band. No Raman bands were observed from the catalyst used at 523 K with the mixed feed. The results are presented in Figure 179 and 180

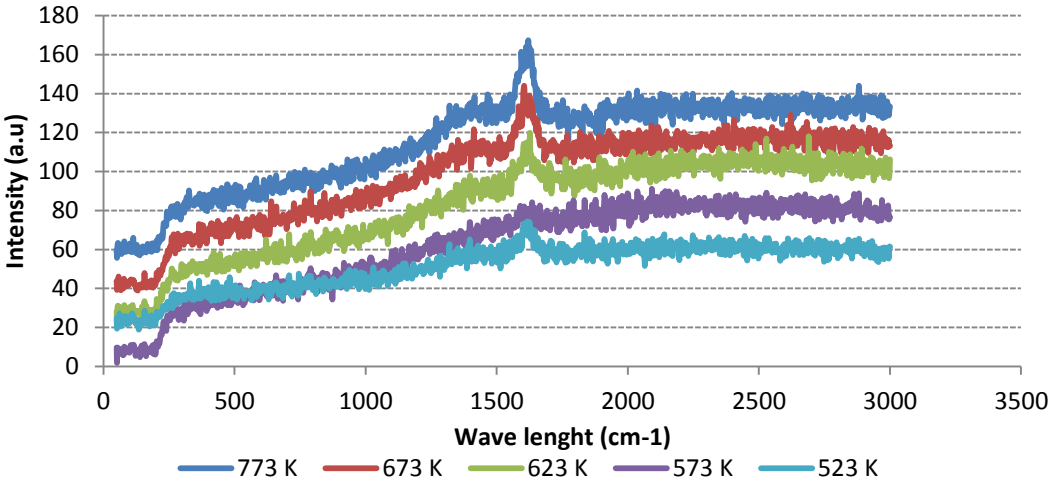

Figure 179: Raman spectra of spent $Pt/A_{l2}O_3$ catalyst for sole 2,4HD obtained using the UV-radiation

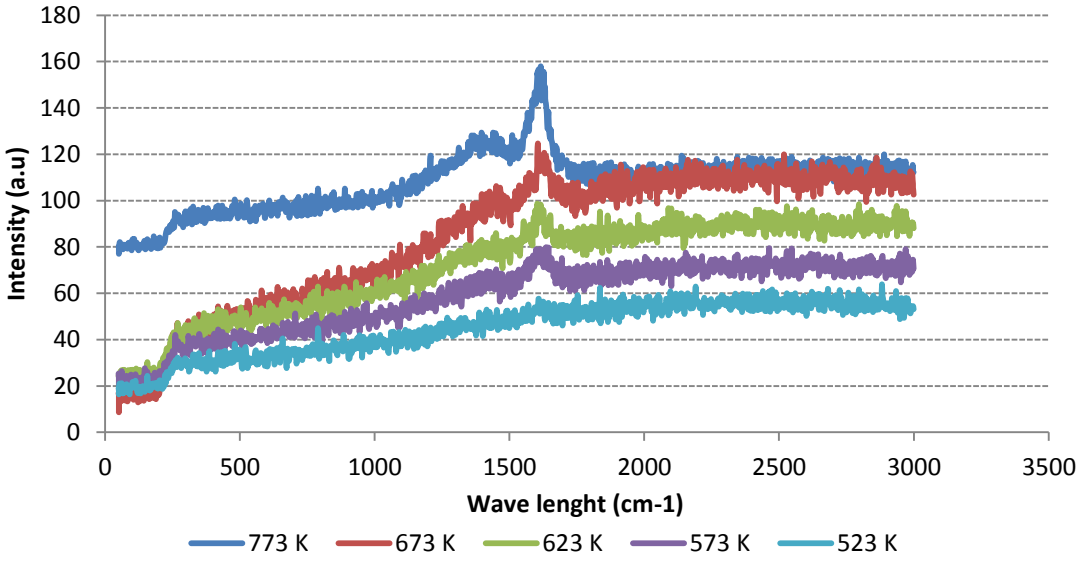

Figure 180: Raman spectra of spent $Pt/A_{l2}O_3$ catalyst for 2,4HD mixed feeds obtained using the UV-radiation

The BET analysis performed on the spent catalyst also suggests that the formation of coke on the catalyst surface using 2,4HD system does not affect the BET surface area and the pore volume. No obvious loss in the S_{BET} was observed with all the samples just similar to 1HY and 1,5 HD systems.

The XRD analysis of the spent catalyst using the 2,4HD system revealed only the diffraction pattern for the alumina support.

The CHN analysis obtained over the platinum catalyst with three reaction systems is presented in Table 85

Table 85: Elemental analysis over platinum catalyst with the three reaction systems

	wt. % C	**Wt. % H**	**wt. % C**	**Wt. % H**	**wt. % C**	**Wt. % H**
	1HY		1,5HD		2,4HD	
773 K	1.41	0.39	1	0.76	1.13	0.41
673 K	1.91	0.53	0.99	0.76	1.72	0.55
623 K	4.21	0.99	1.21	0.89	2.91	0.87
573 K	5.39	1.04	1.21	0.91	2.81	0.82
523 K	5.33	0.94	1.23	0.93	3.86	0.94

3.5 K-Pt/Al_2O_3 catalyst

3.5.1 Pre-reaction catalyst characterisation

3.5.1.1 BET surface area and pore volume determination

Table 86 shows the summary of the parameters extracted from the BET analysis. The result indicated that the S_{BET} is about the same after impregnation of the doped potassium. But, there is a slight decrease in the pore volume and the pore diameter of the platinum catalyst upon impregnation of the potassium

Table 86: BET surface areas, pore volume and average pore diameter of the Pt/$A_{l2}O_3$ and K-Pt/Al_2O_3 catalyst

	S_{BET} (m^2/g)	V_p(cm^3g^{-1})	D_p(Å)
Pt/Y-Al2O3	119	0.54	182
K-Pt/ Y-Al2O3	120	0.47	157

The adsorption isotherm for the catalyst and the support were found to be similar, obeying the type II model. The result is presented in Figure 181

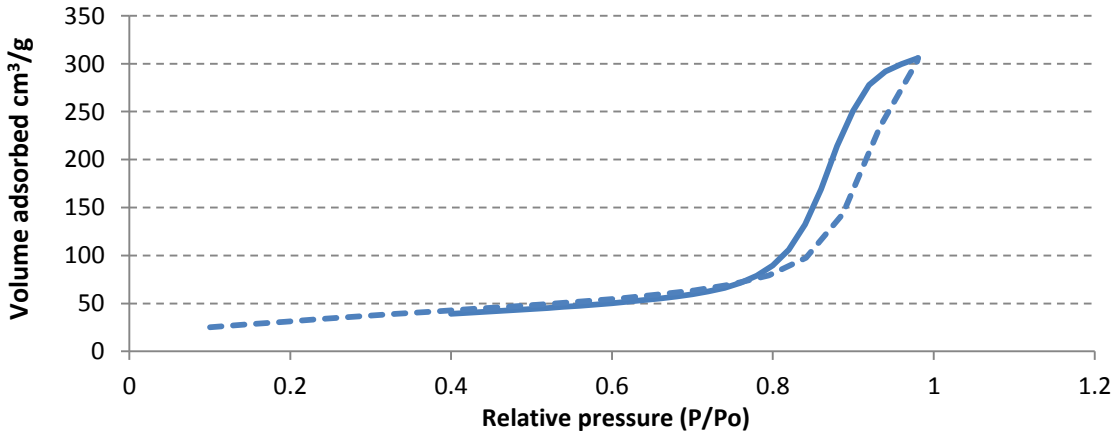

Figure 181: Nitrogen adsorption isotherm at 78K for the K- Pt/$A_{l2}O_3$ catalyst

The pore volume distribution as measured in the micropores range for the support is illustrated in Figure 182. It presents a uniform distribution, but there

is no clear decrease in the pore volume of both mesorpores and microspores of the platinum catalyst upon impregnation of the alkali.

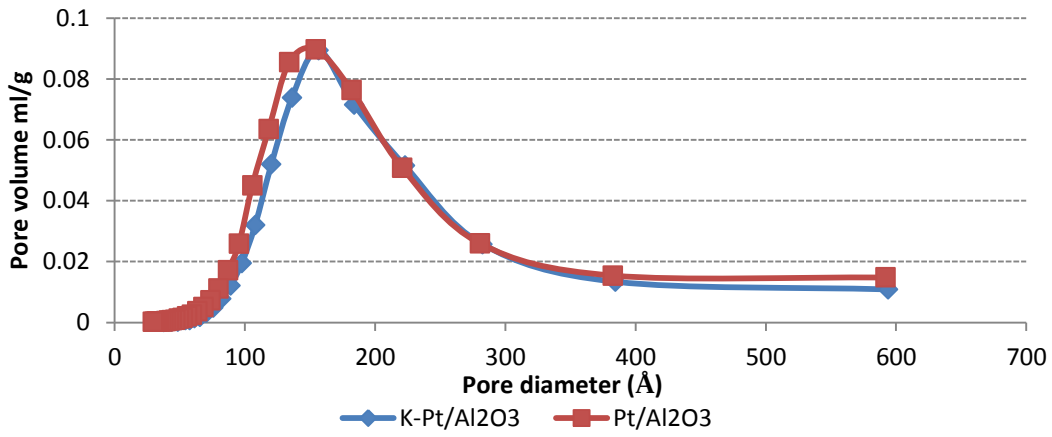

Figure 182: Pore volume distribution of the $Pt/A_{l2}O_3$ and the K- $Pt/A_{l2}O_3$ catalyst

3.5.1.2 XRD analysis

The XRD analysis of the platinum catalyst and the doped catalyst both revealed same diffraction pattern associated with only the alumina support and no evidence was observed for the crystalline phase of the platinum oxide and or the diffraction pattern of the potassium, associated with both α-K_2O/ ß-K_2O crystalline phases as observed with K-CrO_x/Al_2O_3 (Figure 183). This is expected for potassium loading (< 10%)

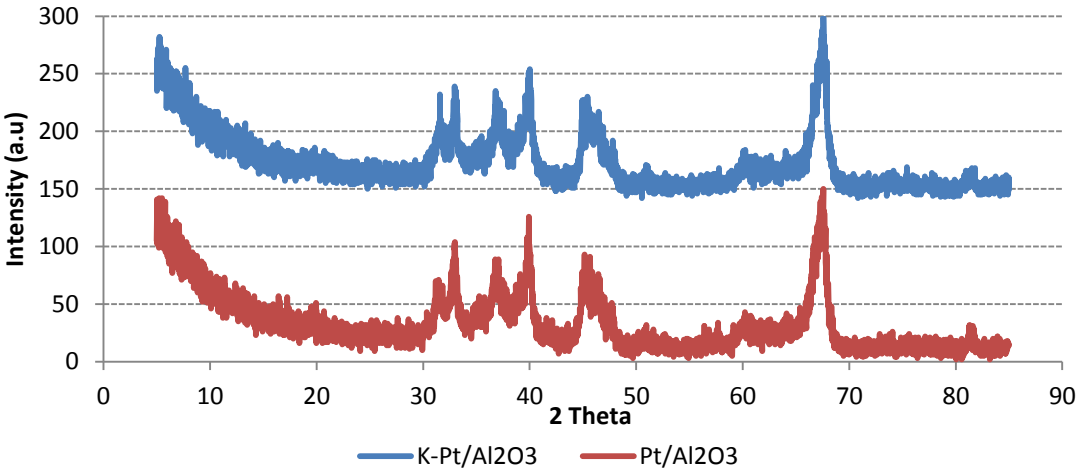

Figure 183: XRD diffraction pattern of the support and the $Pt/A_{l2}O_3$ catalyst

The standard TGA-TPR obtained from ambient temperature to 1273 K revealed an additional peak at ~1120 K. This peak was not observed with the Pt/Al_2O_3 catalyst and was also not observed during the Red/OX cycles, although the Red-Ox cycles were only run to 873 K. The peaks at ~517 and 552 K although at a bit higher temperature, correspond to ones obtained with the platinum catalyst at ~470 and ~506 K. This standard TGA-TPR peak is also consistent with the Red-Ox cycles. This as explained previously could be due to a thermal effect associated with dehydroxylation process that yields platinum oxide species and the thermal decomposition of the platinum complex, plus the reduction of the platinum oxide [91-93]. The oxides of potassium decompose at ~623-773 K and could react with the alumina to form a strong base. However, the potassium itself boils at ~1033 K, and therefore the weight loss (~2 %) at ~1050 K could probably be a loss of the potassium itself due to high temperature effect (Figure 184)

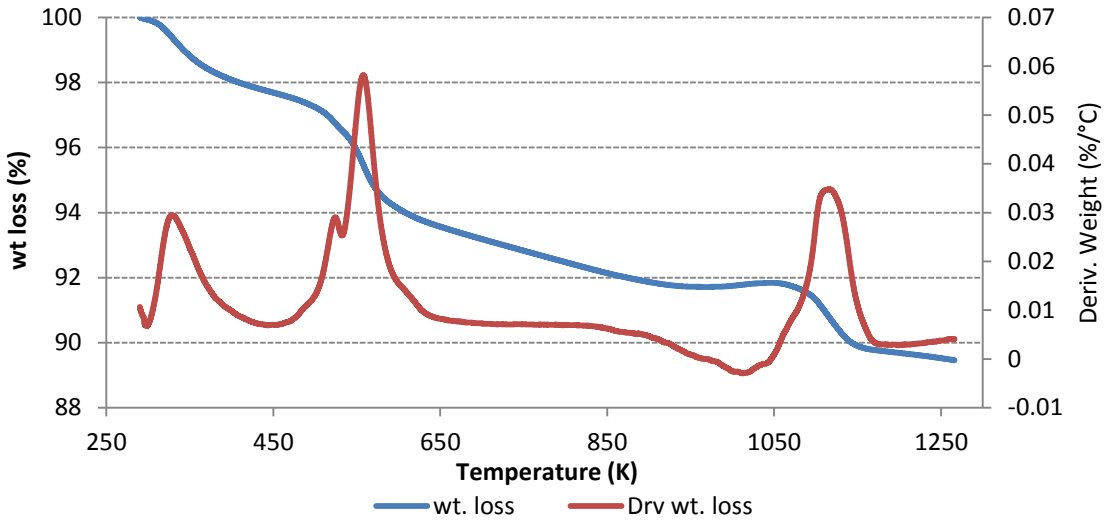

Figure 184: The standard TGA-TPR profile of the K- Pt/Al_2O_3 catalyst

The Ox-red cycles reduction profiles perfectly matches the peaks at ~517 and 552 K. This corresponds to ~4 % weight loss, the peak was only observed with the first reduction cycle which confirms that the loss associated with the peak could be as result of thermal decomposition of the platinum complex and removal of the ligands from the catalyst. The result is presented in Figure 185

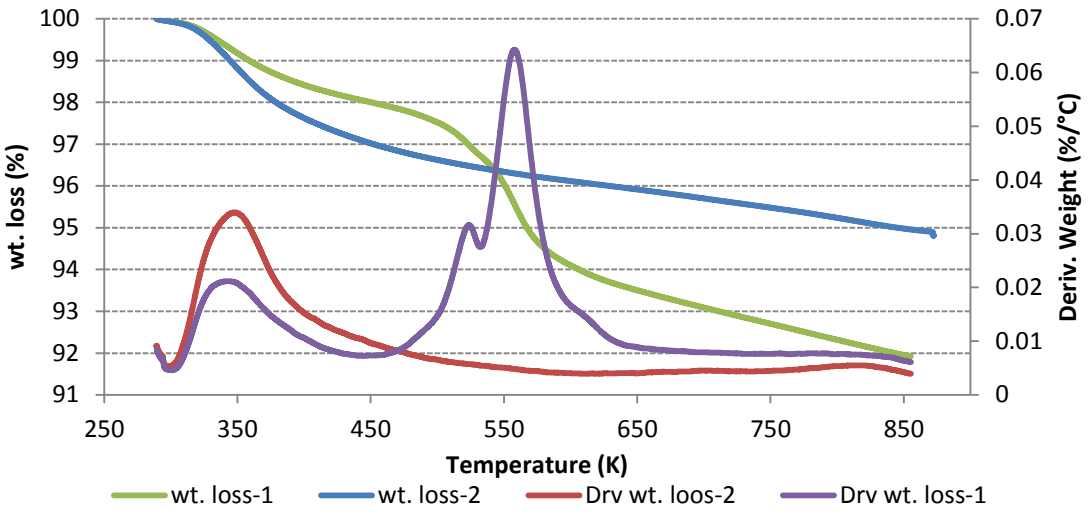

Figure 185: The TGA-TPR profile during the OX-Red cycles of the K-Pt/Al_2O_3 catalyst

The DTA profile during reduction 1st and 2nd cycles showed one endothermic effect in the temperature at ~373 K ascribed to the removal of physiosorbed water corresponding to moisture lost mainly from the alumina support and the weight loss was ~2% and ~1% respectively. Endothermic peaks were also observed at ~517 and 552 corresponding to a weight loss of ~4% similar to the platinum catalyst. This confirms that there is uptake of heat energy due to this loss, and therefore the lost can be assigned predominantly to the thermal effect decomposition of the platinum complex, and obviously a small hydrogen uptake for the reduction process.

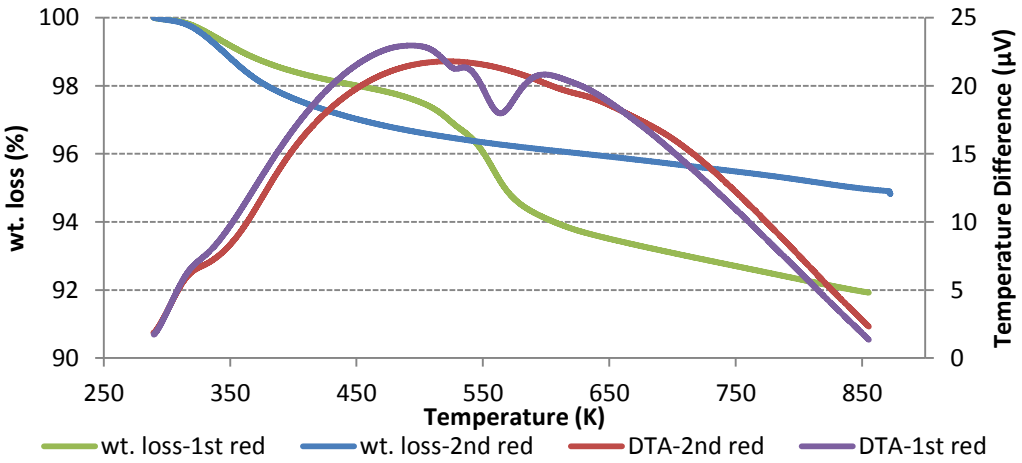

Figure 186: The DTA profile of the catalyst obtained during the TGA-TPR Ox-Red cycle of the K- Pt/$A_{l2}O_3$ catalyst

3.5.2 Pentane/Hexyne (P/1HY) system

3.5.2.1 Reaction analysis and trans-hydrogenation activity evaluation

The reactant conversions were followed individually and during the mixed trans-hydrogenation reaction. There was observed an increase in the conversion of the pentane during the trans-hydrogenation, conversion slightly higher (~3 %) than the pentane dehydrogenation at the two temperatures tested was. However, all of the conversions obtained were higher than the equilibrium conversion of n-pentane at that temperature. This slight increase in conversions was also observed with the hexyne reactant during the trans-hydrogenation. The result is presented in Figure 187.

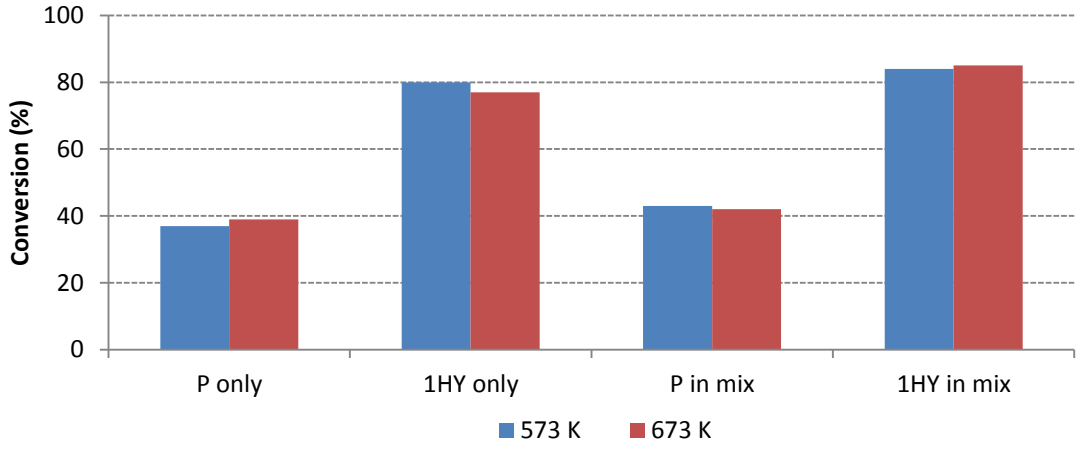

Figure 187: Conversion comparison of P, 1HY and P/1HY mixture using K-Pt/ $Pt/A_{l2}O_3$

The products yields are presented in Table 87 and 88. The product distributions are similar to those observed with the Pt/Al_2O_3 catalyst but with a slight increase in the products yields. Like the Pt/Al_2O_3 catalyst, most of the products obtained are alkylated and alkylated olefinic hydrocarbons.

Table 87: Products yield of the trans-hydrogenation over K-Pt/Al_2O_3 at 673 K

	P	H	P+H	P+H Theory
	Conversion (%)			
Pentane(P)	39		43	39
1-Hexyne(1HY)		77	85	77
	Yield (%)			
Iso-pentane	0.69		2.7	0.69
Pentene	0.84			0.84
Trans-2-Pentene	1.74			1.74
Cis-2-pentene	0.84			0.84
Hexane		2.98	1.62	2.98
1-Hexene		1.46	2.71	1.46
2-Hexene		1.41	0.29	1.41
3-Hexene		3.19	0	3.19
Methyl-2-pentene		7.21	10.59	7.21
3-Methylpentyne		8.6	3.16	8.6
3-methyl-1-hexene		14.23	18.02	14.23
Benzene			0.9	0
3-Methylhexane		1.8	6.39	1.8
2-Methyl-1,3-pentadiene		14.38	18.2	14.38
Methylcyclohexane	29.8	14.56	9.32	44.36

Table 88: Products yield of the trans-hydrogenation over K-Pt/Al_2O_3 at 573 K

	P	H	P+H	P+H Theory
	Conversion (%)			
Pentane(P)	37		42	80.54
1-Hexyne(1HY)		80	84	85.4
	Yield (%)			
Iso-pentane	0.32		1.42	0.32
Pentene	1.39			0.39
Trans-2-Pentene	1.8			0.8
Cis-2-pentene	0.38			0.38
Hexane		0.63	3.91	0.63
1-Hexene		1.03	0.71	1.03
2-Hexene		0.37	0.11	0.37
3-Hexene			0.34	0
Methyl-2-pentene		3.52	6.36	3.52
3-Methylpentyne		19.8	24.12	19.8
3-Methyl-1-hexene		6.4	12.9	6.4
Benzene			0.96	0
3-Methylhexane		6.85	11.43	6.85
2-Methyl-1,3-pentadiene		21.2	12.55	21.2
Methylcyclohexane	21.18	4.59	10.17	**25.77**

3.5.2.2 Post reaction characterization and analysis

The TGA analysis of the spent catalysts show unique weight loss with each type of reactant using the potassium doped platinum catalyst. Variation in the amount of the loss was also observed as a function of reaction temperature. In general there was less weight loss with pentane compared to hexyne and the mixed feed. With the catalyst from pentane only reaction < 2% loss at 673 K and ~1 % loss at 573 K was detected, whilst the catalysts from the hexyne and the mixed feed experiments gave a higher weight loss of ~ 4 % and ~3 % at 673 K respectively, < 1% weight loss was obtained in both cases from the catalysts used at 573 K. As expected, the values are slightly less than the one obtained with

the Pt/Al_2O_3 catalyst. The main loss observed at ~373K with all the three systems could be just due to physiosorbed water and was a similar loss in all the three systems. The other mass losses are due to evolution of CO_2 as confirmed from the TPO analysis. The results are presented in figures 188, 189 and 190

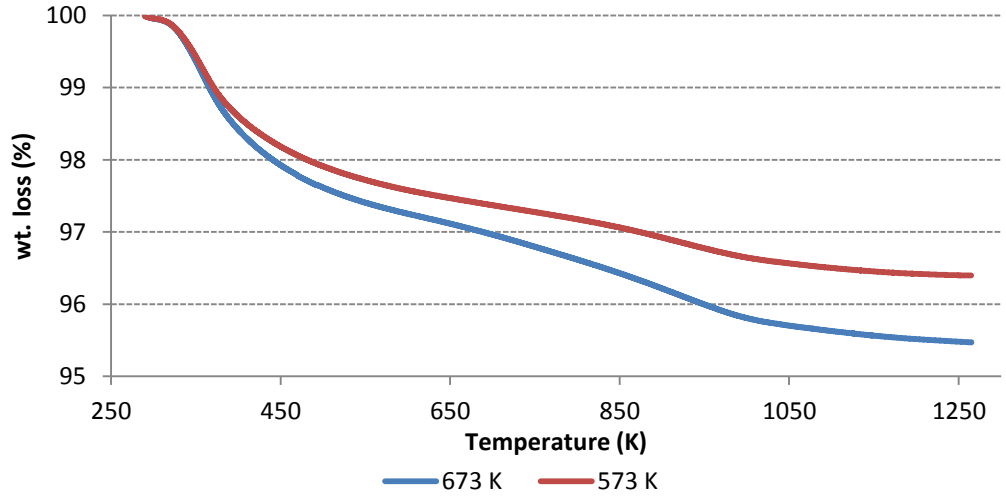

Figure 188: Weight loss profile of pentane run alone over K- Pt/A_2O_3 catalyst

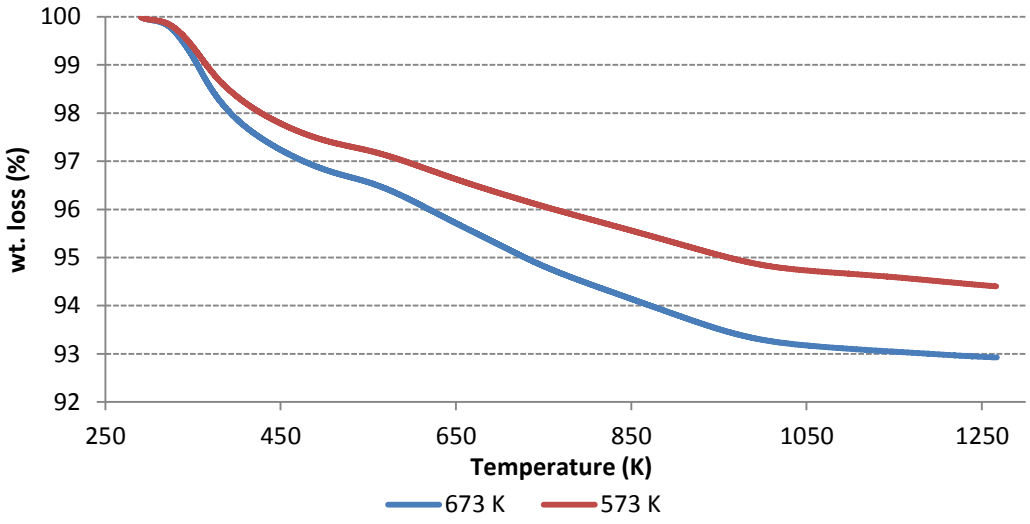

Figure 189: Weight loss profile of hexyne run alone over K- Pt/A_2O_3 catalyst

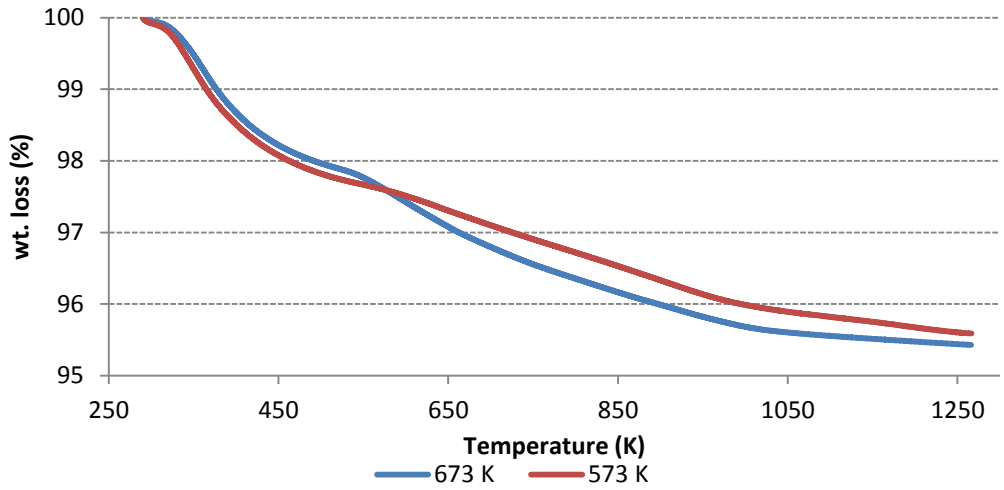

Figure 190: Weight loss profile of P/1HY mixed feed over K-Pt/Al_2O_3 catalyst

The TPO analysis revealed CO_2 as the main desorption species as confirmed by mass spectrometry. Two peaks were observed both with hexyne and the mixed feed. There was a peak at ~560 K and one around 580 K; the peak at lower temperature represented a greater weight loss in both cases except for the run at 573 K using the mixed feed where both carbon dioxide evolutions were about the same. This same effect was observed with the platinum catalyst. Only one obvious carbon dioxide peak was observed with the pentane reactant and it tallied with the second peak when using hexyne or the mixed feed at ~580 K. Possibly, two form of carbonaceous deposit were obtained with the hexyne and the mixed feed and one with the pentane reactant. The results are presented in figures 191, 192 and 193

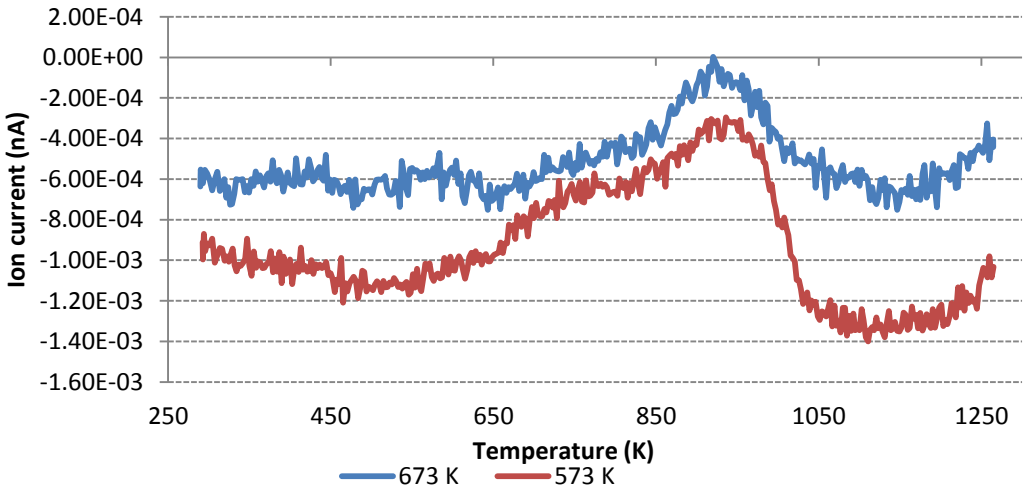

Figure 191: TPO profile of pentane run alone over K-Pt/Al_2O_3 catalyst

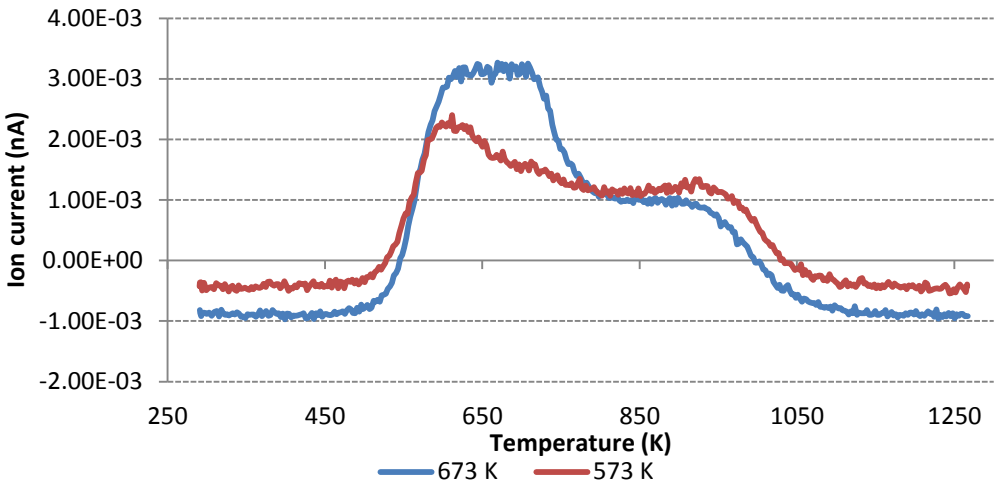

Figure 192: TPO profile of hexyne run alone over K-Pt/Al_2O_3 catalyst

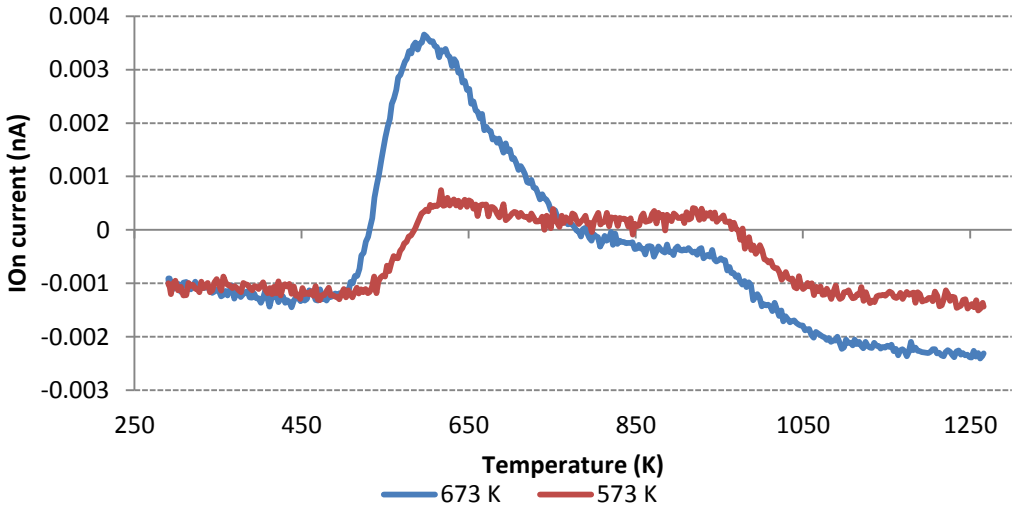

Figure 193: TPO profile of P/1HY mixed feed over K-Pt/Al_2O_3 catalyst

3.5.3 Pentane/1,5-Hexdiene (P/1,5HD) system

3.5.3.1 Reaction analysis and trans-hydrogenation activity evaluation

There is a slight increase in the conversions of pentane using the doped platinum catalyst with the 1,5HD system. More significant increase in conversion (~65 % conversion) of pentane was observed with the trans-hydrogenation and this was about double the conversion obtained with pentane dehydrogenation using this catalyst. Unlike the 1HY system, a decrease in the conversion of the 1,5HD was observed during the trans-hydrogenation of ~8 % at 673 K and ~3 % at 573 K. Higher conversions of pentane were obtained with the doped catalyst compared to the non-doped platinum catalyst. The results are presented in Figure 194

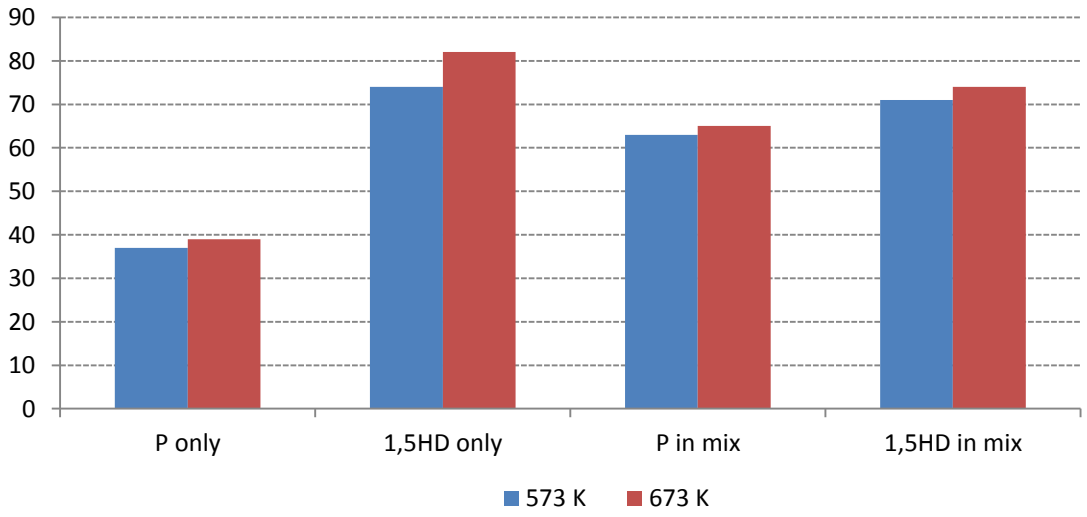

Figure 194: Conversion comparison of P, 1,5HD and P/1,5HD mixture using K-Pt/Al_2O_3

The product yields are presented in table 89 and 90; similar product distributions were obtained using the platinum catalyst with this system. However, there was a slight increase in the yield of the products obtained similar to the 1HY system.

Table 89: Products yield of the trans-hydrogenation: 1,5HD system at 673 K using K-Pt/Al_2O_3

	P	H	P+H	P+H Theory
	Conversion (%)			
Pentane(P)	39		65	74
1,5-Hexadiene (1,5HD)		82	74	82
	Yield (%)			
Iso-pentane	0.69		0.16	0.69
Pentene	0.84			0.84
trans-2-Pentene	1.74			1.74
Cis-2-pentene	0.84			0.84
Hexane		0.97	1.22	0.97
1-Hexene		0.86	0.17	0.86
2-Hexene		0.34	0.91	0.34
3-Hexene		1.62	1.34	1.62
Methyl-2-pentene		9.44	4.53	9.44
3-Methyl-1-hexene		10.88	5.41	10.88
Benzene		0.82		0.82
3-Methylhexane		4.54	3.83	4.54
2-Methyl-1,3-pentadiene		10.53	10.65	10.53
2-Methyl-1-1hexene		6.96	9.38	6.96
Methylcyclohexane	29.8	17.34	12.47	47.14

Table 90: Products yield of the trans-hydrogenation: 1,5HD system at 573 K using K-Pt/Al_2O_3

	P	H	P+H	P+H Theory
	Conversion (%)			
Pentane(P)	37		63	37
1,5-Hexadiene (1,5HD)		74	71	85.4
	Yield (%)			
Iso-pentane	0.32		0.13	0.32
Pentene	1.39			0.39
Trans-2-Pentene	1.8			0.8
Cis-2-pentene	0.38			0.38
Hexane		0.31	0.22	0.31
1-Hexene		1.18	0.28	1.18
2-Hexene		0.61	1.09	0.61
3-Hexene		0.6		0.6
Methyl-2-pentene		6.24	4.17	6.24
3-Methyl-1-hexene		9.48	8.51	9.48
3-Methylhexane		2.59	1.82	2.59
2-Methyl-1,3-pentadiene		8.45	8	8.45
2-methyl-1-1hexene			8.95	0
Methylcyclohexane	21.18	17.2	16.62	38.38

3.5.3.2 Post reaction characterization and analysis

The TGA analysis of the spent catalysts with the 1,5HD system also shows a weight loss. There are two weight losses with both the 1,5HD run and the mixed feed. However, there is not much difference in total weight loss between the two catalysts used at the different reaction temperatures during the mixed feed. The results are presented in Figure 195 and 196

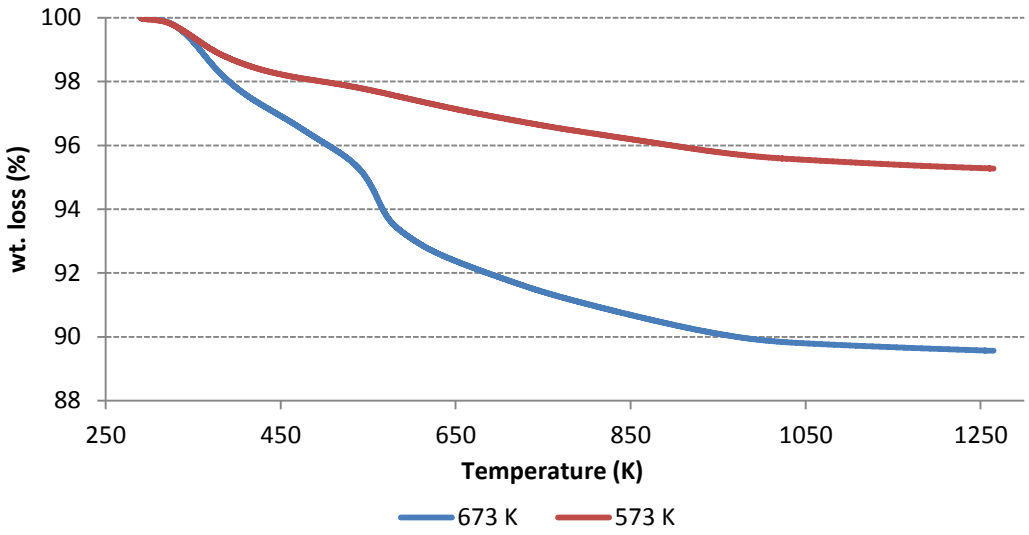

Figure 195: Weight loss profile of 1,5HD run alone over K-Pt/Al_2O_3 catalyst

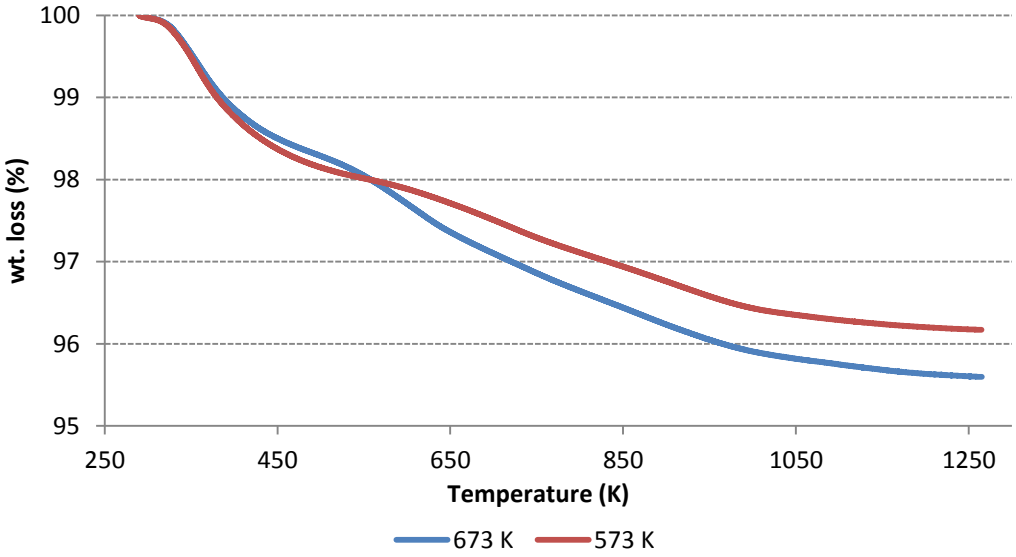

Figure 196: Weight loss profile of P/1,5HD mixed feed over K-Pt/Al_2O_3 catalyst

The TPO analysis of the spent catalyst reveals CO_2 as the main evolved species. However, two forms of carbonaceous deposits were observed with both reactions. There is also observed shift in the evolution of the CO_2 peaks with catalyst reaction temperature, this was only observed with the first peak while the second peak evolved at the same temperature. This peak shift was observed with the 1,5HD system with all the catalysts. The results are presented Figure 197 and 198

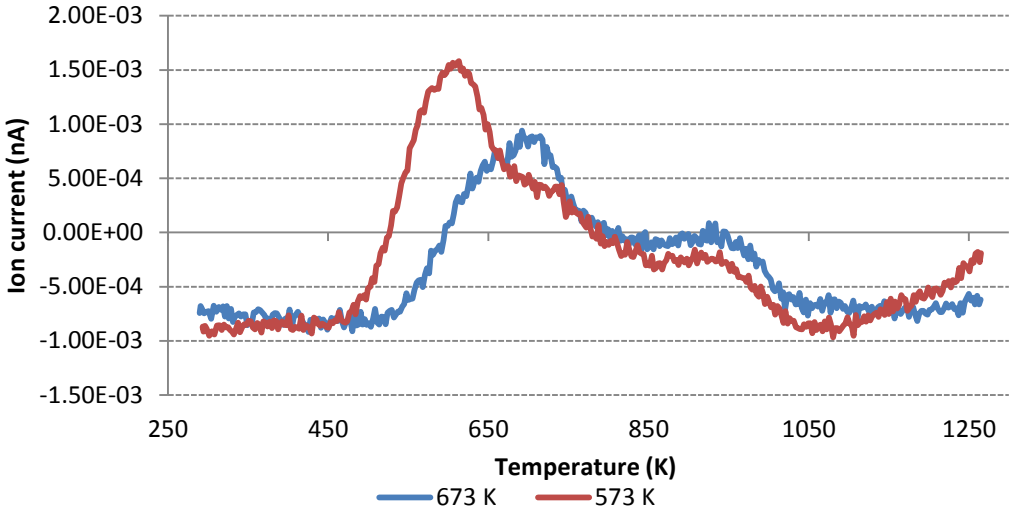

Figure 197: TPO profile of 1,5HD run alone over K-Pt/Al_2O_3 catalyst

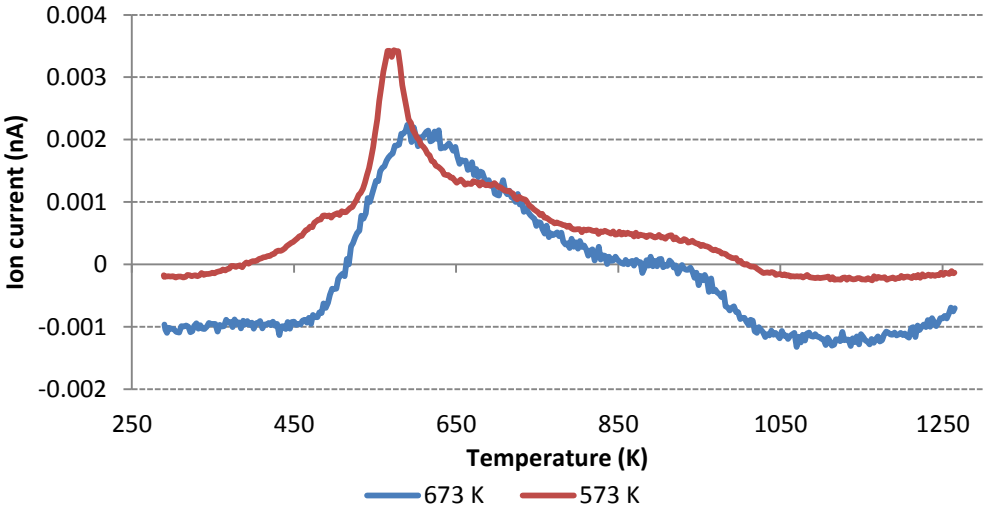

Figure 198: TPO profile of P/1,5HD mixed feed over K-Pt/Al_2O_3 catalyst

3.5.4 Pentane/2,4-Hexadiene (P/2,4HD) system

3.5.4.1 Reaction analysis and trans-hydrogenation activity evaluation

The conversion of pentane was lower during the trans-hydrogenation with this catalyst compared with pentane dehydrogenation. This shows that the doping of the catalyst does not improve the activity of the catalyst. This is very similar to what was observed with the doped chromia catalyst. This is consistent with the thermodynamic limitation as mentioned above. The result is presented Figure 199

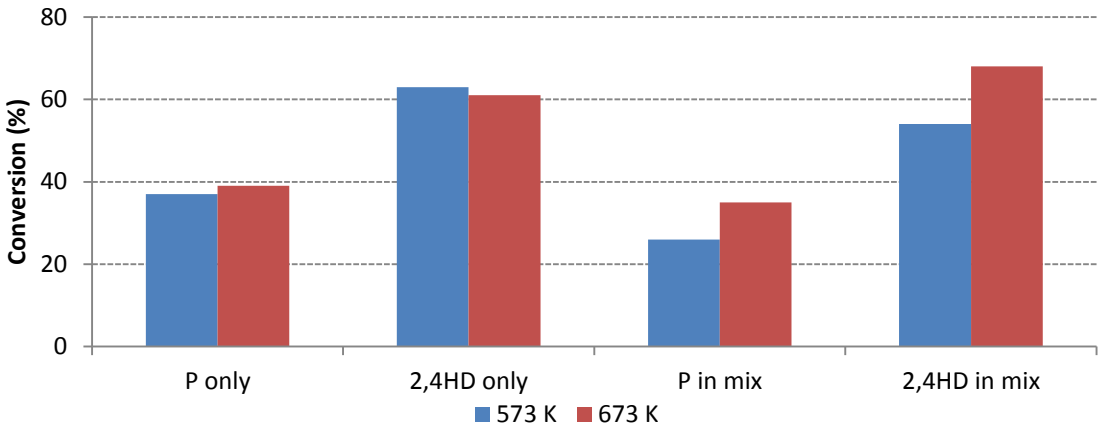

Figure 199: Conversion comparison of P, 2,4HD and P/2,4HD mixture using K-Pt/Al_2O_3

The products yields are presented in table 91 and 92

Table 91: Products yield of the trans-hydrogenation: 2,4HD system at 673 K using K-Pt/Al_2O_3

	P	H	P+H	P+H Theory
	Conversion (%)			
Pentane(P)	39		35	39
2,4-Hexadiene (2,4HD)		61	68	61
	Yield (%)			
Iso-pentane	0.69		1.18	0.69
Pentene	0.84			0.84
Trans-2-Pentene	1.74		0.47	1.74

Cis-2-pentene	0.84			0.84
Hexane		3.65	4.51	3.65
1-Hexene		0.68	0.49	0.68
2-Hexene				0
3-Hexene				0
Methyl-2-pentene		5.03	4.61	5.03
3-Methylhexane		3.28	2.23	3.28
2-Methyl-1,3-pentadiene		18.56		18.56
2-Methyl-1-1hexene		3.5	5.77	3.5
Methylcyclohexane	29.8	12.96	21.16	27.59

Table 92: Products yield of the trans-hydrogenation: 2,4HD system at 573 K using K-Pt/Al_2O_3

	P	**H**	**P+H**	**P+H Theory**
	Conversion (%)			
Pentane(P)	37		26	37
2,4-Hexadiene (2,4HD)		63	54	63
	Yield (%)			
Iso-pentane	0.32			0.32
Pentene	1.39			1.39
Trans-2-Pentene	1.8			1.8
Cis-2-pentene	0.38			0.38
Hexane		3.59	2.12	3.59
1-Hexene				0
2-Hexene				0
3-Hexene				0
Methyl-2-pentene		6.54	2.48	6.54
3-Methyl-1-hexene			4.51	0
3-Methylhexane		0.92	1.61	0.92
2-Methyl-1,3-pentadiene		18.45		18.45
2-Methyl-1-1hexene		5.45	5.98	5.45
Methylcyclohexane	21.18	10.05	19.08	31.23

3.5.4.2 Post reaction characterization and analysis

The TGA analysis of the spent catalyst shows a weight loss with the 2,4HD system. There are two weight losses from the catalysts used with both the 2,4HD run and the mixed feed just like the 1,5HD system but there is less difference in the total weight loss between the two reaction temperatures during the mixed feed compared to both hexyne and the 1,5HD systems. The results are presented in Figure 200, and 201

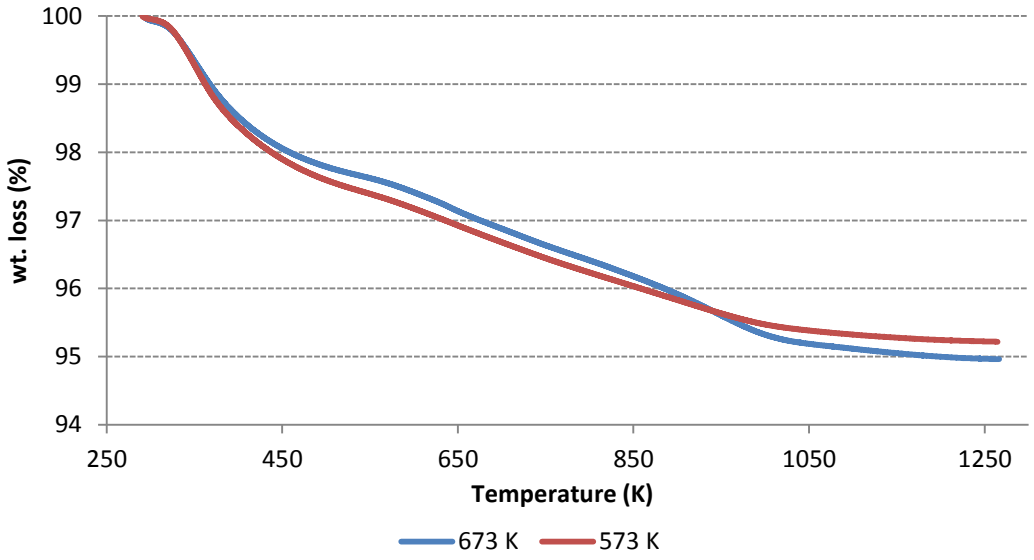

Figure 200: Weight loss profile of 2,4HD run alone over K-Pt/Al_2O_3 catalyst

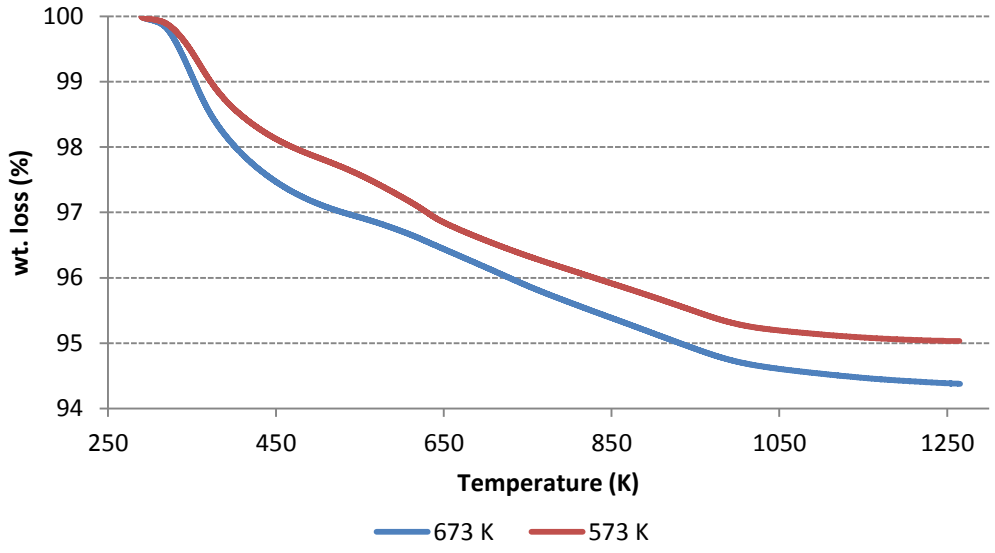

Figure 201: Weight loss profile of P/2,4HD mixed feed over K-Pt/Al_2O_3 catalyst

The TPO analysis of the spent catalyst reveals CO_2 as the main evolved species. However, possible two forms of carbonaceous deposits were observed with both reactions with the 2,4HD system. Unlike the 1,5HD there is no observed shift in the CO_2 peaks. The results are presented in Figure 202 and 203

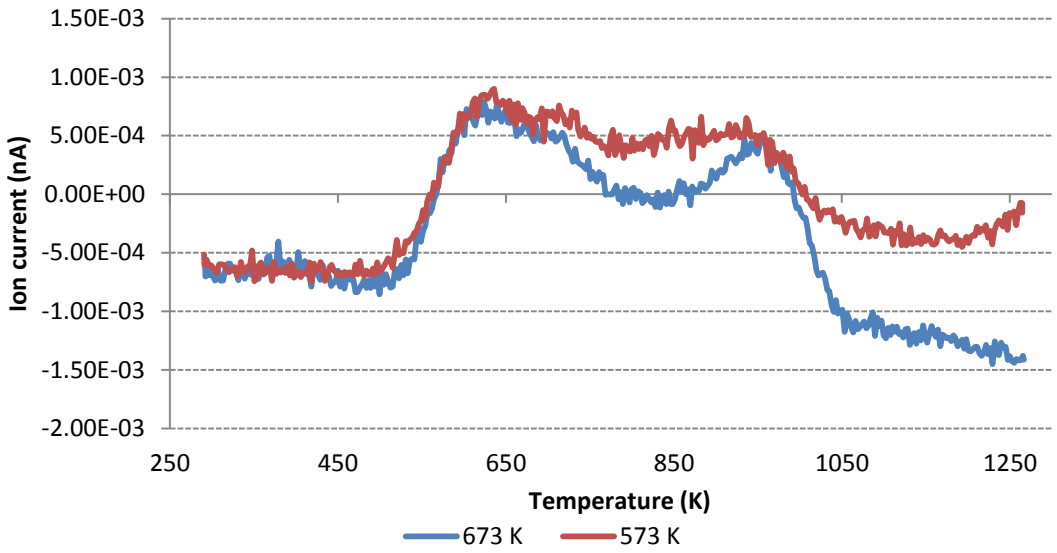

Figure 202: TPO profile of 2,4HD run alone over K-Pt/Al_2O_3 catalyst

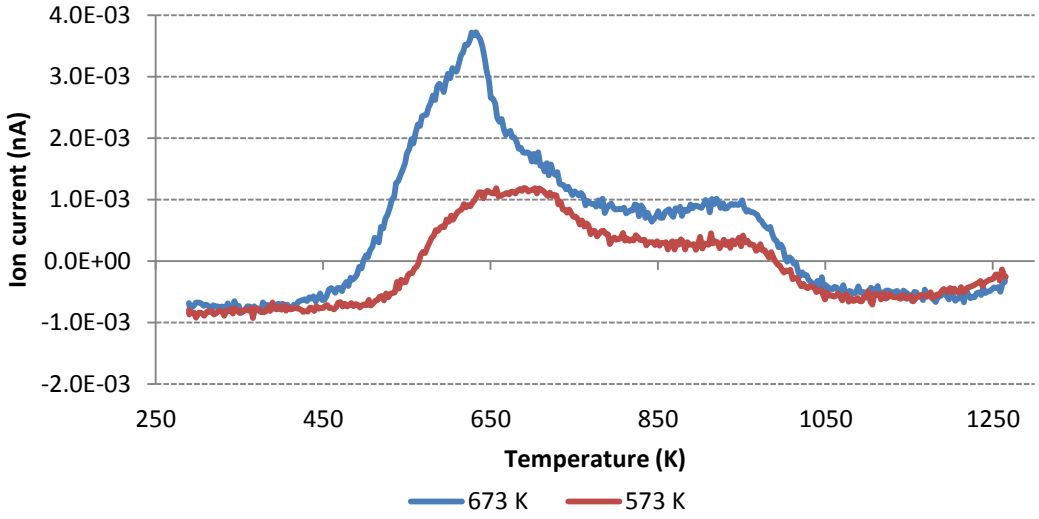

Figure 203: TPO profile of P/2,4HD mixed feed over K-Pt/Al_2O_3 catalyst

3.6 Reaction involving deactivation and regeneration cycles

The catalysts were further analysed for any possible deactivation over an extended period of 8 h. This involved testing of the trans-hydrogenation mixture at 673 K and 573 K. Analyses were taken every 2 h. Any possible deactivation was recorded and the catalysts were regenerated afterwards by flushing the reactor with Ar (30 ml/min) overnight, in order to remove any species remaining in the reactor, before switching the flow to 2% O_2/Ar (100 ml/min) for the *in-situ* TPO of the spent catalysts. The catalysts were heated from ambient temperature to 873 K at a ramp of 10 K/min, the reactor temperature was held at 873 K until evolution of all gases other than O_2 and Ar ceased. The eluent gases from the TPO were analysed by the online mass spectrometer (m/e 2, 16, 28, 32 and 44), for detailed investigation of the deposited carbonaceous material. In this rector configuration, the catalysts could therefore be cycled through this process of reduction/reaction/regeneration.

3.6.1 CrO_x/Al_2O_3 Catalyst

3.6.1.1 Pentane/Hexyne (P/1HY) system

There is less severe reduction in hexyne conversion at 673 K; the conversion only decreases from ~96% to ~80% after 2 hr TOS during the first cycle. Only a slight difference was observed between the two cycles except that the catalyst is more stable after 2 hr during the 2nd cycle (regenerated catalyst). At the lower reaction temperature (573 K), significant deactivation is observed, the conversion of hexyne decreases with time on stream (TOS), from ~50 % observed at 2 h TOS to ~25 % after 8 h. After regeneration hexyne conversion is slightly down from the initial run, whereas the pentane conversion slightly increases. However, at 673 K there is no loss in activity related to pentane conversion and after regeneration conversion of both reactants is slightly higher. The results are presented in Figure 204 and 205

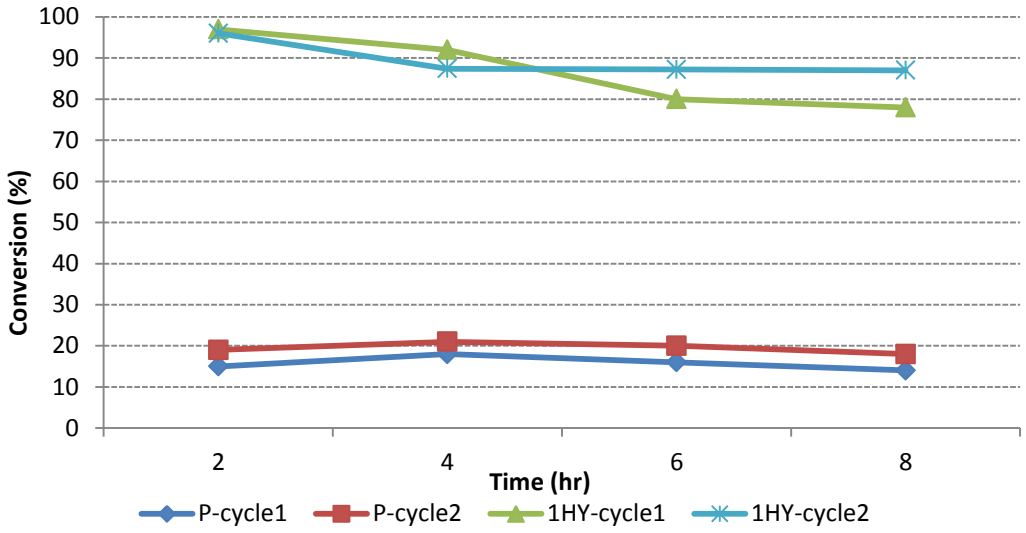

Figure 204: CrO_x/Al_2O_3 catalyst regeneration profile over P/1HY at 673 K

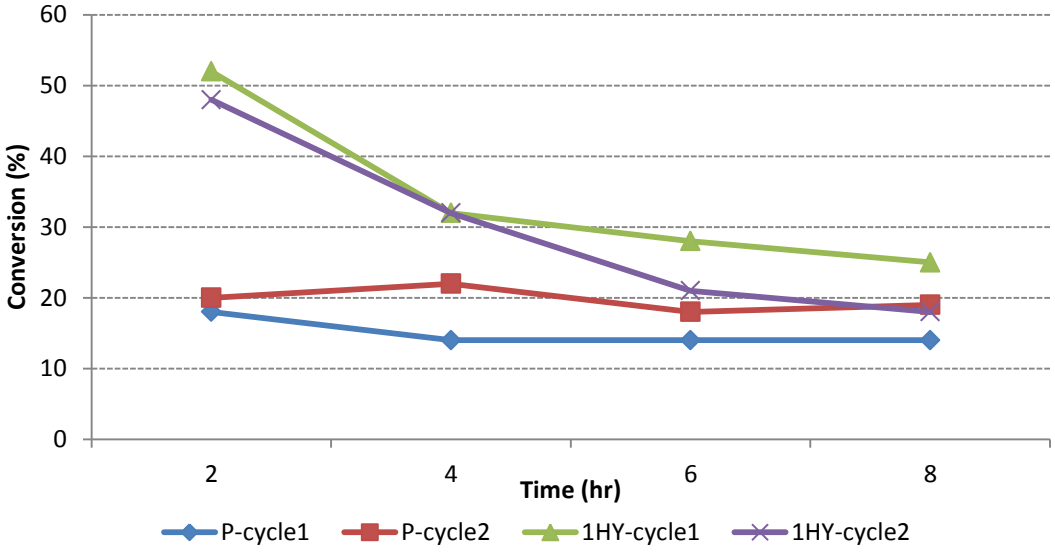

Figure 205: CrO_x/Al_2O_3 catalyst regeneration profile over P/1HY at 573 K

The yield of total olefin (total olefin formed/total feed fed) versus time on stream plots are presented in Figure 206 and 207, for both temperature runs. It indicates that after the first cycle a reduction of the olefin yield is observed after 2 hr during the second cycle. The activity/selectivity of the catalysts is more reproducible with TOS afterward for the period of 8 hrs. It is clearly observed that in both cycles there is approximately the same olefin yield after 4 hr.

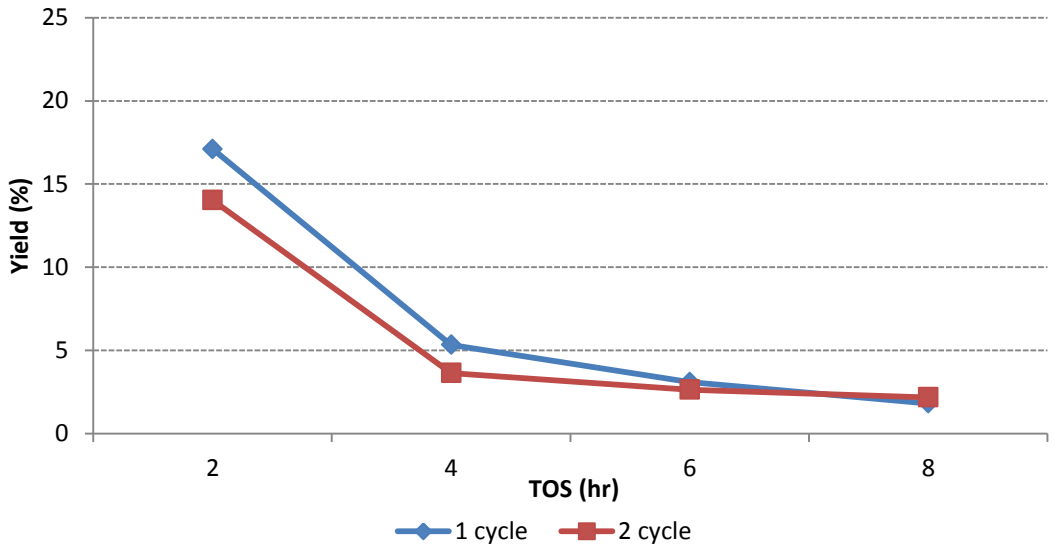

Figure 206: Effect of operating cycles on CrO_x/Al_2O_3 catalyst olefin yield over P/1HY at 673 K

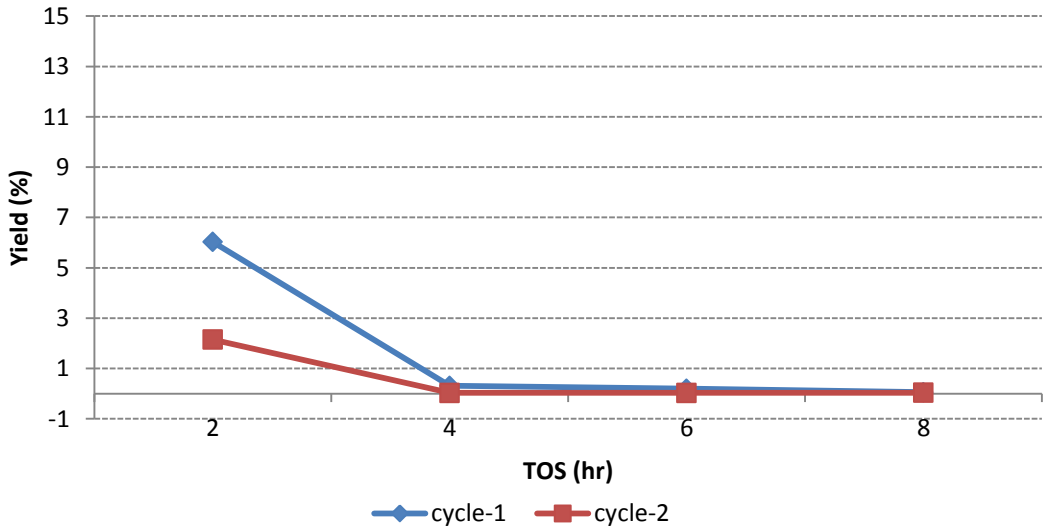

Figure 207: Effect of operating cycles on CrO_x/Al_2O_3 catalyst olefin yield over P/1HY at 573 K

Figure 208 and 209 illustrate the distribution of the valuable products of the reaction at 673K during cycle-1 (fresh catalyst) and cycle-2 (regenerated catalyst). Although there is observed deactivation in regards to the olefin production with both cycles, there is no obvious deactivation in regards to the production of the alkylates and the cyclics. However, there is a slight change in their yield within the 8 hours TOS.

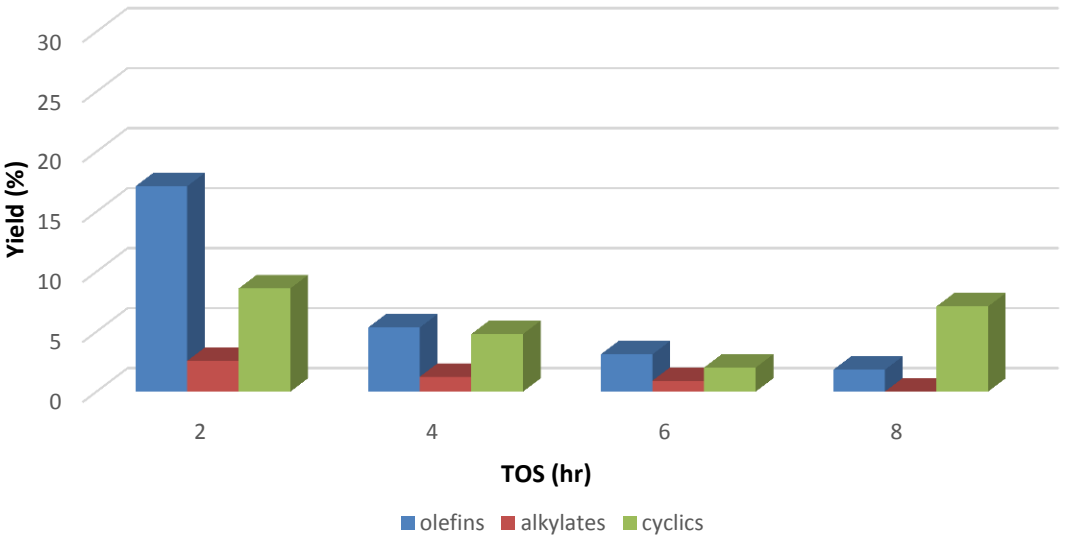

Figure 208: profile of the valuable product during first cycle over CrO_x/Al_2O_3 at 673 K

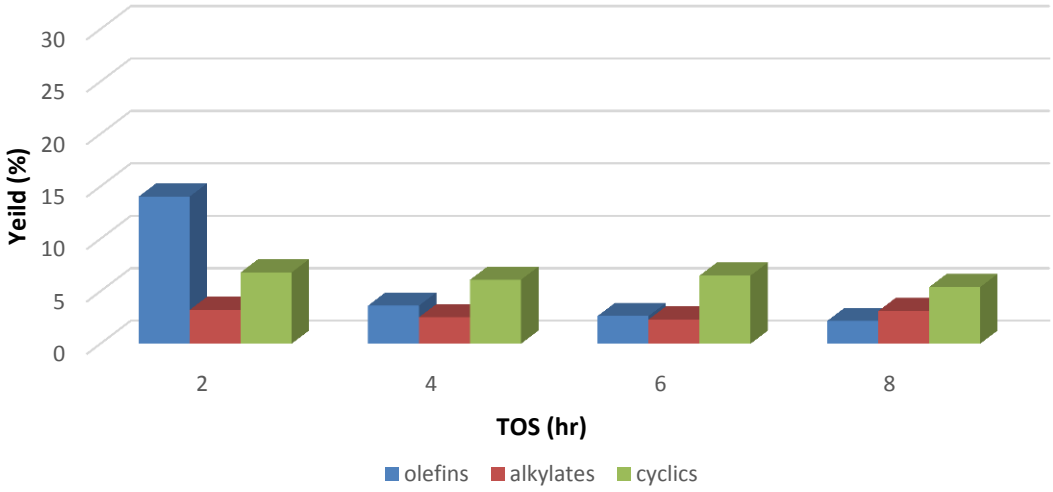

Figure 209: profile of the valuable product during second cycle over CrO_x/Al_2O_3 at 673 K

The two major products 1,4HD and 3MPY obtained using this system follow the same pattern with both cycles and presented a good relationship with reaction time over the 8 hr TOS. There is also observed general reduction during the second cycle compared to the first cycle as illustrated in Figure 210.

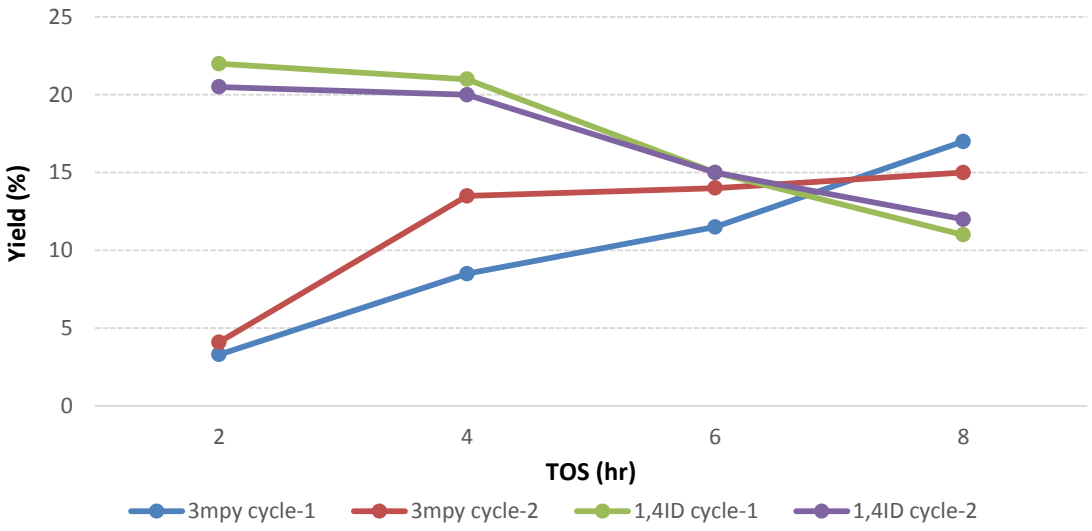

Figure 210: Profile of the two major products at 673 K over CrO_x/Al_2O_3

The reaction at 573 K did not follow the same trend as the reaction at 673 K in regards to the valuable production distribution. There is possible deactivation observed in the production of the both olefin and the cyclic products, whereas the alkylates revealed less consistent effect to the reaction time as illustrated in Figure 211 and 212. Both cycles present the same pattern but only that general reduction in the product yield is observed during the second cycle.

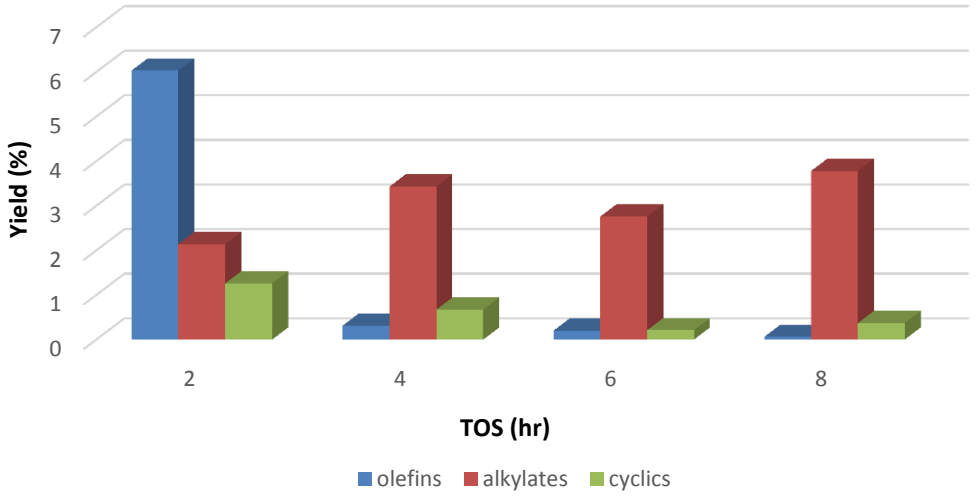

Figure 211: profile of the valuable product during second cycle over CrO_x/Al_2O_3 at 573 K

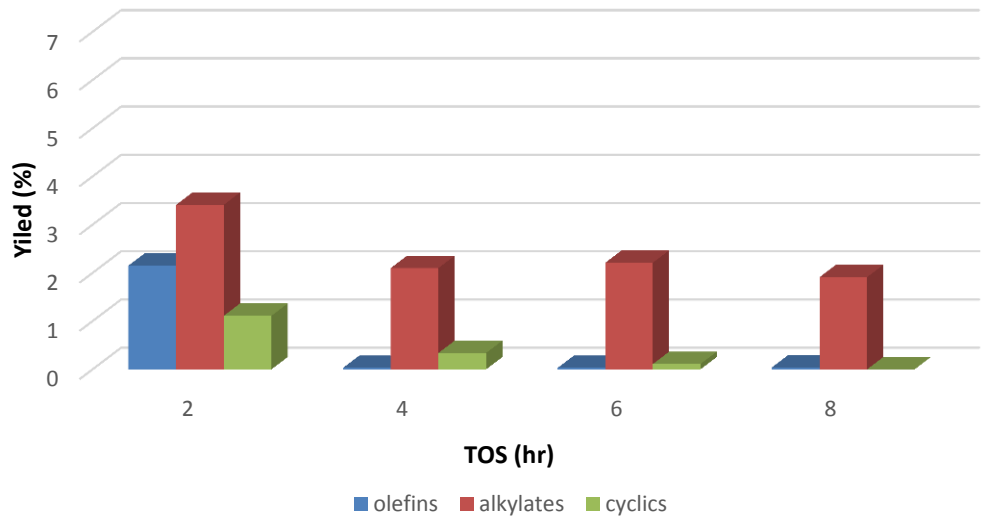

Figure 212: profile of the valuable product during second cycle over CrO_x/Al_2O_3 at 573 K

Figure 213 illustrates the profile of the major products at 573 K, although there is a good similarity with the reaction at 673 K there is observed a general reduction in their yield, which could be related to the differences in the conversion of the reactants using the two temperatures. Only ~8 % 1,4HD with a significant deactivation after 4 hr TOS was obtained at 573 K compared to ~25 % at 673 K. The production of 3MPY was also much more stable during the second cycle at the 573 K

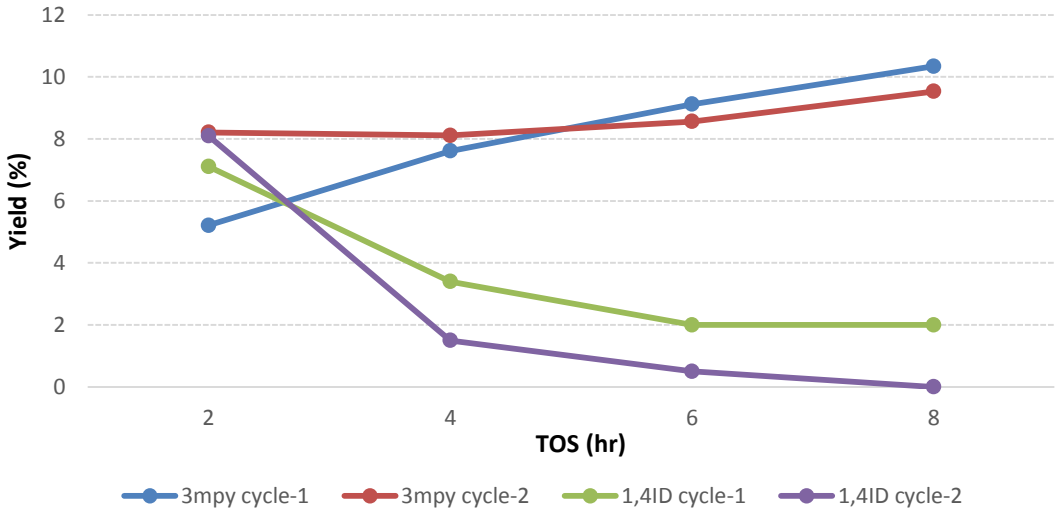

Figure 213: Profile of the two major products at 573 K over CrO_x/Al_2O_3

The TPO analysis on the catalysts used at both 673 K and 573 K are presented in Figure 214 and 215. The graph shows that there has been significant carbon

deposition at both reaction temperatures and CO_2 evolution was observed. In addition, traces of H_2, CO and H_2O were also detected in the course of the TPO. There are possibly two types of carbonaceous material that have formed at both reaction temperatures and all desorption species perfectly matches with the evolution of the CO_2 as two clear distinct evolutions were observed. This suggests that they were formed as a result of combustion of two different types of carbon deposit. Desorption of all these species also matches the consumption of oxygen suggesting that they are from combustion of the carbon deposit. The first CO_2 evolution at ~750 K could be a kind of soft carbon species and hydro-carbonaceous type, while the second CO_2 evolution at the isothermal temperature 873 K after ramping could be a kind of hard carbon species that is less hydro-carbonaceous. This effect is similar to what was observed during the 2 hr short run.

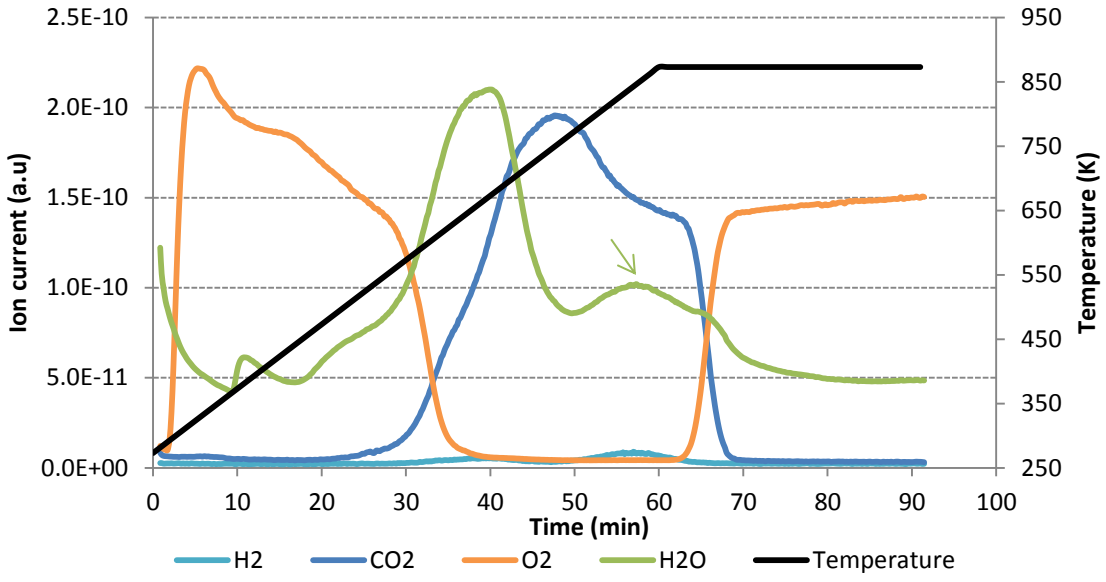

Figure 214: Evolution of CO_2 and other species during the TPO on CrO_x/Al_2O_3 spent catalyst over P/1HY at 673 K

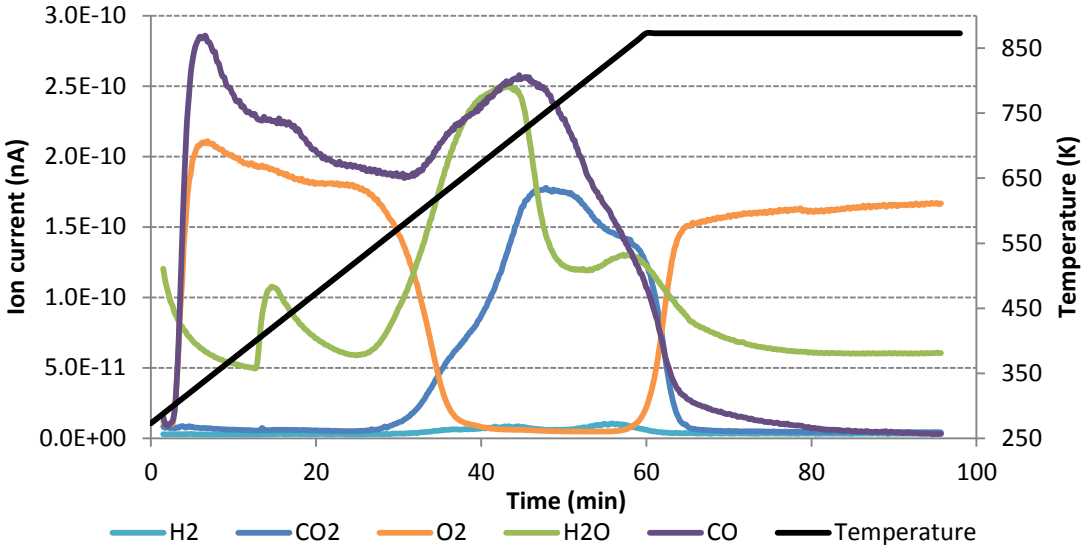

Figure 215: Evolution of CO2 and other species during the TPO on CrO_x/Al_2O_3 spent catalyst over P/1HY at 573 K

Two clear distinct hydrogen evolutions were observed from the catalysts used at 673 K and 573 K, their evolution matches the CO_2 evolution suggesting that the hydrogen evolution could be related to incomplete combustion probably due to high percentage deposition. This distinct hydrogen evolution was not observed during the 2 hr short run. Although the evolution of all the other species were observed in the TPOs from the catalysts used at both reaction. The result is presented in Figure 216

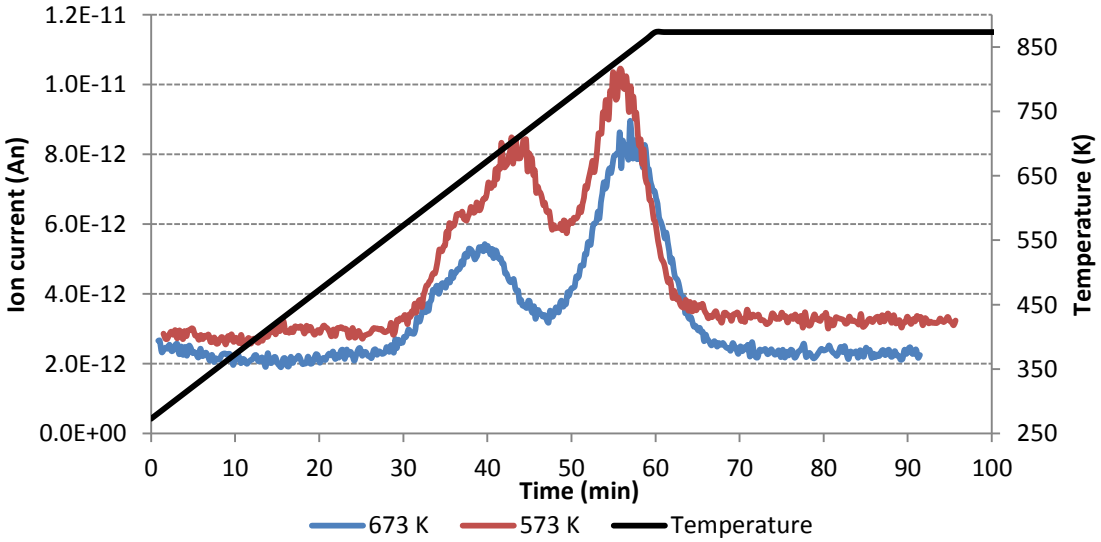

Figure 216: Evolution of hydrogen specie during the TPO on CrO_x/Al_2O_3 spent catalyst over P/1HY

3.6.1.2 Pentane/1,5-hexadiene (P/1,5HD) system

Less severe deactivation was observed with the 1,5HD system over both cycles at 673 K, the activity of the catalyst was observed to be similar during the two cycles. The conversions of the 1,5HD obtained were similar with the 2 hr analysis. The activity of the catalyst only reduced to ~80 % in 8 hr compared to ~96 % obtained in 2 hr observed with 1,5HD reactant at 673 K. However, significant deactivation was only observed with the 2nd cycle during the 573 K reaction. Although the conversion of 1,5HD was maintained at ~80 % in 8 hr during the 1st cycle, severe activity loss was observed in 8 hr during the 2nd cycle (regenerated catalyst)

In general, lower activity was observed with the regenerated catalyst at both reaction temperatures compared to the fresh catalyst. The result are presented in Figure 217 and 218

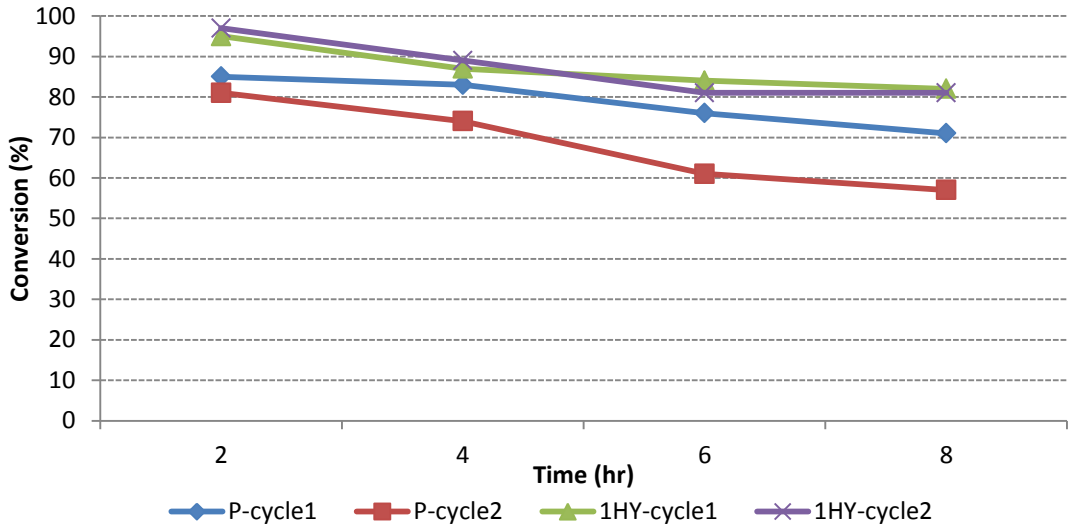

Figure 217: CrO_x/Al_2O_3 catalyst regeneration profile over P/1,5HD at 673 K

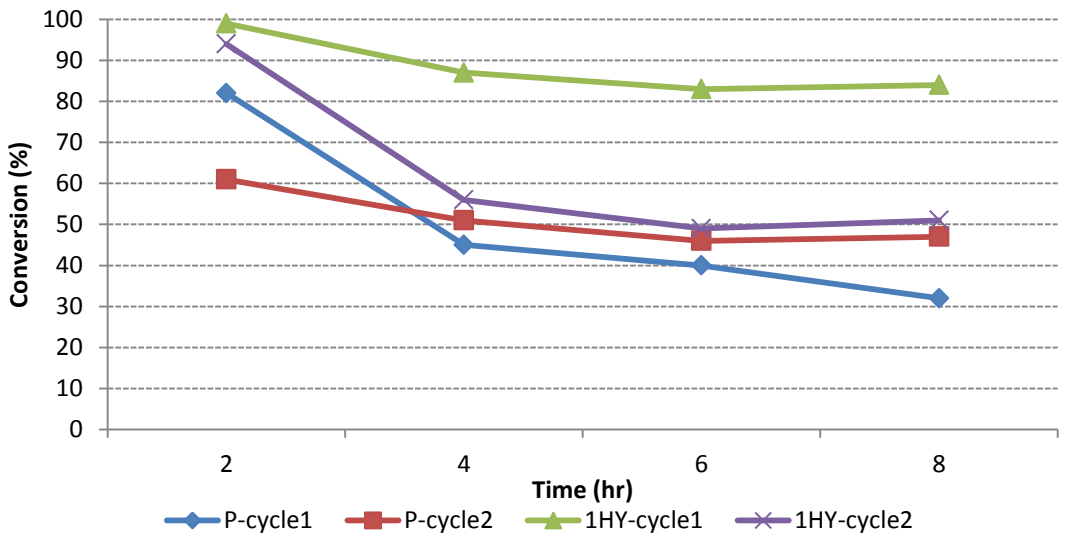

Figure 218: CrO_x/Al_2O_3 catalyst regeneration profile over P/1,5HD at 673 K

The total olefin yield as a function of reaction temperature suggests that, there is a loss in activity/selectivity with time at both temperatures. Significant activity loss down from ~ 55 % after 2 hr to ~ 27% after 8 hr was observed during reaction at 673 K during the 1st cycle. The activity/selectivity is more stable during the 2nd cycle with about same olefin yield obtained in the first 4 hrs and before slightly reducing in the second 4 hrs. The same trend was observed with the test at 573 K. The results are presented in Figure 219 and 220

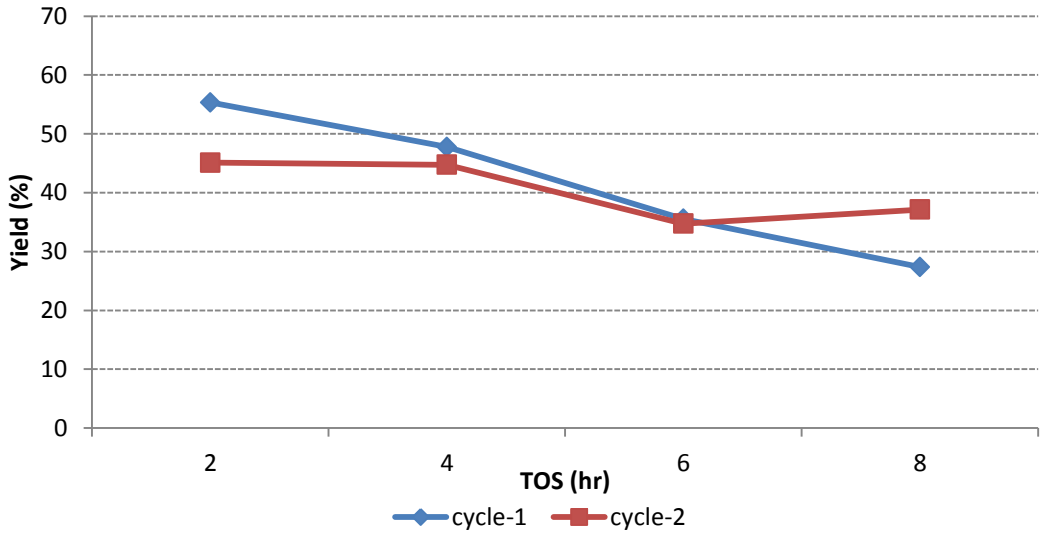

Figure 219: Effect of operating cycles on CrO_x/Al_2O_3 catalyst olefin yield over P/1,5HD at 673 K

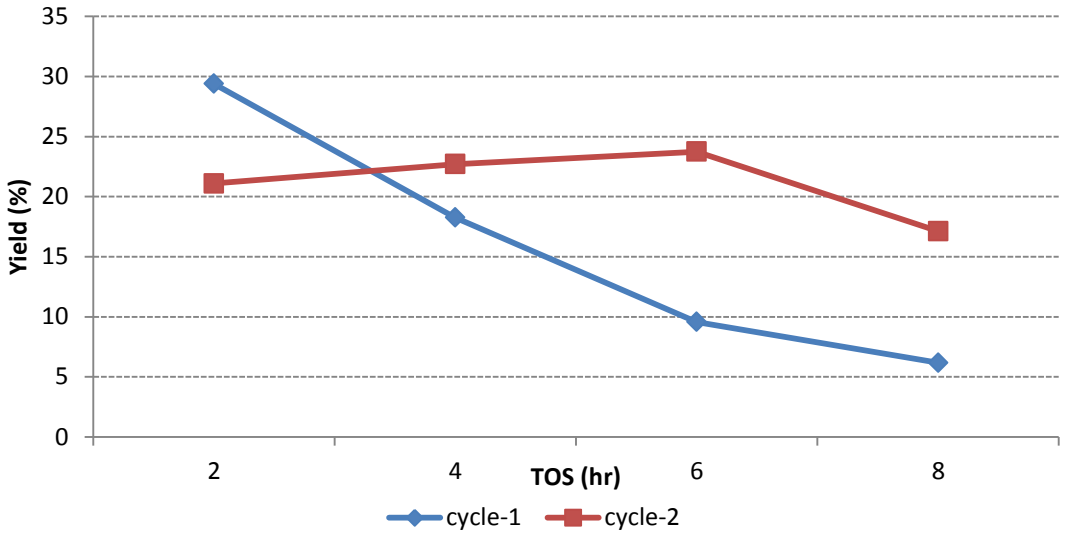

Figure 220: Effect of operating cycles on CrO_x/Al_2O_3 catalyst olefin yield over P/1,5HD at 573 K

The distribution of the valuable products for the reaction at 673 K is presented in Figure 221 and 222 reveals a slight deactivation in regards to the olefin and alkylates with both cycles. Whilst a slight increase in the activity of the catalyst was observed with the regards to the cyclics.

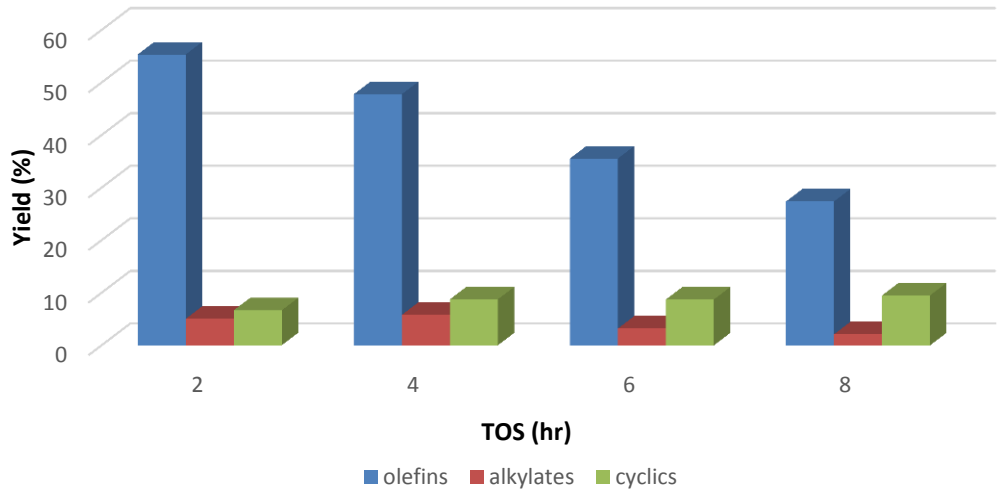

Figure 221: Profile of the valuable product during first cycle using P/1,5HD over CrO_x/Al_2O_3 at 673K

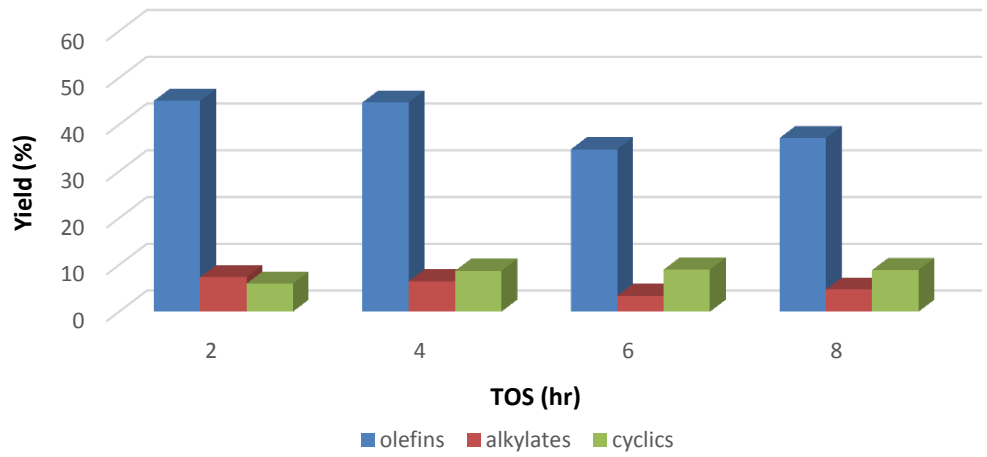

Figure 222: profile of the valuable product during second cycle using P/1,5HD over CrO_x/Al_2O_3 at 673K

The valuable product distribution observed from the reaction at 573 K was similar to the one observed at 673 K. However, there is general reduction in the product yields and the cyclics does not really show a relationship with respect to TOS but they mostly show a stable production. Their production is also most stable during the second cycle. The results are presented in Figure 223 and 224

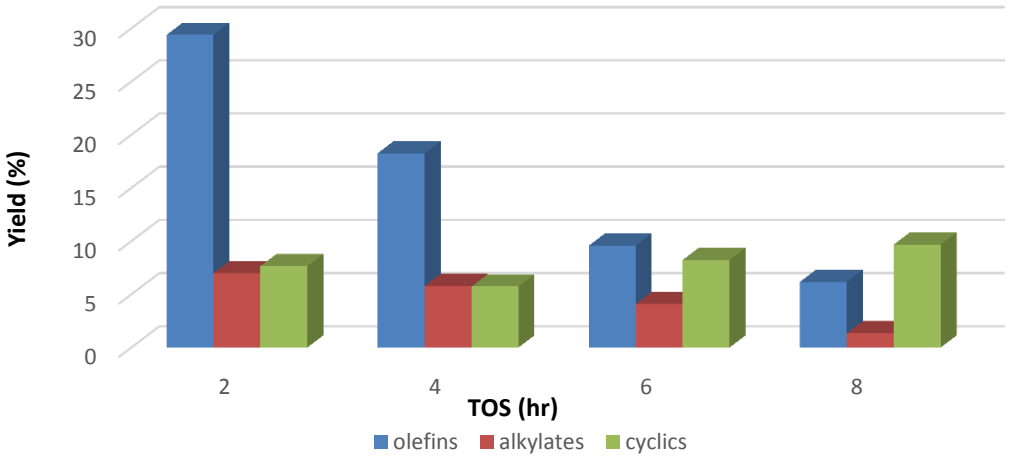

Figure 223: profile of the valuable products during first cycle using P/1,5HD over CrO_x/Al_2O_3 at 573K

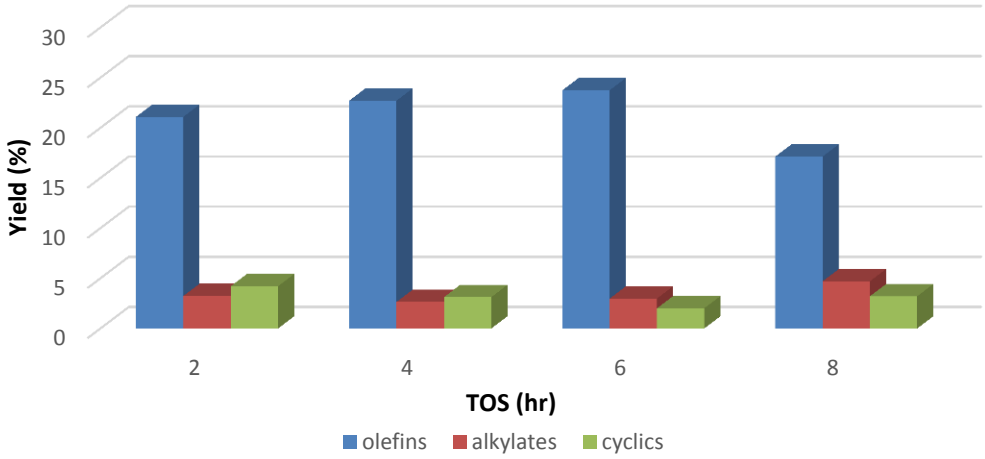

Figure 224: Profile of the valuable product during second cycle using P/1,5HD over CrO_x/Al_2O_3 at 573K

The TPO profile revealed CO_2 as the main evolved species. The TPOs from catalysts at each reaction temperature showed similar TPO profiles. However, there is observed a slight shift in the desorption peaks with reaction temperature. The CO_2 evolution peaks at ~650 K from the catalyst used in the 573 K reaction while the catalyst used in the 673 K reaction evolved carbon dioxide at ~ 740 K revealing that this deposit was harder to burn. This similar to what was observed during the short 2 hr reaction where shifts in the CO_2 evolution peaks with reaction temperature were observed. The lower reaction temperature catalysts have carbonaceous deposits that are easier to burn compared to the deposits on catalysts used in the high temperature reactions. In addition to CO_2 evolution, only traces of H_2O and CO were only observed. There is slight evolution of H_2 although this may be from the cracking pattern of the H_2O. However, during the short 2 hr run CO was not observed during the TPO analysis but only trace of water was detected in some of the samples. It could also be observed that not all of the oxygen is taken up compared to the 1HY system, which is related to the extent of the coke formation. The result are presented in Figure 225 and 226

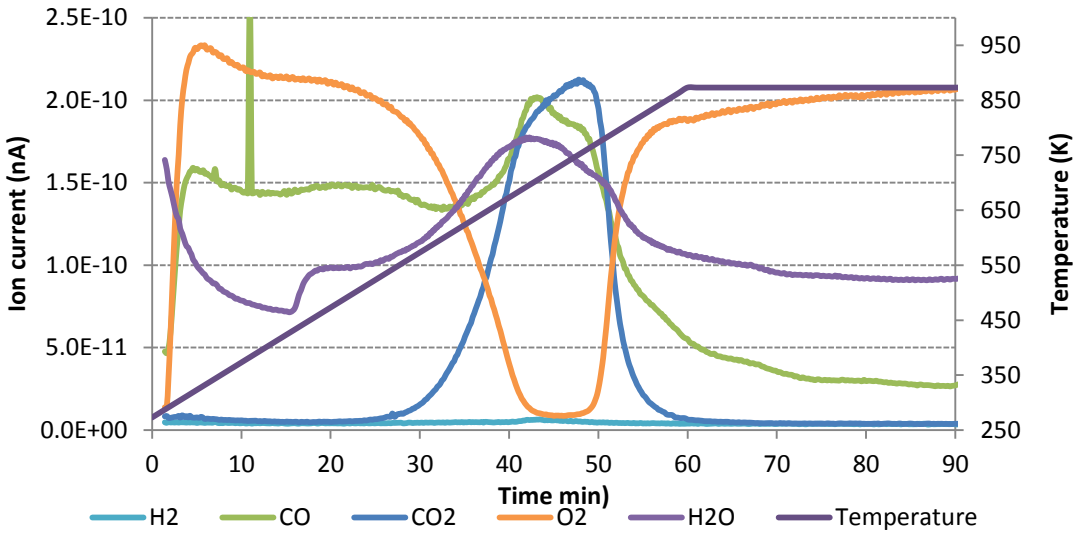

Figure 225: Evolution of CO_2 and other species during the TPO on CrO_x/Al_2O_3 spent catalyst over P/1,5HD at 673 K

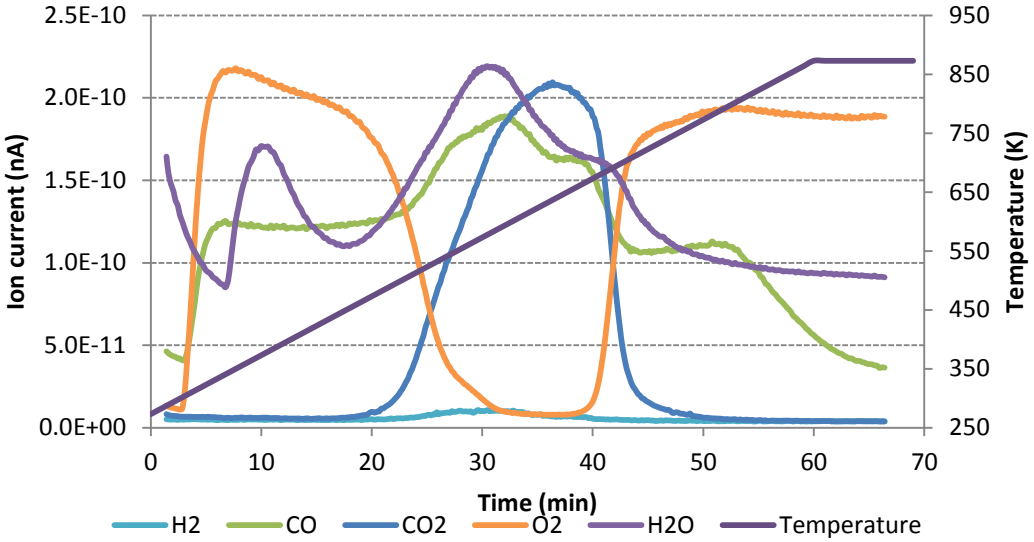

Figure 226: Evolution of CO_2 and other species during the TPO on CrO_x/Al_2O_3 spent catalyst over P/1,5HD at 573 K

3.6.1.3 Pentane/2,4-hexadiene (P/2,4HD) system

Slight deactivation is also observed with pentane/2,4-hexadiene over the 8 hr time-on-stream with ~20 % reduction in the conversion of the 2,4HD. This amount of deactivation was observed with the 2,4HD at both reaction temperatures during the 1st cycle. However, the catalyst was much more stable during the 2nd cycle and the conversions were generally stable for the period of the 8 hr run. There is slight deactivation during the experiment at 573 K. The results are presented in Figure 227 and 228

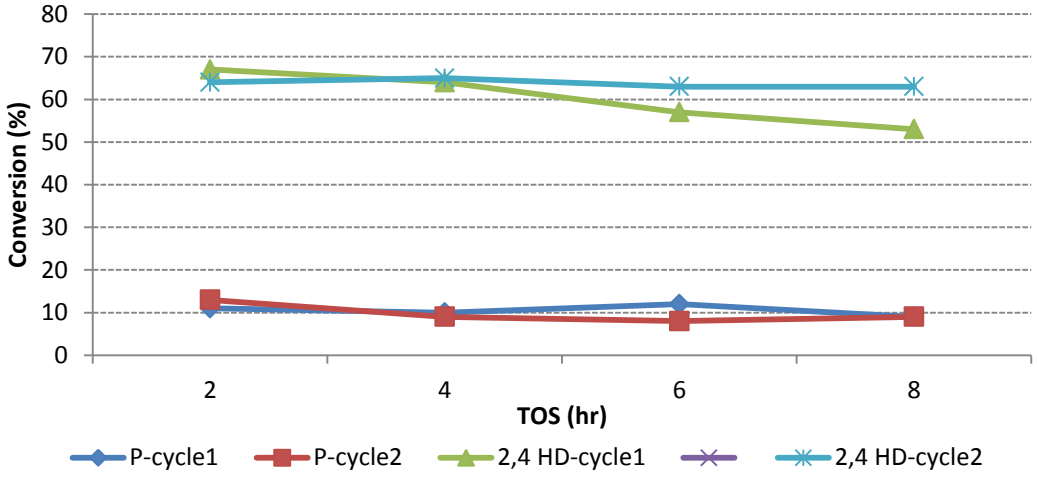

Figure 227: CrO_x/Al_2O_3 catalyst regeneration profile over P/2,4HD at 673 K

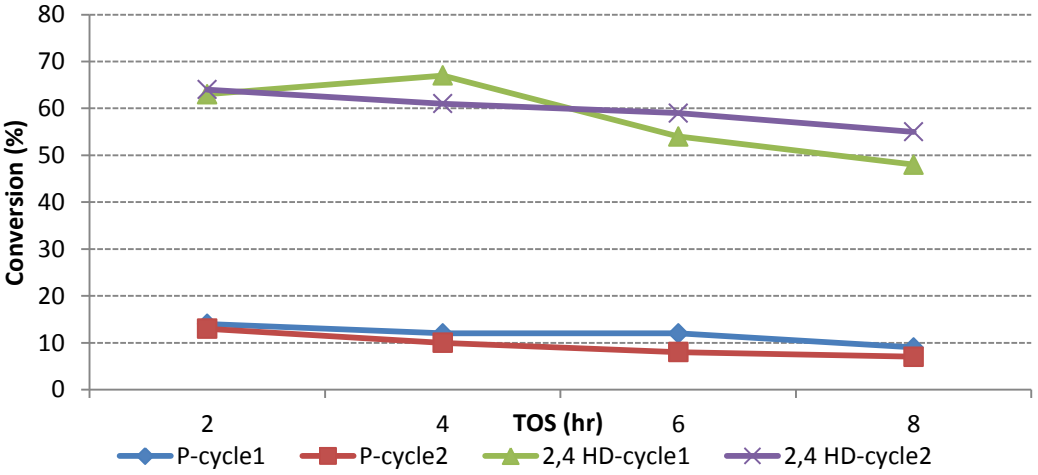

Figure 228: CrO_x/Al_2O_3 catalyst regeneration profile over P/1,5HD at 5 73 K

The total olefin yield was observed to be similar during both cycles at 673 K and there is no evident loss of activity for the generation of the olefin. There is a slight increase in activity after the regeneration with a reaction temperature of 573 K and the yield of the olefin slightly increased during the second cycle. The results are presented in Figure 229 and 230

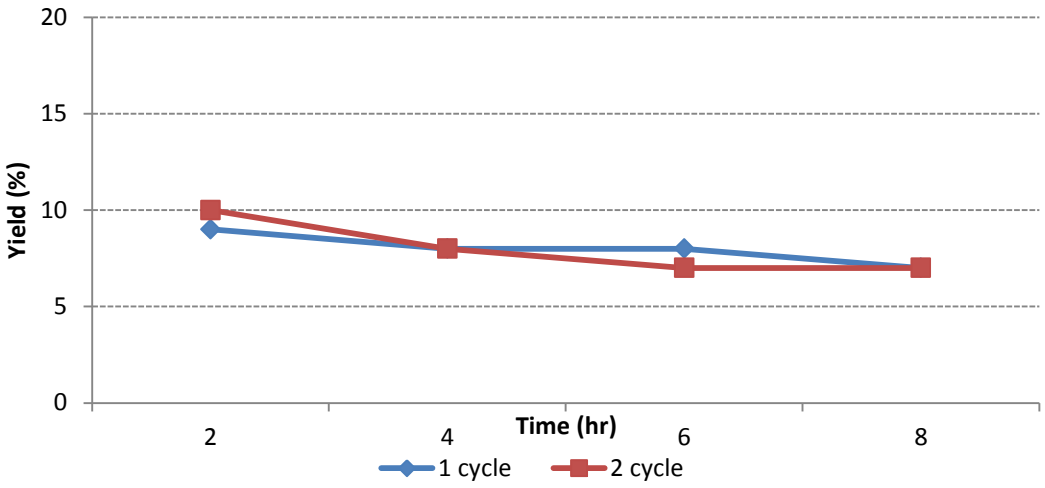

Figure 229: Effect of operating cycles on CrO_x/Al_2O_3 catalyst olefin yield over P/2,4HD at 673 K

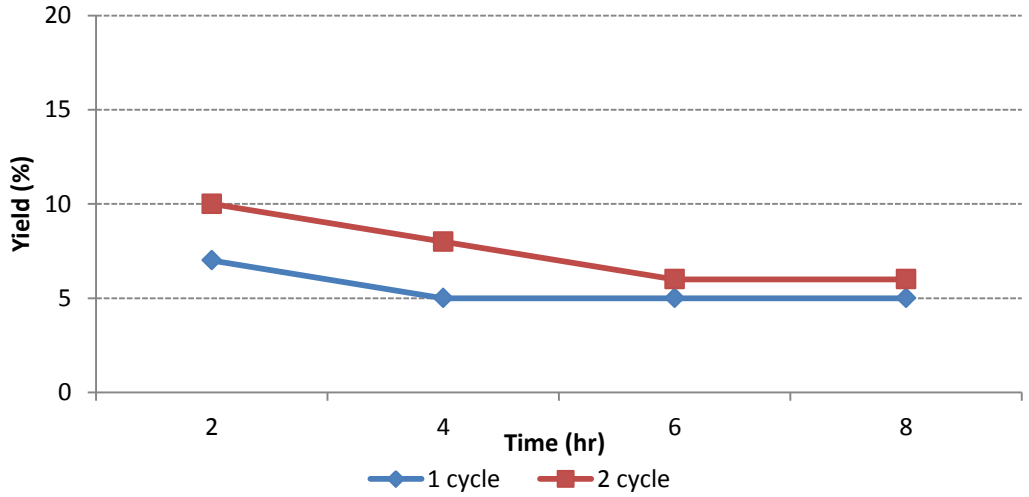

Figure 230: Effect of operating cycles on CrO_x/Al_2O_3 catalyst olefin yield over P/2,4HD at 573 K

Figure 231 and 232 illustrate the valuable products distribution. There is deactivation observed but this is small. Both cycles present the same pattern and a similar product yield.

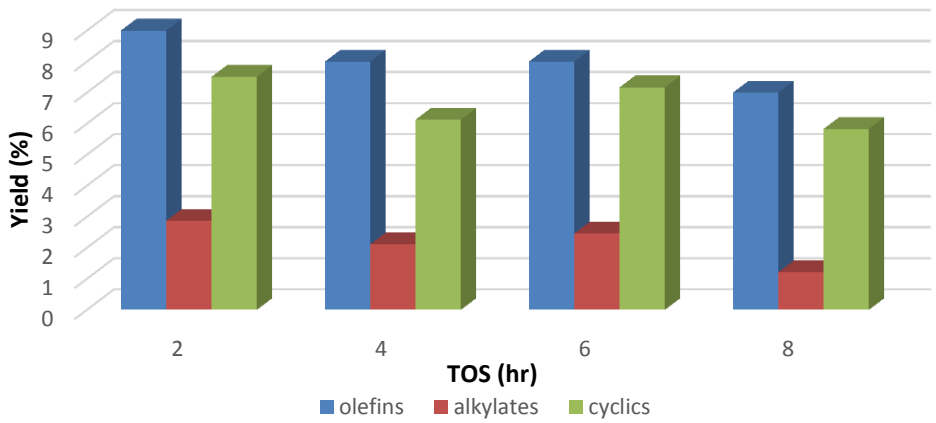

Figure 231: profile of the valuable product during first cycle using P/2,4HD over CrO_x/Al_2O_3

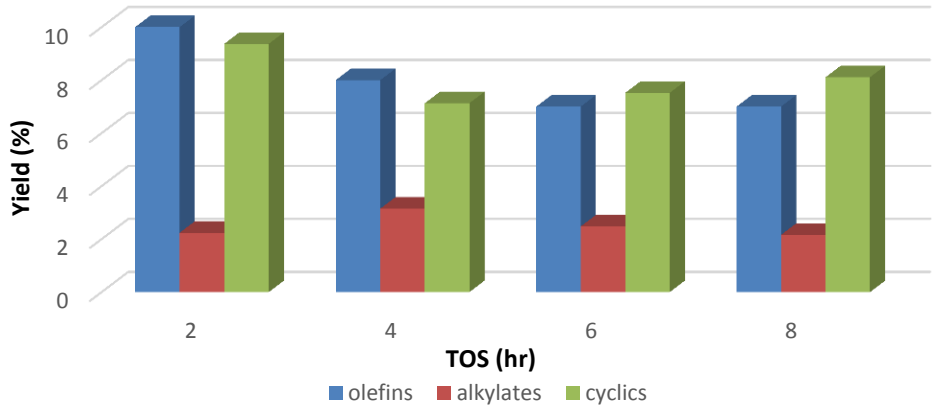

Figure 232: profile of the valuable product during second cycle using P/2,4HD over CrO_x/Al_2O_3 at 673 K

The valuable products distribution during the reaction at 573 K reveals a very similar yield distribution with the reaction at 673 K. The results illustrated in Figure 233 and 234 show that there is a slight increase in the activity of the catalyst after regeneration and the production of alkylates at 563 K is almost stable.

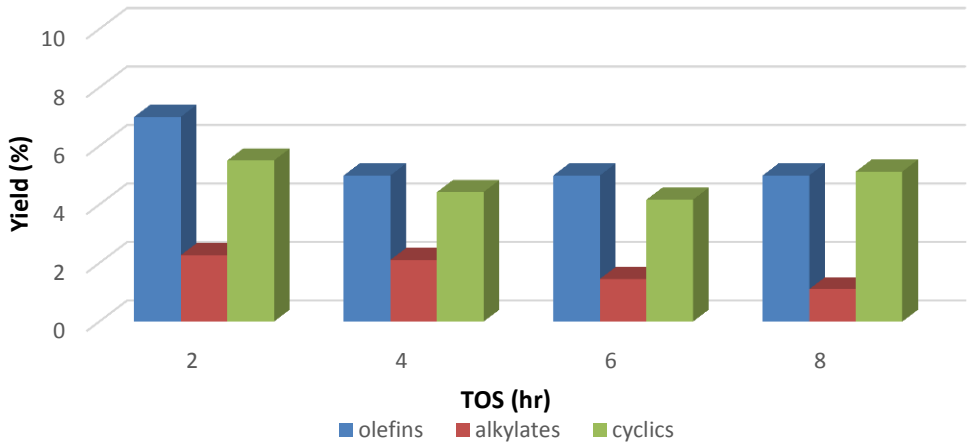

Figure 233: profile of the valuable product during first cycle using P/2,4HD over CrO_x/Al_2O_3 at 573 K

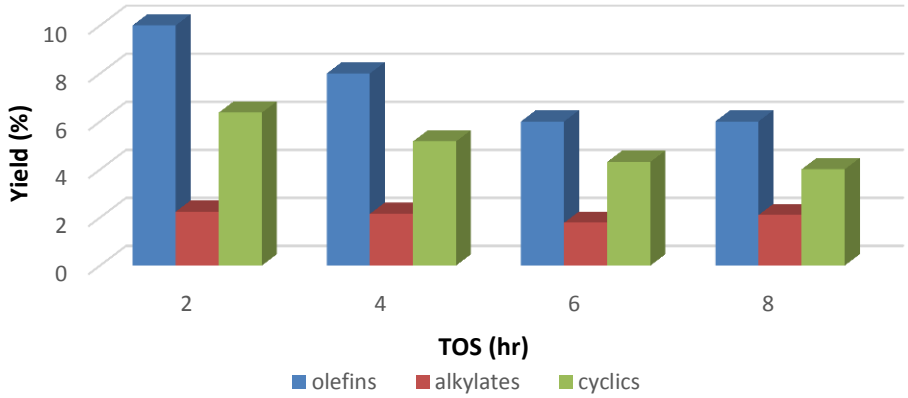

Figure 234: profile of the valuable product during second cycle using P/2,4HD over CrO_x/Al_2O_3 at 573K

The TPO profiles of both catalysts run at 573 K and 673 K show similar desorption species. In addition to the CO_2 peaks, trace CO and H_2O were also observed. However, it is observed that the oxygen consumption is less during the 573 K reaction and could be associated with the amount of carbon deposit being lower than the reaction at 673 K. The results are presented in Figure 235 and 236

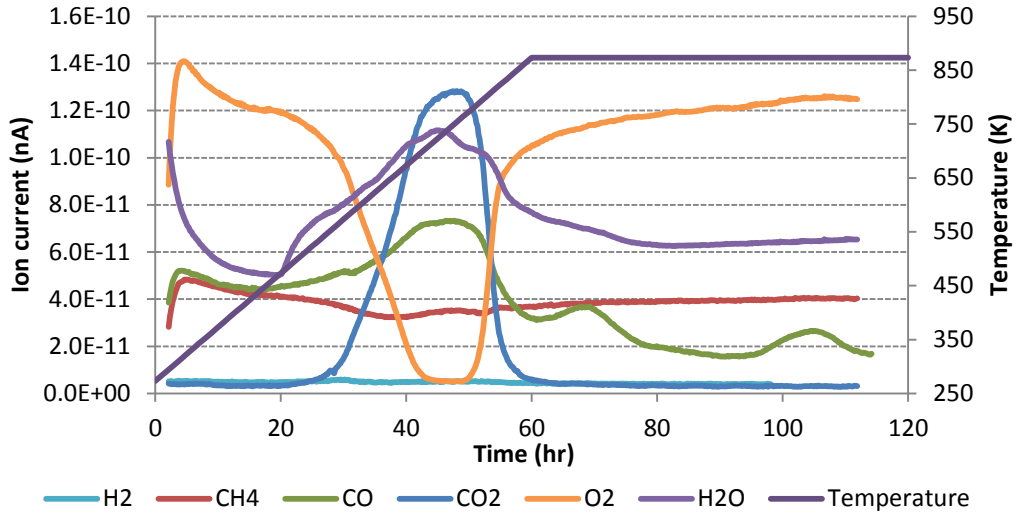

Figure 235: Evolution of CO2 and other species during the TPO on CrO_x/Al_2O_3 spent catalyst over P/2,4HD at 673 K

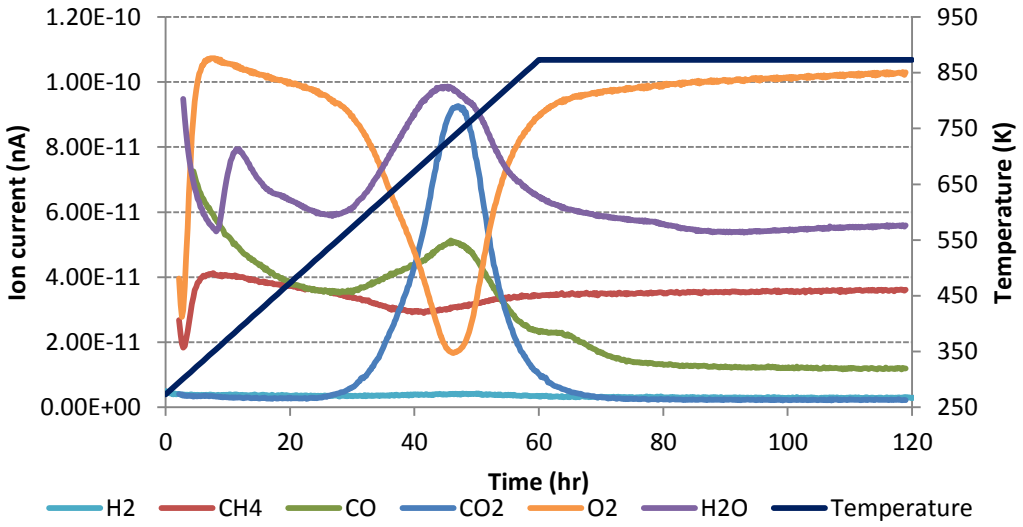

Figure 236: Evolution of CO_2 and other species during the TPO on CrO_x/Al_2O_3 spent catalyst over P/2,4HD at 573 K

3.6.2 Pt/Al_2O_3 Catalyst

3.6.2.1 Pentane/Hexyne (P/1HY) system

The catalyst only slightly deactivated at both reaction temperatures. More deactivation was however observed after 6 hr TOS with the 1HY. There is no obvious deactivation related to the pentane reactant and the conversion is almost stable with both cycles with the reaction at 673 K. The results are presented in Figure 237 and 238

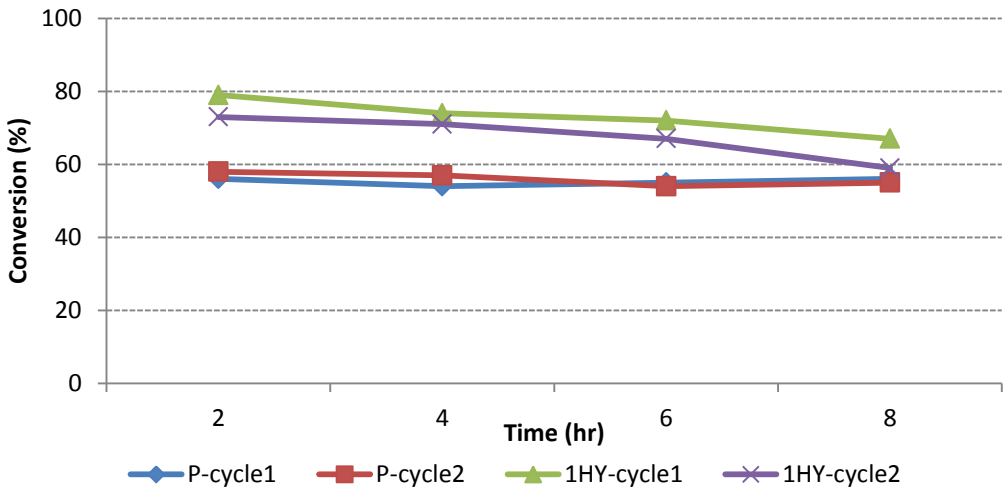

Figure 237: Pt/Al_2O_3 catalyst regeneration profile over P/1HY at 673 K

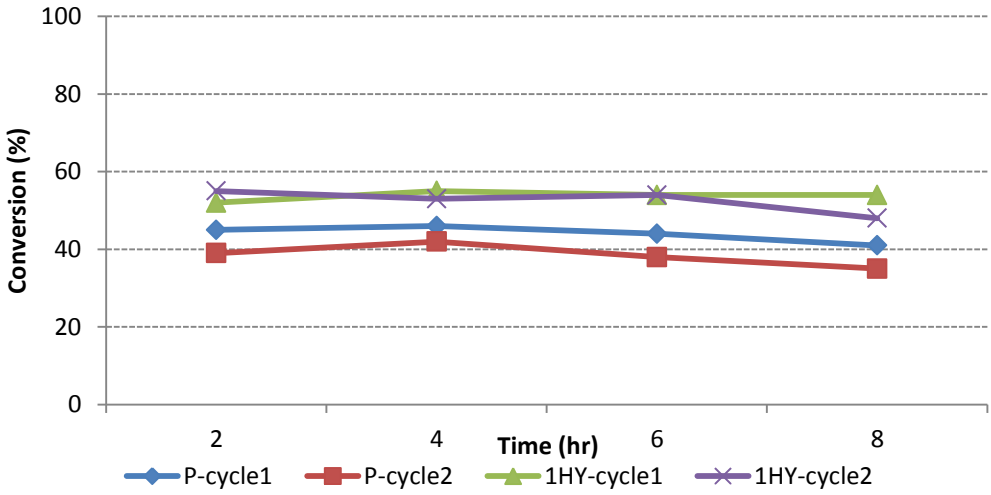

Figure 238: Pt/Al_2O_3 catalyst regeneration profile over P/1HY at 573 K

The total olefin yield analysis suggests that there is a loss of selectivity with time at both reaction temperatures during the first cycle. The olefin yield was reduced by half after 8 hrs TOS with the reaction at 673 K, and an even more severe reduction was observed with the reaction at 573 K. An Increase in selectivity was observed during the 2nd cycle at 673 K, the olefin yield was most stable during the second cycle at 573 K although slight deactivation was observed. The results are presented in Figure 239 and 240

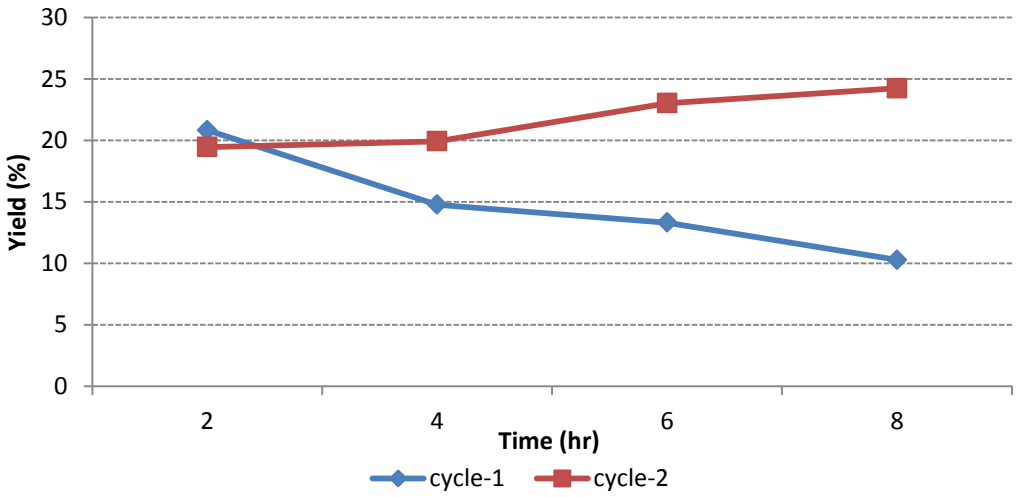

Figure 239: Effect of operating cycles on Pt/Al_2O_3 catalyst olefin yield over P/1HY at 673 K

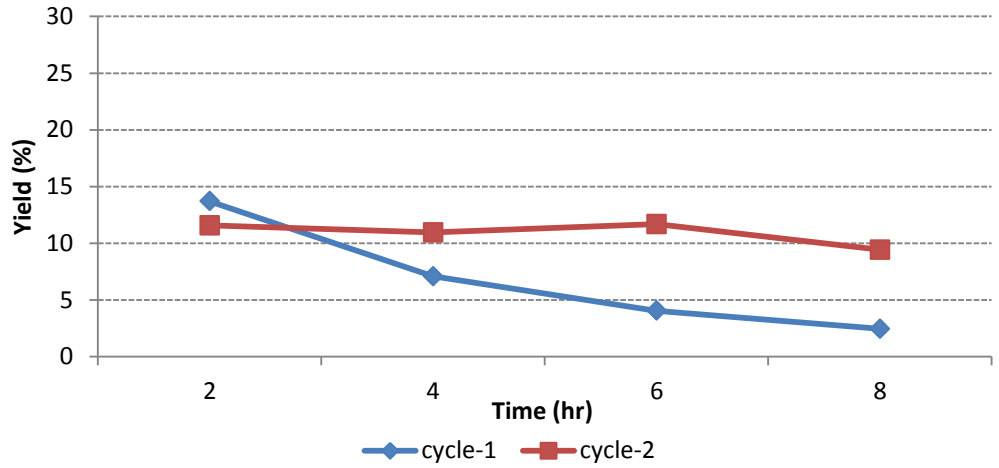

Figure 240: Effect of operating cycles on Pt/Al_2O_3 catalyst olefin yield over P/1HY at 573 K

The valuable products distribution is presented in Figure 241 and 241. It reveals that the production of both the cyclics and the alkylates are about the same for the TOS and there is no obvious deactivation over these products.

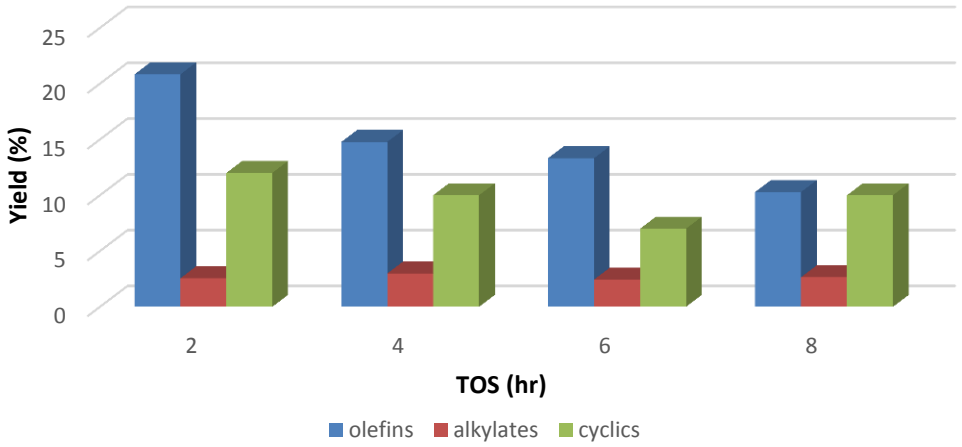

Figure 241: profile of the valuable product during first cycle using P/1HY over Pt/Al_2O_3 at 673 K

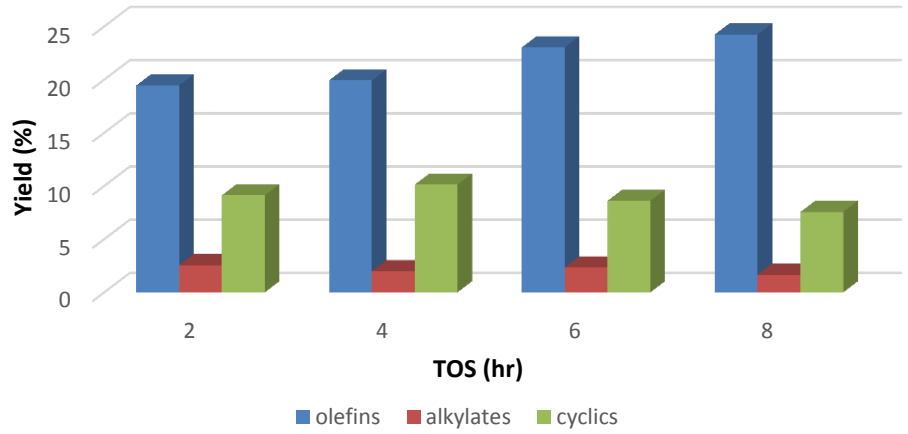

Figure 242: profile of the valuable product during second cycle using P/1HY over Pt/Al_2O_3 at 673 K

Figure 243 illustrates that the profile of the major product 3MPY is similar to that obtained with the chromia catalyst even though 1,4HD product was not observed with this catalyst. Only ~20% was produce with the Pt/Al_2O_3 compared to ~25% with CrO_x/Al_2O_3 catalyst.

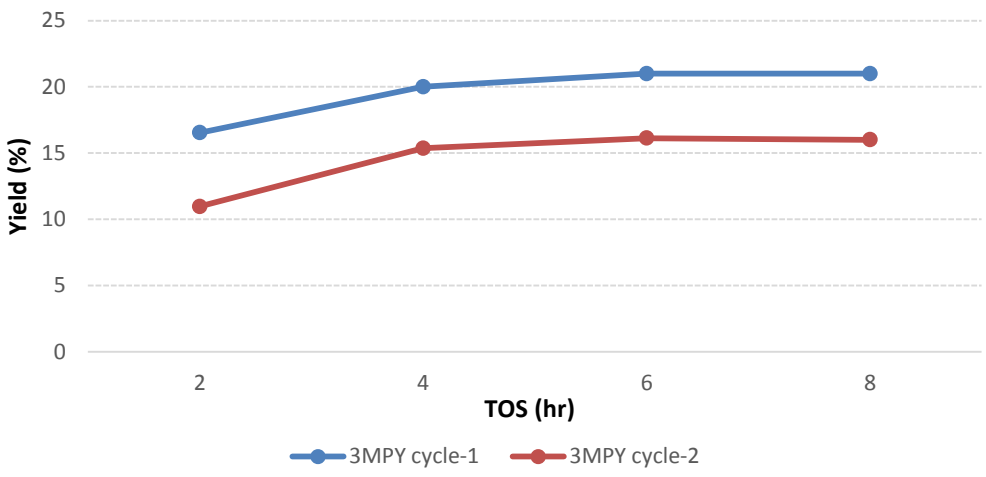

Figure 243: Profile of the 3MPY product at 673 K over Pt/Al_2O_3

The production during the 3MPY at 573 K during first cycle is very similar to that observed at 673 K, but the yield reduced during the second cycle. The result is presented in Figure 244

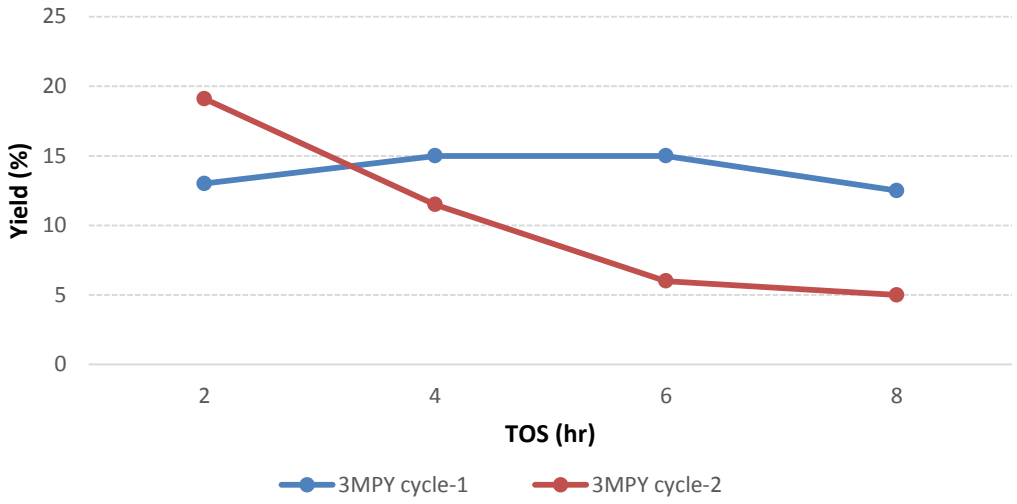

Figure 244: Profile of the 3MPY major products at 573 K over Pt/Al_2O_3

The TPO analyses of both catalysts that had been used at 673 K and 573 K are presented in Figure 245 and 246. The graphs show that there has been significant carbon deposition at both reaction temperatures and CO_2 evolution was observed. There is at least three different carbon species observed with both reaction temperatures. The evolution of the CO_2 perfectly matches the oxygen uptake in all the three places. The TPO profiles at both reaction temperatures present similar evolution profiles. However, there is difference in the evolution

of each CO_2 to the uptake of the oxygen via the two reaction temperatures. For instance, the TPO profile from the catalyst used at 673 K reveals that the oxygen uptake due to CO_2 evolution at 533 K is less, compared to 633 K and 763 K CO_2 evolutions. This suggests that the CO_2 at 533K is a soft carbon specie and the deposition is less, while the carbon species at 763 K are harder carbon species and the deposition is higher. The H_2O evolution is very high at 533 K and smaller at 763 K suggesting that the soft carbon is more of hydro-carbonaceous. However, the higher CO evolution was observed with the carbon species at 633 K and could associate with incomplete combustion. All the other observed species perfectly matches the cracking pattern of the CO_2 evolutions. The TPO profile observed with the catalyst that was used for reaction at 573 K shows that the soft carbon species (533 K) has the highest oxygen uptake and could suggest that this form of carbon is the main deposit on the surface. However, there is general reduction in the oxygen uptakes compared to the TPO of the catalyst that had a reaction temperature of 673 K due to the extent of the carbon deposition. The evolution of other desorbed species perfectly matches the cracking pattern of the CO_2 evolution. The results are presented in Figure 245 and 246

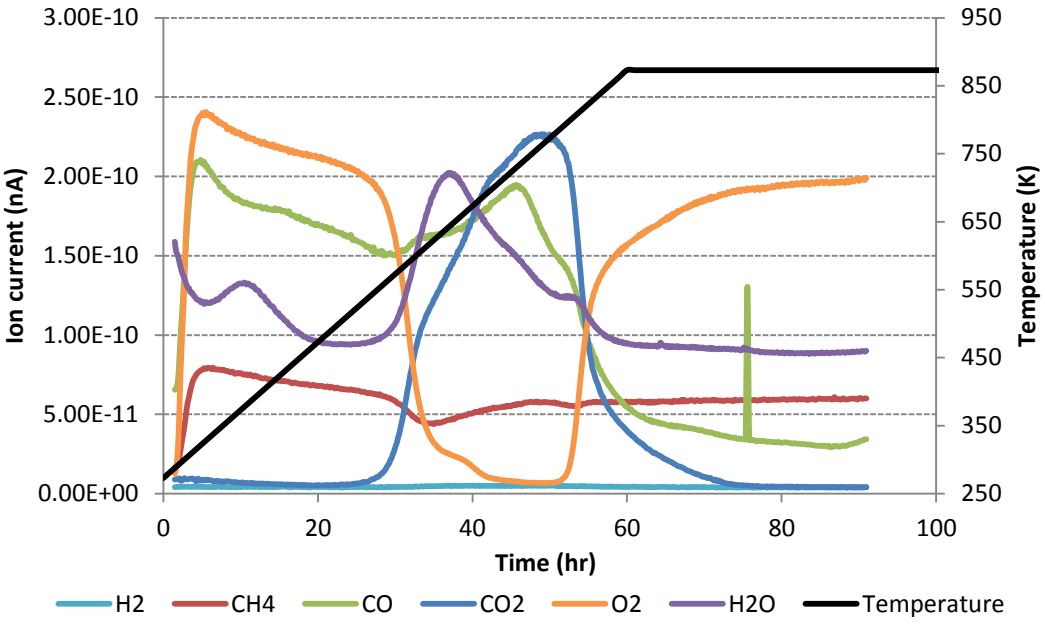

Figure 245: Evolution of CO_2 and other species during the TPO on Pt/Al_2O_3 spent catalyst over P/1HY at 673 K

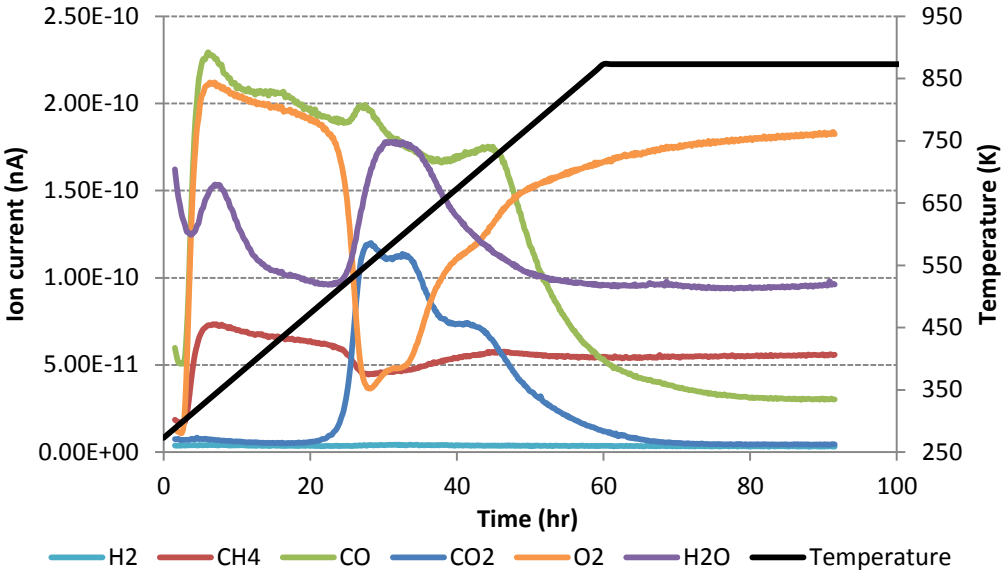

Figure 246: Evolution of CO_2 and other species during the TPO on Pt/Al_2O_3 spent catalyst over P/1HY at 573 K

3.6.2.2 Pentane/1,5-hexadiene (P/1,5HD) system

The fresh catalyst run at 673 K, showed a slight increase in activity. There is slight deactivation during the second cycle resulting in a reduction in the conversion of 1,5HD with TOS. Generally, at both reaction temperatures, there is slight deactivation during the second cycle compared to the fresh catalyst. The activity of the catalyst is almost stable with respect to pentane conversion with very similar activity during both cycles. The results are presented in figure 247 and 248

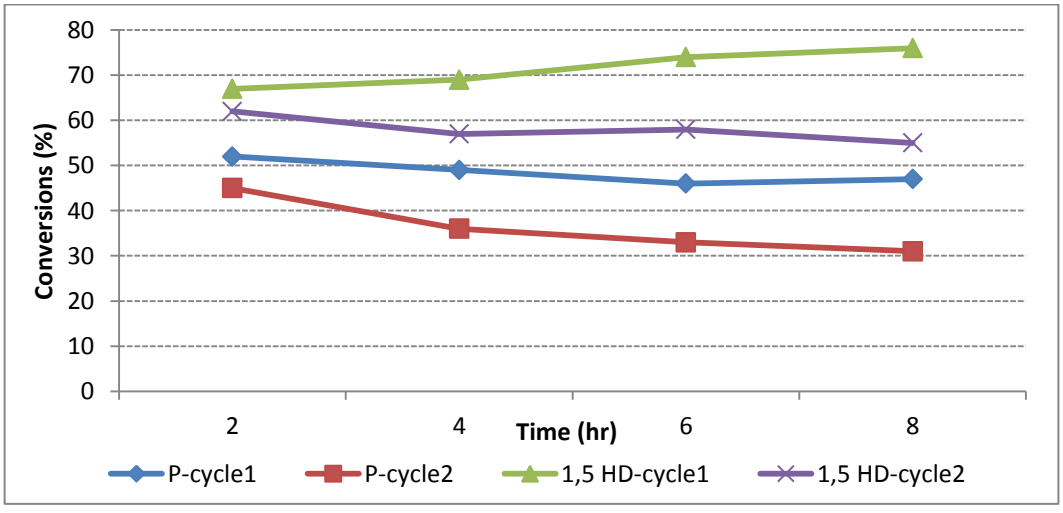

Figure 247: Pt/Al_2O_3 catalyst regeneration profile over P/1,5HD at 673 K

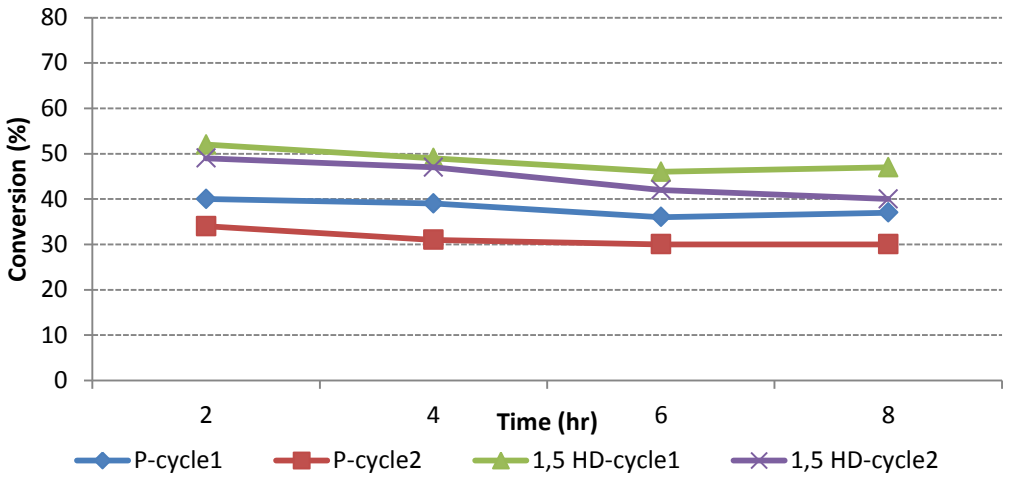

Figure 248: Pt/Al_2O_3 catalyst regeneration profile over P/1,5HD at 573 K

The olefin analysis suggests a similar trend with the P/1HY system. There is observed a decrease in the olefin yield during the first cycle observed with both reaction temperatures, whereas the catalyst activity to olefins is almost stable with the regenerated one. The results are presented in Figure 249 and 250

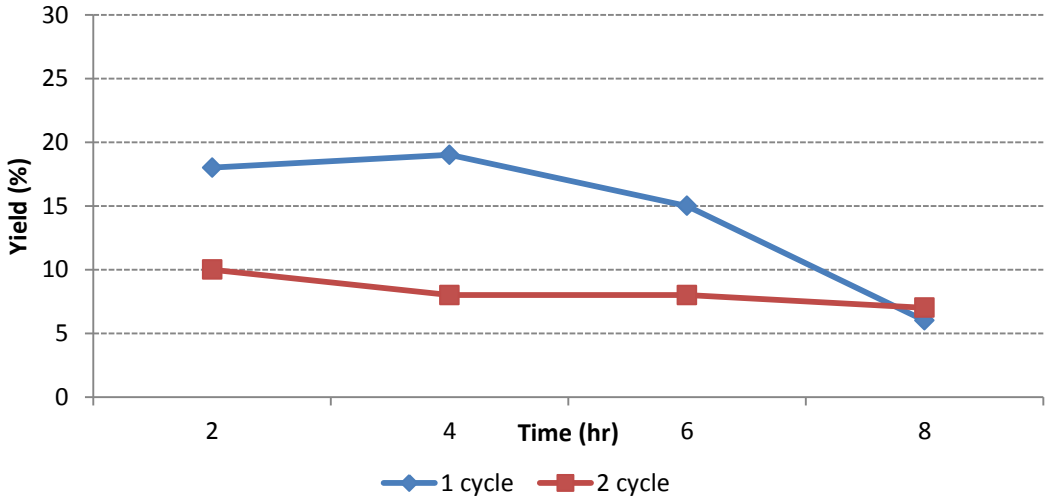

Figure 249: Effect of operating cycles on Pt/Al_2O_3 catalyst olefin yield over P/1,5HD at 673 K

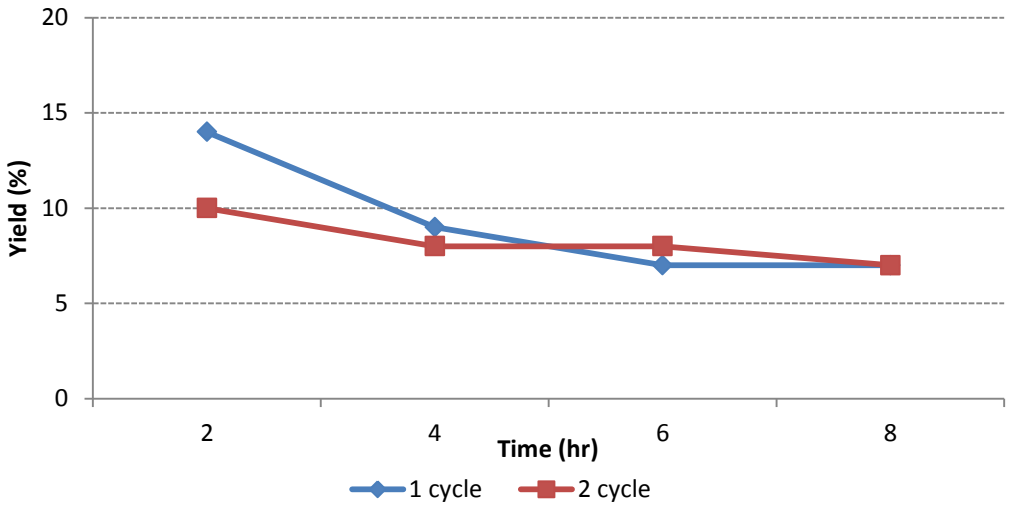

Figure 250: Effect of operating cycles on Pt/Al_2O_3 catalyst olefin yield over P/1,5HD at 573 K

The valuable products distribution illustrated in Figure 251 and 252 reveals that slight deactivation is observed with the alkylates and the cyclics products during the first cycle while production is much more stable during the second cycle. However, there is general reduction observed in the products yield during the second cycle except for the alkylates.

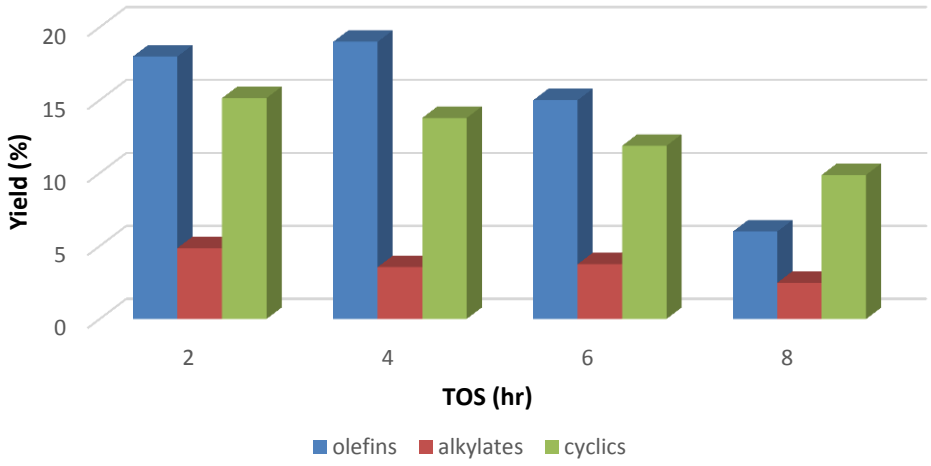

Figure 251: profile of the valuable product during first cycle using P/1,5HD over Pt/Al_2O_3 at 673 K

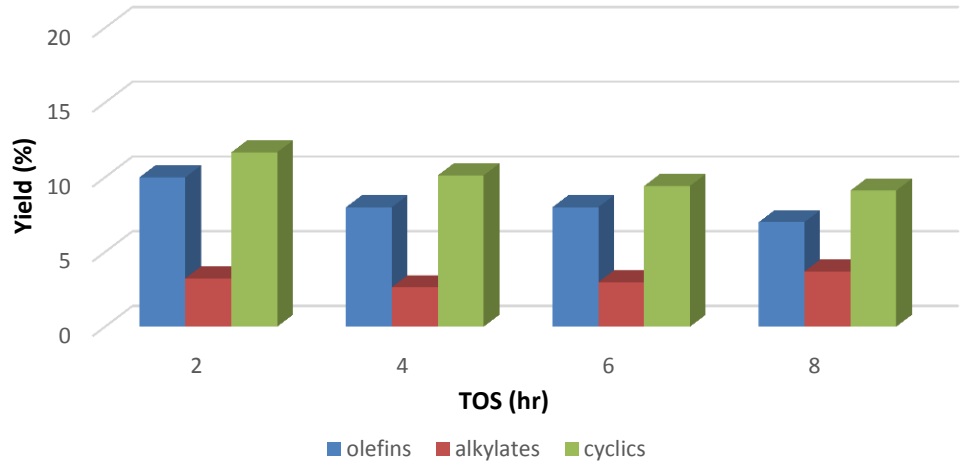

Figure 252: profile of the valuable product during second cycle using P/1,5HD over Pt/Al_2O_3 at 673K

A similar trend was observed with the reaction at 573 K. the results are presented in Figure 253 and 254

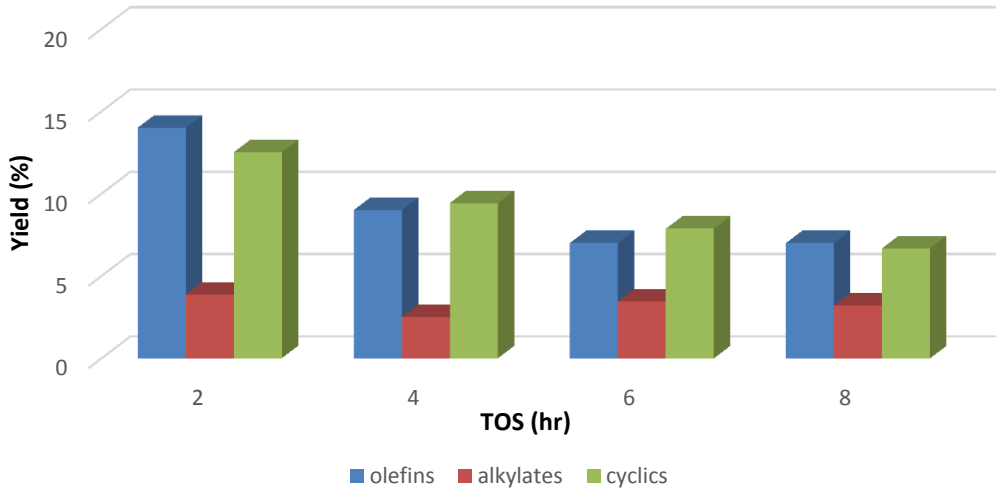

Figure 253: profile of the valuable product during first cycle using P/1,5HD over Pt/Al_2O_3 at 573 K

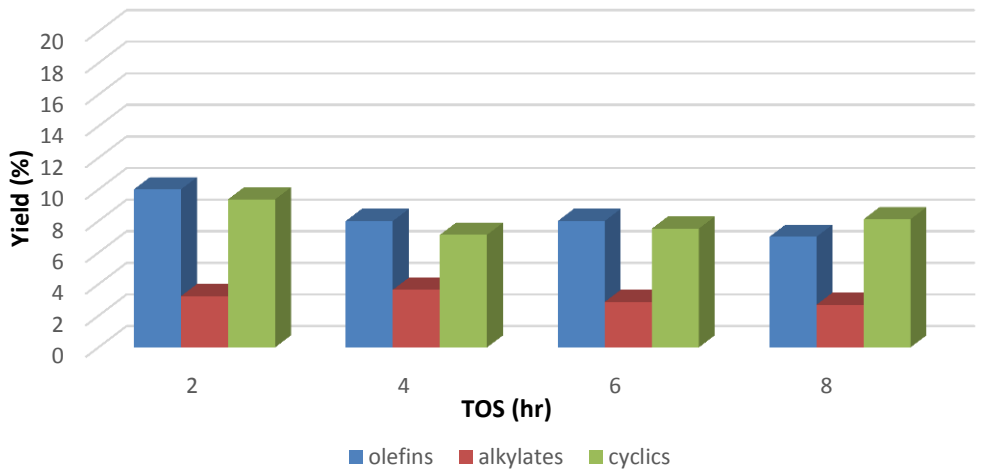

Figure 254: profile of the valuable product during second cycle using P/1,5HD over Pt/Al2O3 at 573K

The TPO analysis indicates CO_2 as the main evolved species with both reaction temperatures. Unlike other previously discussed system there is less CO_2 evolution here. There are possibly two types of carbon specie observed in the TPO from the catalyst run at 673 K but it is not clearly observed with the catalyst used at 573 K but this could be due to lower carbon deposition expected with low temperature. The evolution profile also suggests lower carbon deposition with both catalysts with this system compared to the 1HY system. Very small carbon deposition was also observed during the 2 hr short run. The results are presented in Figure 255 and 256

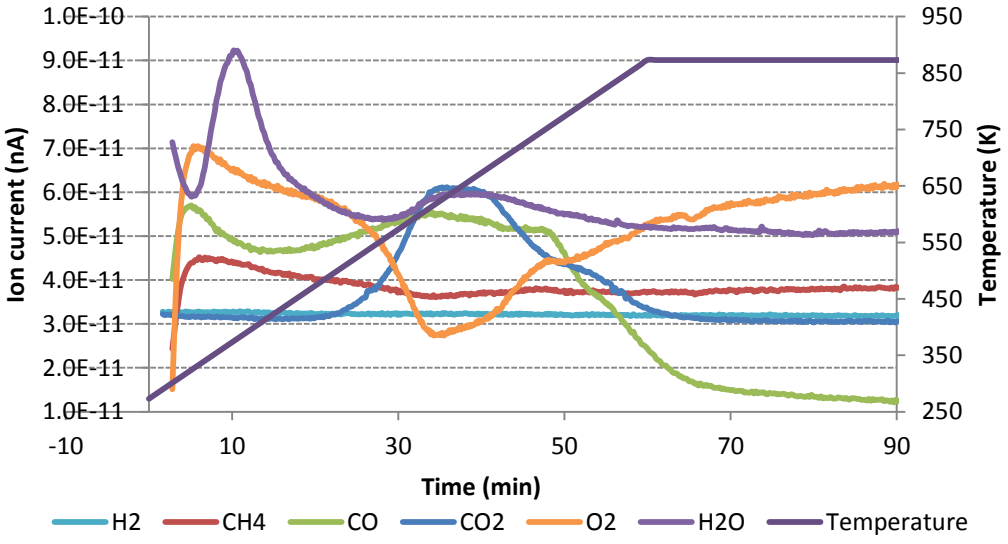

Figure 255: Evolution of CO_2 and other species during the TPO on Pt/Al_2O_3 spent catalyst over P/1,5HD at 673 K

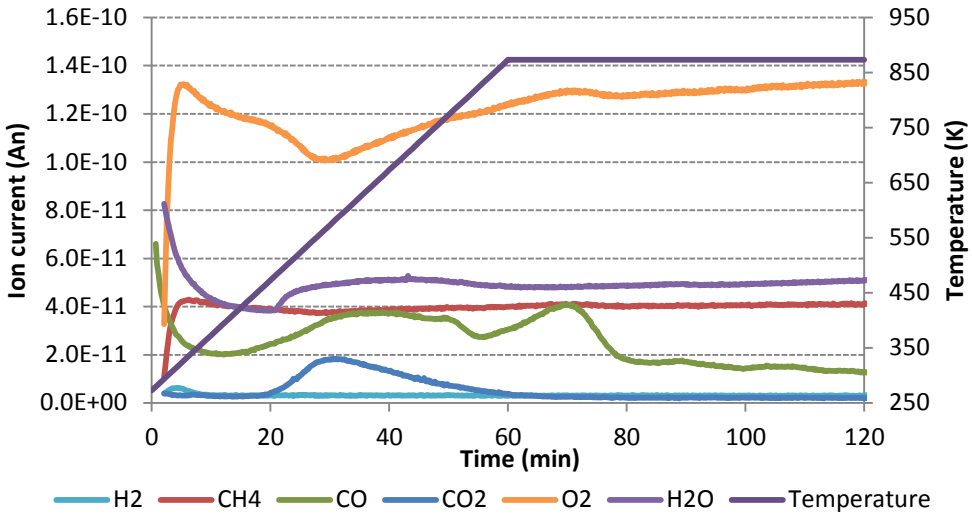

Figure 256: Evolution of CO_2 and other species during the TPO on Pt/Al_2O_3 spent catalyst over P/1,5HD at 573 K

3.6.2.3 Pentane/2,4-hexadiene (P/2,4HD) system

Slight deactivation is also observed with pentane/2,4-hexadiene similar to the chromia catalyst. The activity of the catalyst is reproducible with both pentane and 2,4HD with similar activity observed during the 1st and 2nd cycle. The results are presented in Figure 257 and 258

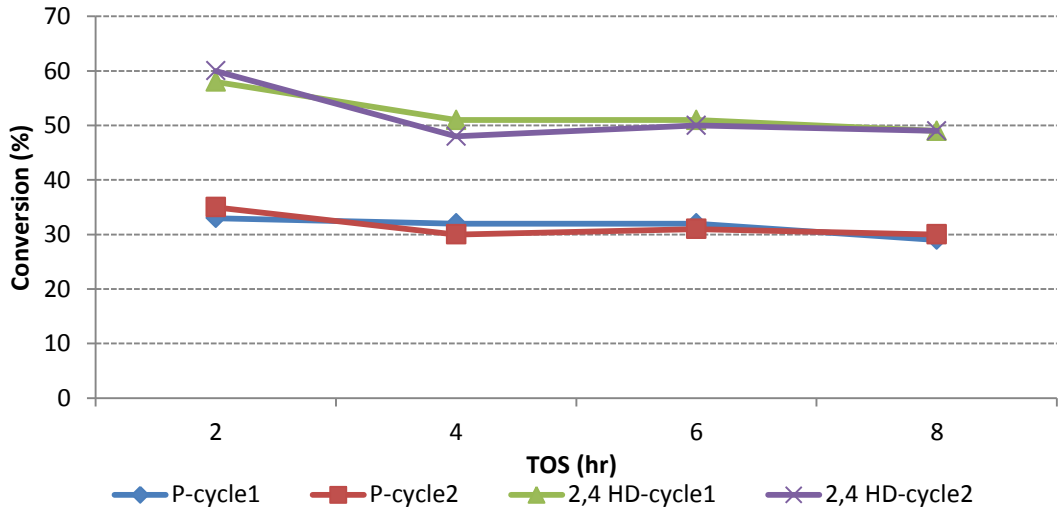

Figure 257: Pt/Al_2O_3 catalyst regeneration profile over P/2,4HD at 673 K

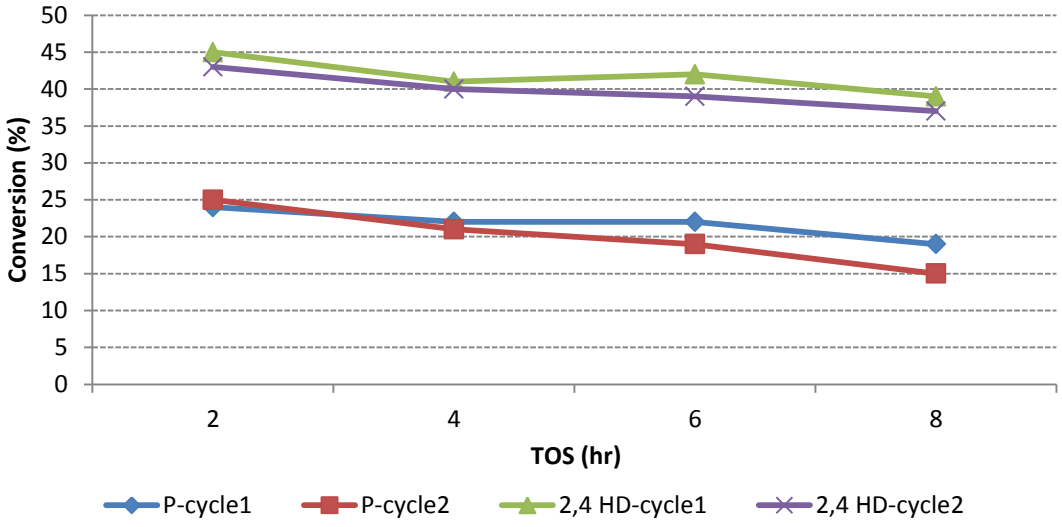

Figure 258: Pt/Al_2O_3 catalyst regeneration profile over P/2,4HD at 573 K

There is deactivation over the total olefin yield. Only ~4 % was observed during the 2nd cycles compared to ~7 % during the 1st cycle at a reaction temperature of 673 K showing a loss activity after regeneration of the catalyst. The production of olefin is generally poorer with this system compared to the other two systems as explained previously. The results are presented in Figure 259 and 260

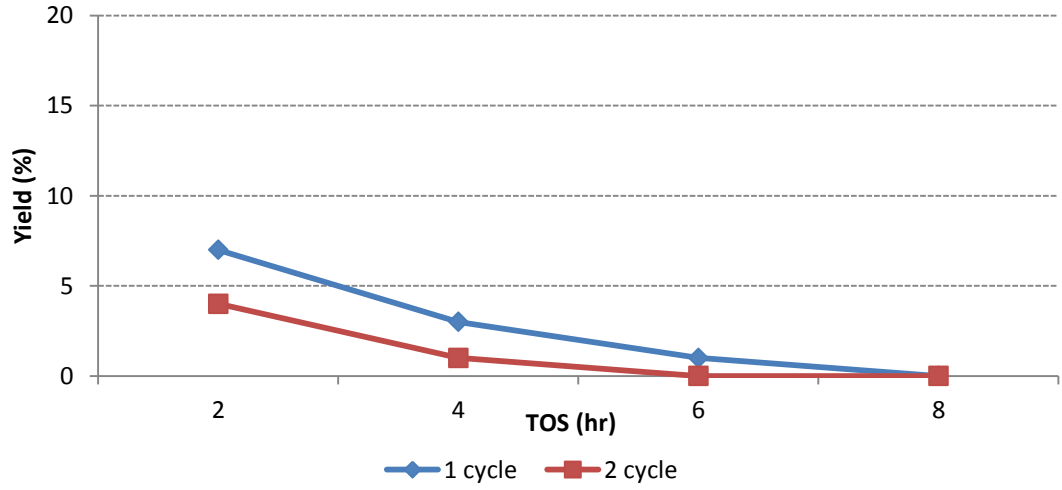

Figure 259: Effect of operating cycles on Pt/Al_2O_3 catalyst olefin yield over P/2,4HD at 673 K

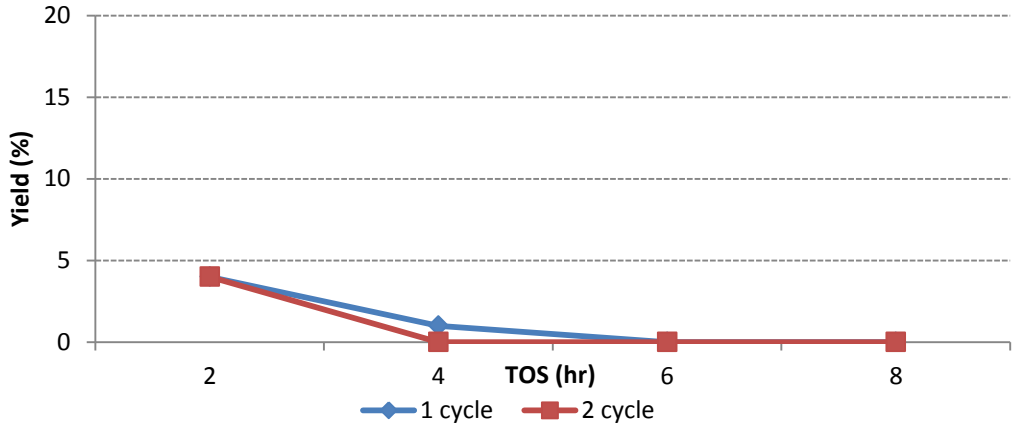

Figure 260: Effect of operating cycles on Pt/Al_2O_3 catalyst olefin yield over P/2,4HD at 573 K

The valuable product distribution presented in Figure 261 and 262 reveals that the production of alkylates and cyclics is almost stable over the reaction TOS with both cycles. The yield of these products is about the same with both cycles.

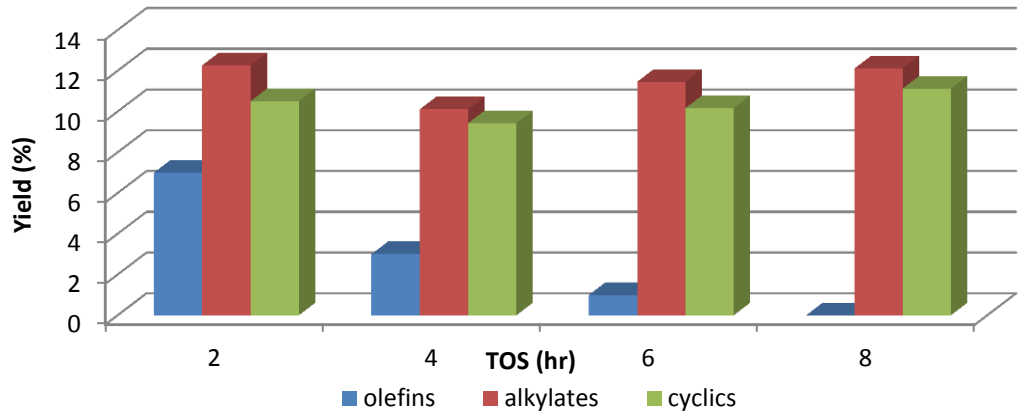

Figure 261: profile of valuable product during first cycle using P/2,4HD over Pt/Al_2O_3 at 673K

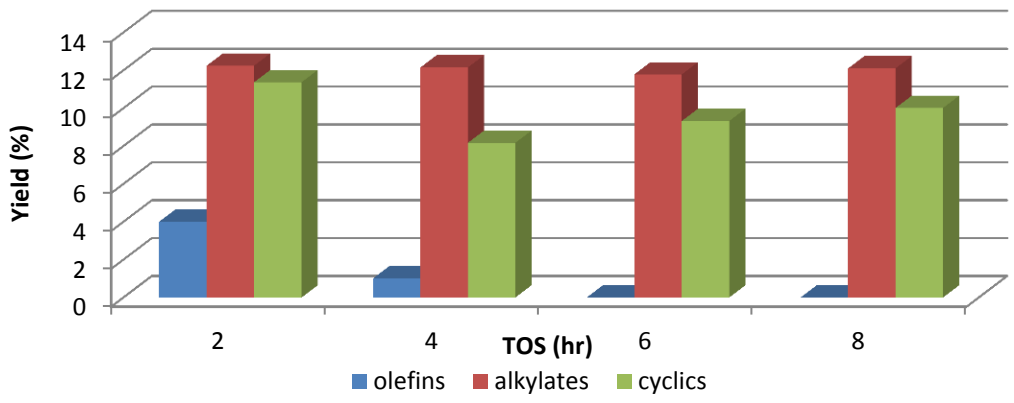

Figure 262: profile of valuable product during 2nd cycle using P/2,4HD over Pt/Al_2O_3 at 673K

The distribution of the valuable product at 573 K is almost similar to the observed at 673 K reactions and the correlation between the two cycles in respect to the alkylates and the cyclic production is about the same. There is no evidence of the activation regarding to these products over the reaction TOS. The result are presented in Figure 263 and 264

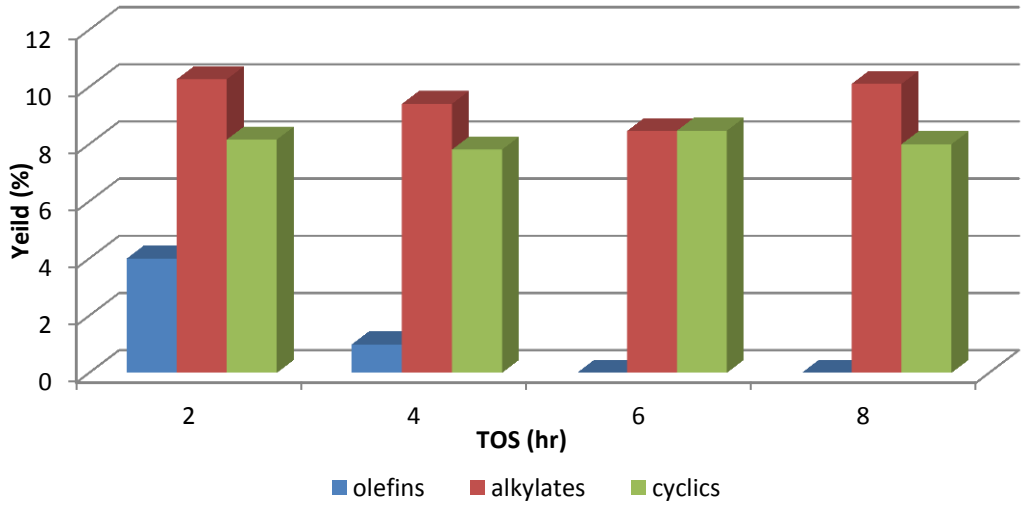

Figure 263: profile of the valuable product during first cycle using P/2,4HD over Pt/Al_2O_3 at 573 K

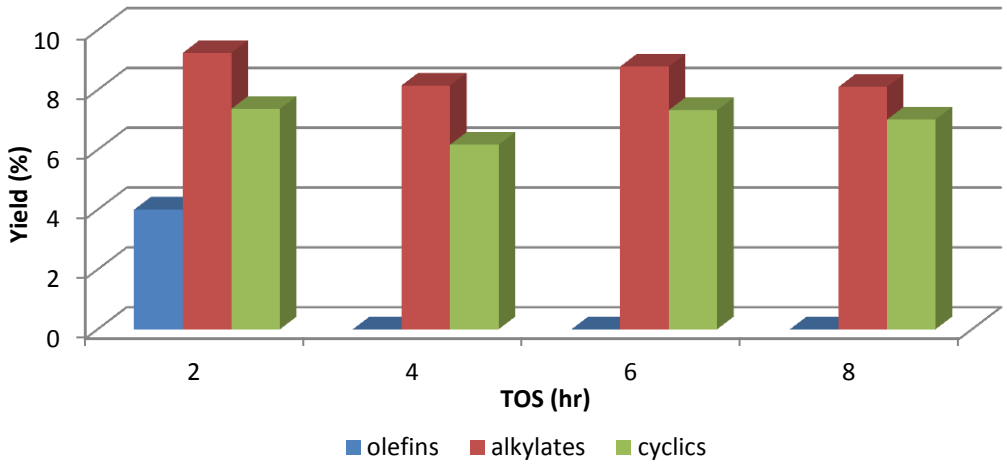

Figure 264: profile of the valuable product during second cycle using P/2,4HD over Pt/Al_2O_3 at 573 K

The TPO profile of both catalysts shows similar desorption species. Possibly three types of carbon species are observed. There is less oxygen uptake with the

harder carbon species (~853 K) compared to the uptake observed with the soft carbon species (~600 K). In addition to the CO_2 peaks, traces of CO and H2O were also observed with both catalysts. The soft carbon species is more predominant with the Pt/Al_2O_3 catalyst, and it is observed with all the reaction systems. The results are presented in Figure 265 and 266

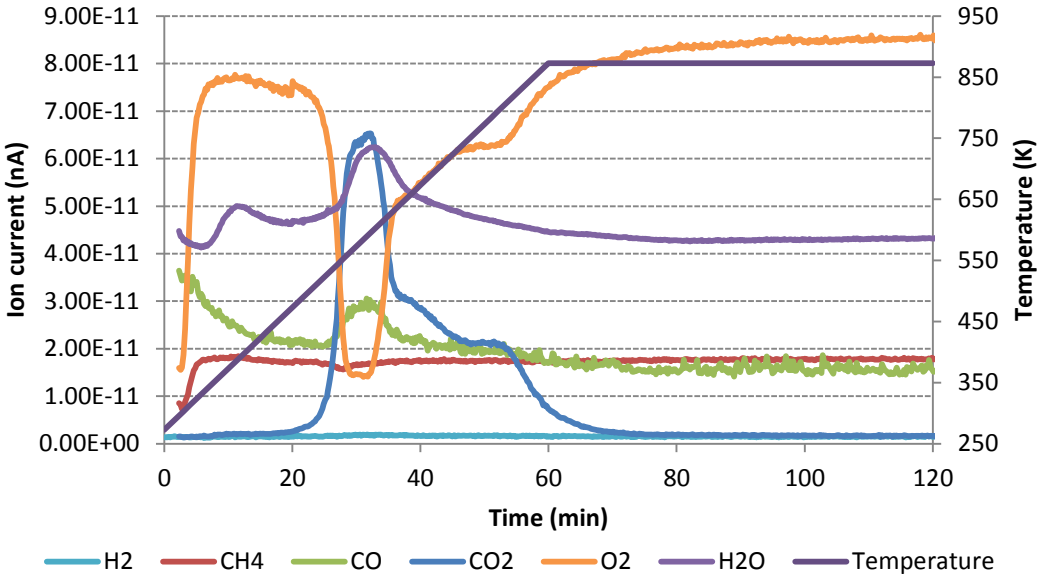

Figure 265: Evolution of CO2 and other species during the TPO on Pt/Al_2O_3 spent catalyst over P/2,4HD at 573 K

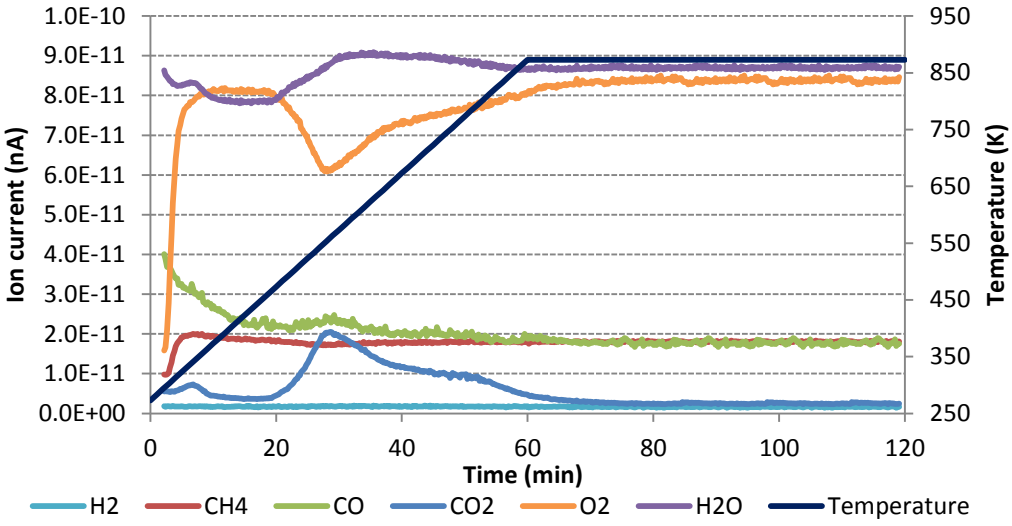

Figure 266: Evolution of CO2 and other species during the TPO on Pt/Al_2O_3 spent catalyst over P/2,4HD at 573 K

4. Discussion

4.1 Reaction analysis and trans-hydrogenation activity evaluation

4.1.1 Catalyst efficacy on trans-hydrogenation

Catalyst efficacy for trans-hydrogenation has been observed at all temperatures. However, this is more pronounced at high temperatures. Unique product distributions were observed during the trans-hydrogenation compared to the [P + HY] theory with all reaction and catalyst systems. As illustrated (Table 12-16) using the CrO_x/Al_2O_3 catalyst with 1HY system, it is evident that there is a clear trans-hydrogenation process occurring. It could be observed that the primary olefin products were either initially not produced or only traces were produced when the reactants were feed individually over the catalyst. Pentene, 2-hexene and their isomers initially produced from pentane and hexyne respectively increase during the trans-hydrogenation process. For instance, (Table 14), the yield of 2-hexene increased from 0.33% to 1.81% in the mixed feed and this trend could also be observed with all other temperatures. However these figures were subject to change with temperature, but in general, a clear trans-hydrogenation process were observed. Meanwhile, the olefin product initially produced from the pentane dehydrogenation experiments were sometimes consumed in the trans-hydrogenation process, 8.59% trans-2-pentene was observed with pentane dehydrogenation (Table 13) and was totally consumed during the trans-hydrogenation. However, this may be related to the formation of other products. This type of effect where the olefins initially produced with dehydrogenation process were consumed in the trans-hydrogenation has also been observed with other alkane molecules [26, 27]. Similar behaviour was also observed with the 1,5HD system (Table 22-26), nevertheless all the yield of valuable products increased during trans-hydrogenation. In general, more valuable products were observed with P/1,5HD system and the efficacy of the catalyst is obviously more predominant here. This activity was not observed with the P/2,4HD system; instead the general production of the valuable product is poorer (Table 32-36). In (Table 33) the yield of hexene reduces from 0.3% to 0.26% and 3-hexene from 2.35 to 2.17%. Overall, the yields of these products are either similar or lower during the trans-hydrogenation process compared to the (P+H) theory. This is

associated with the thermodynamics of the reaction (section 3.1). There is almost about the same efficacy observed with the Pt/Al_2O_3 catalyst as the CrO_x/Al_2O_3 catalyst. Clear increases in the production of valuable products were observed with all the reaction systems. However, more of the primary targeted products were observed with the platinum catalyst. For instance, at 773 K using the chromia catalyst, 0.66% hexene was obtained (Table 12); while, 2.79% hexene was obtained with the same system using the platinum catalyst (table 56). This trend could also be observed at other reaction temperatures. However, although the efficacy of the two catalysts for trans-hydrogenation with the 1HY system is about the same, the platinum catalyst is less efficient with the P/1,5HD system and the reaction with P/2,4HD is also poorer. Therefore, it could be suggested that there is higher trans-hydrogenation activity with the chromia catalyst than the platinum catalyst.

Although, the total olefin yields were observed to have generally increased during the trans-hydrogenation process most of them are isomers of the primary target product and their alkylated olefins. Other alkylation products were also observed. However, much of this chemistry may take place over the alumina support as it is known to promote alkylation and isomerization on its acid site [94-96]. This phenomenon was observed to have reduced with the doped catalysts, and increases in the target primary products were observed, for instance, (Table 12), 0.27% hexene was produced with the chromia catalyst and 2.72% (Table 44) was obtained with the doped catalyst. The same trend was also observed with the P/1,5HD system (Table 23) 1.61% hexene was produced with the chromia catalyst and 2.23% (Table 52) was obtained with the doped catalyst. The two catalyst systems exhibited different major products, 3-methylpentyne and 1,4-hexadiene were the major products using CrO_x/Al_2O_3 and 3-methylhexene and methyl-2-pentene were the major products with K-CrO_x/Al_2O_3. However these major products mentioned above were observed to be consumed and producing other products across the reaction temperature range. This could be that temperature may have effect changing the mechanism of the reaction. Like the doped chromia system, there is observed an increase in target products with the K-Pt/Al_2O_3 catalyst using the P/1HY system. However, in contrast, less activity was observed with the doped platinum catalyst using

the P/1,5HD system. There is little improvement with both doped catalysts when using the P/2,4HD system.

Hexyne is very reactive[36, 97], and when run individually in the absence of hydrogen, it is expected to undergo cracking and dehydrogenation[28]. It can also influence the reactivity of alkenes and other alkynes in a competitive environment [37, 38]. Some products were initially formed when hexyne was fed alone over the catalyst but increased in the mixed feed cf. in (table 14) 11.6% of 3-methylpentyne was obtained with hexyne alone but increased to 19.24% in the mixed feed using the CrO_x/Al_2O_3 catalyst. This was also observed with the doped catalyst. Other products from cyclization and further dehydrogenation were also observed. In principle, a unique product distribution has been observed for each of the reaction systems. The product distribution is summarized and presented in Figure 267. There were five possible reaction processes occurring in addition to the trans-hydrogenation (TH) as listed below:

i. Dehydrogenation (D)

ii. Hydrogenation (H)

iii. Isomerisation (I)

iv. Alkylation (A)

v. Cyclisation (C)

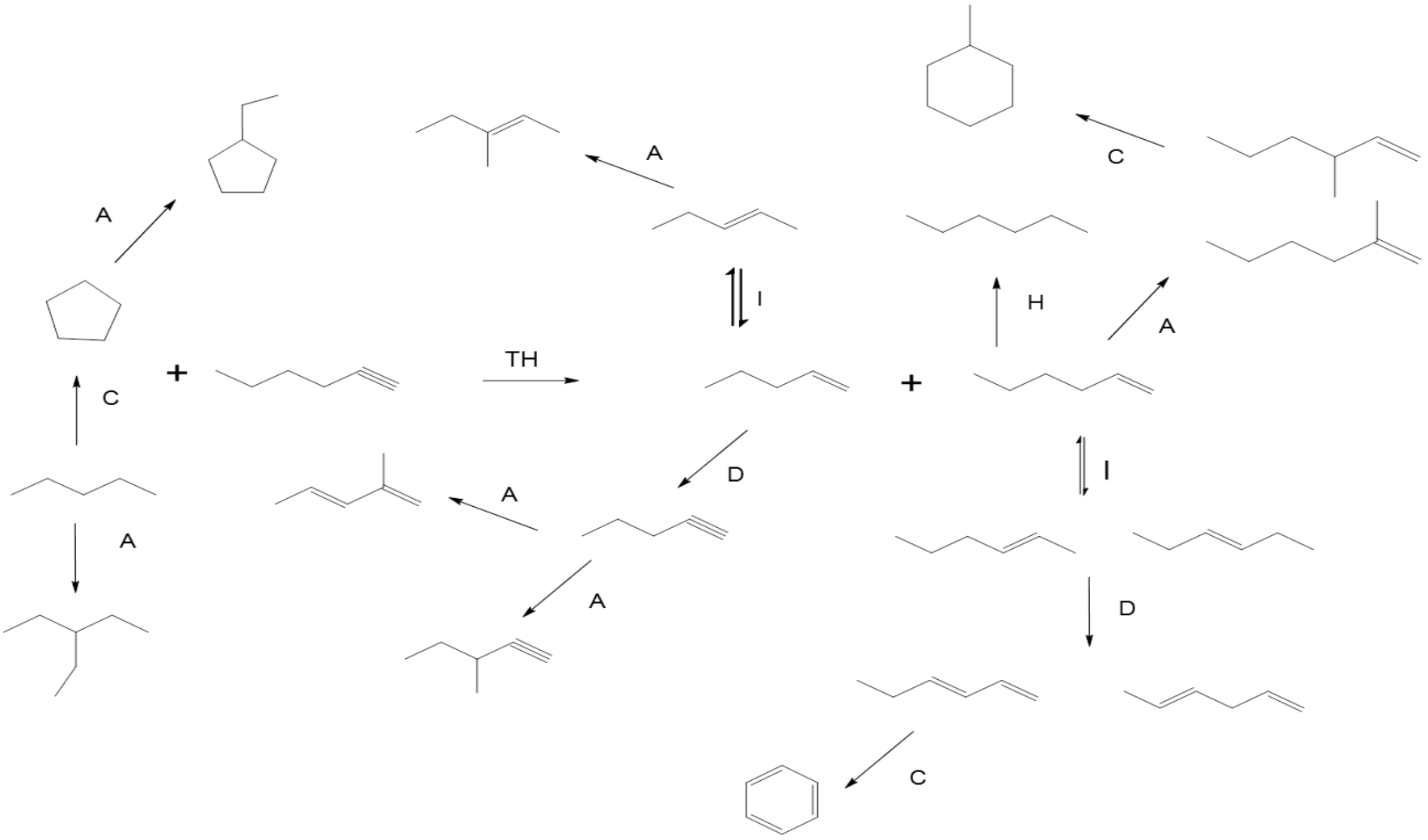

Figure 267: The product distribution showing multiple processes occurring

As expected the product yield varies with reaction temperature. This could be the distribution pattern changes with the reaction temperature but generally the effect of the trans-hydrogenation can easily be depicted despite the pattern change. Partial differences were both observed in the products patterns and distribution comparing the K-CrO_x/ Al_2O_3 with CrO_x/ Al_2O_3 and Pt/ Al_2O_3 with K-Pt/ Al_2O_3. The efficacy of the catalyst in general, for trans-hydrogenation was observed to decline at the lower temperatures, 573 K and 523 K. The doped catalysts provided more selectivity and more appreciable yield as could clearly be seen in tables presented in the result chapter. It could be suggested that the activity of the tested catalyst on trans-hydrogenation follow the order below.

K-Pt/Al_2O_3 < Pt/ Al_2O_3 < CrO_x/ Al_2O_3 < K-CrO_x/ Al_2O_3

4.1.2 Reactant conversions and products yield

One of the aims of trans-hydrogenation is to lift the conversion limitations posed on the dehydrogenation process of the pentane reactant. The conversions of pentane was obtained individually and compared to the mixed feed. There is an increase in the conversion of pentane at all temperatures during trans-hydrogenation, indicating removal of the constraint. A maximum increase of ~26% conversion of pentane was observed with the mixed trans-hydrogenation feed compared to ~10% conversion with the single feed at 623 K using the CrO_x/Al_2O_3 catalyst. However, the constraint is specific to the pentane dehydrogenation reaction. Thus, if other products are formed, then conversions higher than the thermodynamic limits for the dehydrogenation reaction are easily obtainable.

A ratio of pentane conversion during trans-hydrogenation (P+H) to the dehydrogenation (P) noted as (P+H: P) was calculated. The result indicates a ratio of ~2 with the P/1HY system at 773 K using the CrO_x/Al_2O_3. This ratio was found to increase with decreasing reaction temperature with the same P/1HY system. On using the P/1,5HD over the same catalyst system, a significant increase in the pentane conversion was observed, ~91% during trans-hydrogenation at 773K. The P+H: P ratio was found to be ~10 for the P/1,5HD system, and, in contrast to the P/1HY system, where higher ratios were obtained at lower reaction temperatures (~80 at 523K). A ratio (P+H: P) of only ~ 0.8 was

observed for the 2,4HD system over the chromia catalyst and, it is almost stable with reaction temperature. The analysis with the various reaction temperatures is presented in Figure 268. All the conversions obtained for the pentane run using the chromia catalyst are around the equilibrium conversions of pentane dehydrogenation.

A trend was observed using the Pt/Al_2O_3 catalyst. For instance, the increase in the conversion of pentane using the P/1HY system indicates a ratio (P+H: P) of ~ 2 at 773 K. Higher pentane conversions were achievable with Pt/Al_2O_3; ~71% was observed during the trans-hydrogenation and ~37% during the pentane dehydrogenation. However, the trend is in opposite of what was observed with the chromia catalyst. Similarly, unlike the chromia catalyst, the ratio only slightly reduces with reaction temperature here, a ratio of only ~1 was observed at 523 K. This could suggest that the platinum catalyst exhibited lower trans-hydrogenation activity compared to the chromia catalyst. Slightly lower ratios were observed for reaction with P/1,5HD and 2,4HD system. The result is presented in Figure 269

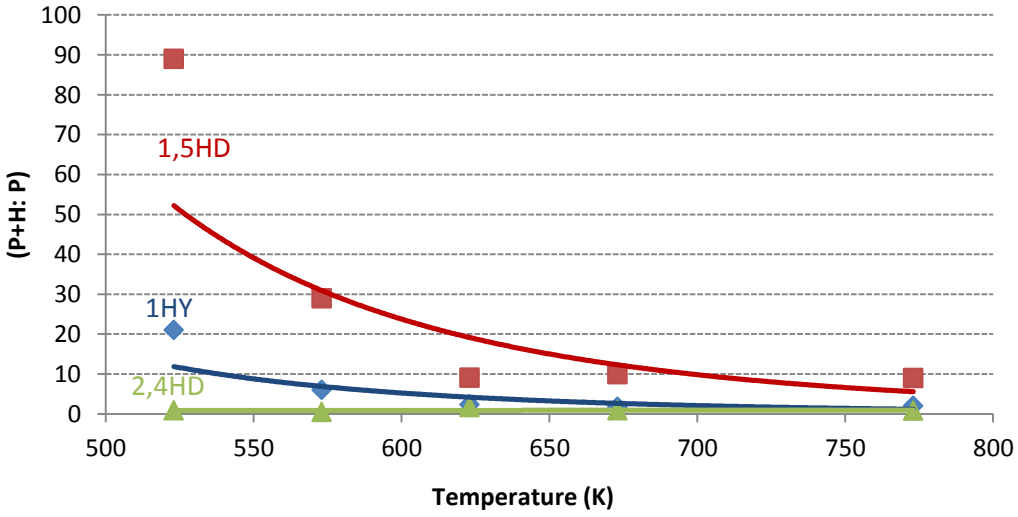

Figure 268: profile of the (P+H: P) ratio with reaction temperature over the three reaction systems with CrO_x/Al_2O_3 catalyst

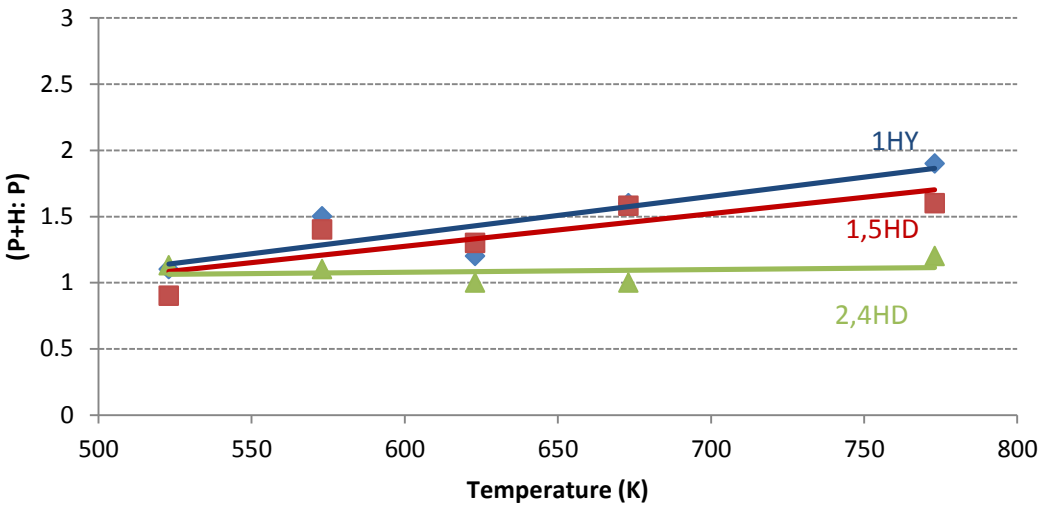

Figure 269: Figure: profile of the (P+H: P) ratio with reaction temperature over the three reaction systems with Pt/Al_2O_3 catalyst

However, the platinum catalyst has higher dehydrogenation activity compared to the chromia catalyst and it makes more alkene products. It could be observed that all the pentane conversions with the platinum are higher than the equilibrium conversions (~19% for n-pentane). There is ~37% pentane conversion obtained with the platinum catalyst and only ~11% with the chromia catalyst at 773K, suggesting that the platinum is active for the conversion of pentane to more than just pentene.

Unlike the chromia catalyst, the platinum catalyst was less active with the P/1,5HD system. About 59% (table 93) conversion of pentane was obtained during the trans-hydrogenation at 773 K, which is lower than that observed with the P/1HY system, whereas with the chromia catalyst, the reaction with the 1,5HD gave higher pentane conversion than reaction with P/1HY system. Meanwhile the activity of the platinum catalyst only slightly reduces with reaction temperature, and a conversion of ~47% was still achieved at 573 K during the trans-hydrogenation using the 1,5HD system. In contrast the activity was almost maintained over the range of reaction temperature using the chromia catalyst, suggesting that chromia catalyst gives better activity using 1,5HD system.

The platinum catalyst presented better activity with using P/2,4HD system compared to the chromia catalyst. All the conversions of pentane during the

trans-hydrogenation using the chromia catalyst are about the same or lower than the pentane dehydrogenation. However, higher pentane conversion was obtained during the trans-hydrogenation using the platinum catalyst which suggests a lifting of the thermodynamic constraint using the platinum catalyst with the 2,4HD system. The result is presented in table 93.

Table 93: Summary of the conversions result obtained at 773 K over $CrOx/Al_2O_3$ and Pt/Al_2O_3

	Conversions (%)			
	P	P/1HY	P/1,5HD	P/2,4HD
CrOx/Al2O3	11	19	91	9
Pt/Al2O3	37	71	59	46

Interestingly, ~90% pentane conversion was obtained with the doped chromia catalyst using the P/1HY system at 673 K compared to 13% with the chromia catalyst. Also, when the pentane was run individually over the doped catalyst, conversions higher than the equilibrium conversion of the pentane were obtained (~43% at 673 K), indicating a poor selectivity to the dehydrogenation reaction. Similarly, about the same conversions of pentane were obtained with the P/1,5HD system (~89% at 673K) just like the 1HY system. This suggests that the trans-hydrogenation activity over the K-CrO_x/Al_2O_3 catalyst is about the same based on pentane conversion with both P/1HY and P/1,5HD systems. This is in contrast to the chromia catalyst where reaction with P/1,5HD gave a better activity compared to P/1HY. Reaction using K-CrO_x/Al_2O_3 does not indicate that there has been a lifting of the thermodynamic constraint with the 2,4HD. Only ~11% was observed with the trans-hydrogenation compared to ~43% with pentane dehydrogenation. Summary comparison of the two catalysts using the three systems at 673 K is presented in table 94

Table 94: Summary of the conversions result obtained at 673 K over $CrOx/Al_2O_3$ and K- $CrOx/Al_2O_3$

	Conversions (%)			
	P	P/1HY	P/1,5HD	P/2,4HD
CrOx/Al2O3	8	13	91	7
K-CrOx/Al2O3	43	87	89	11

In contrast, the trans-hydrogenation process only slightly increased the conversion of pentane with the doped platinum catalyst. With the P/1HY system only ~ 42% pentane conversion was observed at 673K during the trans-hydrogenation, compared to ~39% conversion for pentane dehydrogenation. Slightly higher conversion was obtained using the P/1,5HD system (~65 % at 673 K) while the P/2,4HD revealed poorer conversion (~35 % at 673 K). The remarkable increase in activity observed with the doped chromia catalyst compared to the chromia catalyst was not observed with the doped platinum catalyst compared to the platinum catalyst

With the exception of Pt/Al_2O_3 catalyst, the reaction with P/2,4HD exhibited poor pentane conversions during the trans-hydrogenation. This is expected with P/2,4HD system as the thermodynamics of the trans-hydrogenation reaction with 2,4HD suggested that it would be under severe equilibrium control (see section). The increase in the conversion of the pentane with the trans-hydrogenation is related to the Free energy (ΔG) of reaction of pentane with the hydrogen acceptors [98]. The trans-hydrogenation reaction of pentane with 1- hexyne is thermodynamically favoured at most temperatures (ΔG = -50 kJ/mol at 773 K) while, dehydrogenation of n-pentane is under thermodynamic constraint (ΔG = +27 kJ/mol at 773 K).

The differences in the conversion of pentane obtained with the chromia catalysts and the doped catalyst was expected because the potassium doped catalyst would block the acid site of the catalyst preventing coke deposition deactivating the catalyst[99, 100]. There is a slight reduction in hexyne conversion observed in the mixed feed compared to when it was fed alone. The

conversion of hexyne feed alone at the various run temperature is ~95% at 773 K, which reduced to ~87 % with mixed feed, over the CrO_x/Al_2O_3 system. This reduction could be due to a reduction in cracking because of the trans-hydrogenation process, because alkynes are very reactive and thermodynamically less stable [101]. The conversion of 1HY, 1,5HD and the 2,4HD with doped catalyst was almost constant when either fed alone or as part of the trans-hydrogenation process

4.1.3 Side reactions

The primary aim of trans-hydrogenation is to produce pentenes and hexenes from the three systems (i.e. P/1HY, P/1,5HD and P/2,4HD). However, side reactions are expected. Isomerisation products were clearly observed from three mentioned systems. These isomers add to the production of total olefin which is either not initially formed when the reactants were passed alone, or the yield increased during the trans-hydrogenation. For instance, 3.08% cis/trans 2-hexene and 3.44% cis/trans 3-hexene were obtained during the trans-hydrogenation compared to 0.81% cis/trans 2-hexene and 2.34% cis/trans 3-hexene obtained when hexyne was run alone using the CrO_x/Al_2O_3 catalyst (table 6 Cr chapter). A similar trend was also observed with the same catalyst using the P/1,5HD system, but more alkylated olefins were observed, with 20% of 3-methylhexene obtained at 773 K. The 3-methylhexene product was not observed using the P/1HY system. It is observed that in both reaction systems, there is increase in the total olefin yield during the trans-hydrogenation, but the P/1,5HD system presented higher alkylated olefinic products. This could be a reason why the total olefin yield was observed to be higher with the P/1,5HD system

There are also observed side reactions due to isomerism and alkylation using the platinum catalyst; it is the same trend with the chromia catalyst where the isomers formed increase during the trans-hydrogenation. However, unlike the chromia catalyst, more of the primary olefins are observed with the platinum catalyst, 2.79% 1-hexene was observed with the platinum catalyst compared to the 0.66% obtained with the chromia catalyst using the P/1HY system at 773 K.

Meanwhile, it is also observed that more of the primary olefins are obtained at lower reaction temperatures during the trans-hydrogenation with both catalysts; 3.06 and 3.64% 1-hexene were observed with chromia and platinum catalysts at 573 K respectively. This is a higher yield if compared with the reaction at 773 K highlighted above, but the total olefin yield (primary olefin + secondary olefin + alkylated olefin) was observed to be higher with high reaction temperatures, suggesting that the side reactions predominate at higher reaction temperatures

This same trend was also observed using the doped, K-CrO_x/Al_2O_3 and K-Pt/Al_2O_3 catalysts, with more significant yields obtained in the case of the K-CrO_x/Al_2O_3 catalyst compared to the chromia counterpart. Generally, there are fewer isomers of pentene observed compared to hexene isomers, and presumably the pentenes may have been consumed in the by-product reactions.

Alkylated species are major products observed in most of the reaction systems. However, most of these alkylation products are olefin alkylated. This suggests that in essence, rapid isomerization and alkylation occurs immediately when the trans-hydrogenation process occurs. The olefin produced in **(a)** could be re-adsorbed on the catalyst and used in the formation of surface carbeniun ion intermediate on the acid site of the catalyst **(b),** which could either isomerize **(c),** or undergo alkylation **(d)**

a) metal side dehydrogenation/hydrogenation)

$$n\text{-}C_nH_{2n-2} / n\text{-}C_nH_{2n+2} \rightarrow n\text{-}C_nH_{2n} + H_2 / -H_2$$

b) Carbenium ion intermediate

$$n\text{-}C_nH_{2n} \rightarrow n\text{-}C_nH^+_{2n+1}$$

C) Alumina acid site isomerization

$$n\text{-}C_nH^+_{2n+1} \rightarrow i\text{-}C_nH_{2n}$$

d) Alumina acid site alkylation

$n\text{-}C_nH^+_{2n+1} + R \rightarrow R\text{-}C_nH_{2n+1}$

As expected there are variations and differences in the yield of the side reaction products, dependent on the catalyst system, the reaction system and the reaction temperatures. Thus, the trans-hydrogenation could be masked by subsequent isomerisation and alkylation as highlighted previously above. (Figure 270). The illustrated process in figure is dependent on, the catalyst system, reaction temperature, GHSV and reaction time.

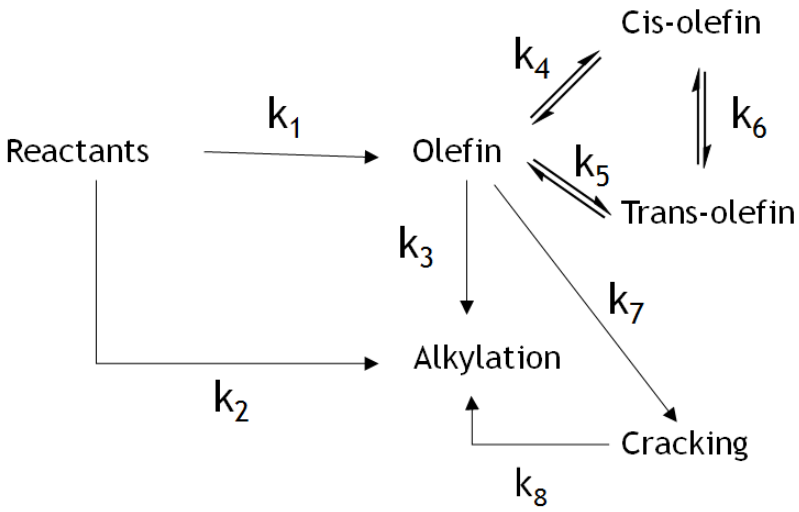

Figure 270: Suggested reaction path-way during the trans-hydrogenation

One may speculate that in the case of the trans-hydrogenation, (k_1) is fast. Therefore, one may expect more of the targeted primary product (olefin) as in the case of the Platinum. The rate at which each product occurs varies and summarized below are three possible causes for these differences:

1. The isomerisation activity (i.e rate constant K_4 or k_5) is much lower on the Pt than the Cr catalyst

2. The reactants and the products adsorption competition is more on the Cr than on the Pt catalyst

3. The site reaction competition with unreacted compound making (i.e. rate constant K_2, K_3, K_7 or K_8) faster, in the case of 1,5HD system with both catalysts

4.1.4 Evolved gas analysis

The evolved gas products occur due to cracking processes on the surface of the catalyst. Hydrocarbon molecules are said to crack at elevated temperatures on acid sites of a catalyst through ß-scission into smaller fragments [102-104]. Methane, ethylene, propylene, and butylene are the main cracked products observed. The reactants are suggested to have cracked with the stoichiometric ratios as illustrated bellow:

Methane

$C_5H_{12} \rightarrow 3CH_4 + 2C$

$C_6H_{10} \rightarrow 2CH_4 + 2HCC$

Ethylene

$C_5H_{12} \rightarrow 2C_2H_4 + CH_4$

$C_6H_{10} \rightarrow 2C_2H_4 + 2HC$

Propylene

$C_5H_{12} \rightarrow C_3H_6 + CH_4 + C$

$C_6H_{10} \rightarrow C_3H_6 + CH_4 + 2C$

Butylene

$C_5H_{12} \rightarrow C_4H_8 + HHC$

$C_6H_{10} \rightarrow C_4H_8 + 2HC$

During pentane dehydrogenation over the CrO_x/Al_2O_3 catalyst, CH_4 and C_2H_6 were both observed. The gases evolved after ~40 min of the reaction on stream and were maintained for the whole 2 h reaction period. This is the same time when the hydrogen completely declined from the reaction stream. Thus, this could

suggest that the catalyst could have died with respect to dehydrogenation activity. A similar trend observed with the trans-hydrogenation using the P/1HY system and it could be that the hydrogen is completely taken up for the trans-hydrogenation process or the trans-hydrogenation could have stopped when there is no hydrogen on the stream. C_3H_6 and C_4H_8 were observed with the P/1,5HD system. Unlike the P/1HY system, hydrogen was observed to gradually decrease from the reaction with TOS and was maintained to ~80 min before it completely declined from the stream. This is similar to what was observed with the P/2,4HD system but the hydrogen production was only maintained to ~70 min before ceasing.

However, only pulses of these gases were observed with the platinum catalyst with all the reaction systems and they were maintained only for ~20-30 min TOS, whereas the hydrogen production was maintained in the reaction stream for the period time of the reaction (2 hr). The gases productions are highlighted in Table 95.

Pulses of both methane and ethylene were observed using the potassium doped catalysts but were only maintained for ~30 min after which they declined from the stream. A similar trend was observed with the doped platinum but only maintained for ~20 min of the reaction. The pulse of hydrogen was also observed and was at the highest intensity at ~20 min but subsequently decreased with time for the duration of the reaction with both catalyst systems. This is expected as the potassium reduces the acid site formations and so did the gaseous species. All other followed masses (m/z 30, 40, 44, 54, 58, 72 & 84) were not observed but only their pulses were seen at the beginning of the reaction. There were five suggested postulation that could possible occurs:

1. The trans-hydrogenation stops when the hydrogen completely declined from the reaction stream

2. The hydrogen completely taken up for the trans-hydrogenation and was not observed on the stream

3. There could be good hydrogen production which may been used in the trans-hydrogenation and also still maintained in the reaction stream

4. The trans-hydrogenation stops when the dehydrogenation activity dies up

5. The hydrogen could also be taken up by the C, -CH_3 and -C_2H_5 intermediates to produce the methane, ethylene

Table 95: Summary of the gases formed with reaction system and catalyst

	1HY	**1,5HD**	**2,4HD**
CrO_x/Al_2O_3	CH4/C2H4	C3H6/C4H8	C3H6/C4H8
K-CrO_x/Al_2O_3	CH4/C2H4 pulses	C3H6/C4H8 pulses	C3H6/C4H8 pulses
Pt/Al_2O_3	CH4/C2H4 pulses	CH4/C2H4 pulses	CH4/C2H4 pulses
K-Pt/Al_2O_3	CH4/C2H4 pulses	CH4/C2H4 pulses	CH4/C2H4 pulses

4.1.5 Effect of changing the reaction temperatures on olefin products

In order to determine the effect of reaction temperatures on the trans-hydrogenation process, the reaction was run for at temperatures of 523, 573, 623, 673, and 773 K as indicated previously. Significant changes were observed in the yield of the olefinic products with reaction temperatures. This also depended on either the reaction system or the catalyst used. However, there are no significant changes observed in the products distribution pattern. It was previously highlighted that the use of temperature does not really change the product distribution pattern. Nevertheless there is observed a relationship between the yield of olefin products and reaction temperature. In each reaction system, it is observed that the reaction gets more selective to the production of these olefin products with the higher reaction temperatures as presented in Figure 271-273

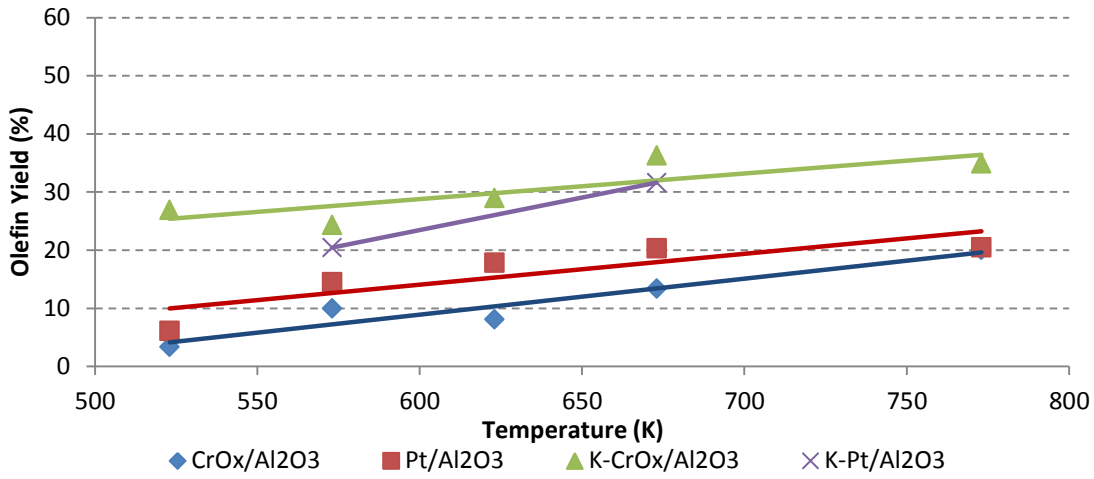

Figure 271: comparison of the olefin yield with the various catalysts using 1HY system

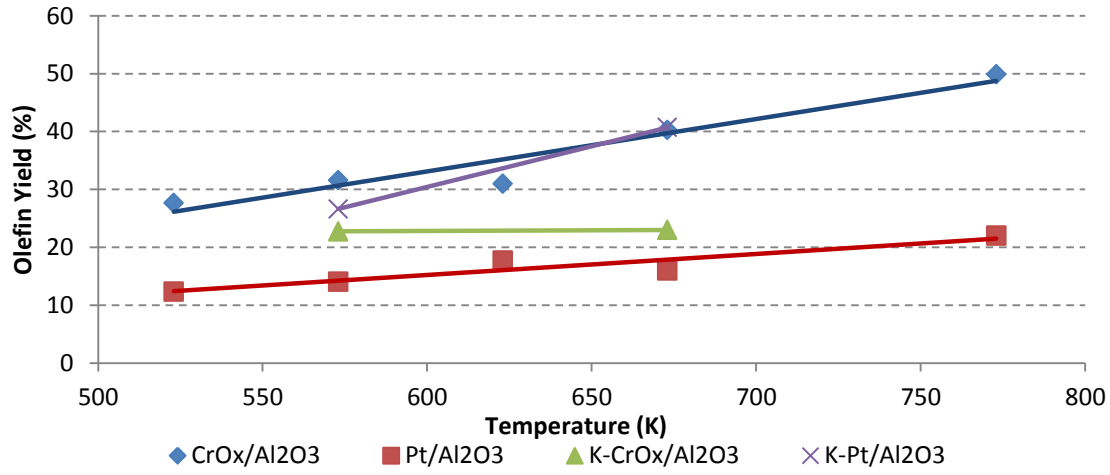

Figure 272: comparison of the olefin yield with the various catalysts using 1,5HD system

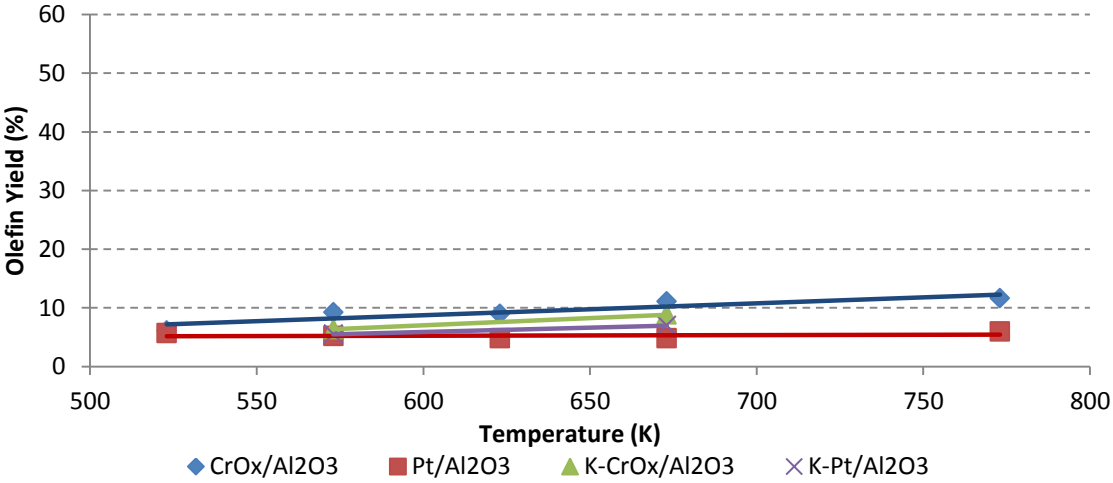

Figure 273: comparison of the olefin yield with the various catalysts using 2,4HD system

It could be observed that an overall higher product yield was obtained with the chromia systems compared to the platinum systems even though the platinum gave better reactant conversions during the trans-hydrogenation. Taking individual systems and relating to activity of each tested catalyst, it can be suggested that the selectivity to the total olefinic products follow the order as below:

For 1HY system

$K\text{-}CrO_x/Al_2O_3 > K\text{-}Pt/Al_2O_3 > Pt/Al_2O_3 > CrO_x/Al_2O_3$

For the 1,5HD system

$CrO_x/Al_2O_3 > K\text{-}Pt/Al_2O_3 > K\text{-}CrO_x/Al_2O_3 > Pt/Al_2O_3$

For the 2,4HD system

$CrO_x/ Al_2O_3 > K\text{-}CrOx/ Al_2O_3 = K\text{-}Pt/ Al_2O_3 > Pt/ Al_2O_3$

4.1.6 Effect of using alternative catalyst on the valuable products yields

Generally, the result analysis of the valuable products from each reaction system shows that there is good relationship with the yield of these products and the reaction temperatures. An increase in the valuable products was observed with higher reaction temperature and with different catalysts. The reaction at 673 K was used to obtain this comparison and we can clearly see which catalyst gives a higher valuable products yield. This is presented in Figure 274.

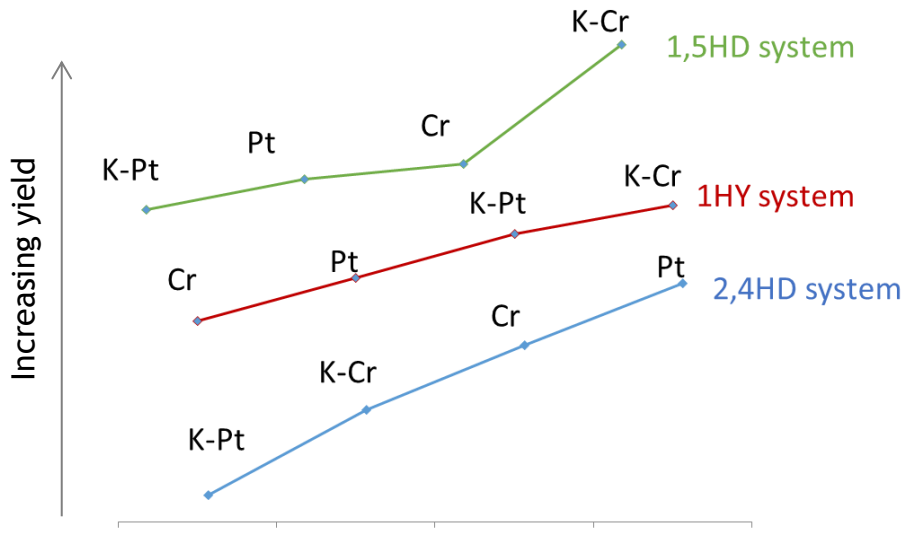

Figure 274: effect of the alternative catalyst on the yield of the valuable products

4.1.7 Comparisons of the trans-hydrogenation products with hydrogenation of hexyne/hexadienes

The trans-hydrogenation process is limited by the dehydrogenation of the alkane as highlighted previously in the introduction chapter. Therefore, the activity of the trans-hydrogenation could be determined by the available hydrogen species made available during the process. However, in comparison with the hydrogenation of the alkyne and the alkadienes, it was observed that the reaction product distribution remain almost the same for both hydrogenation and trans-hydrogenation, only that the yield of the valuable products changes (i.e. olefins, alkylates olefins, alkylates and cyclics), as more of these products were observed during the hydrogenation process. Meanwhile, there was a significant similarity in the product distribution obtained during both the trans-hydrogenation and the hydrogenation compared to when the reaction was observed individually. In essence, there is an appreciable increase in the product yield/selectivity to the valuable products obtained during the trans-hydrogenation compared to when the reactants were run individually, even though higher selective was achievable with the hydrogenation. This suggests a clear indication that there is a trans-hydrogenation process occurring. For instant, (table 14), only 0.33% 1-hexene was observed during when the hexyne was run individually, this then increased to 1.81% with the trans-hydrogenation and 3.39% with the hydrogenation. This is the same trend observed with other

products and with the other reaction systems. Thus you can clearly depict the change as a result of trans-hydrogenation. However, products sometimes got more selective with hydrogenation compared to trans-hydrogenation by a factor of ~2-3. This could be related to that the amount of hydrogen available.

4.2 Post reaction characterization and analysis

4.2.1 TGA-TPO analysis of the post reaction catalysts

The TGA-TPO-MS analysis on the catalysts confirms presence of carbon deposition with all the reaction systems. However, changes were observed in the type of carbon deposit. For instance, from the derivative weight loss/MS profile plot of the CrO_x/Al_2O_3 spent catalyst used for the P/1HY reaction reveals evolution of carbon species at ~515 K and further evolution up to ~890 K indicating that the carbonaceous deposit is complex. The spent catalyst obtained with the P/1,5HD system reveals evolution of CO_2 at ~515-775 K indicating the absence of a more recalcitrant coke with this system compared to the P/1HY. There is also a observed shift of the CO_2 evolution with reaction temperature. A ~8 K reduction with reducing reaction temperature was observed; suggesting that softer coke is formed with a lower reaction temperature. The spent catalyst obtained with the P/2,4HD system reveals a similar coke formation to the P/1,5HD system except for the observed additional CO_2 evolutions at higher temperature with reactions at 623 K and 573K, suggesting possible formation of harder coke. However, two clear distinct evolution peaks were observed unlike what was observed with the P/1HY system.

The TGA-TPO profile obtained with the Pt/Al_2O_3 catalyst showed similar formation of deposited surface species with all three reaction systems. Two types of carbonaceous deposit were formed with this catalyst, one at lower temperature and a higher temperature species. However, little changes were observed between the systems. For instant, using the 1HY system, the low temperature evolution was observed at ~510 K and the high temperature evolution at ~540-850 K with hexyne alone. A similar profile was observed during the P/1HY trans-hydrogenation except for that the low temperature evolution was lost from the catalyst used in the 523 K reaction, suggesting temperature influences in the formation of this carbonaceous species. With the 2,4HD system

the low temperature evolution was observed at ~450 K and the higher temperature broad evolution at ~523-850 K. There is also a clear shift in the evolution with the reaction temperature similar to that observed with P/1,5HD using the chromia catalyst. The TPO profile from the used Pt/alumina catalyst after P/1,5HD trans-hydrogenation does not clearly showed the distinction between the two, evolutions which could be attributed to a smaller amount of carbon deposit compared to the P/2,4HD system. This is confirmed from the carbon laydown analysis. The first CO_2 evolution could be derived from the more hydrogen rich coke attributed to the formation of "soft coke". The second broad peak of the CO_2 evolution could be attributed to the reaction of hard coke-hydrogen deficient/aromatic species which are considered as intermediates for the formation of hard coke [105-107], and/or coke deposited in the deep pores of the catalyst

The TGA-TPO-MS profile of the K-CrO_x/Al_2O_3 spent catalysts used with the 1HY reaction system reveal a sharp–weight loss–at ~547 K and two further weight losses at ~631 K and ~707 K indicating that three form of carbonaceous deposit have been formed. The low temperature carbon dioxide evolution may be attributed to a soft form of coke similar to that observed with the Pt/Al_2O_3 catalyst. The subsequent weight loss could be related to graphitic aromatic precursors of different types, as carbon deposition occurs due to progressive condensation and cyclisation of hydrocarbons that leads to this type of coke. Only two CO_2 evolutions were observed with the 2,4HD and 1,5HD systems at ~608 K and ~700K and are similar the two broad carbon dioxide evolutions observed with the 1HY system. The doped platinum catalyst reveals also two CO_2 evolutions, the first evolution at ~600 K could be a similar carbon species to that found with the K-CrO_x/Al_2O_3 catalyst while the second weight loss is very broad and the combustion is only completed at ~1050 indicating the presence of a hard carbon species that is not observed with the other catalyst systems.

Meanwhile, the pentane dehydrogenation reveals a different profile with the weight loss associated with the evolution of the CO_2 observed at ~ 605 K using CrO_x/Al_2O_3. No obvious carbon dioxide evolution was observed using the K-CrO_x/Al_2O_3 catalyst or the Pt/Al_2O_3 catalyst. However, the doped platinum catalyst shows a CO_2 evolution similar to the one obtained during reactions with

the mixed feeds at ~1050 K. All the spent catalysts show a weight loss at ~373 K associated with physisorbed water evolution. Detailed analysis on how many CO_2 evolutions are observed with different systems and catalyst is presented in table 96

Table 96: Forms of the carbonaceous species formed over three system using different catalyst

	1HY system	1,5HD system	2,4HD system
CrO_x/Al_2O_3	1	1	1 or 2
Pt/Al_2O_3	2	2	2 or 3
K-CrO_x/Al_2O_3	3	2	2
K-Pt/Al_2O_3	2	2	2

4.2.3 TGA-TPO-MS desorbed species analysis

Desorbed species including H_2, CH_4, CO and predominantly CO_2 were observed with the 1HY system during the TPOs from the chromia catalyst. Formation of this kind of species can occur during burning of hydrocarbons in limited supply of air. The CH_4 could be generated from aliphatic species and aliphatic side chains attached to aromatic coke [107]. This type of behaviour is observed only with this system and the CrO_x/Al_2O_3 catalyst. The spent catalyst from the 1HY hydrogenation reaction also presented this same behaviour suggesting that the carbon deposit formed from the 1-hexyne reactant plays a major role in their formation. There is not much of the carbon deposition and there is no competitive C and H reaction with the oxygen and hence complete combustion

In general, it is clearly observed that the potassium reduces the total amount of the carbon formation on the catalyst compared to the chromia and the platinum

catalysts and could be attributed to the removal of the support acid site that promote cracking activities [108].

4.2.4 The coke formation and deposition

For a generic trans-hydrogenation reaction it is suggested that, the reactant can form the olefin product via the H_2 transfer and the resulting olefin could also be adsorbed on the catalyst, undergoing oligomerization and polymerization after forming radical species. This leads to the production of coke precursors and finally to coke formation.

4.2.5 CHN elemental analysis

On the basis of CHN elemental analysis, the composition of the carbon deposit likely varies with the reaction temperature and nature of the reactants. Over the chromia catalyst, the carbonaceous deposit formed during the hexyne reaction feeds presented a more hydrogen deficient carbonaceous deposit, a 1.6 H:C atomic ratio was observed at 773K. There is general increase in these ratios observed with the 1,5HD and 2,4HD systems, with ratio ranges from 3.1-2.3 and 3.5-2.6 respectively. This suggests that the coke formation with the 1,5HD and 2,4HD systems is a more hydrogenated coke compared to the 1HY system. A slightly higher ratio was observed with both the 1HY and 2,4HD system 3.3-2.1 and 4.1-2.9 respectively using the Pt/Al_2O_3 catalyst. Unexpectedly, ~9 H/C ratio similar to what was observed with pentane run was obtained with the 1,5HD system and could be attributed to low carbon laydown observed with this system. Hence, this could suggest that the more hydrogenated coke is formed with the Pt/ Al_2O_3 catalyst and more hydrogen deficient were formed with the chromia catalyst especially with the 1HY system. The results are presented in figures 275 and 276

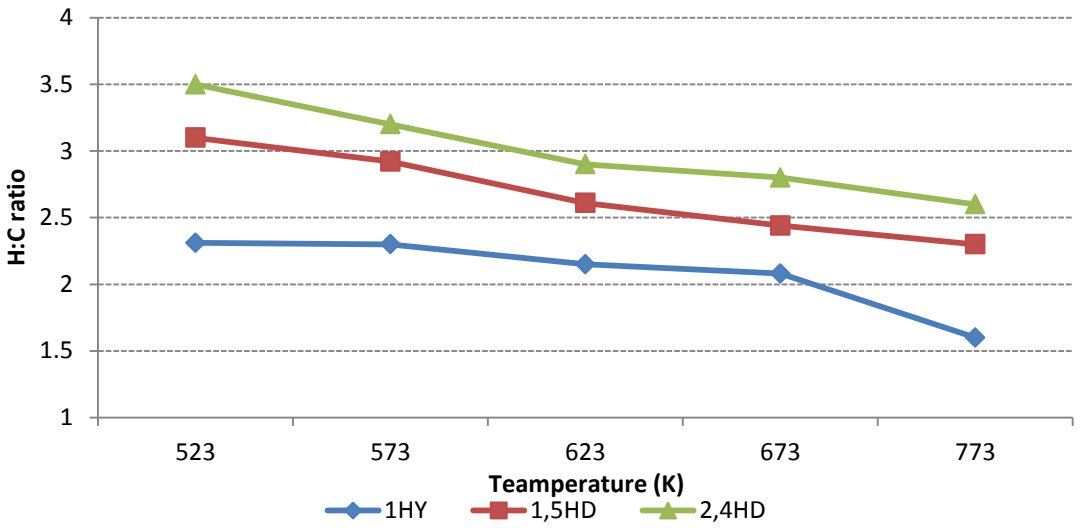

Figure 275: H:C atomic ratio of the coke formed over the CrO_x/Al_2O_3 catalyst using the three reaction system at different reaction temperatures

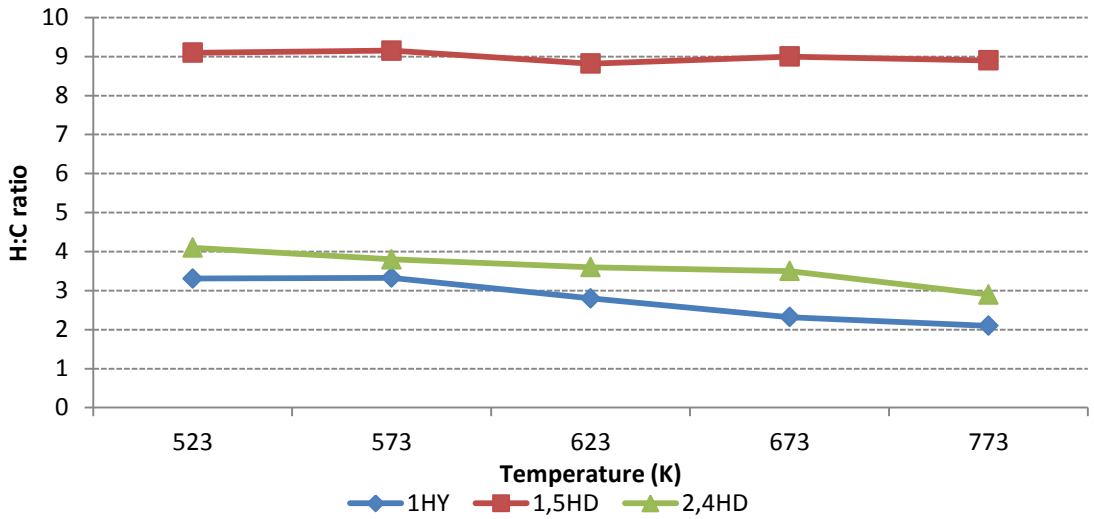

Figure 276: H:C atomic ratio of the coke formed over the Pt/Al_2O_3 catalyst using the three reaction system at different reaction temperatures

Similarly, the significance of potassium doping has been observed with a higher H/C ratio observed with the doped chromia catalyst. The data is presented in table 97. The Lower H:C ratio suggests more hydrogenated coke and a lower carbon formation. This could be observed with all reaction temperatures compared to the chromia catalyst.

Table 97: H/C ratio of coke obtained over CrO_x/Al_2O_3 and K-CrO_x/Al_2O_3 using 1HY system

Temperature (K)	H/C ratio of coke		
	P	1HY	P/1HY
CrOx/Al2O3			
773	9.2	1.60	1.80
673	10.1	2.08	2.20
623	9.4	2.15	2.30
573	9.1	2.30	2.50
523	9.6	2.31	2.50
K-CrOx/Al2O3			
773	7.20	3.31	3.61
673	9.32	4.05	3.96
623	9.46	4.57	4.20
573	9.21	4.71	4.31
523	10.10	5.01	5.12

4.2.6 Effect of the reaction temperatures on the carbon formation

Higher carbon formation was always observed with higher reaction temperatures. However, higher carbon formation was obtained with the chromia catalyst as presented in Figure 277.

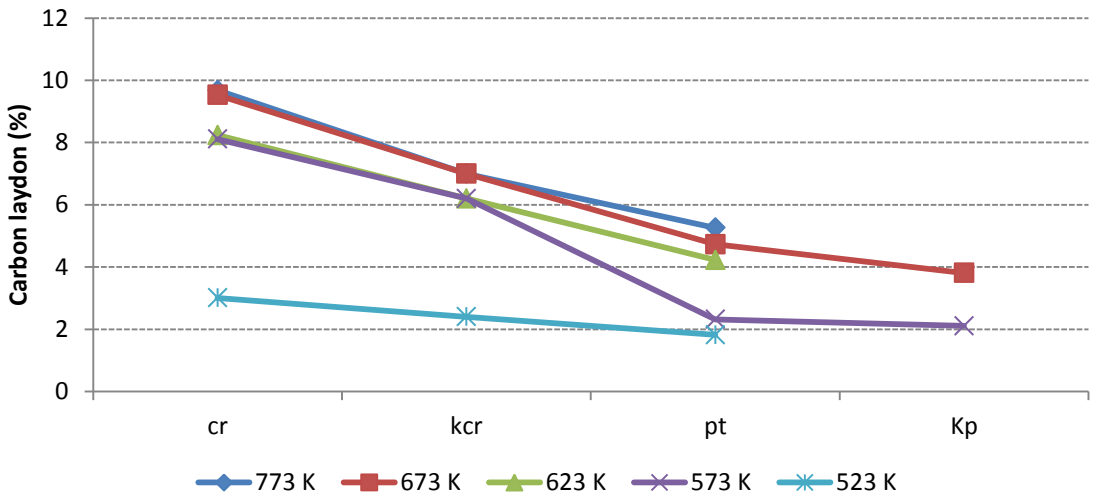

Figure 277: comparison of the carbon laydown over the catalysts at different reaction temperatures

There is clear different between the chromia catalyst and the potassium doped counterpart. This difference is suggested to have linked to the reduction of the carbonaceous formation with doped catalyst. However, if the data is plotted as a pseudo-Arrhenius plot (fig 278) then, the carbon laydown formation shows about the same gradients for both the K- CrO_x/Al_2O_3 and CrO_x/Al_2O_3 catalyst. Using the gradient it is poosible to generate a pseudo-Ea number, so the reactions with K-CrOx/Al_2O_3 have activation energy (~59 $kJmol^{-1}$) whilst reactions with CrO_x/Al_2O_3 also have activation energy (~59 $kJmol^{-1}$). Both catalysts show a good linearity of the plots for the reaction temperature range (Figure 278). This suggests that the potassium doping as expected, does not change the mechanism of the reaction but have only reduce the acid site of the catalyst

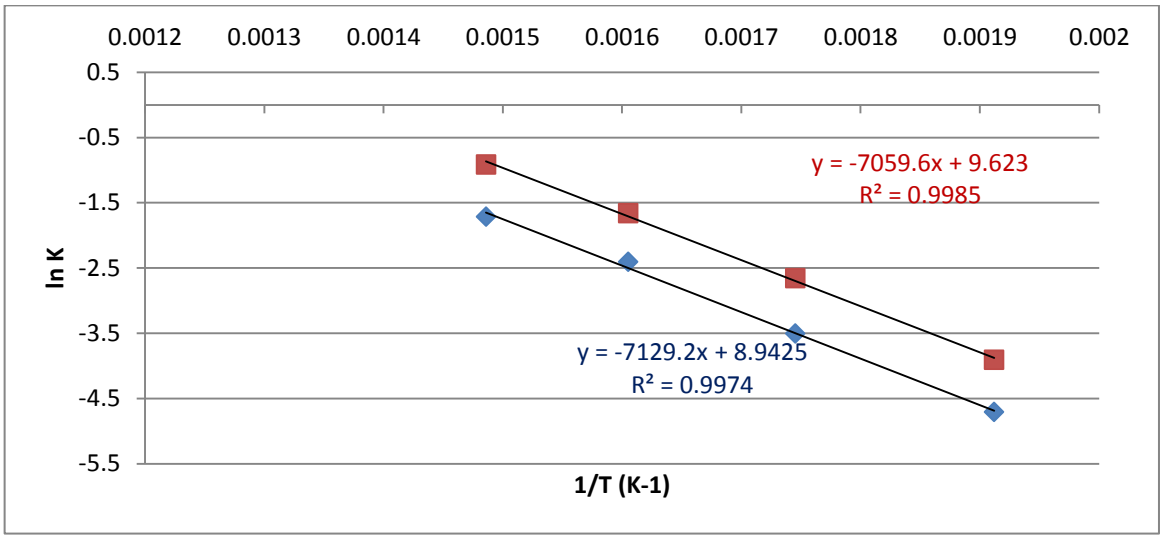

Figure 278: Coke formation during trans-hydrogenation over ■ CrO_x/Al_2O_3 ♦K- CrO_x/Al_2O_3

4.2.7 Raman analysis

The Raman spectrum obtained from all the catalyst system confirms the presence of graphitic species. Spectra showing two overlapping bands with peaks at ~1380 cm^{-1} and ~1600 cm^{-1} were observed on the chromia catalyst after use with hexyne and the mixed feed trans-hydrogenation. These bands are associated with coke deposition and are the D and G bands respectively related to graphite. The graphene G band at ~1600 cm^{-1} is a graphitic lattice vibrational mode mainly of an aromatic nature[109]. While the D type at ~1380 cm^{-1} is related to defects characteristic of disorder of the graphene[110]. The degree of disorder in the graphitic structure [106, 111] denoted as (I_D/I_G) can be measured and the ratio of D and G band intensities are presented in table (11). However, for the reaction systems that are not presented, they have zero ratios. The I_D/I_G shows that the intensity and the disorder in the graphitic type carbon with all the catalysts increases as temperature increases. However, this ratio was found to reduce with the trans-hydrogenation process (Figure 279). There is also a reduction in the I_D/I_G ratio observed between the 1HY and 1,5HD/2,4HD systems suggesting that the carbon deposits obtained with 1HY are more disordered while 1,5HD and 2,4HD presented about the same I_D/I_G ratios.

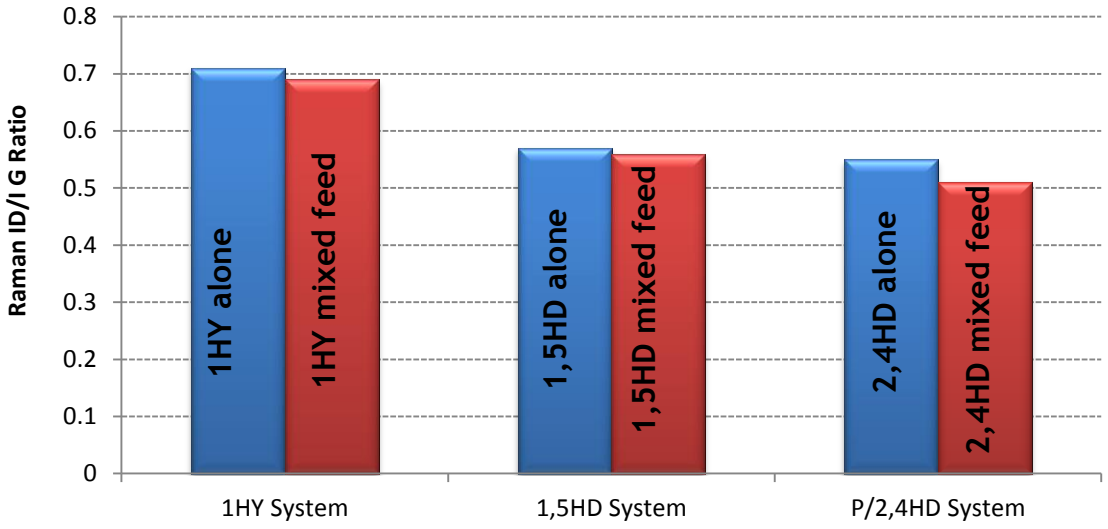

Figure 279: Raman I_D/I_G Ratio ratios of the three systems over the chromia catalyst at 623 K

The similarities between 1,5HD and 2,4HD reactant have been observed in some of the spent catalyst characterization and could be attributed that 1,5HD and 2,4HD both have two double bond compared to hexyne which has triple bond. The microcrystalline planar size of the carbon was evaluated using the relationship $La(nm) = 4.4[I_D/I_G]^{-1}$ [112] and it is observed that the carbon species are more crystalline with trans-hydrogenation and with the 1,5HD and 2,4HD feeds compared to the 1HY feed as presented in table 98

Table 98: Microcrystalline planar size (La) of carbon at 623 K using CrO_x/Al_2O_3

	$La (nm) = 4.4[I_D/I_G]^{-1}$		
	1HY	1,5HD	2,4HD
Mixed feed with pentane	6.4	7.9	8.6
Single feed	6.2	7.7	8.0

The D-band was not observed on catalysts used at the low reaction temperatures of 573 K and 523 K with most of the reaction systems during trans-hydrogenation suggesting that the effect of temperature is in making the carbon species less disordered during the trans-hydrogenation. The Raman spectra obtained using pentane alone over the CrO_x/Al_2O_3 catalyst, shows that the spent catalyst still

reveals bands ~357, ~ 836 and ~973 cm^{-1} due to bending modes and symmetric stretch of CrO_2 suggesting that the deposited coke is not enough to cover the surface of the chromia on the catalyst.

Table 99: Ratio of D and G band intensities obtained from the various reactions

Catalyst/Reactants	D:G Ratio				
	523 K	573 K	623 K	673 K	773 K
CrOx/Al2O3					
P	0	0	0	0	0
1HY	0.64	0.64	0.68	0.70	0.72
P/1HY	0	0	0.65	0.68	0.71
1,5HD	0	0	0.57	0.61	0.65
P/1,5HD			0.56	0.59	0.61
2,4HD			0.55	0.57	0.59
P/2,4HD			0.51	0.54	0.57
Pt/Al2O3					
P	0	0	0	0	0
1HY	0	0	0.58	0.71	0.72
P/1HY	0	0	0	0	0.71
1,5HD	0	0	0.66	0.73	0.74
P/1,5HD	0	0	0	0	0.69

4.2.8 Formation of yellow oil (wax-like species)

The formation of the polycyclic aromatics is of considerable importance for understanding the mechanism involved in the carbon deposition and coke formation [113-115]. Yellow oil was observed to build up in the reactor tube with time and a considerable amount was made visible after a series of trans-hydrogenation reactions. Hence all the material carbon which goes to produce this material will be normally considered and classified under carbon deposition. The chromia and the platinum catalysts, and the alumina support were noticeable to produce this material. These materials are believed to be poly

aromatic species of C_{16}-C_{22} as listed in the table 100 below. There is also a possibility that the material could also have attachment of aliphatic side chain. Therefore, it could also range to >C_{22}

Table 100: Typical analysis of the yellow wax deposit

component	Molecular formula
Pyrene	$C_{16}H_{10}$
Fluoranthene	$C_{16}H_{10}$
Methyl Pyrenes	$C_{17}H_{12}$
Benzo (GHI) Flouranthene	$C_{18}H_{10}$
Benzo Anthracene	$C_{18}H_{12}$
Benzo (K) Fluoranthene	$C_{22}H_{12}$
Perylene	$C_{20}H_{12}$
Benzo Perylene	$C_{22}H_{12}$

Such species are often postulated as intermediates in coke formation but are rarely detected. Therefore, series of experiments have to be conducted to allow a large enough of the sufficient material to be produce and collected. These materials only volatilize at temperatures >723 K and hence there is a high probability that they can be retained on the catalyst surface. The formation of this coke precursor and the final coke, have been previously studied in both reflection and transmittance using UV-Visible spectroscopy [116-119]. Absorption at the highest energies (200-240 nm) are assigned to neutral molecules having single aromatic ring such as alkylated benzenes, while absorptions in the region between (250-500 nm) are assigned to carbocationic and neutral species (poly-aromatic but also linear having an extensive conjugated double bond system)[116]. The UV-Visible spectra obtained from both the yellow oil (wax) and the extract of the catalyst surface reveal absorption bands between 200-400 nm. Similar absorption spectra were obtained for both catalyst systems and wax as presented in Figure 280

Table 101: CHN elemental analysis of the yellow wax deposit

	Elemental analysis		
	%C	%H	H/C Ratio
Wax	64.6	4.52	~1.2

This may suggest that the wax is a product that could have desorbed off the catalyst surface and of course a precursor to the coke formation as highlighted previously. Similarly the CHN elemental analysis of the wax reveals that the H/C atomic ratio is ~1.2 suggesting that unsaturated forms of hydrocarbon species probably of a poly-aromatic type are formed. Note that this ratio is similar to the figure obtained from the coke observed with 1HY system using the chromia catalyst (~1.6 at 773K). The result is presented in table 101

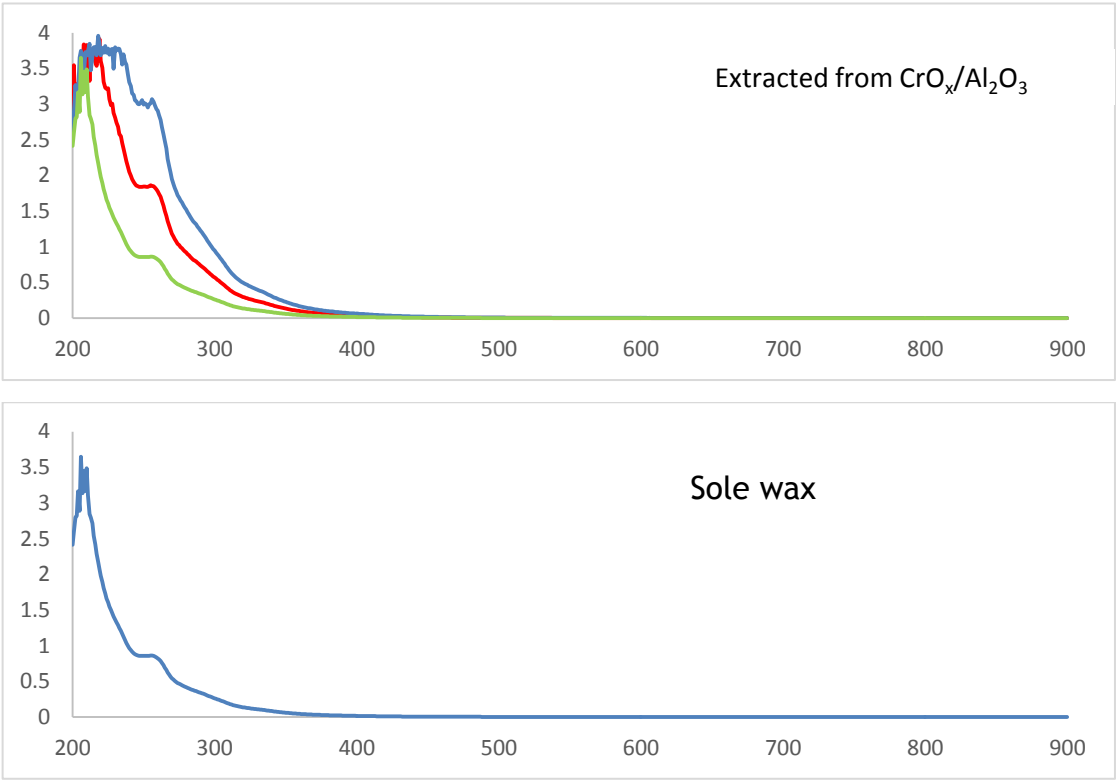

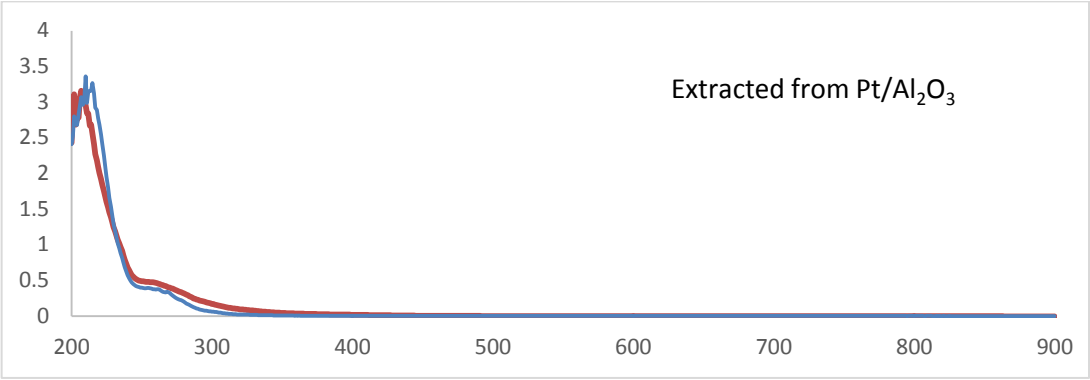

Figure 280 UV-Visible analysis of the yellow wax in comparison with the catalyst extracts

ESI mass spectroscopy has been proposed to be viable for the investigation of the oil deposit. Thus it makes it an attractive possibility for the determination of molecular weight of the species formed. The ESI-MS spectra shows multiple peak cluster for a possible higher hydrocarbon of molecular weight up to (m/e ~330) and are similar to that of higher hydrocarbons of possibly poly-fused ring or poly-aromatic as presented in Figure 281

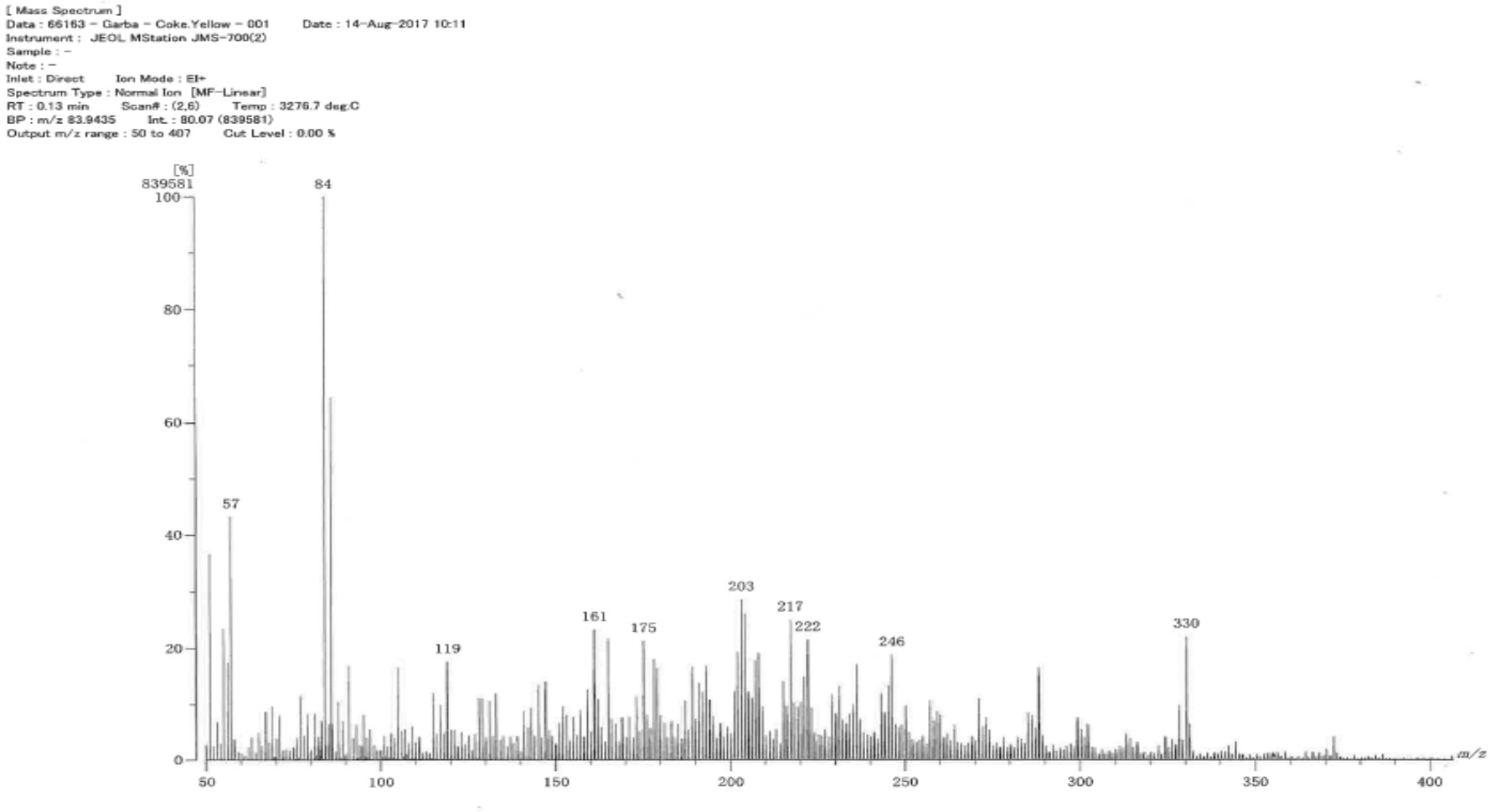

Figure 281: ESI mass spectrometry analysis of the yellow wax

Multiple line EPR spectra and a broad signal with a linewidth $\Delta H \geq 0.8$ mT would suggest the formation of oligomeric olefinic or allylic and hydrogen rich species, whereas a narrow single line EPR spectrum with a linewidth $\Delta H \geq 0.5$ mT and g = ~2, would be due to highly condensed aromatic coke[120]. The calculated linewith from both EPR spectra reveals (ΔH ~ 0.5 mT and g_{eff} = ~2) suggesting similar species to that of the yellow deposit are formed. This also suggests a highly condensed aromatic coke.

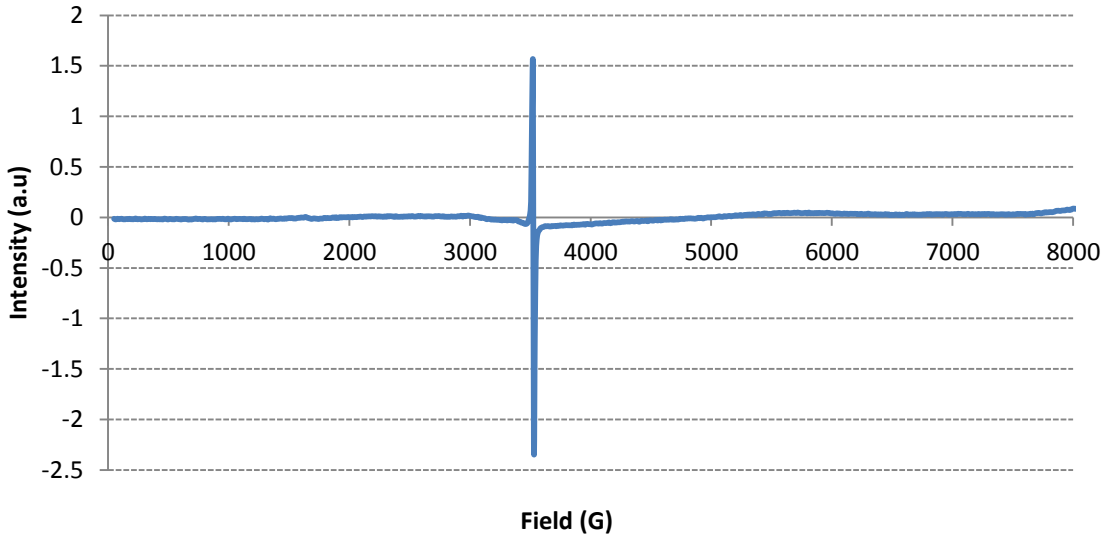

Figure 282: The EPR spectra obtained from alumina spent catalyst

The graph is presented below on a smaller range.

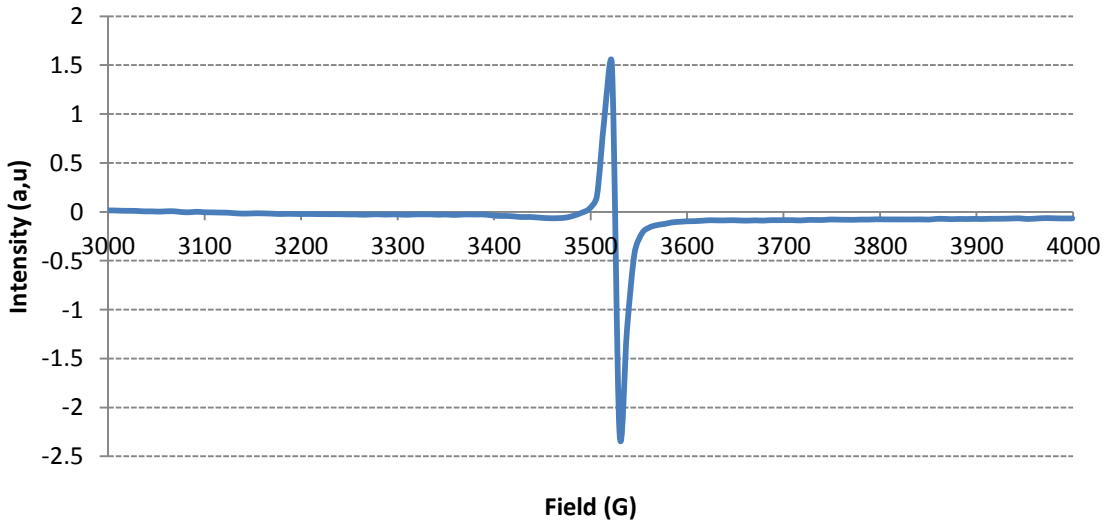

5. Conclusion

In the initial stage of the research project work, the fresh catalysts were characterized using BET, XRD, Raman and TGA-MS to investigate the morphology of each catalyst. The catalyst were then used to performed the trans-hydrogenation reactions over 523-773 K temperature range. From the XRD result, it was observed that the Al_2O_3 existed as either gamma for the chromia catalysts or as mixed gamma and theta for the platinum catalyst, and the impregnation of the Al_2O_3 with the metal precursor has no observable effect on the structure of the Al_2O_3 support.

The reactions were initially performed with the alumina support to evaluate its effect on the various reactants. The results were mainly cracking and alkylation products with ~50 % and ~1 % conversion at 623 K for the hexyne and pentane respectively. There was only a slight difference obtained in the trans-hydrogenation over the alumina, with conversion of hexyne still ~50 % but the pentane conversion was ~2 % showing an increase of 1 % compared to when it was run alone. The product distribution was very similar to when hexyne was run alone. This behaviour of alumina has been reported elsewhere in literature [121-123]. Therefore, the alumina support on its own does not performed well for the trans-hydrogenation process. The addition of the metals reduces the propensity for both cracking and alkylation observed with the support and added dehydrogenation activity

The primary aim of this thesis was to study the trans-hydrogenation of 1-hexyne (1HY), 1,5-hexadiene (1,5HD) and 2,4-hexadiene (2,4HD) with pentane (P) using heterogeneous catalysis. In-line with the research objectives as outlined in section… , the following conclusions can be made.

- The results obtained clearly showed a promising trans-hydrogenation processes occurring with the P/1HY and P/1,5HD, while results obtained for the P/2,4HD system were poorer due to thermodynamic constraints. The trans-hydrogenation of 1HY, 15HD and 2,4HD to hexene was detected with an enhanced yield of hexene when the pentane/hexyne mix was passed over the catalyst. The yield of the olefin increases during the trans-hydrogenation. The conversion of pentane to value-added products

ceis also enhanced with all the increase in pentane conversion accounted for in the production of the isomers, alkylates and the cyclic products.

- Instead of the targeted primary olefinic product, most of the products observed are secondary products. These secondary products are however, products from isomerisation, alkylation and cyclisation and accounted as valuable products. Most of the generated olefin were cis/trans 2-hexene, cis/trans 3-hexene and alkylated olefins (3-methyl-1-hexene, 2-methyl-1-hexene). However, the addition of the alkali reduced secondary alkylation and more of the primary olefins were produced with the doped catalyst.

- Catalyst deactivation was attributed to coke deposition from poly aromatic type species. Only slight deactivation was observed over the 8 hr time reaction period, but the carbon deposition could lead to severe deactivation with longer reaction time. There is an increase in the amount of the coke deposition with increased reaction temperature with all the catalyst except reaction with 1,5HD using the Pt/Al_2O_3 catalyst which shows about the same deposition with all reaction temperatures. The coke deposition could be on the metal, metal-support interface, doped alkali and or the support. All the types of the coke deposited were clearly distinguishable except with the CrO_x/Al_2O_3 catalyst. The Raman spectroscopy results show that carbon formed was graphitic in type and present on all the catalyst, the disorder in the graphitic carbon increased with increasing reaction temperature

- Finally, It has proved that it is possible to up-grade mixed hydrocarbon feed streams with this methodology as most of the reaction products are valuable products used in the daily activities of petrochemical industries.

6. Reference

1. L Peskett, R Slater, C Stevens, A Dufey, *Biofuels, agriculture and poverty reduction*. (2007), Natural Resource Perspectives.
2. Bhasin, M.M., et al., *Dehydrogenation and oxydehydrogenation of paraffins to olefins.* Applied Catalysis A: General, (2001). **221**(1–2): p. 397-419.
3. Alvin, H.W., *The Manufacture of Propylene*, in *Refining Petroleum for Chemicals*. (1970), AMERICAN CHEMICAL SOCIETY. p. 153-178.
4. Craig RG, Spence DC, *Catalytic dehydrogenation of liquefied petroleum gas by the Houdry Catofin and Catadiene processes*. Handbook of Petroleum Refining Processes.(2007), New York: McGraw-Hill Education.
5. Bipin, V.V. and R.P. Peter, *Catalytic Dehydrogenation*, in *Encyclopedia of Chemical Processing*. (2007), Taylor & Francis. p. 379-395.
6. Erofeev, V.I., I.S. Khomyakov, and L.A. Egorova, *Production of high-octane gasoline from straight-run gasoline on ZSM-5 modified zeolites.* Theoretical Foundations of Chemical Engineering, (2014). **48**(1): p. 71-76.
7. Song H, Wang N, Song H-L, Li F, *La-Ni modified S2O82−/ZrO2-Al2O3 catalyst in n-pentane hydroisomerization.* Catalysis Communications, (2015). **59**: p. 61-64.
8. Galadima, A., R.P.K. Wells, and J.A. Anderson, *n-Alkane hydroconversion over carbided molybdena supported on sulfated zirconia.* Applied Petrochemical Research, (2012). **1**(1-4): p. 35-43.
9. Ou J, Guo H, Zheng J, Cheung K, Louie PKK, Ling Z, Wang D, *Concentrations and sources of non-methane hydrocarbons (NMHCs) from 2005 to 2013 in Hong Kong: A multi-year real-time data analysis.* Atmospheric Environment, (2015). **103**: p. 196-206.
10. Agarwal AK, Gupta T, Bothra P, Shukla PC, *Emission profiling of diesel and gasoline cars at a city traffic junction.* Particuology, (2015). **18**: p. 186-193.
11. Dyer, P.N., R. Pierantozzi, and H.P. Withers, *Supported fischer-tropsch catalyst and method of making the catalyst*. (1987), US 4681867.
12. Chang, M.E., L.; Herman, R.; Wasielewski, P., *GASOLINE CONSUMPTION IN URBAN TRAFFIC*. (1976), USA: Transportation Research Board. 25-30.
13. KBR. *Olefins: market situation*. (2015) [cited 2015 10/08/15]; Available from: http://www.kbr.com/Technologies/Olefins/.
14. Bender, M., *An Overview of Industrial Processes for the Production of Olefins – C4 Hydrocarbons.* ChemBioEng Reviews, (2014). **1**(4): p. 136-147.
15. Givens EN, Charles PJ, Rosinski E J. , *Converting low molecular weight olefins over zeolites* in *US Patent 3960978* (1976), Assigned to Mobil Oil Corporation (New York, NY).
16. Coleman, S.T., *Process for cracking heavy hydrocarbon feed* in *US Patent 8658023*. (2014), Assigned to Equistar Chemicals, LP (Houston, TX) USA.
17. Ward, AM, Oprins AM, Housmans THM, *Process for The Production of Light Olefins and Aromatics From a Hydrocarbon Feedstock* in *WIPO Patent*

2015000842. (2015), Assigned to Saudi Basic Industries Corporation, Sabic Global Tech B.V.

18. OSAH, *Petroleum Refining Process*, U.s.o. Labor, Editor. (2014), OSAH: USA.
19. Garba, M.D. and A. Galadima, *Efficiencies of Green Chemistry Metrics in the Activities of Petroleum Refinery Process*. Vol. 4. (2015).
20. Dessau R, Partridge M, Randall D, *Production of Olefins by Transhydrogenation* in *WIPO Patent 1995030635*. (1995), Assigned to MOBIL OIL CORPORATION; 3225 Gallows Road, Fairfax, VA 22037 (US).
21. Biland-Thommen A, Ashford N, Ellis D, Escher T, Smyth D, *TRANSHYDROGENATION PROCESSES*, in *WIPO Patent 2009085826*. (2009), Assigned to SI GROUP, INC. 2750 Balltown Road, Schenectady, NY 12309 (US).
22. Gough A, Turner SK, Mercer J, Stitt EH, *Process for Cracking and Transhydrogenation of Hydrocarbon Feedstock*, in *WIPO Patent 1994010264*. (1994), Assigned to IMPERIAL CHEMICAL INDUSTRIES PLC; Imperial Chemical House, Millbank, London SW1P 3JF (GB).
23. Arthur, RJ, Lee AC, Seine M, *Process for forming olefins by hydrogen transfer*, in *US Patent 3267170*. (1966), Assigned to Exxon Research Engineering Co.
24. Parris DA, Nunawading U, *Process for the manufacture of methyl t-butyl ether*, in *US Patent 4546204*. (1985), Assigned to Imperial Chemical Industries Australia Limited (Melbourne, AU) USA.
25. Turner SK, Gough A, *Process for producing a branched chain olefin by isomerization and transhydrogenation*, in *US Patent 5639926*. (1997), Assigned to Institut Francais Du Petrole (Rueil-Malmaison Cedex, FR)
26. Jackson SD, Matheson I M, Webb G, *Carbon deposition during transhydrogenation over chromia catalysts*. PREPRINTS- AMERICAN CHEMICAL SOCIETY DIVISION OF PETROLEUM CHEMISTRY, (2003). **49;**: p. 50-53.
27. Jackson SD, Matheson MI, Webb G, *An isotopic study of the transhydrogenation of propyne with propane over a potassium-doped chromia/alumina catalyst*. Applied Catalysis A: General, (2005). **289**(1): p. 16-21.
28. Wigzell, F., S. Rugmini, and S.D Jackson, *Transhydrogenation of propyne with butane over a vanadia/θ-alumina catalyst*. Applied Petrochemical Research, (2015): p. 1-7.
29. Cavani, F. and F. Trifiró, *Classification of industrial catalysts and catalysis for the petrochemical industry*. Catalysis Today, (1997). **34**(3–4): p. 269-279.
30. Germain, J.E., *Catalytic Conversion of Hydrocarbons*. (1969), London-New York: Academic Press.
31. Jackson SD, Grenfell J, Matheson IM, Munro S, Raval R, Webb G, *Deactivation and regeneration of alkane dehydrogenation catalysts*, in

Studies in Surface Science and Catalysis, C.H. Bartholomew and G.A. Fuentes, Editors. (1997), Elsevier. p. 167-174.
32. Jackson SD, Grenfell J, Matheson IM, Webb G, *Modelling of alkane dehydrogenation under transient and steady state conditions over a chromia catalyst using isotopic labelling*. (1999), Elsevier. p. 149-155.
33. Froment, G.F., Waugh, K.C. , *Reaction Kinetics and the Development of Catalytic Processes*. 1st ed. (1999), Amsterdam: Elsevier science.
34. Weckhuysen, B.M. and R.A. Schoonheydt, *Alkane dehydrogenation over supported chromium oxide catalysts*. Catalysis Today, (1999). **51**(2): p. 223-232.
35. Vora, B.V., *Development of Dehydrogenation Catalysts and Processes*. Topics in Catalysis, (2012). **55**(19): p. 1297-1308.
36. Hauwert, P., et al., *Mechanism of Pd(NHC)-Catalyzed Transfer Hydrogenation of Alkynes*. Journal of the American Chemical Society, (2010). **132**(47): p. 16900-16910.
37. Hamilton CA, Jackson SD, Kelly GJ, Spence R, de Bruin D, *Competitive reactions in alkyne hydrogenation*. Applied Catalysis A: General, (2002). **237**(1–2): p. 201-209.
38. Canning, A.S., et al., *C-5 alkene hydrogenation: Effect of competitive reactions on activity and selectivity*. Catalysis Today, (2006). **116**(1): p. 22-29.
39. Campbell, K.N. and B.K. Campbell, *The Addition of Hydrogen to Multiple Carbon-Carbon Bonds*. Chemical Reviews, (1942). **31**(1): p. 77-175.
40. Bond, G.C., *Platinum Metals as Hydrogenation Catalysts*. Platinum Metals Rev, (1957). **1**(3): p. 87-93.
41. James OO, Sandip M, NkemA, Biswajit C, Sudip M, *Lower alkanes dehydrogenation: Strategies and reaction routes to corresponding alkenes*. Fuel Processing Technology, (2016). **149**: p. 239-255.
42. Resasco, D.E. and G.L. Haller, *Catalytic dehydrogenation of lower alkanes*, in *Catalysis: Volume 11*, J.J. Spivey and S.K. Agarwal, Editors. (1994), The Royal Society of Chemistry. p. 379-411.
43. Quicker, P., V. Höllein, and R. Dittmeyer, *Catalytic dehydrogenation of hydrocarbons in palladium composite membrane reactors*. Catalysis Today, (2000). **56**(1–3): p. 21-34.
44. Weckhuysen, B.M., et al., *Redox Behavior and Dispersion of Supported Chromium Catalysts*. The Journal of Physical Chemistry, (1995). **99**(1): p. 320-326.
45. Weckhuysen BM, Schoonheydt RA, Mabbs FE, Collison D, *Electron paramagnetic resonance of heterogeneous chromium catalysts*. Journal of the Chemical Society, Faraday Transactions, (1996). **92**(13): p. 2431-2436.
46. Lugo, H.J. and J.H. Lunsford, *The dehydrogenation of ethane over chromium catalysts*. Journal of Catalysis, (1985). **91**(1): p. 155-166.
47. Derossi, S., et al., *Propane Dehydrogenation on Chromia/Silica and Chromia/Alumina Catalysts*. Journal of Catalysis, (1994). **148**(1): p. 36-46.

48. Weckhuysen BM, Verberckmoes AA, Buttiens AL, Schoonheydt RA, *Diffuse reflectance spectroscopy study of the thermal genesis and molecular structure of chromium-supported catalysts.* The Journal of Physical Chemistry, (1994). **98**(2): p. 579-584.
49. Weckhuysen, B.M., L.M. De Ridder, and R.A. Schoonheydt, *A quantitative diffuse reflectance spectroscopy study of supported chromium catalysts.* The Journal of Physical Chemistry, (1993). **97**(18): p. 4756-4763.
50. Stephanie J.S, Marwan H, Andrew P, and David M.H, *Dispersion and Coverage of Cr/Al2O3 Catalysts.* The Journal of Physical Chemistry, (1995). **99**(5): p. 1537-1542.
51. Grünert W, W. Saffert, R. Feldhaus,and K. Anders, *Reduction and aromatization activity of chromia-alumina catalysts.* Journal of Catalysis, (1986). **100**(1): p. 138-148.
52. Du G, Sangyun Lim, Pinault M, Chuan W, Fang F, Lisa P, Gary L.H, *Synthesis, characterization, and catalytic performance of highly dispersed vanadium grafted SBA-15 catalyst.* Journal of Catalysis, (2008). **253**(1): p. 74-90.
53. Jackson, S.D. and S. Rugmini, *Dehydrogenation of n-butane over vanadia catalysts supported on θ-alumina.* Journal of Catalysis, (2007). **251**(1): p. 59-68.
54. Rahman A, Mohamed MH, Ahmed M, Aitani AM, *Characterization of chromia/alumina catalysts by X-ray photoelectron spectroscopy, proton induced X-ray emission and thermogravimetric analysis.* Applied Catalysis A: General, (1995). **121**(2): p. 203-216.
55. Dines, T.J. and S. Inglis, *Raman spectroscopic study of supported chromium(vi) oxide catalysts.* Physical Chemistry Chemical Physics, (2003). **5**(6): p. 1320-1328.
56. Weckhuysen, B.M. and I.E. Wachs, *In Situ Raman Spectroscopy of Supported Chromium Oxide Catalysts: 18O2−16O2 Isotopic Labeling Studies.* The Journal of Physical Chemistry B, (1997). **101**(15): p. 2793-2796.
57. Wang, L. and W.K. Hall, *The preparation and properties of rhenia-alumina catalysts.* Journal of Catalysis, (1983). **82**(1): p. 177-184.
58. Chan, S.S. and I.E. Wachs, *In situ laser Raman spectroscopy of nickel oxide supported on γ-Al2O3.* Journal of Catalysis, (1987). **103**(1): p. 224-227.
59. Williams, K.P.J. and K. Harrison, *Raman spectroscopic studies of the effects of tin promotion on a rhenium/alumina dismutation catalyst.* Journal of the Chemical Society, Faraday Transactions, (1990). **86**(9): p. 1603-1606.
60. Vuurman, M.A., I.E. Wachs, and A.M. Hirt, *Structural determination of supported vanadium pentoxide-tungsten trioxide-titania catalysts by in situ Raman spectroscopy and x-ray photoelectron spectroscopy.* The Journal of Physical Chemistry, (1991). **95**(24): p. 9928-9937.

61. Dines, T.J., C.H. Rochester, and A.M. Ward, *Raman spectroscopic study of titania-supported vanadia catalysts.* Journal of the Chemical Society, Faraday Transactions, (1991). **87**(4): p. 653-656.
62. Gough A, Turner SK , *Transhydrogenation,* in *US Patent 5585530.* (1996), Assigned to Institut Francais Du Petrole (Rueil-Malmaison Cedex, FR): USA.
63. Jackson SD, Grenfell J, Matheson IM, Webb G, *Production of alkenes over chromia catalysts: Effect of potassium on reaction sites and mechanism*, in *Studies in Surface Science and Catalysis*, F.V.M.S.M. Avelino Corma and G.F. José Luis, Editors. (2000), Elsevier. p. 2213-2218.
64. Ralph MD, Ernest WV, James CV, *Catalytic dehydrogenation of hydrocarbons over tin-containing crystalline microporous materials*, in *US Patent 4886926.* (1989), Assigned to Mobil Oil Corporation.
65. Iglesias-Jueza A, Andrew MB, Karin M, Tsu CW, Pieter G, Bert M.W, *A combined in situ time-resolved UV-Vis, Raman and high-energy resolution X-ray absorption spectroscopy study on the deactivation behavior of Pt and PtSn propane dehydrogenation catalysts under industrial reaction conditions.* Journal of Catalysis, (2010). **276**(2): p. 268-279.
66. Hagen, J., *Heterogeneous Catalysis: Fundamentals*, in *Industrial Catalysis*. (2015), Wiley-VCH Verlag GmbH & Co. KGaA. p. 99-210.
67. Isobel, M., Matheson, *Reactions of C3-hydrocarbons on Pt/alumina and chromia/alumina catalyst*, in *chemistry*. (1995), Glasgow: University of Glasgow.
68. Lagauche M, Kim L, Elsa J, Karin B, Céline C, Loïc F, and Michèle P, *Thermodynamic Characterization of the Hydroxyl Group on the γ-Alumina Surface by the Energy Distribution Function.* The Journal of Physical Chemistry C, (2017). **121**(31): p. 16770-16782.
69. Knözinger, H. and P. Ratnasamy, *Catalytic Aluminas: Surface Models and Characterization of Surface Sites.* Catalysis Reviews, (1978). **17**(1): p. 31-70.
70. Morterra C, Salvatore C, Edoardo G, and Giovanna G, *Surface acidity of [small eta]-alumina. Part 1.-Pyridine chemisorption at room temperature*. Journal of the Chemical Society, Faraday Transactions 1: Physical Chemistry in Condensed Phases, (1979). **75**(0): p. 271-288.
71. Hendriksen, B.A., D.R. Pearce, and R. Rudham, *Heats of adsorption of water on a- and γ-alumina.* Journal of Catalysis, (1972). **24**(1): p. 82-87.
72. J. Haber, JH Block, B. Delmon , *PHYSICAL AND BIOPHYSICAL CHEMISTRY DIVISION COMMISSION ON COLLOID AND SURFACE CHEMISTRY INCLUDING CATALYSIS.* Pure Appl. Chem., (1995). **67**(8-9): p. 1257-1306.
73. Yeboah, Y.D. and A.M. Aitani, *Thermal analysis of spent steam-reforming catalysts.* Thermochimica Acta, (1989). **149**: p. 147-156.
74. Mackenzie, R.C., *Thermal Analysis*, in *Physicochemical Methods of Mineral Analysis*, A. Nicol, Editor. (1975), Springer US. p. 389-420.
75. Daniel RS, Edgar FW, Gerard CS, *The Chemical Thermodynamics of Organic Compounds*. (1987), Malabar, Florida: Robert E. Krieger Publishing Company.

76. Vuurmana M A, Israel EW, Derk JS, and Ad O, *Characterization of chromium oxide supported on Al2O3, ZrO2, TiO2, and SiO2 under dehydrated conditions.* Journal of Molecular Catalysis, (1993). **80**(2): p. 209-227.
77. Michel, G. and R. Cahay, *Raman spectroscopic investigations on the chromium(VI) equilibria part 2—species present, influence of ionic strength and CrO42−▫Cr2O72− equilibrium constant*. Journal of Raman Spectroscopy, (1986). **17**(1): p. 79-82.
78. Vuurman, M.A. and I.E. Wachs, *In situ Raman spectroscopy of alumina-supported metal oxide catalysts*. The Journal of Physical Chemistry, (1992). **96**(12): p. 5008-5016.
79. Nakamura O., J. Silvio, T. Mambrim, H. O. Pastore, E. J. S. Vichi, F. G. Gandra, E. C. da Silva, H. Vargas and J. Pelzl, *Electron paramagnetic resonance study of chromosilicalite.* Journal of the Chemical Society, Faraday Transactions, (1992). **88**(14): p. 2071-2073.
80. Evans, J.C., C.R. Owen, and C.C. Rowlands, *Electron paramagnetic resonance study of monoclinic zirconium dioxide polycrystalline powders doped with paramagnetic transition-metal ions.* Journal of the Chemical Society, Faraday Transactions 1: Physical Chemistry in Condensed Phases, (1989). **85**(12): p. 4039-4046.
81. Calizo I, Igor B, Muhammad R, Guanxiong L, and Alexander AB, *Ultraviolet Raman microscopy of single and multilayer graphene.* Journal of Applied Physics, (2009). **106**(4): p. 043509.
82. Jin, S., et al., *UV Raman Spectroscopic Characterization of Catalysts and Catalytic Active Sites*. Catalysis Letters, (2015). **145**(1): p. 468-481.
83. Li, C. and P.C. Stair, *Ultraviolet Raman spectroscopy characterization of coke formation in zeolites.* Catalysis Today, (1997). **33**(1): p. 353-360.
84. Li, C. and P.C. Stair, *Ultraviolet Raman spectroscopy characterization of sulfated zirconia catalysts: fresh, deactivated and regenerated.* Catalysis Letters, (1996). **36**(3): p. 119-123.
85. Chua, Y.T., P.C. Stair, and I.E. Wachs, *A Comparison of Ultraviolet and Visible Raman Spectra of Supported Metal Oxide Catalysts*. The Journal of Physical Chemistry B, (2001). **105**(36): p. 8600-8606.
86. Edussuriya, M., S.D. Jackson, and S. Rugmini, *Deactivation and regeneration of chromia and vanadia catalysts in alkane dehydrogenation.* Current Topics in Catalysis, (2010). **9**: p. 15-24.
87. Song S, Yu J, Qiang X, Ye X, Yijun Zhong, and Weidong Z, *A stepwise loading method to magnetically responsive Pt-Fe(3)O(4)/MCNT catalysts for selective hydrogenation of 3-methylcrotonaldehyde*. Nanoscale Research Letters, (2014). **9**: p. 677.
88. Regalbuto, J.R., T.H. Fleisch, and E.E. Wolf, *An integrated study of Pt/WO3/SiO2 catalysts for the NO · CO reaction.* Journal of Catalysis, (1987). **107**(1): p. 114-128.
89. Jackson, S.D., G.J. Kelly, and G. Webb, *Supported Metal Catalysts; Preparation, Characterisation, and Function.* Journal of Catalysis, (1998). **176**(1): p. 225-234.

90. Graham, G.W., W.H. Weber, and K. Otto, *Raman investigation of the standard Pt/SiO2 catalyst EUROPT-1.* Applied Surface Science, (1992). **59**(1): p. 87-89.
91. Lieskeb H., G.Lietzb, H.Spindler, and J.Völter, *Reactions of platinum in oxygen- and hydrogen-treated Pty-Al2O3 catalysts.* Journal of Catalysis, (1983). **81**(1): p. 8-16.
92. Lieskeb H., G.Lietzb, H.Spindler, and J.Völter, *Reactions of platinum in oxygen- and hydrogen-treated Pty-Al2O3 catalysts.* Journal of Catalysis, (1983). **81**(1): p. 17-25.
93. Straguzzi, G.I., H.R. Aduriz, and C.E. Gigola, *Redispersion of platinum on alumina support.* Journal of Catalysis, (1980). **66**(1): p. 171-183.
94. Gorriz, O.F., V. Cortes Corberan, and J.L.G. Fierro, *Propane dehydrogenation and coke formation on chromia-alumina catalysts: effect of reductive pretreatments.* Industrial & Engineering Chemistry Research, (1992). **31**(12): p. 2670-2674.
95. Perego, C. and P. Ingallina, *Recent advances in the industrial alkylation of aromatics: new catalysts and new processes.* Catalysis Today, (2002). **73**(1): p. 3-22.
96. Hirofumi I,Tadashi H, Katsuhito S, and Yuichi M, *Role of acid and base sites in the side-chain alkylation of alkylbenzenes with methanol on two-ion-exchanged zeolites.* Journal of Catalysis, (1983). **79**(1): p. 21-33.
97. Holme A, Sæthre LJ, Børve KJ, Thomas TD., *Chemical Reactivity of Alkenes and Alkynes As Seen from Activation Energies, Enthalpies of Protonation, and Carbon 1s Ionization Energies.* The Journal of Organic Chemistry, (2012). **77**(22): p. 10105-10117.
98. Garba, M.D. and S.D. Jackson, *Catalytic upgrading of refinery cracked products by trans-hydrogenation: a review.* Applied Petrochemical Research, (2016): p. 1-8.
99. Mross, W.D., *Alkali Doping in Heterogeneous Catalysis.* Catalysis Reviews, (1983). **25**(4): p. 591-637.
100. Caspary, K.J., et al., *Dehydrogenation of Alkanes*, in *Handbook of Heterogeneous Catalysis*. (2008), Wiley-VCH Verlag GmbH & Co. KGaA.
101. Jonathan, C.N., Greeves; Stuart, Warren;, *Organic chemistry*, ed. s. edition. (2001), New York , USA: Oxford University Press Inc. .
102. Seo, YH., K.H Lee, and D.H. Shin, *Investigation of catalytic degradation of high-density polyethylene by hydrocarbon group type analysis.* Journal of Analytical and Applied Pyrolysis, (2003). **70**(2): p. 383-398.
103. Fogassy G , Nicolas T , Yves S and Claude M, *From biomass to bio-gasoline by FCC co-processing: effect of feed composition and catalyst structure on product quality.* Energy & Environmental Science, (2011). **4**(12): p. 5068-5076.
104. Frash MV, Kazansky VB, Rigby AM, and van Santen RA, *Cracking of Hydrocarbons on Zeolite Catalysts: Density Functional and Hartree−Fock Calculations on the Mechanism of the ß-Scission Reaction.* The Journal of Physical Chemistry B, (1998). **102**(12): p. 2232-2238.

105. Alessandro GB, Andrew MH, JT McKinnon, Robert LM, and Glen HK, *Coke and Byproduct Formation during 1,2-Dichloroethane Pyrolysis in a Laboratory Tubular Reactor*. Industrial & Engineering Chemistry Research, (2001). **40**(11): p. 2428-2436.
106. Bilal, M. and S.D. Jackson, *Ethanol steam reforming over Pt/Al2O3 and Rh/Al2O3 catalysts: The effect of impurities on selectivity and catalyst deactivation*. Applied Catalysis A: General, (2017). **529**: p. 98-107.
107. Shi, J., et al., *Nitrogen Chemistry and Coke Transformation of FCC Coked Catalyst during the Regeneration Process*. Scientific Reports, (2016). **6**: p. 27309.
108. Comstock, M.J., *Fluid Catalytic Cracking II, Copyright, ACS Symposium Series, Foreword*, in *Fluid Catalytic Cracking II*, M.J. Comstock, Editor. (1991), American Chemical Society. p. i-iv.
109. Sattler, J.J.H.B., A.M. Beale, and B.M. Weckhuysen, *Operando Raman spectroscopy study on the deactivation of Pt/Al2O3 and Pt-Sn/Al2O3 propane dehydrogenation catalysts*. Physical Chemistry Chemical Physics, (2013). **15**(29): p. 12095-12103.
110. Sadezky, A., et al., *Raman microspectroscopy of soot and related carbonaceous materials: Spectral analysis and structural information*. Carbon, (2005). **43**(8): p. 1731-1742.
111. Bilal, M. and S.D. Jackson, *Ethanol steam reforming over Rh and Pt catalysts: effect of temperature and catalyst deactivation*. Catalysis Science & Technology, (2013). **3**(3): p. 754-766.
112. Ruijun, Z. and S. Zhibin, *Structures and high temperature frictional behaviors of carbonaceous mesophases doped with metallic element nickel (Ni) through mechanical alloying*. Tribology Letters, (2006). **22**(1): p. 113-118.
113. Bernardo, C.A., *The Fouling of Catalysts by Deposition of Filamentous Carbon*, in *Fouling Science and Technology*, L.F. Melo, T.R. Bott, and C.A. Bernardo, Editors. (1988), Springer Netherlands: Dordrecht. p. 369-389.
114. Bartholomew, C.H., *Mechanisms of catalyst deactivation*. Applied Catalysis A: General, (2001). **212**(1): p. 17-60.
115. Rostami RB, Mohammad G, Zuoxing D, Yao W, and Reza MB, *Study of coke deposition phenomena on the SAPO_34 catalyst and its effects on light olefin selectivity during the methanol to olefin reaction*. RSC Advances, (2015). **5**(100): p. 81965-81980.
116. Bauer, F. and H.G. Karge, *Characterization of Coke on Zeolites*, in *Characterization II*, H.G. Karge and J. Weitkamp, Editors. (2007), Springer Berlin Heidelberg: Berlin, Heidelberg. p. 249-364.
117. Karge, H.G., S. Trevizan de Suarez, and I.G. Dalla Lana, *A new cell for combined IR and ESR investigations on solid catalysts*. The Journal of Physical Chemistry, (1984). **88**(9): p. 1782-1784.
118. Karge, H.G., M. Łaniecki, and M. Ziołek, *UV-visible spectroscopic investigations of the modified claus reaction on NaX zeolite catalysts*. Journal of Catalysis, (1988). **109**(2): p. 252-262.

119. Förster H, Jürgen S, Pal F and Imre K, *Formation of carbocations from C3 compounds in zeolites of different acidities.* Journal of the Chemical Society, Faraday Transactions 1: Physical Chemistry in Condensed Phases, (1987). **83**(4): p. 1109-1117.
120. Retcofsky, H.L., et al., *Studies of e.s.r. linewidths in coals and related materials.* Fuel, (1975). **54**(2): p. 126-128.
121. Greensfelder, B.S., H.H. Voge, and G.M. Good, *Catalytic and Thermal Cracking of Pure Hydrocarbons: Mechanisms of Reaction.* Industrial & Engineering Chemistry, (1949). **41**(11): p. 2573-2584.
122. Guisnet, M. and N.S. Gnep, *Mechanism of short-chain alkane transformation over protonic zeolites. Alkylation, disproportionation and aromatization.* Applied Catalysis A: General, (1996). **146**(1): p. 33-64.
123. Sterte, J. and J.E. Otterstedt, *Catalytic cracking of heavy oil: use of alumina—montmorillonites both as catalysts and as matrices for rare earth exchanged zeolite Y molecular sieve.* Applied Catalysis, (1988). **38**(1): p. 131-142.